4.0 REACTOR

4.1 SUMMARY DESCRIPTION

4.1.1 GENERAL

This chapter describes the mechanical components of the reactor core including the fuel rods, fuel assemblies, and control rods; the nuclear design; and the thermal-hydraulic design.

The core is cooled and moderated by light water at a normal operating pressure of 2250 psia in the Reactor Coolant System. The moderator reactor coolant contains boron as a neutron poison. The concentration of boron in the reactor coolant is varied as required to control relatively slow reactivity changes including the effects of fuel burnup. In addition, gadolinia poison is employed in the core to establish the desired initial reactivity.

The reactor core is comprised of an array of fuel assemblies each made up of two hundred and sixty-four fuel rods in a square 17 x 17 array. The fuel rods are supported in intervals along their length by grid assemblies which maintain the lateral spacing between the rods throughout the design life of the assembly. The grid assembly consists of an "egg-crate" arrangement of interlocked straps. The straps contain castellations or spring fingers and dimples for fuel rod support as well as reactor coolant mixing channels or vanes. The fuel rods consist of slightly enriched uranium dioxide ceramic cylindrical pellets contained in slightly cold worked and stress relieved Zircaloy-4 tubing, or recrystalized M5 tubing which are plugged and seal welded to encapsulate the fuel. All fuel rods are pressurized with helium during fabrication.

The center position in the assembly is reserved for the incore instrumentation, while the remaining 24 positions in the array are equipped with guide thimbles joined to the grids and the top and bottom nozzles. Depending upon the position of the assembly in the core, the guide thimbles may be used as core locations for rod cluster control assemblies (RCCA's).

The bottom nozzle is a box-like structure which serves as a bottom structural element of the fuel assembly and directs the reactor coolant flow distribution to the assembly.

The top nozzle assembly functions as the upper structural element of the fuel assembly in addition to providing a partial protective housing for the RCCA or other components.

The RCCAs each consist of a group of individual absorber rods fastened at the top end to a common hub or spider assembly. These assemblies contain adsorber material to control the reactivity of the core under operating conditions.

The nuclear design analyses and evaluation establish physical locations for control rods, burnable poison and physical parameters such as fuel and gadolinia enrichments and boron concentration in the reactor coolant. The nuclear design evaluation established that the reactor core has inherent characteristics which together with corrective actions of the reactor coolant and protective systems provide adequate reactivity control even if the highest reactivity worth RCCA is stuck in the fully withdrawn position.

The design also provides for inherent stability against diametral and azimuthal power oscillations and for control of induced axial power oscillations.

The thermal-hydraulic design analyses and evaluation establish reactor coolant flow parameters which assure that adequate heat transfer is provided between the fuel clad and the reactor coolant. The thermal design takes into account local variations in dimensions, power generation, flow distribution and mixing. The mixing channels or vanes incorporated in the fuel assembly spacer grid designs induce additional flow mixing between the various flow channels within a fuel assembly as well as between adjacent assemblies.

Instrumentation is provided in and out of the core to monitor the nuclear, thermal-hydraulic and mechanical performance of the reactor, and to provide inputs to automatic control functions.

Table 4.1.1-1 presents a comparison of the principal nuclear thermal-hydraulic and mechanical design parameters for the original core between the Shearon Harris Nuclear Station and the Virgil C. Summer Nuclear Station.

The analysis techniques employed in the core design are tabulated in Table 4.1.1-2.

4.2 FUEL SYSTEM DESIGN

The plant design conditions are divided into four categories in accordance with their anticipated frequency of occurrence and risk to the public: ANS Condition I - Normal Operation; ANS Condition II - Incidents of Moderate Frequency; ANS Condition III - Infrequent Incidents; ANS Condition IV - Limiting Faults. Chapter 15 describes the bases, plant operational conditions, and events involving each ANS Condition.

The reactor is designed so that its components meet the following performance and safety criteria:

a) The mechanical design of the reactor core components and their physical arrangement, together with corrective actions of the reactor control, protection, and emergency cooling systems (when applicable) ensure that:

   1) Fuel damage is not expected during ANS Condition I and ANS Condition II events. Fuel damage as used here is defined as penetration of the fission product barrier (i.e., the fuel rod clad). It is not possible, however, to preclude a very small number of rod failures resulting in the release of fission products. The CVCS is designed to remove these fission products from the reactor coolant, keeping the reactor coolant activity within plant design basis limits.

   2) The reactor can be brought to a safe state following a ANS Condition III event with only a small fraction of fuel rods damaged although sufficient fuel damage might occur to preclude immediate resumption of operation. In any case, the fraction of fuel rods damaged must be limited to meet the dose guidelines of 10 CFR 50.67.

   3) The reactor can be brought to a safe state and the core can be kept subcritical with acceptable heat transfer geometry following transients arising from ANS Condition IV events.

b) The fuel assemblies are designed to withstand loads induced during shipping, handling, and core loading without exceeding the criteria of Section 4.2.1.5.

c) The fuel assemblies are designed to accept control rod insertions in order to provide the required reactivity control for power operations and reactivity shutdown conditions.

d) All fuel assemblies have provisions for the insertion of incore instrumentation necessary for plant operation.

e) The reactor internals, in conjunction with the fuel assemblies and incore control components, direct reactor coolant through the core. This achieves acceptable flow distribution and restricts bypass flow so that the heat transfer performance requirements can be met for all modes of operation.

4.2.1 DESIGN BASES

The fuel rod and fuel assembly design bases are established to satisfy the general performance and safety criteria presented in Section 4.2.

The AREVA fuel rods are designed for a peak rod average burnup of up to 62,000 megawatt days per metric ton of uranium (MWD/MTU). The Westinghouse fuel rods are designed for a lead rod average burnup of up to 60,000 MWD/MTU in the fuel cycle equilibrium condition.

The detailed fuel rod design establishes such parameters as pellet size and density, clad/pellet diametral gap, gas plenum size, and helium pre-pressurization level. The design also considers effects such as fuel density changes, fission gas release, clad creep, and other physical properties which vary with burnup. The integrity of the fuel rods is ensured by designing to prevent excessive fuel temperatures, excessive internal rod gas pressures due to fission gas releases, and excessive cladding stresses and strains. This is achieved by designing the fuel rods so that the conservative design bases in the following subsections are satisfied during ANS Condition I and ANS Condition II events over the fuel lifetime. For each design basis, the performance of the limiting fuel rod must not exceed the limits specified by the design basis.

Integrity of the fuel assembly structure is ensured by setting limits on stresses and deformations due to various loads and by preventing the assembly structure from interfering with the functioning of other components. Three types of loads are considered:

1. Non-operational loads such as those due to shipping and handling.

2. Normal and abnormal loads which are defined for ANS Conditions I and II.

3. Abnormal loads which are defined for ANS Conditions III and IV.

The design bases for the incore control components are described in Section 4.2.1.6.

4.2.1.1 Cladding

Zircaloy-4 and M5 combine neutron economy (low absorption cross section); high corrosion resistance to reactor coolant, fuel, and fission products; and high strength and ductility at operating temperatures. References 4.2.1-1, 4.2.1-13, and 4.2.1-14 document the operating experience with Zircaloy-4 as a clad material while Reference 4.2.3-6 documents the operating experience with M5. Additional information on the materials, chemical, and mechanical

properties is given in References 4.2.1-2 and 4.2.1-10 for Zircaloy-4 and in Reference 4.2.3-6 for M5.

2. Stress Limits

   a. The Zircaloy-4 clad stresses are less than the ASME Section III allowable stresses, with due consideration of temperature and irradiation effects. Limits for M5® cladding are contained in Reference 4.2.3-6 and are considered proprietary to AREVA.

   b. Clad Tensile Strain - The total tensile creep strain is less than one percent from the unirradiated condition. The elastic tensile strain during a transient is less than one percent from the pre-transient value. This limit is consistent with proven practice (References 4.2.1-1, 4.2.1-13, and 4.2.1-14).

3. Vibration and Fatigue

   a. Strain Fatigue - The cumulative strain fatigue cycles are less than the design strain fatigue life. This basis is consistent with proven practice (References 4.2.1-1, 4.2.1-13, and 4.2.1-14).

   b. Vibration - Potential fretting wear due to vibration is limited by the spacer grid design. Without proper grid design, fretting of the clad surface can occur due to flow-induced vibration between the fuel rods and fuel assembly grid contact areas. Rod support by the spacer grids varies during the fuel life due to clad diameter creepdown combined with grid cell relaxation. Acceptability of the spacer grid design to prevent fretting is based on a combination of analysis and testing, as described in Reference 4.2.1-15.

4. Chemical properties of the cladding are discussed in Reference 4.2.1-2.

4.2.1.2 Fuel Material

1. Thermal-Physical Properties and fuel pellet temperatures--The center temperature of the hottest pellet is to be below the melting temperature of UO_2. While a limited amount of center melting can be tolerated, the design conservatively precludes center melting.

   The normal design density of the fuel is 95 percent theoretical. The normal design density of the fuel is 96 percent of theoretical beginning with Cycle 19. Additional information on fuel properties is given in Reference 4.2.1-2.

2. Fuel densification and fission product swelling - The design bases and models used for fuel densification and swelling are provided in References 4.2.1-4, 4.2.1-5, 4.2.1-13 and 4.2.1-16.

3. Chemical properties - Reference 4.2.1-2 provides a basis for justifying that no adverse chemical interactions occur between the fuel and its adjacent material.

4.2.1.3 Fuel Rod Performance

1. Fuel rod models - The basis fuel rod models and the ability to predict operating characteristics are given in References 4.2.1-5, 4.2.1-13 and 4.2.1-14 and Section 4.2.3.

2. Mechanical design limits - Cladding collapse is conservatively predicted not to occur during the fuel rod design lifetime (Reference 4.2.1-11 and 4.2.1-17). The models described in References 4.2.1-6 and 4.2.1-13 are used for this evaluation.

   The rod internal gas pressure shall remain below the value which causes the fuel/clad diametral gap to increase due to outward cladding creep during steady state operation. Rod pressure is also limited such that extensive departure from nucleate boiling (DNB) propagation will not occur during normal operation and any accident event. Section 4.4 shows that DNB propagation criteria is satisfied.

   For the calculated internal rod pressure of AREVA fuel, the NRC has approved a proprietary limit above system pressure. If system pressure is exceeded using the NRC approved methodology, then calculations are performed to show that the diametral gap does not increase during steady-state operation.

   For Westinghouse fuel, the NRC staff has completed its review of the revised fuel rod internal pressure design criteria and has decided on the following acceptable amended criteria:

   > "The internal pressure of the lead fuel rod in the reactor will be limited to a value below that which could cause (1) the diametrical gap to increase due to outward cladding creep during steady-state operation and (2) extensive DNB propagation to occur."

4.2.1.4 Spacer Grids

1. Mechanical limits and materials properties - The grid component strength criteria are based on experimental tests. The limit is established with a 95% confidence limit on the mean Pc (AREVA fuel) or at 0.9 Pc (Westinghouse fuel), where Pc is the experimental collapse load. This limit is sufficient to assure that under worst-case combined seismic and blowdown loads from an ANS Condition IV loss-of-coolant accident, the core will maintain a geometry amenable to cooling. As an integral part of the fuel assembly structure, the grids must satisfy the applicable fuel assembly design bases and limits defined in Section 4.2.1.5.

   Grid material and chemical properties are given in Reference 4.2.1-2.

4.2.1.5 Fuel Assembly

1. Structural Design - As previously discussed in Section 4.2.1, the structural integrity of the fuel assembly is ensured by setting design limits on stresses and deformations due to various non-operational, operational, and accident loads. These limits are applied to the design and evaluation of the top and bottom nozzles, guide thimbles, grids, and thimble joints.

The design bases for evaluating the structural integrity of the fuel assemblies are:

a. Non-operational
   - 2.5 g's for handling and 4-6 g's for shipping (AREVA fuel)
   - 4-6 g's loading with dimensional stability (Westinghouse fuel)

b. For the normal operating and upset conditions, the fuel assembly component structural design criteria are established for the two primary material categories, namely austenitic steels and Zircaloy. The stress categories and strength theory presented in the ASME Boiler and Pressure Vessel Code, Section III, are used as a general guide. The maximum shear-theory (Tresca criterion) for combined stresses is used to determine the stress intensities for the austenitic steel components. The stress intensity is defined as the numerically largest difference between the various principal stresses in a three-dimensional field. The design stress intensity, Sm, value for austenitic steels, such as nickel-chromium-iron alloys, is given by the lowest of the following:

   1) One-third of the specified minimum tensile strength or 2/3 of the specified minimum yield strength at room temperature;

   2) One-third of the tensile strength or 90 percent of the yield strength at operating temperature but not to exceed 2/3 of the specified minimum yield strength at room temperature.

   The stress limits for the austenitic steel components are given below. All stress nomenclature is per the ASME Code, Section III.

Stress Intensity Limits

Categories	Limit
Local primary membrane stress intensity	1.5 Sm
Primary membrane plus bending stress intensity	1.5 Sm
Total primary plus secondary stress intensity	3.0 Sm
Where: Sm is the design stress intensity	

For austenitic steel components of AREVA fuel, acceptable strength to perform the design function are based on direct testing of the articles. The testing consisted of conservative loadings, with consideration of temperature effects and both static and dynamic conditions.

The Zircaloy structural components, which consist of guide thimble and fuel tubes, are in turn subdivided into two categories because of material differences and functional requirements. The fuel cladding design criteria is covered separately in Section 4.2.1.1.

The maximum shear theory is used to evaluate the guide thimble design. For conservative purposes, the Zircaloy unirradiated properties are used to define the stress limits.

3) Abnormal loads during ANS Conditions III or IV - worst cases represented by combined seismic and blowdown loads.

a) Deflections or failures of components cannot interfere with reactor shutdown or emergency cooling of the fuel rods.

b) The fuel assembly structural component stresses under faulted conditions are evaluated using primarily the methods outlined in Appendix F of the ASME Code, Section III. Since the current analytical methods utilize elastic analysis, the stress allowables are defined as the smaller value of 2.4 Sm or 0.70 Su for primary membrane and 3.6 Sm or 1.05 Su for primary membrane plus primary bending. For the austenitic steel fuel assembly components, the design stress intensity is defined in accordance with the rules described in the previous section for normal operating conditions. For the Zircaloy components the design stress intensity is set at 2/3 of the material yield strength, Sy, or 1/3 of the ultimate strength, Su, at reactor operating temperature. This results in Zircaloy stress limits being the smaller of 1.6 Sy or 0.70 Su for primary membrane and 2.4 Sy or 1.05 Su for primary membrane plus bending. For conservative purposes, the Zircaloy unirradiated properties are used to define the stress limits.

Material and chemical properties of the fuel assembly components are given in Reference 4.2.1 2.

c) Thermal-hydraulic design - This topic is discussed in Section 4.4.

4.2.1.6 Core Components

The core components are subdivided into permanent and temporary devices.

The permanent components are the full length rod cluster control assemblies (RCCAs) and thimble plug assemblies. The thimble plug assemblies were removed from the core for Cycle 12. New AREVA RCCAs were installed during the Cycle 16 core reload. The temporary components are the burnable poison assemblies and the primary neutron source assemblies, which will no longer be used and are no longer addressed in detail in this document.

Materials are selected for compatibility in a pressurized water reactor environment, for adequate mechanical properties at room and operating temperature, for resistance to adverse property changes in a radioactive environment, and for compatibility with interfacing components. Material properties are given in Reference 4.2.1-2 for original core components and Reference 4.2.1-18 for AREVA RCCAs.

For ANS Conditions I and II, the stress categories and strength theory presented in the ASME Boiler and Pressure Vessel Code, Section III, Subsection NB 3000 are used as a general guide to establish core component rod cladding stress/strain limits. The code methodology is applied, as with fuel assembly structural design where possible. For ANS Conditions III and IV, code stresses are not limiting.

Additional design bases for each of the mentioned components are given in the following subsections.

1. Control rods - Design conditions which are considered under Article NB 3000 of the ASME Code, Section III are as follows:

   a. External pressure equal to the reactor coolant system operating pressure with appropriate allowance for overpressure transients.

   b. Wear allowance for continuous load follow operation during control rod assembly lifetime.

   c. Bending of the rod due to a misalignment in the guide tube.

   d. Forces imposed on the rods during rod drop.

   e. Loads imposed by the accelerations of the control rod drive mechanism.

   f. Radiation exposure during maximum core life.

The control rod cladding is cold drawn Type 304 stainless steel tubing for the original Westinghouse design and low contaminant Type 316L stainless steel tubing for the AREVA design installed for cycle 16. The stress intensity limit S_m, for this material is defined at 2/3 of the 0.2 percent offset yield stress.

The absorber material temperature does not exceed its melting temperature (1454 F for Ag-In-Cd absorber material - Reference 4.2.1-8 and 4.2.1-18). The melting point basis is determined by the nominal melting point minus uncertainty.

2. Thimble plug assembly - The thimble plug assembly, if used, restricts bypass flow through those thimbles not occupied by rod cluster control assemblies or burnable poison assemblies.

   The thimble plug assemblies satisfy the following criteria:

   a. Accommodate the differential thermal expansion between the fuel assembly and the core internals.

   b. Maintain positive contact with the fuel assembly and the core internals.

   c. Limits the flow through each occupied thimble to acceptable design value.

4.2.1.7 Surveillance Program

Section 4.2.4.5 and Sections 8 and 23 of Reference 4.2.1-9 discuss the testing and fuel surveillance operational experience programs which are being conducted to verify the adequacy of the fuel performance and design bases. Fuel surveillance and testing results, as they become available, are used to improve fuel rod design and manufacturing processes and ensure that the design bases and safety criteria are satisfied.

4.2.2 DESIGN DESCRIPTION

Three fuel designs may be used in the SHNPP core. The initial core and first reload were composed of standard Westinghouse 17 x 17 low-parasitic (LOPAR) fuel assemblies. The next three reloads introduced Westinghouse 17 x 17 VANTAGE 5 fuel. Subsequent reloads consist of AREVA 17 x 17 High Thermal Performance (HTP) fuel. The AREVA 17x17 design is intended to replace and be compatible with a core containing fuel of the VANTAGE 5 and LOPAR designs. The three fuel designs are essentially equivalent with regards to exterior assembly envelope dimensions and reactor internals interface. A comparison of the three fuel assembly designs is provided in Table 4.2.2-1. The AREVA 17 x 17 and VANTAGE 5 fuel assembly designs are described in detail in References 4.2.1-17 and 4.2.2-1 respectively.

Each 17 x 17 fuel assembly consists of 264 fuel rods (technical specifications allow limited substitution of fuel rods by filler rods consisting of Zircaloy-4 clad or M5 clad, or vacancies subject to a cycle-specific evaluation), 24 guide thimble tubes, and one instrumentation thimble tube arranged within a supporting structure. The instrumentation thimble is located in the center position and provides a channel for insertion of an incore neutron detector, if the fuel assembly is located in an instrumented core position. The guide thimbles provide channels for insertion of either a rod cluster control assembly or a thimble plug assembly. Figures 4.2.2-1A, 4.2.2-1B, and 4.2.2-1C show cross-sections of the LOPAR, VANTAGE 5, and AREVA 17 x 17 fuel assembly arrays, and Figures 4.2.2-2A and 4.2.2-2B show fuel assembly full-length views. The fuel rods are loaded into the fuel assembly structure so that there is clearance between the fuel rod ends and the top and bottom nozzles.

Improper orientation of fuel assemblies within the core is prevented by the use of an indexing hole in one corner of the top nozzle top plate. The assembly is oriented with respect to the handling tool and the core by means of a pin which is inserted into this indexing hole. Visual confirmation of proper orientation is also provided by an engraved identification number on the opposite corner clamp for the Westinghouse and AREVA designs.

4.2.2.1 Fuel Rods

The fuel rods consist of uranium dioxide ceramic pellets contained in slightly cold worked and stress relieved Zircaloy-4 tubing, or recrystalized M5 tubing which is plugged and seal welded at the ends to encapsulate the fuel. A schematic of the fuel rods for the VANTAGE 5 and LOPAR designs is shown in Figure 4.2.2-3A and for the AREVA design in Figures 4.2.2-3B and 4.2.2-3C. The fuel pellets are right circular cylinders consisting of slightly enriched uranium dioxide powder which has been compacted by cold pressing and then sintered to the required density. The ends of each pellet are dished slightly to allow greater axial expansion at the center of the pellets. Neutron absorbing characteristics to provide reduced peaking at the beginning of irradiation are provided by gadolinia bearing pellets in the AREVA design. The AREVA gadolinia bearing pellets (UO_2-Gd_2O_3) are geometrically similar to the enriched uranium dioxide pellets. The Westinghouse IFBA coated fuel pellets are identical to the enriched uranium dioxide pellets except for the addition of a thin enriched zirconium diboride (ZrB_2) coating on the pellet cylindrical surface. Both types of absorber pellets occupy the central portion of the fuel column (up to 126 inches for AREVA). The number and pattern of fuel rods containing absorber pellets within an assembly may vary depending on the specific application. The ends of the absorber pellets, like the enriched uranium pellets, are also dished to allow for greater axial expansion at the pellet centerline and void volume for fission gas release.

Void volume and clearances are provided within the rods to accommodate fission gases released from the fuel, differential thermal expansion between the clad and the fuel, and fuel density changes during irradiation. Shifting of the fuel within the clad during handling or shipping prior to core loading is prevented by an Alloy X-750 (AREVA fuel) or a stainless steel (Westinghouse fuel) helical spring which bears on top of the fuel.

4.2.2.2 Fuel Assembly Structure

The fuel assembly structure consists of a bottom nozzle, top nozzle, guide thimbles and grids, as shown in Figures 4.2.2-2A and 4.2.2-2B.

4.2.2.2.1 Bottom nozzle

The bottom nozzle serves as a bottom structural element of the fuel assembly and directs the reactor coolant flow distribution to the assembly. The AREVA bottom nozzle is of the FUELGUARD design: it consists of stainless steel bushings and curved blades brazed into a stainless steel cast and machined frame. This array of curved blades significantly improves the debris capturing effectiveness of the bottom nozzle compared to more standard designs. The Westinghouse nozzle is fabricated from Type 304 stainless steel and consists of a perforated plate and four angle legs with bearing plates as shown in Figure 4.2.2-2A. In both designs, the legs form a plenum for the inlet coolant flow to the fuel assembly. The grid of the nozzle also prevents accidental downward ejection of the fuel rods from the fuel assembly. The bottom nozzle is fastened to the fuel assembly guide tubes by mechanically locked screws which penetrate through the nozzle and mate with a threaded plug in each guide tube.

Reactor coolant flows from the plenum in the bottom nozzle upward through the penetrations in the grid to the channels between the fuel rods. For the Westinghouse design, the penetrations in the plate are positioned between the rows of the fuel rods.

Axial loads (holddown) imposed on the fuel assembly and the weight of the fuel assembly are transmitted through the bottom nozzle to the lower core plate. Indexing and positioning of the fuel assembly are provided by alignment holes in two diagonally opposite bearing plates which mate with locating pins in the lower core plate. Lateral loads on the fuel assembly are transmitted to the lower core plate through the locating pins.

4.2.2.2.2 Top nozzle

The top nozzle assembly functions as the upper structural element of the fuel assembly in addition to providing a partial protective housing for the rod cluster control assembly or other components, which are installed in the guide thimble tubes. The top nozzle assembly consists of a machined casting with two spring clamps in the AREVA design. The Westinghouse top nozzle assembly consists of an adapter plate, enclosure, top plate, and pads. Holddown springs are mounted on the assembly as shown in Figures 4.2.2-2A and 4.2.2-2B. The springs are Alloy 718 and the bolts are made of Alloy 718 whereas other components are made of Type 304 stainless steel.

The bottom plate of the top nozzle (referred to hereon as the adapter plate) is provided with round penetrations and semicircular ended slots to permit the flow of coolant upward through the top nozzle. Other holes are provided for the mechanical attachment of the guide thimble tubes. The AREVA design attachment consists of two latching rings and a spring which interact

with the adapter plate and the guide tube upper sleeve which is welded to the guide thimble tube. This quarter-turn mechanism provides for remote detachment/reattachment capability. On the Westinghouse design, round holes in the top nozzle are provided to accept sleeves which are mechanically attached to the thimble tubes. With the LOPAR fuel design, these sleeves are then welded to the adapter plate. The VANTAGE 5 fuel design uses a locking mechanism to attach the sleeves to the adapter plate which permits top nozzle removal.

The ligaments in the adapter plate cover the tops of the fuel rods and prevent their upward ejection from the fuel assembly. The top of the nozzle has a large square hole in the center to permit access for the control rods and the control rod spider. Holddown springs are mounted on the top plate and are fastened in place by bolts and clamps located at two diagonally opposite corners. On the other two corners, integral pads are positioned which contain alignment holes for locating the upper end of the fuel assembly.

4.2.2.2.3 Guide and instrument thimbles

The guide thimbles are structural members which also provide channels for the neutron absorber rods or thimble plug assemblies. Each thimble is fabricated from Zircaloy-4 tubing having two different diameters. The tube diameter at the top section provides the annular area necessary to permit rapid control rod insertion during a reactor trip. The lower portion of the guide thimble is swaged to a smaller diameter to reduce diametral clearances and produce a dashpot action near the end of the control rod travel during normal trip operation. MONOBLOC guide tube introduced in Cycle 19 where the lower portion of the guide tube ID is reduced to produce a dashpot action while maintaining constant OD to provide additional assembly stiffness. Holes are provided in the thimble tube above the dashpot to reduce the rod drop time and provide cooling for inserted or partially inserted RCCAs. The dashpot is closed at the bottom by means of an end plug. A small flow port is provided to avoid fluid stagnation in the dashpot volume during normal operation. The top end of the guide thimble is fastened to the top nozzle, as explained in Section 4.2.2.2.2 The lower end of the guide thimble is fitted with an end plug which is then fastened to the bottom nozzle by a mechanically locked screw.

Fuel rod support grids are fastened to the guide thimble assemblies to create an integrated structure. As shown in Figure 4.2.2-4, the AREVA spacers are resistance spot welded to the guide thimble tubes.

Since welding of the Westinghouse Inconel grid and Zircaloy thimble is not possible, a mechanical fastening technique depicted in Figures 4.2.2-5A, and 4.2.2-5B is used. An expanding tool is inserted into the inner diameter of the Zircaloy thimble tube at the elevation of stainless steel sleeves which have been brazed into the inconel grid assembly. The four lobed tool forces the thimble and sleeve outward to a predetermined diameter, thus joining the two components. The methods of grid fastening are standard and have been used successfully since the introduction of Zircaloy guide thimbles in 1969.

The central instrumentation thimble of each fuel assembly is constrained by seating in counterbores in each nozzle. This tube is of constant diameter and guides the incore neutron detectors. The instrument tube is also welded to end spacers in the AREVA design. For the Westinghouse designs, this thimble is expanded at the top and mid grids in the same manner as the previously discussed expansion of the guide thimbles to the grids. Figures 4.2.2-6 and 4.2.2-7 show the guide and instrument thimbles for all three fuel designs. For the Advanced W17 HTP™ design, the instrument tube is captured as noted in Figure 4.2.2-4.

4.2.2.2.4 Grid assemblies

The fuel rods, as shown in Figure 4.2.2-2A and 4.2.2-2B, are supported at intervals along their length by grid assemblies which maintain the lateral spacing between the rods. Each fuel rod is supported within each grid by the combination of support castellations, dimples, and springs. The grid assembly consists of slotted straps interlocked and welded or brazed in an "egg-crate" arrangement to join the straps permanently at their points of intersection. The straps contain castellations, spring fingers, support dimples, mixing channels, and mixing vanes.

The magnitude of the grid restraining force on the fuel rod and the contact area with the rod surface (for the AREVA Zircaloy and Nickel Alloy 718 spacers) are designed to minimize possible fretting, without overstressing the cladding at the points of contact between the grids and fuel rods. The grid assemblies also allow axial thermal expansion of the fuel rods without imposing restraint sufficient to develop buckling or distortion of the fuel rods.

The LOPAR fuel design utilizes two types of grid assemblies in each fuel assembly. Six grids, with mixing vanes projecting from the edges of the straps into the reactor coolant stream, are used in the high heat flux region of the fuel assemblies to promote mixing of the reactor coolant. Two grids, one at each end of the assembly, do not contain mixing vanes on the internal straps. The outside straps on all grids contain mixing vanes which, in addition to their mixing function, aid in guiding the grids and fuel assemblies past projecting surfaces during handling or during loading and unloading of the core. All LOPAR grids are made of Inconel-718.

The VANTAGE 5 fuel design uses three types of grid assemblies in each fuel assembly. The top and bottom grids are identical to the Inconel non-mixing vane grids used on the LOPAR design. The six internal grids are Zircaloy-4 structural grids with mixing vanes. In addition, non-structural Zircaloy-4 intermediate flow mixers (IFM) are included in the three uppermost spans between the Zircaloy mixing vane structural grids. The prime function of the IFM grids is to provide mid-span flow mixing in the hottest region of the fuel assembly.

The AREVA fuel design uses three types of grid assemblies in each fuel assembly. The top and bottom grids consist of Zircaloy-4 structural members with Alloy 718 spring strips. These end spacers restrain the rods in a dimple to spring contact arrangement. The six internal grids are Zircaloy-4 High Thermal Performance (HTP) designs. These grids consist of welded internal "doublet" strips which contain mixing channels that induce a swirling pattern in the coolant flow. Additional mixing is provided by three Intermediate Flow Mixers (IFMs) located between HTP grids in the upper region of the assembly. Like the HTP grids, the IFMs are of all-Zircaloy-4 construction, and they contain welded internal "doublet" strips with mixing channels. However, the IFM grids do not serve as structural members of the cage design.

The AREVA fuel design (Advanced W17 HTP) introduced in Cycle 19 uses three types of grid assemblies in each fuel assembly. The upper most spacer is a Zircaloy-4 High Thermal Performance (HTP) design as are the six intermediate spacers. These grids consist of welded internal “doublet” strips which contain mixing channels that induce a swirling pattern in the coolant flow. Additional mixing is provided by three Intermediate Flow Mixers (IFMs) located between HTP grids in the upper region of the assembly. Like the HTP grids, the IFMs are all of Zircaloy-4 construction and they contain welded internal “doublet” strips with mixing channels. However, the IFM grids do not serve as structural members of the cage design. The lower most spacer in the Adv. W17 HTP assembly is a High Mechanical Performance (HMP) design. The

HMP™ spacer is of nickel alloy 718 construction. The HMP™ grid consists of a similar welded internal “doublet” strips but with straight mixing channels.

4.2.2.3 Core Components

Reactivity control is provided by neutron absorbing rods and a soluble chemical neutron absorber (boric acid). The boric acid concentration is varied to control long term reactivity changes such as:

1. Fuel depletion and fission product buildup.
2. Cold to hot, zero power reactivity change.
3. Reactivity change produced by intermediate term fission products such as xenon and samarium.
4. Burnable poison depletion.

The Chemical and Volume Control System is discussed in Section 9.3.4.

The rod cluster control assemblies provide reactivity control for:

1. Shutdown.
2. Reactivity changes due to reactor coolant temperature changes in the power range.
3. Reactivity changes associated with the power coefficient of reactivity.
4. Reactivity changes resulting from void formation.

It is desirable to have a negative moderator temperature coefficient throughout the entire cycle in order to reduce possible deleterious effects caused by a positive coefficient during loss-of-coolant, loss-of-flow, or steam line break accidents. A combination of burnable poison with soluble boron is used to ensure a negative moderator coefficient during all portions of the fuel operating cycle.

The rod cluster control assemblies and their control rod drive mechanisms are the only moving parts in the reactor. Figure 4.2.2-8 illustrates the rod cluster control and control rod drive mechanism assembly, in addition to the arrangement of these components in the reactor, relative to the interfacing fuel assembly and guide tubes. In the following paragraphs, each reactivity control component is described in detail. The control rod drive mechanism assembly is described in Section 3.9.4.

The thimble plug assemblies, if used, limit bypass flow through those fuel assembly thimbles which do not contain control rods.

4.2.2.3.1 Full length rod cluster control assembly

The rod cluster control assemblies are divided into two categories: control and shutdown. The control groups compensate for reactivity changes associated with variations in operating

conditions of the reactor, i.e., power and temperature variations. Two nuclear design criteria have been employed for selection of the control group. First, the total reactivity worth must be adequate to meet the nuclear requirements of the reactor. Second, in view of the fact that these rods may be partially inserted at power operation, the total power peaking factor should be low enough to ensure that the power capability is met. The control and shutdown groups provide adequate shutdown margin.

The rod cluster control assembly is comprised of 24 neutron absorber rods fastened at the top end to a common spider assembly, as illustrated in Figure 4.2.2-9 and 4.2.2-9A.

The absorber materials used in the control rods is a silver-indium-cadmium or Hafnium alloy which is essentially "black" to thermal neutrons and has sufficient additional resonance absorption to significantly increase their worth. The alloy is in the form of extruded rods which are sealed in cold worked stainless steel tubes to prevent the rods from coming in direct contact with the reactor coolant (Figure 4.2.2-10). Sufficient diametral and end clearance is provided to accommodate relative thermal expansions.

The bottom plugs are made bullet-nosed to reduce the hydraulic drag during reactor trip and to guide smoothly into the dashpot section of the fuel assembly guide thimbles.

The absorber rod end plugs are Type 308 stainless steel. The design stresses used for the Type 308 material are the same as those defined in the ASME Code, Section III, for Type 304 stainless steel. At room temperature, the yield and ultimate stresses per ASTM 580 are the same for the two alloys. In view of the similarity of the alloy composition, the temperature dependence of strength for the two materials is also assumed to be the same.

The allowable stresses used as a function of temperature are listed in Table 1-1.2 of Section III of the ASME Code. The fatigue strength for the Type 308 material is based on the S N curve for austenitic stainless steels in Figure 1-9.2 of Section III.

The Westinghouse spider assembly is in the form of a central hub with radial vanes containing cylindrical fingers from which the absorber rods are suspended. Handling detents and detents for connection to the drive rod assembly are machined into the upper end of the hub. A coil spring inside the spider body absorbs the impact energy at the end of a trip insertion. The radial vanes are joined to the hub by tack weld and braze and the fingers are joined to the vanes by brazing. A centerpost which holds the spring and its retainer is threaded into the hub within the skirt and welded to prevent loosening in service. All components of the spider assembly are made from Types 304 and 308 stainless steel except for the retainer which is of 17-4 PH material and the springs which are Alloy 718.

The absorber rods are fastened securely to the spider. The rods are first threaded into the spider fingers and then pinned to maintain joint tightness, after which the pins are welded in place. The end plug below the pin position is designed with a reduced section to permit flexing of the rods to correct for small operating or assembly misalignments.

The AREVA NP Inc., spider assembly is in the form of a central hub with radial vanes containing cylindrical fingers from which the absorber rods are suspended. A coil spring inside the spider body absorbs the impact energy at the end of a trip insertion. The RCCA spider is cast rather than brazed to increase reliability of the spider by reducing the amount of welded or brazed connections. The spider body material is type CF3M stainless steel. All other components are

made from Types 304 and 308 stainless steel except for the spring retainer which is 17-4PH material and the springs which are alloy 718.

The rod connection to the spider consists of an upper end plug that is pinned and bolted to the spider boss to form a "flex joint". The upper end plug has a reduced diameter shank that provides flexibility to the joint for any misaligned control rod/fuel assembly/upper internals/handling equipment condition.

The overall length is such that when the assembly is withdrawn through its full travel, the tips of the absorber rods remain engaged in the guide thimbles so that alignment between rods and thimbles is always maintained. Since the rods are long and slender, they are relatively free to conform to any small misalignments with the guide thimble.

4.2.2.3.2 Thimble plug assembly

Thimble plug assemblies, if used, limit bypass flow through the rod cluster control guide thimbles in fuel assemblies which do not contain control rods. The thimble plug assemblies were removed from the core in cycle 12.

The thimble plug assemblies consist of a flat base plate with short rods suspended from the bottom surface and a spring pack assembly, as shown in Figure 4.2.2-15. The 24 short rods, called thimble plugs, project into the upper ends of the guide thimbles to reduce the bypass flow. Each thimble plug is permanently attached to the base plate by a nut which is lock-welded to the threaded end of the plug. When in the core, the thimble plug assemblies interface with both the upper core plate and with the fuel assembly top nozzles by resting on the adapter plate. The spring pack is compressed by the upper core plate when the upper internals assembly is lowered into place.

All components in the thimble plug assembly, except for the springs, are constructed from Type 304 stainless steel. The springs are Alloy 718.

4.2.2.4 GAIA Lead Assemblies

4.2.2.4.1 Fuel Material

The nominal density of the fuel for the AREVA 17 x 17 GAIA lead assemblies is 96.75 percent of theoretical.

4.2.2.4.2 Design Description

In Cycle 20, eight lead assemblies of the AREVA 17 x 17 GAIA design were inserted. See Figure 4.2.2-1D for the cross-section of AREVA 17 x 17 GAIA Fuel Assembly.

4.2.2.4.2.1 Fuel Rods

The fuel rods consist of uranium dioxide ceramic pellets contained in recrystalized M5® tubing which is plugged and seal welded at the ends to encapsulate the fuel. A schematic of the fuel rod for the AREVA 17 x 17 GAIA is shown in Figure 4.2.2-3C. The fuel pellets are right circular cylinders consisting of slightly enriched uranium dioxide powder which has been compacted by cold pressing and then sintered to 96.75% of theoretical density. The UO_2-Gd_2O_3 pellets

occupy the 123” central portion of the fuel column. Shifting of the fuel within the clad during handling or shipping prior to core loading is prevented by a nickel alloy X750 helical spring which bears on top of the fuel column.

4.2.2.4.2.2 Fuel Assembly Structure

The fuel assembly structure consists of a bottom nozzle, top nozzle, guide thimbles, spacer grids and fuel rods as shown in Figure 4.2.2-2C.

4.2.2.4.2.3 Bottom Nozzle

The bottom nozzle for the AREVA 17 x 17 GAIA fuel design is of the GRIP design; it consists of a stainless steel machined frame with a debris filtering plate attached underneath. The machining configuration of the frame includes recess areas to capture fuel rod end caps as they seat in the bottom nozzle and prevents accidental downward ejection of the fuel rods from the fuel assembly. The legs form a plenum for the inlet coolant flow to the fuel assembly. The bottom nozzle is fastened to the fuel assembly guide tubes by a lower connection screw which penetrates through the bottom nozzle and mates with a threaded plug in each guide tube.

4.2.2.4.2.4 Top Nozzle

The top nozzle design for the AREVA 17 x 17 GAIA design consists of a machined plate and frame. Holddown springs are mounted on the assembly as shown in Figure 4.2.2-2C.

4.2.2.4.2.5 Guide and Instrument Thimbles

For the AREVA 17 x 17 GAIA design, each thimble is fabricated from Q12™ alloy and is a MONOBLOC™ design. For the AREVA 17 x 17 GAIA, the instrument tube is captured as noted in Figure 4.2.2-4.

4.2.3 DESIGN EVALUATION

The fuel assemblies, fuel rods, and incore control components are designed to satisfy the performance and safety criteria of the introduction to Section 4.2, the mechanical design bases of Section 4.2.1, and other interfacing nuclear and thermal-hydraulic design bases specified in Section 4.3 and 4.4. AREVA analyses address the above by demonstrating compliance to the criteria in Reference 4.2.3-5 for Zircaloy-4 clad fuel rods and Reference 4.2.3-6 for M5 clad fuel rods.

Effects on fuel integrity of ANS Conditions II, III, and IV, or anticipated transients without trip are presented in Chapter 15 or supporting topical reports.

The initial step in fuel rod design evaluation for a region of fuel is to determine the limiting rod(s). Limiting rods are defined as those rod(s) whose predicted performance provides the minimum margin to each of the design criteria. For a number of design criteria the limiting rod is the lead burnup rod of a fuel region. In other instances it may be the maximum power or the minimum burnup rod. For the most part, no single rod will be limiting with respect to all design criteria. For the AREVA evaluation, the selection of the limiting rod power histories is in accordance with the NRC approved methodology described in Reference 4.2.1-13.

After identifying the limiting rod(s), a worst-case performance evaluation is made which includes the limiting rod design basis power history and considers the effects of model uncertainties and dimensional variations.

Furthermore, to verify adherence to the design criteria, the conservative case evaluation also considers the effects of postulated transient power increases which are achievable during operation consistent with ANS Conditions I and II. These transient power increases can affect both rod average and local power levels. The analytical methods used in the evaluation result in performance parameters which demonstrate the fuel rod behavior. Examples of parameters considered include rod internal pressure, fuel temperature, clad stress, and clad strain. In fuel rod design analyses, these performance parameters provide the basis for comparison between expected fuel rod behavior and the corresponding design criteria limits.

Fuel rod and assembly models used for the various evaluations are documented and maintained under an appropriate control system.

4.2.3.1 Cladding

1. Vibration and wear - Fuel rod vibrations are flow induced. The effect of vibrations on fuel assemblies and individual fuel rods is minimal. The cyclic stress range associated with deflections of such small magnitude is insignificant and has no effect on the structural integrity of the fuel rods.

   The reaction force on the grid supports due to rod vibration motions is also small and is much less than the spring preload. On certain grid designs, firm fuel clad spring contact is maintained. On the AREVA all-Zircaloy grid designs, the spring contact force may reach zero, but a large interfacing surface area at the rod support location is maintained. For all of the designs types, no significant wear of the clad or grid supports is expected during the life of the fuel assembly based on out-of-pile flow tests, performance of similarly designed fuel in operating reactors, and design analyses.

   Clad fretting and fuel vibration has been experimentally investigated, as shown in References 4.2.3-1 and 4.2.1-17.

2. Fuel rod internal pressure and cladding stresses - The burnup dependent fission gas release models (References (4.2.1-5 and 4.2.1-16) are used in determining the internal gas pressures as a function of irradiation time. The plenum height of the fuel rod has been designed to ensure that the maximum internal pressure of the fuel rod will not exceed the criteria described in Section 4.2.1.3. Exceeding these criteria could cause, (1) the fuel/clad diametral gap to increase during steady state operation and, (2) extensive DNB propagation to occur.

   The following description pertains to the Westinghouse fuel design stress analysis, although the general physical phenomenon apply to fuel rod designs in general. The clad stresses at a constant local fuel rod power are low. Compressive stresses are created by the pressure differential between the reactor coolant pressure and the rod internal gas pressure. Because of the pre-pressurization with helium, the volume average effective stresses are always less than approximately 10,000 psi at the pressurization level used in the fuel rod design. Stresses due to the temperature gradient are not included in the average effective stress because thermal stresses are, in general, negative at the clad inside diameter and

positive at the clad outside diameter, and their contribution to the clad volume average stress is small. Furthermore, the thermal stress decreases with time during steady state operation due to stress relaxation. The stress due to pressure differential is highest in the minimum power rod at the beginning-of-life due to low internal gas pressure and the thermal stress is highest in the maximum power rod due to steep temperature gradient.

The internal gas pressure of beginning-of-life is approximately 1,400 psia for a typical lead power fuel rod. The total tangential stress at the clad inside diameter at beginning-of-life is approximately 14,400 psi compressive (~13,000 psi due to ΔP and ~1,400 due to ΔT) for an average power rod operating at 5 kW/ft and approximately 12,000 psi compressive (~8,500 psi due to ΔP and ~3,500 psi due to ΔT) for a high power rod operating at 15 kW/ft. However, the volume average effective stress at beginning-of-life is between approximately 8000 psi (high power rod) and approximately 10,000 psi (low power rod). These stresses are substantially below even the unirradiated clad strength (~55,000 psi) at a typical clad mean operating temperature of 700 F.

For the AREVA clad stress analysis, both steady-state and vibratory stresses are considered. These stresses are caused by differential pressure, flow-induced vibration, spacer spring contact stresses, differential expansion, thermal gradients, pellet cladding interaction, and mechanical bow. As described above, the contribution from these categories changes during the irradiation of the fuel. Design tolerances are included in the evaluation with the use of conservative dimensional parameters. The evaluation shows the applicable stress criteria are met in all cases for Zircaloy-4 and M5® cladding. The limits for Zircaloy-4 are described in the 1977 ASME Boiler and Pressure Vessel Code Section III. The limits for M5 cladding are contained in Reference 4.2.3-6 and are considered proprietary to AREVA.

Tensile stresses could be created once the clad has come in contact with the pellet. These stresses would be induced by the fuel pellet swelling during irradiation. Fuel swelling can result in small clad strains (<1 percent for expected discharge burnups but the associated clad stresses are very low because of thermal and irradiation-induced clad creep). The 1 percent strain criterion is extremely conservative for fuel-swelling driven clad strain because the strain rate associated with solid fission products swelling is very slow. A detailed discussion of fuel rod performance is given in Section 4.2.3.3.

3. Materials and chemical evaluation - Zircaloy-4 and M5 clad has a high corrosion resistance to the reactor coolant, fuel, and fission products. As shown in Reference 4.2.1-1, there is considerable pressurized water reactor operating experience on the capability of Zircaloy as a clad material. Controls on fuel fabrication specify maximum moisture levels to preclude clad hydriding.

   Metallographic examinations of irradiated commercial fuel rods have shown occurrences of fuel/clad chemical interaction. Reaction layers of <1 mil in thickness have been observed between fuel and clad at limited points around the circumference. Metallographic data indicates that this interface layer remains very thin even at high burnup. Thus, there is no indication of propagation of the layer and eventual clad penetration.

   Stress corrosion cracking is another postulated phenomenon related to fuel/clad chemical interaction. Out-of-pile tests have shown that in the presence of high clad tensile stresses, large concentrations of iodine can chemically attack the Zircaloy tubing and can lead to

eventual clad cracking. Extensive post-irradiation examination has produced no inpile evidence that this mechanism is operative in commercial fuel.

4. Rod bowing - Section 4.4 presents the model used for evaluation of fuel rod bowing.

5. Consequences of power-coolant mismatch - This subject is discussed in Chapter 15.

6. Creep collapse and creepdown - This subject and the associated irradiation stability of cladding have been evaluated using the models described in References 4.2.1-6 and 4.2.1-13. It has been established that the design basis of no clad collapse during planned core life can be satisfied by limiting fuel densification, by having a sufficiently high initial internal rod pressure, and by a properly designed plenum spring.

4.2.3.2 Fuel Materials Considerations

Sintered high density uranium dioxide fuel reacts only slightly with the clad, at core operating temperatures and pressures. In the event of clad defects, the high resistance of uranium dioxide to attack by water, protects against fuel deterioration; although limited fuel erosion can occur. As has been shown by operating experience and extensive experimental work, the thermal design parameters conservatively account for changes in the thermal performance of the fuel elements due to pellet fracture which may occur during power operation. The consequences of defects in the clad are greatly reduced by the ability of uranium dioxide to retain fission products including those which are gaseous or highly volatile. Observations from several operating Westinghouse pressurized water reactors (Reference 4.2.1-9) have shown that fuel pellets can densify under irradiation to a density higher than the manufactured values. Fuel densification and subsequent settling of the fuel pellets can result in local and distributed gaps in the fuel rods. Fuel densification has been minimized by improvements in the fuel manufacturing process and by specifying a nominal 95-96 percent initial fuel density.

The evaluation of fuel densification effects and their consideration in fuel design are described in References 4.2.1-4, 4.2.1-5, 4.2.1-13 and 4.2.1 16. The treatment of fuel swelling and fission gas release are described in References 4.2.1-5, 4.2.1-13 and 4.2.1-16.

The effects of waterlogged fuel behavior are discussed in Section 4.2.3.3.

4.2.3.3 Fuel Rod Performance

In the calculation of the steady state performance of a nuclear fuel rod, the following interacting factors must be considered:

- Clad creep and elastic deflection.
- Pellet density changes, thermal expansion, gas release, and thermal properties as a function of temperature and fuel burnup.
- Internal pressure as a function of fission gas release, rod geometry, and temperature distribution.

These effects are evaluated by using a fuel rod design model (References 4.2.1-5 and 4.2.1-16). The Westinghouse model modifications for time dependent fuel densification are given in References 4.2.1-4 and 4.2.1-5.

With the above interacting factors considered, the models determine the fuel rod performance characteristics for a given rod geometry, power history, axial power shape, thermal hydraulic conditions, and irradiation environment. In particular, internal gas pressure, fuel and clad temperatures, and fuel and clad deflections are calculated. The fuel rod is divided into several axial sections and radially into a number of annular zones. Fuel density changes are calculated separately for each segment. The effects are integrated to obtain the internal rod pressure.

The initial rod internal pressure is selected to delay fuel/clad mechanical interaction and to avoid the potential for flattened rod formation. It is limited, however, by the design criteria for the rod internal pressure (see Section 4.2.1.3).

The gap conductance between the pellet surface and the clad inner diameter is calculated as a function of the composition, temperature, and pressure of the gas mixture, and the gap size or contact pressure between clad and pellet.

The Westinghouse fuel performance model includes the following processes. After computing the fuel temperature for each pellet annular zone, the fractional fission gas release is assessed using an empirical model derived from experimental data (Reference 4.2.1-5). The total amount of gas released is based on the average fractional release within each axial and radial zone and the gas generation rate which in turn is a function of burnup. Finally, the gas released is summed over all zones and the pressure is calculated.

The Westinghouse code shows good agreement in fit for a variety of published and proprietary data on fission gas release, fuel temperatures and clad deflections (Reference 4.2.1-5). These data include variations in power, time, fuel density, and geometry.

The AREVA fuel performance code consists of a time dependent model with the rod design divided into both axial and radial zones. Types of fuel rod phenomena modelled by the code include gap conductance; fission gas release; pellet grain growth; fuel densification, swelling, and cracking; fuel cladding contact; and cladding corrosion. This thermal-mechanical-chemical evaluation provides simulation of a fuel rod under normal operating conditions, as well as starting conditions for the analysis of transient conditions at various exposures. Detailed description and benchmarking of the fuel performance code is provided in Reference 4.2.1-13 and 4.2.1-16.

1. Fuel/cladding mechanical interaction - One factor in fuel element duty is potential mechanical interaction of fuel and clad. This fuel/clad interaction produces cyclic stresses and strains in the clad, and these in turn consume clad fatigue life. The reduction of fuel/clad interaction is therefore a goal of design. The technology of using pre-pressurized fuel rods has been developed to further this objective.

   The gap between the fuel and clad is initially sufficient to prevent hard contact between the two. However, during power operation a gradual compressive creep of the clad onto the fuel pellet occurs due to the external pressure exerted on the rod by the reactor coolant. Clad compressive creep eventually results in the fuel/clad contact. Once fuel/clad contact occurs, changes in power level result in changes in clad stresses and strains. By using pre-pressurized fuel rods to partially offset the effect of the reactor coolant external pressure, the rate of clad creep toward the surface of the fuel is reduced. Fuel rod pre-pressurization delays the time at which fuel/clad interaction and contact occur and hence significantly reduces the number and extent of cyclic stresses and strains experienced by the clad both

before and after fuel/clad contact. These features result in an increase in the fatigue life margin of the clad and lead to greater clad reliability. If gaps should form in the fuel stacks, clad flattening will be prevented by the rod pre-pressurization so that the flattening time will be greater than the fuel core life. Furthermore, the plenum spring in the AREVA fuel is designed to preclude the development of such gaps.

In addition to uniform clad stresses, stress concentrations develop in the clad adjacent to radial cracks in the pellet. These radial cracks have a tendency to open during a power increase but the frictional forces between fuel and clad oppose the opening of these cracks and result in localized increases in clad stress. As the power is further increased, large tensile stresses exceed the ultimate tensile strength of UO_2, and additional cracks in the fuel are created which limit the magnitude of the stress concentration in the clad.

Models of pellet cracking and pellet cladding mechanical interaction are part of the AREVA fuel performance modelling code for normal operation. Furthermore, results from the normal operation code are used as starting conditions for the AREVA mechanical transient model. This model includes stress effects from pellet cladding mechanical interaction as well as lodged pellet chips. Results from these benchmarked codes are compared to conservative fuel rod criteria to ensure acceptable in-reactor behavior.

For the Westinghouse evaluation, a two-dimensional (r,θ) finite element model has been developed to investigate the effects of radial pellet cracks on stress concentrations in the clad. Stress concentration is defined as the difference between the maximum clad stress in the θ-direction and the mean clad stress. The first case has the fuel and clad in mechanical equilibrium and as a result the stress in the clad is close to zero. In subsequent cases the pellet power is increased in steps and the resultant fuel thermal expansion imposes tensile stress in the clad.

As part of the standard Westinghouse fuel rod design analysis, the maximum stress concentration evaluated from finite element calculations is added to the volume averaged effective stress in the clad as determined from one-dimensional stress/strain calculations. The resultant clad stress is then compared to the temperature dependent Zircaloy yield stress in order to assure that the stress/strain criteria are satisfied.

Transient Evaluation Method - Pellet thermal expansion due to power increases is one way by which significant stresses and strains can be imposed on the clad. Such increases are a consequence of fuel shuffling (e.g., Region 3 positioned near the center of the core for Cycle 2 operation after operating near the periphery during Cycle 1), reactor power escalation following extended reduced power operation, and full-length control rod movement.

In the Westinghouse mechanical design model, lead rod burnup values are obtained by using best estimate power histories, as determined by core physics calculations. During burnup, the amount of diametral gap closure is evaluated, based upon the pellet expansion cracking model, clad creep model, and fuel swelling model. At various times during the depletion, the power is increased locally on the rod to the burnup-dependent attainable power density, as determined by core physics calculations. The radial, tangential, and axial clad stresses resulting from the power increase are combined into a volume average effective clad stress.

The Von Mises criterion is used to evaluate if the clad yield stress has been exceeded. This criterion states that an isotropic material in multiaxial stress will begin to yield plastically when the effective stress exceeds the yield stress, as determined by an axial tensile test. The yield stress correlation is that for irradiated cladding, since fuel/clad interaction occurs at high burnup. Furthermore, the effective stress is increased by an allowance, which accounts for stress concentrations in the clad adjacent to radial cracks in the pellet prior to the comparison with the yield stress. This allowance was evaluated using a two-dimensional (r,θ) finite element model.

In the AREVA evaluation, a transient model is coupled with the normal operation model to determine the rod behavior during power ramps. The ability of a fuel rod to resist failure from pellet-cladding interaction resulting from power increases is dependent upon the thermal-mechanical state of the fuel and the cladding and the chemical environment of the fuel/cladding interface. The transient model evaluates the mean and localized cladding deformations and the stress state of the cladding/pellet interface. Input to this model includes initial conditions of the rod at the time of the power increase taken from the AREVA normal operation fuel model and a time dependent history of the power fluctuation during the power ramp. The power fluctuations are analyzed at various times throughout irradiation. The power levels are based on the allowed peaking limits of the core, adjusted to the local power level of the rod being analyzed. This transient model was benchmarked using ramp test results from the Studsvik international programs; INTERRAMP, OVERRAMP, and SUPERRAMP. The results of this evaluation are compared to the applicable strain criterion, and stress results are used as input for the fatigue evaluation.

Slow transient power increases can result in large clad strains without exceeding the clad yield stress because of clad creep and stress relaxation. Therefore, in addition to the yield stress criterion, a criterion on allowable clad strain is necessary. Based upon high strain rate burst and tensile test data on irradiated tubing, 1 percent strain was determined to be a conservative lower limit on irradiated clad ductility and thus adopted as a design criterion.

A comprehensive review of the available strain-fatigue models was conducted by Westinghouse as early as 1968. This included the Langer-O'Donnell model (Reference 4.2.3 3), the Yao-Munse model, and the Manson-Halford model. Upon completion of this review and using the results of the Westinghouse experimental programs discussed below, it was concluded that the approach defined by Langer-O'Donnel would be retained and the empirical factors of their correlation modified in order to conservatively bound the results of the Westinghouse testing program.

The Langer-O'Donnel empirical correlation has the following form:

$$S_a = \frac{E}{4\sqrt{N_f}} \ln\left(\frac{100}{100 - RA}\right) + S_e$$

where:

S_a = 1/2 E $\Delta\varepsilon_t$ = pseudo - stress amplitude which causes failure in N_f cycles (lb./in.^{2})

$\Delta\varepsilon_t$ = total strain range (in./in.)

E = Young's Modulus (lb./in.^{2})

N_f = number of cycles to failure

RA = reduction in area at fracture in a uniaxial tensile test (%)

S_e = endurance limit (lb./in.^{2})

Both RA and Se are empirical constants which depend on the type of material, the temperature, and irradiation. The Westinghouse testing program was subdivided into the following subprograms:

a. A rotating bend fatigue experiment on unirradiated Zircaloy-4 specimens at room temperature and at 725F. Both hydrided and non-hydrided Zircaloy-4 cladding were tested.

b. A biaxial fatigue experiment in gas autoclave on unirradiated Zircaloy-4 cladding both hydrided and non-hydrided.

c. A fatigue test program on irradiated cladding from the Carolina-Virginia Tube Reactor and Yankee Core V conducted at Battelle Memorial Institute.

The results of these test programs provided information on different cladding conditions including the effect of irradiation, of hydrogen level, and temperature.

The design equations followed the concept for the fatigue design criterion according to the ASME Code, Section III. Namely,

1) The calculated pseudo-stress amplitude (S_a) has to be multiplied by a factor of 2 in order to obtain the allowable number of cycles (N_f).

2) The allowable cycles for a given S_a is 5 percent of N_f, or a safety factor of 20 on cycles.

The lesser of the two allowable number of cycles is selected. The cumulative fatigue life fraction is then computed as:

$$\sum_{1}^{k} \frac{n_k}{N_{fk}} \leq 1$$

where:

n_k = number of daily cycles of mode k

N_{fk} = number of allowable cycles

It is recognized that a possible limitation to the satisfactory behavior of the fuel rods in a reactor which is subjected to daily load follow is the failure of the clad by low-cycle strain fatigue. During their normal residence time in reactor, the fuel rods may be subjected to

approximately 1,000 cycles with typical changes in power level from 50 to 100 percent of their steady state values.

The assessment of the fatigue life of the fuel rod clad is subject to a considerable uncertainty due to the difficulty of evaluating the strain range which results from the cyclic interaction of the fuel pellets and clad. This difficulty arises, for example, from such highly unpredictable phenomena as pellet cracking, fragmentation, and relocation. Nevertheless, since early 1968, this particular phenomenon has been investigated analytically and experimentally (Reference 4.2.3 3). Strain fatigue tests on irradiated and nonirradiated hydrided Zircaloy-4 claddings were performed which permitted a definition of a conservative fatigue life limit and recommendation of a methodology to treat the strain fatigue evaluation of the Westinghouse reference fuel rod designs.

Experience in load follow operation dates back to early 1970 with the load follow operation of the Saxton reactor. Successful load follow operation has been performed on reactor A (~400 load follow cycles) and reactor B (500 load follow cycles). In both cases, there was no significant reactor coolant activity increase that could be associated with the load follow mode of operation.

In the AREVA evaluation, the stresses obtained from the transient model analysis along with the Langer-O'Donnel relationship are used in determining the fatigue usage factor. The transient stresses are calculated based on power fluctuations that are conservatively high both in quantity and in power level change. The calculated usage factor is then compared to a conservative fatigue usage criterion to ensure acceptability of the design.

2. Irradiation experience - Fuel operational experience is presented in References 4.2.1-1, 4.2.1-13 and 4.2.1-14. Additional test assembly and test rod experience are given in Sections 8 and 23 of Reference 4.2.1-9.

3. Fuel and cladding temperature - The methods used for evaluation of fuel rod temperatures are presented in Section 4.4.2.11.

4. Waterlogging - Waterlogging damage of a previously defective fuel rod has occasionally been postulated as a mechanism for subsequent rupture of the cladding. Such damage has been postulated as a consequence of a power increase on a rod after water has entered such a rod through a clad defect of appropriate size. Rupture is postulated upon power increase if the rod internal pressure increase is excessive due to insufficient venting of water to the reactor coolant. Local cladding deformations typical for waterlogging bursts have never been observed in commercial Westinghouse fuel. Experience has shown that the small number of rods which have acquired clad defects, regardless of primary mechanism, remain intact and do not progressively distort or restrict reactor coolant flow. In fact, such small defects are normally observed through reductions in reactor coolant activity to be progressively closed upon further operation due to the buildup of zirconium oxide and other substances. Secondary failures which have been observed in defective rods are attributed to hydrogen embrittlement of the cladding.

   Post-irradiation examinations point to the hydriding failure mechanism rather than a waterlogging mechanism; the secondary failures occur as axial cracks in the cladding and

are similar regardless of the primary failure mechanism. Such cracks do not result in flow blockage or increase the effects of any postulated transients.

5. Potentially damaging temperature effects during transients - The fuel rod experiences many operational transients (intentional maneuvers) during its residence in the core. A number of thermal effects must be considered when analyzing the fuel rod performance.

   The clad can be in contact with the fuel pellet at some time in the fuel lifetime. Clad/pellet interaction occurs if the fuel pellet temperature is increased after the clad is in contact with the pellet. Clad/pellet interaction is discussed in Section 4.2.3.3 item 1.

   The potential effects of operation with waterlogged fuel are discussed in Section 4.2.3.3 item 4, which concluded that waterlogging is not a concern during operational transients.

   Clad flattening, as shown in Reference 4.2.1-6, has been observed in some operating power reactors. Thermal expansion (axial) of the fuel rod stack against a flattened section of clad could cause failure of the clad. This is no longer a concern because clad flattening is precluded during the fuel residence in the core (see Section 4.2.3.1).

   Potential differential thermal expansion between the fuel rods and the guide thimbles during a transient is considered in the design. Excessive bowing of the fuel rods is precluded because the grid assemblies allow axial movement of the fuel rods relative to the grids. Specifically, thermal expansion of the fuel rods is considered in the grid design so that axial loads imposed on the fuel rods during a thermal transient will not result in excessively bowed fuel rods.

6. Fuel element burnout and potential energy release - As discussed in Section 4.4.2.2, the core is protected from DNB over the full range of possible operating conditions. In the extremely unlikely event that DNB should occur, the clad temperature will rise due to the steam blanketing at the rod surface and the consequent degradation in heat transfer. During this time there is potential for chemical reaction between the cladding and the reactor coolant. However, because of the relatively good film boiling heat transfer following DNB, the energy release resulting from this reaction is insignificant compared to the power produced by the fuel.

4.2.3.4 Spacer Grids

The reactor coolant flow channels are established and maintained by the structure composed of grids and guide thimbles. The lateral spacing between fuel rods is provided and controlled by the support dimples or castellations of adjacent grid cells. On certain spacer designs, contact of the fuel rods on the dimples is maintained through the clamping force of the grid springs. In the case of the AREVA HTP and IFM grid designs, the relatively large contact area with the rods prevents fretting wear. Lateral motion of the fuel rods is opposed by the spacer cell designs. Grid testing is discussed in References 4.2.3-4 and 4.2.1-17. As shown in References 4.2.3-4 and 4.2.1-17, grid crushing tests and seismic and loss-of-coolant accident evaluations show that the grids will maintain a geometry that is capable of being cooled under the worst-case accident ANS Condition IV event.

4.2.3.5 Fuel Assembly

4.2.3.5.1 Stresses and deflections

The fuel assembly component stress levels are limited by the design. For example, stresses in the fuel rod due to thermal expansion and Zirconium alloy irradiation growth are limited by the relative motion of the rod as it slips through the grid cells. Clearances between the fuel rod ends and nozzles are provided so that Zirconium alloy irradiation growth does not result in rod end interferences. Stresses in the fuel assembly caused by tripping of the rod cluster control assembly have little influence on fatigue because of the small number of events during the life of an assembly. Assembly components and prototype fuel assemblies made from production parts have been subjected to structural tests to verify that the design bases requirements are met.

The fuel assembly design loads for shipping have been established at 4-6 g's for Westinghouse fuel and for AREVA fuel. Accelerometers are placed into the shipping container to monitor and detect fuel assembly accelerations that would exceed the criteria. Past history and experience has indicated that loads which exceed the allowable limits rarely occur. Exceeding the limits requires reinspection of the fuel assembly for damage. Tests on various fuel assembly components such as the grid assembly, sleeves, inserts, and structure joints have been performed to assure that the shipping design limits do not result in impairment of fuel assembly function. Seismic Analysis of the Fuel assembly is presented in Reference 4.2.3-4.

4.2.3.5.2 Dimensional stability

A prototype fuel assembly and/or individual components have been subjected to vertical loads in excess of those expected in normal service and faulted conditions (see References 4.2.3-4 and 4.2.1-17). No interference with control rod insertion into thimble tubes will occur during a postulated loss-of-coolant accident transient due to fuel rod swelling, thermal expansion, or bowing. In the early phase of the transient following the reactor coolant break, the high axial loads, which could be generated by the difference in thermal expansion between fuel clad and thimbles, are relieved by slippage of the fuel rods through the grids. The relatively low drag force restraint on the fuel rods will induce only minor thermal bowing, which is insufficient to close the fuel rod-to-thimble tube gap.

4.2.3.5.2.1 Seismic/LOCA Effects on the SHNPP Fuel Assemblies

The Westinghouse fuel assembly responses resulting from the lateral safe shutdown earthquake, SSE and the most limiting main coolant pipe break accident, LOCA are analyzed using time history numerical integration techniques. Since the reactor vessel motions resulting from the transient loadings are asymmetric with respect to the geometrical center of the reactor core, the full assembly core finite element model described in References 4.2.1-13 and 4.2.3-4 is used to determine the fuel assembly deflection and grid impact forces.

The reactor core finite element model consisting of the maximum number of fuel assemblies across the core diameter was used to analyze the fuel assembly responses. The SHNPP has fifteen fuel assemblies arranged in a planar array with gaps to simulate the geometric clearance between the fuel assemblies as well as the clearance between the peripheral fuel assemblies and baffle plate.

The fuel assembly finite element model is constructed by preserving the essential dynamic properties such as the fuel assembly vibration frequencies, mode shapes, and mass distribution. The time history motion for the upper and lower core plates and the barrel at the upper core plate elevation are simultaneously applied to the simulated core model. The time history inputs representing the safe shutdown earthquake motion and the coolant pipe rupture transient were obtained from the time history analysis of the reactor vessel and internals finite element model.

The introduction of AREVA fuel into the core is facilitated by the more flexible AREVA structural grid spacer. Uniform and mixed core finite element studies with 17x17 assemblies showed lower core loads with the utilization of the AREVA design. The evaluation is described in more detail in Reference 4.2.1-17.

For the GAIA fuel design the SHNPP seismic/LOCA evaluation has been reanalyzed using Reference 4.2.3-7 in conjunction with the introduction of the GAIA Lead Assembly design. Reference 4.2.3-7 is approved for this application. Using the methodology the GAIA fuel assemblies have demonstrated margin to the maximum impact forces experienced by the fuel during the postulated seismic/LOCA event.

1. Grid Analysis. The maximum grid impact forces for both the seismic and asymmetric LOCA accidents occur at the peripheral fuel assembly locations adjacent to the baffle wall. The maximum grid impact forces obtained from the safe shutdown earthquake and the nozzle inlet break analyses were approximately 38 and 30 percent of the allowable Westinghouse grid strength, respectively.

   In order to comply with the requirements in the USNRC 4.2 standard review plan, the maximum grid impact responses obtained from the two transient analyses shall be combined using the square-root-of-sum-of-squares (SRSS) method. The combined grid impact forces are determined at all the grid elevations. The resulting maximum combined impact force for the Shearon Harris fuel assemblies was approximately 48 percent of the allowable Westinghouse grid strength which is determined experimentally based on the 95% confidence level on the true mean as taken from the distribution of measurements. Using the same type of statistical reduction, the strength of the AREVA grids is higher than the load criterion. Furthermore, as described above, uniform and mixed core studies of the AREVA design show that the resultant accident loads would be reduced with the introduction of the AREVA design (Reference 4.2.1-17).

   The effect of steam flashing on grid impact load was analyzed. The results indicated that the effect of steam flashing on fuel grid impact load is negligible. Therefore, the 30 percent increase in the grid impact load specified in the Appendix A of SRP Section 4.2 to account for steam flashing effects was not included in the grid load calculation.

2. Non-Grid Component Analyses. The stresses induced in the various fuel assembly non-grid components are assessed based on the most limiting seismic and LOCA accident conditions. The fuel assembly axial force resulting from the LOCA accident are the primary sources of stresses in the thimble guide tube and the fuel assembly nozzles. The induced stresses in the fuel rods result from the fuel assembly relative deflection during the seismic and LOCA accidents and are generally very small. The combined seismic and LOCA induced stresses of the various fuel assembly components for both the Westinghouse and AREVA designs are below the allowable limit. Consequently, the fuel assembly

components are structurally acceptable under the postulated accident design conditions for the SHNPP.

References 4.2.3-4 and 4.2.1-17 show that the fuel assemblies will maintain a geometry amenable to cooling during a combined seismic and double-ended loss-of-coolant accident.

4.2.3.6 Reactivity Control Assembly

1. Internal Pressure and Cladding Stresses During Normal, Transient, and Accident Conditions - Rod, guide thimble, and dashpot flow analyses indicate that the flow is sufficient to prevent coolant boiling. Therefore, clad temperatures at which the clad material has adequate strength to resist reactor coolant operating pressures and rod internal pressures are maintained.

2. Thermal Stability of the Absorber Material Including Phase Changes and Thermal Expansion - The radial and axial temperature profiles have been determined by considering gap conductance, thermal expansion, and neutron or gamma heating of the contained material as well as gamma heating of the clad.

   The maximum temperature of the Ag-In-Cd or Hafnium absorber material was calculated to be less than 850 F, and occurs axially at only the highest flux region. This temperature is well below the absorber melting temperature bases of Section 4.2.1.6.1. The thermal expansion properties of the absorber material and the phase changes are discussed in References 4.2.1-2, 4.2.1-8, and 4.2.1-18.

   Sufficient diametral and end clearances have been provided in the neutron absorber to accommodate the relative thermal expansions between the enclosed material and the surrounding clad and end plug.

3. Irradiation Stability of the Absorber Material, Taking into Consideration Gas Release and Swelling - The irradiation stability of the absorber material is discussed in References 4.2.1-2, 4.2.1-3, and 4.2.1-18. Irradiation produces no deleterious effects in the absorber material. Sufficient diametral and end clearances are provided to accommodate swelling of the absorber material.

   Gas release is not a concern for the absorber rod because no gas is released by the absorber material. Sufficient diametral and end clearances are provided to accommodate swelling of the absorber material.

4. Potential for chemical interaction, including possible waterlogging rupture - The selected structural materials have good resistance to irradiation damage and are compatible with the reactor environment.

   The current design type reactivity controls have been in service with no unanticipated degradation of construction material.

   Corrosion of the materials exposed to the reactor coolant is quite low, and proper control of chloride and oxygen in the coolant will prevent the occurrence of stress corrosion. The potential for the interference with rod cluster control movement due to possible corrosion phenomena is very low.

Waterlogging rupture is not a failure mechanism associated with Westinghouse-designed control rods. However, a breach of the cladding for any postulated reason does not result in serious consequences. The silver-indium-cadmium or Hafnium absorber material is relatively inert and would still remain remote from high reactor coolant velocity regions. Rapid loss of material resulting in significant loss of reactivity control material would not occur. Bettis test results (Reference 4.2.1-8) concluded that additions of indium and cadmium to silver, in the amounts to form the Westinghouse absorber material composition, result in small corrosion rates.

4.2.4 TESTING AND INSPECTION PLAN

4.2.4.1 Quality Assurance Program

The AREVA and Westinghouse fuel assemblies have been designed and fabricated under a NRC approved quality assurance program. The quality assurance program for AREVA is described in Reference 4.2.4-2.

The program provides for control over all activities affecting product quality, commencing with design and development and continuing through procurement, materials handling, fabrication, testing and inspection, storage, and transportation. The program also provides for the indoctrination and training of personnel and for the auditing of activities affecting product quality through a formal auditing program.

The drawings and product, process, and material specifications identify the requirements that must be inspected.

4.2.4.2 Quality Control

Quality control philosophy is generally based on critical features being performed to at least a 95 percent confidence that at least 95 percent of the product meets specification.

1. Fuel system components and parts - The characteristics inspected depend upon the component parts and include dimensional and visual checks, audits of test reports, material certifications and nondestructive examinations (such as X-ray and ultrasonic).

   All material used in the core is accepted and released by quality control.

2. Pellets - Inspection is performed for dimensional characteristics such as diameter, density, length, and squareness of ends. Additional visual inspections are performed for cracks, chips, and surface conditions according to approved standards.

   Density and chemical analyses are taken on a specified sample basis throughout pellet production.

3. Rod inspection - Fuel rod and control rod inspection consists of the following nondestructive examination techniques and methods, as applicable.

   a. Leak testing - Each rod is tested by using a calibrated mass spectrometer with helium being the detectable gas.

b. Enclosure welds - All weld enclosures are X-rayed using weld correction forms. AREVA fuel rod weld quality is ensured through 100% verification of critical weld parameters, in addition to burst test samples at specified frequencies.

c. Dimensional - All rods are dimensionally inspected prior to final release. Requirements of rod dimensions include such items as length, straightness, and visual appearance.

d. Plenum dimensions - The plenum lengths of all of the fuel rods are inspected.

e. Pellet-to-pellet gaps - All of the fuel rods are inspected by fluoroscope, gamma scanning or other methods as discussed in Section 4.2.4.4 to ensure that no significant gaps exist between pellets.

f. All of the fuel rods are gamma scanned to verify enrichment control prior to acceptance for assembly loading.

g. Traceability - Traceability of rods and associated rod components is established by quality control.

4. Assemblies - Each fuel and control rod is inspected for drawing and/or specification requirements. Other incore control component inspection and specification requirements are given in Section 4.2.4.3.

5. Other inspections - The following inspections are performed as part of the routine inspection operation:

   a. Gage inspection and control including standardization to primary and/or secondary working standards. Gage inspection is performed at prescribed intervals on all serialized gages. Complete records of calibration and conditions of gages are kept.

   b. Audits of inspection activities and records are performed to ensure that prescribed methods are followed and that records are correct and properly maintained.

   c. Surveillance inspection, where appropriate, and audits of outside contractors are performed to ensure conformance with specified requirements.

6. Process control - To prevent the possibility of mixing enrichments during fuel manufacture and assembly, strict enrichment segregation and other process controls are exercised.

   The UO_2 powder is kept in enclosed containers. The contents are fully identified by descriptive tagging. An identification tag completely describing the contents is affixed to the containers before transfer to powder storage. Isotopic content is confirmed by analysis.

   Finished pellets are placed on trays identified by lot and transferred to segregated storage racks within the confines of the pelleting area. Samples from each pellet lot are tested for isotopic content and impurity levels prior to acceptance by quality control. Physical barriers prevent mixing of pellets of different nominal densities and enrichments in the storage area.

A serialized traceability code is placed on each lower end plug for AREVA fuel built through reload SHA-6. The end plugs are inserted and then are welded to seal the tube. Starting with reload SHA-7 fuel, the serialized traceability code is placed on the fuel rod tube. The information on the lower end cap or tube provides traceability for the contract and rod composition.

Traceability of each rod and its component parts is maintained. This traceability is also maintained within a given assembly. The top nozzle is inscribed with a permanent identification number providing traceability to the fuel contained in the assembly.

Similar traceability is provided for control rodlets as required.

4.2.4.3 Incore Control Component Testing and Inspection

Tests and inspections are performed on each reactivity control component to verify the mechanical characteristics. In the case of the full length rod cluster control assembly, prototype testing has been conducted and both manufacturing test/inspections and functional testing at the plant site are performed.

During the component manufacturing phase, the following requirements apply to the reactivity control components to assure the proper functioning during reactor operation:

1. All materials are procured to specifications to attain the desired standard of quality.

2. A Westinghouse spider from each braze lot is proof tested by applying a 5000 pound load to the spider body, so that approximately 310 pounds is applied to each vane. This proof load provides a bending moment at the spider body approximately equivalent to 1.4 times the load caused by the acceleration imposed by the control rod drive mechanism.

3. All rods are checked for integrity by the methods described in Section 4.2.4.2.3, item c.

4. To ensure proper fitup with the fuel assembly, the rod cluster control assemblies are installed in the fuel assembly or equivalent gage fixture for AREVA RCCAs without restriction or binding in the dry condition. Also a straightness of 0.01 in./ft. is required on the entire inserted length of each rod assembly.

   The rod cluster control assemblies are functionally tested following core loading. Prior to the initial criticality, in order to demonstrate reliable operation of the assemblies, each assembly was operated (and tripped) one time at no flow/cold conditions, full flow/hot conditions, no flow/hot conditions, and full flow/cold conditions. Also, for each test, all rods falling outside the statistical 2σ limit were tripped at least an additional six times. Thus each assembly was tested four times minimum to ensure the assemblies were properly functioning.

   In order to demonstrate continuous free movement of the full length rod cluster control assemblies, and to ensure acceptable core power distributions during operations, partial movement checks are performed on every full length rod cluster control assembly, as required by the technical specifications. In addition, periodic drop tests of the full length rod cluster control assemblies are performed after each refueling shutdown to demonstrate continued ability to meet trip time requirements, as required by the technical specifications.

If a rod cluster control assembly cannot be moved by its mechanism, adjustments in the boron concentration ensure that adequate shutdown margin would be achieved following a trip. Thus inability to move one rod cluster control assembly can be tolerated. More than one inoperable rod cluster control assembly could be tolerated, but would impose additional demands on the plant operator. Therefore, the number of inoperable rod cluster control assemblies is limited to one.

4.2.4.4 Tests and Inspections by Others

If any tests and inspections are to be performed on core components or fuel subassemblies on behalf of AREVA or Westinghouse, AREVA or Westinghouse (as appropriate) will assure that the vendor quality control procedures and inspection plans are in accordance with the positions of the applicable approved QA plan.

4.2.4.5 Inservice Surveillance

Westinghouse is conducting a program to examine detailed aspects of the 17 x 17 fuel assembly. This program is described in Section 23 of Reference 4.2.1-9. Reference 4.2.1-1 is periodically updated in order to provide recent results of operating experience with Westinghouse fuel and incore control components.

AREVA continues to monitor the performance of its 17x17 and other PWR fuel designs with surveillance programs. Furthermore, development of improved designs is facilitated by in-reactor performance programs which include detailed characterized assemblies, slight material variations, and tighter controls on particular design attributes being monitored.

Refer to Section 9.3.6 for a discussion of the Failed Fuel Detection System.

4.2.4.6 Inspection of Discharged Fuel Assemblies

After each refueling, some recently discharged fuel assemblies will be subjected to a qualitative visual examination. Such an examination will be sufficient to identify gross problems of structural integrity, fuel rod failure, rod bowing or crud deposition. If unusual behavior is noticed in the visual examination or if, during power operations, plant instrumentation indicates gross fuel failures, then additional surveillance may be performed and analyzed to determine the causes.

REFERENCES: SECTION 4.2

4.2.1-1 Skaritka, J. and Iorii, J. A., "Operational Experience with Westinghouse Cores," (Up to December 31, 1977)," WCAP-8133, Revision 8, August 1978.

4.2.1-2 Beaumont, M. D., et al., "Properties of Fuel Core Component Materials," WCAP-9179, Revision 1 (Proprietary) and WCAP-9224 (Non-Proprietary), July 1978, and Appendix A, "Hafnium."

4.2.1-3 Deleted by Amendment No. 45.

4.2.1-4 Hellman, J. M. (Ed.), "Fuel Densification Experimental Results and Model for Reactor Operation," WCAP-8281 P A (Proprietary) and WCAP-8219 A (Non-Proprietary), March 1975.

4.2.1-5 Miller, J. V. (Ed.), "Improved Analytical Models Used in Westinghouse Fuel Rod Design Computations," WCAP-8720 (Proprietary) and WCAP-8785 (Non-Proprietary), October 1976.

4.2.1-6 George, R. A., Lee, Y. C. and Eng, G. H., "Revised Clad Flattening Model," WCAP-8377 (Proprietary) and WCAP-8381 (Non-Proprietary), July 1974.

4.2.1-7 Deleted by Amendment No. 45.

4.2.1-8 Cohen, J., "Development and Properties of Silver Base Alloys as Control Rod Materials for Pressurized Water Reactors," WAPD 214, December 1959.

4.2.1-9 Eggleston, F. T., "Safety-Related Research and Development for Westinghouse Pressurized Water Reactors, Program Summaries - Winter 1977 -Summer 1978," WCAP-8768, Revision 2, October 1978.

4.2.1-10 "Reference Core Report 17 x 17 Optimized Fuel Assembly" WCAP-9500.

4.2.1-11 Kersting, P. J., et al., "Extended Burnup Evaluation of Westinghouse Fuel," WCAP-10125 (Proprietary), July 1982 (acceptability documented in NRC letter to W dated 10 11 85).

4.2.1-12 Deleted by Amendment No. 45.

4.2.1-13 "Qualification of Exxon Nuclear Fuel for Extended Burnup," XN NF 82 06 (P)(A) Revision 1 & Supplements 2, 4, & 5, October 1986.

4.2.1-14 "Qualification of Advanced Nuclear Fuels' PWR Design Methodology for Rod Burnups of 62 GWd/MTU," ANF-88-133 (P)(A) & Supplement 1, December 1991.

4.2.1-15 "Generic Mechanical Design Report High Thermal Performance Spacer and Intermediate Flow Mixer," ANF-89-060 (P)(A) & Supplement 1, March 1991.

4.2.1-16 "RODEX 2 Fuel Rod Thermal-Mechanical Response Evaluation Model", XN NF-81-58 (P)(A) Revision 2 & Supplement 1 & 2, March 1984.

4.2R-1 Amendment No. 51

4.2.1-17 "Generic Mechanical Licensing Report for Advanced 17 x 17 Fuel Design," EMF-93-074 (A) & Supplement 1, June 1994.

4.2.1-18 "Shearon Harris Unit 1 RCCA Final Design Report" AREVA NP, Inc., Document No: 51-9098915-003

4.2.2-1 Davidson, S. L. and Kramer, W. R (Ed.), "Reference Core Report VANTAGE 5 Fuel Assembly," WCAP-10444-P-A, September 1985.

4.2.3-1 Demario, E. E., "Hydraulic Flow Test of the 17 x 17 Fuel Assembly," WCAP-8278 (Proprietary) and WCAP-8279 (Non-Proprietary), February 1974.

4.2.3-2 Deleted by Amendment No. 45.

4.2.3-3 O'Donnel, W. J. and Langer, B. F., "Fatigue Design Basis for Zircaloy Components," Nuclear Science and Engineering, 20, 1-12, 1964.

4.2.3-4 Gesinski, L. and Chiang, D., "Safety Analysis of the 17 x 17 Fuel Assembly for Combined Seismic and Loss-of-Coolant Accident," WCAP-8236 (Proprietary) and WCAP-8288 (Non-Proprietary), December 1973.

4.2.3-5 "Generic Mechanical Design Criteria for PWR Fuel Design", EMF 92 116 (P)(A), and Supplement 1 (P)(A), February 1999 and May 2015.

4.2.4-1 Deleted by Amendment No. 60

4.2.4-2 FMM, Rev. 5, AREVA Front End Business Group, Fuel Business Unit Management Manual, July 2014.

4.2.3-6 "Incorporation of M5™ Properties in Framatome ANP Approved Methods," BAW-10240(P)(A), Revision 0, May 2004.

4.3 NUCLEAR DESIGN

4.3.1 DESIGN BASES

This section describes the design bases and functional requirements used in the nuclear design of the fuel and reactivity control system and relates these design bases to the General Design Criteria (GDC) presented in 10 CFR 50, Appendix A. Where appropriate, supplemental criteria such as the "Final Acceptance Criteria for Emergency Core Cooling Systems" are addressed. Before discussing the nuclear design bases, it is appropriate to briefly review the four major categories ascribed to conditions of plant operation.

The full spectrum of plant conditions is divided into four categories, in accordance with the anticipated frequency of occurrence and risk to the public:

1) ANS Condition I - Normal Operation

2) ANS Condition II - Incidents of Moderate Frequency

3) ANS Condition III - Infrequent Faults

4) ANS Condition IV - Limiting Faults

In general, the ANS Condition I occurrences are accommodated with the margin between any plant parameter and the value of that parameter which would require either automatic or manual protective action. ANS Condition II incidents are accommodated with, at most, a shutdown of the reactor with the plant capable of returning to operation after corrective action. Fuel damage (fuel damage as used here is defined as penetration of the fission product barrier, i.e., the fuel

rod clad) is not expected during ANS Condition I and ANS Condition II events. It is not possible, however, to preclude a very small number of rod failures resulting in the release of small quantities of fission products. The CVCS is designed to remove the fission products from the reactor coolant, keeping the reactor coolant activity within the plant design bases limits.

ANS Condition III incidents will not cause more than a small fraction of the fuel elements in the reactor to be damaged, although sufficient fuel element damage might occur to preclude immediate resumption of operation. The release of radioactive material due to ANS Condition III incidents should not be sufficient to interrupt or restrict public use of these areas beyond the exclusion area. Furthermore, an ANS Condition III incident will not, by itself, generate an ANS Condition IV fault or result in a consequential loss of function of the reactor coolant or reactor containment barriers.

ANS Condition IV occurrences are faults that are not expected to occur but are defined as limiting faults which must be designed against. ANS Condition IV faults will not cause a release of radioactive material that results in an undue risk to public health and safety.

The core design power distribution limits related to fuel integrity are met for ANS Condition I occurrences through conservative design and maintained by the action of the control system. The requirements for ANS Condition II occurrences are met by providing an adequate protection system which monitors reactor parameters. The control and protection systems are described in Chapter 7 and the consequences of ANS Condition II, III, and IV occurrences are given in Chapter 15.

4.3.1.1 Fuel Burnup

1. Basis - The fuel rod design basis is described in Section 4.2. The nuclear design basis is to install sufficient reactivity to support the discharge burnup limits associated with each of the fuel designs used. These limits are:

   - For AREVA High Thermal Performance (HTP) fuel and GAIA lead assemblies: peak rod average burnup limit is 62,000 MWD/MTU. (Reference 4.3.1-5)

   - For Westinghouse fuel: peak rod average burnup limit is 60,000 MWD/MTU (Reference 4.3.1-6)

   The above, along with the design basis in Section 4.3.1.3, satisfies GDC-10.

2. Discussion - Fuel burnup is a measure of fuel depletion which represents the integrated energy output of the fuel (MWD/MTU) and is a convenient means for quantifying fuel exposure criteria.

   The core design lifetime or design discharge burnup is achieved by installing sufficient initial excess reactivity in each fuel region and by following a fuel replacement program (such as that described in Section 4.3.2) that meets all safety-related criteria in each cycle of operation.

   Initial excess reactivity installed in the fuel, although not a design basis, must be sufficient to maintain core criticality at full power operating conditions throughout cycle life with equilibrium xenon, samarium, and other fission products present. The end of design cycle

life is defined to occur when the chemical shim concentration is essentially zero with no control rod insertion.

A limitation on initial installed excess reactivity is not required other than as is quantified in terms of other design bases, such as core negative reactivity feedback and shutdown margin discussed below.

4.3.1.2 Negative Reactivity Feedbacks (Reactivity Coefficient)

1. Basis - The fuel temperature coefficient will be negative and the moderator temperature coefficient of reactivity will be nonpositive for full power operating conditions, thereby providing negative reactivity feedback characteristics. The design basis meets GDC-11.

2. Discussion - When compensation for a rapid increase in reactivity is considered, there are two major effects. These are the resonance absorption effects (Doppler) associated with changing fuel temperature and the spectrum effect resulting from changing moderator density. These basic physics characteristics are often identified by reactivity coefficients. The use of slightly enriched uranium ensures that the Doppler coefficient of reactivity is negative. This coefficient provides the most rapid reactivity compensation. The core is also designed to have an overall negative moderator temperature coefficient of reactivity at full power operating conditions so that average reactor coolant temperature or void content provides another, slower compensatory effect. Nominal full power operation is permitted only in a range of overall negative moderator temperature coefficient. The negative moderator temperature coefficient at full power operating conditions can be achieved through use of gadolinia bearing fuel rods or control rods by limiting the reactivity held down by soluble boron.

4.3.1.3 Control of Power Distribution

1. Basis - The nuclear design basis is that, with at least a 95 percent confidence level:

   a. The fuel will not be operated at greater than 14.0 Kw/ft under normal operating conditions. At a rated thermal power of 2948 MW this Kw/ft limit corresponds to the core average LHGR of 5.77 Kw/ft augmented by the F_Q limit. This value is then increased by the 0.034% calorimetric uncertainty.

      For the AREVA mechanical design evaluation a rated thermal power of 2948 was analyzed. For this case, the Kw/ft limit corresponds to a core average LHGR of 5.77 Kw/ft.

   b. Under abnormal conditions including the maximum overpower condition, the fuel peak power will not cause melting as defined in Section 4.4.1.2.

   c. The fuel will not operate with a power distribution that violates the departure from nucleate boiling (DNB) design basis (i.e., that DNBR will not be less than the safety analysis limit, as discussed in Section 4.4.1) under ANS Condition I and II events, including the maximum overpower condition.

   d. Fuel management will be such as to produce rod powers and burnups consistent with the assumptions in the fuel rod mechanical integrity analysis of Section 4.2.

The above basis meets GDC-10.

2. Discussion - Calculation of extreme power shapes which affect fuel design limits is performed with proven methods and verified frequently with measurements from operating reactors. The conditions under which limiting power shapes are assumed to occur are chosen conservatively with regard to any permissible operating state.

   Even though there is good agreement between calculated peak power and measurements, a nuclear uncertainty (see Section 4.3.2.2) is applied to calculated peak local power. Such a margin is provided both for the analysis for normal operating states and for anticipated transients.

4.3.1.4 Maximum Controlled Reactivity Insertion Rate

1. Basis - The maximum reactivity insertion rate due to withdrawal of rod cluster control assemblies at power or by boron dilution is limited. During normal at power operation, the maximum controlled reactivity rate change is less than 35 pcm/sec. (1pcm = $10^{-5}\Delta\rho$). A maximum reactivity change rate of 100 pcm/sec.(Section 15.4.2.2) for accidental withdrawal of control banks is set such that peak heat generation rate and DNBR do not exceed the maximum allowable at overpower conditions. This satisfies GDC-25.

   The maximum reactivity worth of control rods and the maximum rates of reactivity insertion employing control rods are limited so as to preclude rupture of the reactor coolant pressure boundary or disruption of the core internals to a degree which would impair core cooling capacity due to a rod withdrawal or ejection accident (see Chapter 15).

   Following any ANS Condition IV event, the reactor can be brought to the shutdown condition and the core will maintain acceptable heat transfer geometry. This satisfies GDC-28.

2. Discussion - Reactivity addition associated with an accidental withdrawal of a control bank (or banks) is limited by the maximum rod speed (or travel rate) and by the worth of the bank(s). The maximum control rod speed is 45 inches per minute, (or 72 steps/minute) and the maximum rate of reactivity change considering two control banks moving is less than 100 pcm/sec. During normal operation at power and with control rod overlap, the maximum reactivity change rate is less than 35 pcm/sec.

   The reactivity change rates are conservatively calculated assuming unfavorable axial power and xenon distributions. The peak xenon burnout rate is 15 pcm/min., which is lower than the maximum reactivity addition rate of 35 pcm/sec. for normal operation and 100 pcm/sec. for accidental withdrawal of two banks.

4.3.1.5 Shutdown Margins

1. Basis - Minimum shutdown margin as specified in the Technical Specifications is required in all modes of operation.

   In all analyses involving reactor trip, the single, highest worth rod cluster control assembly is postulated to remain untripped in its full-out position (stuck rod criterion). This satisfies GDC-26.

2. Discussion - Two independent reactivity control systems are provided, namely control rods and soluble boron in the reactor coolant. The Control Rod System can compensate for the reactivity effects of the fuel and water temperature changes accompanying power level changes over the range from full-load to no-load. In addition, the Control Rod System provides the minimum shutdown margin under ANS Condition I events and is capable of making the core subcritical rapidly enough to prevent exceeding acceptable fuel damage limits assuming that the highest worth control rod is stuck out upon trip.

   The boron (Chemical Shim Control System) can compensate for all xenon burnout reactivity changes and will maintain the reactor in the cold shutdown. Thus, backup and emergency shutdown provisions are provided by a mechanical and a Chemical Shim Control System which satisfies GDC-26.

3. Basis - When fuel assemblies are in the pressure vessel and the vessel head is not in place, k_{eff} will be maintained at or below 0.95 with control rods and soluble boron. Further, the fuel will be maintained sufficiently subcritical that removal of all rod cluster control assemblies will not result in criticality.

4. Discussion - ANSI Standard N18.2 specifies a k_{eff} not to exceed 0.95 in spent fuel storage racks and transfer equipment flooded with pure water and a k_{eff} not to exceed 0.98 in normally dry new fuel storage racks assuming optimum moderation. No criterion is given for the refueling operation, however a 5 percent margin, which is consistent with spent fuel storage and transfer and the new fuel storage, is adequate for the controlled and continuously monitored operations involved.

   The boron concentration required to meet the refueling shutdown criteria is specified in the Technical Specifications. Verification that this shutdown criteria is met, including uncertainties, is achieved using standard AREVA design methods. The subcriticality of the core is continuously monitored as described in the Technical Specifications.

4.3.1.6 Stability

1. Basis - The core will be inherently stable to power oscillations at the fundamental mode. This satisfies GDC-12.

   Spatial power oscillations within the core with a constant core power output, should they occur, can be reliably and readily detected and suppressed.

2. Discussion - Oscillations of the total power output of the core, from whatever cause, are readily detected by the reactor coolant loop temperature sensors and by the nuclear instrumentation. The core is protected by these systems, a reactor trip would occur if power increased unacceptably, preserving the design margins to fuel design limits. The stability of the Turbine/Steam, Generator/Core Systems and the Reactor Control System is such that total core power oscillations are not normally possible. The redundancy of the protection circuits ensures an extremely low probability of exceeding design power levels.

   The core is designed so that diametral and azimuthal oscillations due to spatial xenon effects are self-damping and no operator action or control action is required to suppress them. The stability to diametral oscillations is so great that this excitation is highly improbable. Convergent azimuthal oscillations can be excited by prohibited motion of

individual control rods. Such oscillations are readily observable and alarmed, using the excore long ion chambers. Indications are also continuously available from incore thermocouples and loop temperature measurements. Movable incore detectors can be activated to provide more detailed information. In all proposed cores, the horizontal plane oscillations are self-damping by virtue of reactivity feedback effects designed into the core.

However, axial xenon spatial power oscillations may occur late in core life. The control bank and excore detectors are provided for control and monitoring of axial power distributions. Assurance that fuel design limits are not exceeded is provided by the reactor overtemperature ΔT trip function which uses the measured axial power imbalance as an input.

4.3.1.7 Anticipated Transients Without Trip

The effects of anticipated transients with failure to trip are not considered in the design bases of the plant. Analysis has shown that the likelihood of such a hypothetical event is negligibly small. Furthermore, analysis of the consequences of a hypothetical failure to trip following anticipated transients has shown that no significant core damage would result, system peak pressures would be limited to acceptable values and no failure of the Reactor Coolant System would result (Reference 4.3.1-4).

4.3.2 DESCRIPTION

4.3.2.1 Nuclear Design Description

The reactor core consists of a specified number of fuel rods which are held in bundles by spacer grids and top and bottom fittings. The fuel rods are constructed of zircaloy or M5 cylindrical tubes containing UO_2 or UO_2-Gd_2O_3 fuel pellets. The bundles, known as fuel assemblies, are arranged in a pattern which approximates a right circular cylinder.

Each fuel assembly contains a 17 x 17 rod array composed of 264 fuel rods, 24 rod cluster control thimbles and an incore instrumentation thimble. Figure 4.2.2 1 shows a cross sectional view of a 17 x 17 fuel assembly and the related rod cluster control locations. Further details of the fuel assembly are given in Section 4.2.

Starting with the first reload (Cycle 2), fresh fuel has axial zoning of uranium enrichment; however, the enrichment in the radial direction of an assembly was maintained at a consistent enrichment. Generally, axial zoning consists of making the top and bottom six (6) inches of the fuel slightly enriched (0.74 w/o U-235). Blankets, as the slightly enriched uranium regions are referred to, reduce the axial neutron leakage, thereby contributing to better fuel utilization.

Starting with the first reload of AREVA fuel in Cycle 6, the blanket region for a fuel pin was altered so that the top and bottom three (3) inches contained natural uranium. Starting with Batch 21 (Cycle 19), the blanket region of UO_2 fuel pin is six (6) inches and contains mid-enriched uranium. The blanket region of UO_2-Gd_2O_3 fuel pin is 10.5 inches. The enrichment in the radial direction was no longer held constant as the enrichment of U-235 in the gadolinia bearing fuel was reduced relative to that of the non-gadolinia fuel to account for the reduced thermal conductivity and melting point due to the gadolinia. Figure 4.3.2-1a shows the typical axial zoning of the fuel and the axial placement of the absorber for the AREVA pin designs.

The loading of fresh fuel in the interior of the core decreases the radial neutron leakage by reducing the power produced on the core periphery. This type of reload pattern increases the fuel utilization and is referred to as a low leakage loading pattern.

Each cycle will typically operate for approximately 500 EFPD, equal to about 17 months of operation at 98% capacity factor. The exact reloading pattern, initial and final positions of assemblies and the number of fresh assemblies are dependent on the energy requirement for the cycle and power histories of the previous cycles.

The core average enrichment is determined by the amount of fissionable material required to provide the desired core lifetime and energy requirements. The physics of the burnout process is such that operation of the reactor depletes the amount of fuel available due to the absorption of neutrons by the U 235 atoms and their subsequent fission. The rate of U 235 depletion is directly proportional to the power level at which the reactor is operated. In addition, the fission process results in the formation of fission products, some of which readily absorb neutrons. These effects, depletion and the buildup of fission products, are partially offset by the buildup of plutonium shown in Figure 4.3.2-2 for a typical 17 x 17 fuel assembly, which occurs due to the non-fission absorption of neutrons in U-238. Therefore, at the beginning of any cycle, a reactivity reserve equal to the depletion of the fissionable fuel and the buildup of fission product poisons over the specified cycle life must be "built" into the reactor. This excess reactivity is controlled by removable neutron absorbing material in the form of boron dissolved in the reactor coolant and gadolinia bearing fuel.

The concentration of boric acid in the reactor coolant is varied to provide control and to compensate for long term reactivity requirements. The concentration of the soluble neutron absorber is varied to compensate for reactivity changes due to fuel burnup, fission product poisoning including xenon and samarium, burnable poison depletion, and the cold-to-operating moderator temperature change. Based on a conservatively low Boric Acid Transfer Pump flow of only 30 gpm and a conservatively low estimate for differential boron worth (pcm/ppm), the Chemical and Volume Control System (CVCS) is capable of inserting negative reactivity at a rate of approximately 19 pcm/minute when the reactor coolant boron concentration is 1500 ppm and approximately 31.5 pcm/minute when the reactor coolant boron concentration is zero ppm. A conservatively high estimate for the peak burnout rate for xenon is +15 pcm/minute. (Section 9.3.4 discusses the capability of the CVCS to counteract xenon decay). Rapid transient reactivity requirements and safety shutdown requirements are met with control rods.

As the boron concentration is increased, the moderator temperature coefficient (MTC) becomes less negative. The use of a soluble poison alone could result in the MTC exceeding the technical specifications limit. Therefore, gadolinia bearing fuel is used to reduce the soluble boron concentration sufficiently to ensure that the MTC is negative for full power operating conditions, and within safety limits for part power operating conditions. During operation, the gadolinia content of the fuel is depleted thus adding positive reactivity to offset some of the negative reactivity from fuel depletion and fission product buildup.

In addition to reactivity control, the gadolinia bearing fuel rods are strategically located to provide a favorable radial power distribution. Figure 4.3.2-4a shows the gadolinia distributions within a fuel assembly for typical symmetric and non-symmetric gadolinia configurations used in a 17 x 17 array.

Tables 4.3.2-1 through 4.3.2-3 contain a summary of the reactor core design parameters for a typical cycle, including reactivity coefficients, delayed neutron fraction, and neutron lifetimes. Sufficient information is included to permit an independent calculation of the nuclear performance characteristics of the core.

4.3.2.2 Power Distributions

The accuracy of power distribution calculations has been confirmed through comparisons of measured and predicted flux maps for various core designs and operating strategies.

4.3.2.2.1 Definitions

Power distributions are quantified in terms of hot channel factors. These factors, which are a measure of the peak pellet power within the reactor core and the total energy produced in a reactor coolant channel, are expressed in the following terms of quantities related to the nuclear or thermal design:

Power density is the thermal power produced per unit volume of the core (kW/liter).

Linear Power density is the thermal power produced per unit length of active fuel (kW/ft). Since fuel assembly geometry is standardized, this is the unit of power density most commonly used. For all practical purposes it differs from kW/liter by a constant factor which includes geometry and the fraction of the total thermal power which is generated in the fuel rod.

Average linear power density is the total thermal power produced in the fuel rods divided by the total active fuel length of all rods in the core.

Local heat flux is the heat flux at the surface of the cladding (Btu ft.2 hr) For nominal rod parameters this differs from linear power density by a constant factor.

Rod power or rod integral power is the length integrated linear power density in one rod (kW).

Average rod power is the total thermal power produced in the fuel rods divided by the number of fuel rods (assuming all rods have equal length).

The hot channel factors used in the discussion of power distributions in this section are defined as follows:

F_Q, heat flux hot channel factor, is defined as the maximum local heat flux on the surface of a fuel rod divided by the average fuel rod heat flux, allowing for manufacturing tolerances on fuel pellets and rods.

F_Q^N, nuclear heat flux hot channel factor, is defined as the maximum local fuel rod linear power density divided by the average fuel rod linear power density, assuming nominal fuel pellet and rod parameters.

F_Q^E, engineering heat flux hot channel factor, is the allowance on heat flux required for manufacturing tolerances. The engineering factor allows for local variations in enrichment, as-sintered pellet density and diameter, and in-reactor densification.

Combined statistically the net effect is bounded by a factor of 1.03 to be applied to fuel rod surface heat flux.

F_U^N, factor for measurement uncertainties, assumed to be 1.05.

$F_{\Delta H}^N$, nuclear enthalpy rise hot channel factor, is defined as the ratio of the integral of linear power along the rod with the highest integrated power to the average rod power.

Manufacturing tolerances, hot channel power distribution and surrounding channel power distributions are treated explicitly in the calculation of the DNBR described in Section 4.4.

4.3.2.2.2 Radial power distributions

The power shape in horizontal sections of the core at full power is a function of the fuel and burnable poison loading patterns and the presence or absence of a single bank of full length control rods. Thus, at any time in the cycle a horizontal section of the core can be characterized as unrodded or with group D control rods. These two situations combined with burnup effects determine the radial power shapes which can exist in the core at full power. The effect on radial power shapes of power level, xenon, samarium and moderator density effects are also considered but these are quite small. The effect of non-uniform flow distribution is negligible. While radial power distributions in various planes of the core are often illustrated, the core radial enthalpy rise distribution as determined by the integral of power up each channel is of greater interest. Figure 4.3.2-6 through 4.3.2-11 show typical radial power distributions for one-quarter of the core for representative operating conditions. These conditions are: 1) hot full power (HFP) at beginning-of-life (BOL) - unrodded - no xenon, 2) HFP at BOL - unrodded - equilibrium xenon, 3) HFP near BOL -bank D in -equilibrium xenon, 4) HFP near middle-of-life (MOL) -unrodded -equilibrium xenon, 5) HFP near end-of-life (EOL) -unrodded -equilibrium xenon, and 6) HFP at EOL - bank D in -equilibrium xenon.

Since the position of the hot channel varies from time to time a single reference radial design power distribution is selected for DNB calculations. This reference power distribution is chosen conservatively to concentrate power in one area of the core, minimizing the benefits of flow redistribution. Assembly powers are normalized to core average power. The radial power distribution within a fuel rod and its variation with burnup as utilized in thermal calculations and fuel rod design is discussed in Section 4.4.

4.3.2.2.3 Assembly power distributions

For the purpose of illustration, typical assembly power distributions from the BOL and EOL conditions corresponding to Figures 4.3.2-7 and 4.3.2-10, respectively, are given for the same assembly in Figures 4.3.2-12 and 4.3.2-13 respectively.

Since the detailed power distribution surrounding the hot channel varies from time to time, a conservatively flat assembly power distribution is assumed in the DNB analysis, described in Section 4.4, with the rod of maximum integrated power artificially raised to the design value of $F_{\Delta H}^N$. Care is taken in the nuclear design of all fuel cycles and all operating conditions to ensure that a flatter assembly power distribution does not occur with limiting values of $F_{\Delta H}^N$.

4.3.2.2.4 Axial power distributions

The shape of the power profile in the axial or vertical direction is largely under the control of the operator through either the manual operation of the full length control rods or automatic motion of full length rods responding to manual operation of the CVCS. Nuclear effects which cause variations in the axial power shape include moderator density, Doppler Effect on resonance absorption, spatial xenon, and burnup. Automatically controlled variations in total power output and full length rod motion are also important in determining the axial power shape at any time. Signals are available to the operator from the excore ion chambers which are long ion chambers outside the reactor vessel running parallel to the axis of the core. Separate signals are taken from the top and bottom halves of the chambers. The difference between top and bottom signals from each of four pairs of detectors is displayed on the main control board and called the flux difference, ΔI. Calculations of core average peaking factor for many plants and measurements from operating plants under many operating situations are associated with either ΔI or axial offset in such a way that an upper bound can be placed on the peaking factor. For these correlations, axial offset is defined as:

$$\text{axial offset} = \frac{\varphi t - \varphi b}{\varphi t + \varphi b}$$

and φt and φb are the top and bottom detector readings.

Representative axial power shapes for BOL, MOL, and EOL conditions are shown in Figures 4.3.2-14 through 4.3.2-16. These figures cover a wide range of axial offset, including values not permitted at full power.

The radial power distributions shown in Figures 4.3.2-8 and 4.3.2-11 involving the partial insertion of control rods represent a synthesis of power shapes from the rodded and unrodded planes. The applicability of the separability assumption upon which this procedure is based is assured through extensive three-dimensional calculations of possible rodded conditions. As an example, Figure 4.3.2-17 compares the axial power distribution for several assemblies at different distances from inserted control rods with the core average distribution. The only significant difference from the average occurs in the low power peripheral assemblies, thus confirming the validity of the separability assumption.

4.3.2.2.5 Local power peaking

Fuel densification, which has been observed to occur under irradiation in several operating reactors, causes the fuel pellets to shrink both axially and radially. The pellet shrinkage combined with random hang-up of fuel pellets results in gaps in the fuel column when the pellets below the hung-up pellet settle in the fuel rod. The gaps vary in length and location in the fuel rod. Because of decreased neutron absorption in the vicinity of the gap, power peaking occurs in the adjacent fuel rods resulting in an increased power peaking factor. Densification effects are included in the 3% manufacturing uncertainty used in the transient analyses (see Section 4.4.2.2.4).

4.3.2.2.6 Limiting power distributions

According to the ANSI classification of plant conditions (see Chapter 15), ANS Condition I occurrences are those which are expected frequently or regularly in the course of power

operation, maintenance, or maneuvering of the plant. As such, ANS Condition I occurrences are accommodated with margin between any plant parameter and the value of that parameter which would require either automatic or manual protective action. As ANS Condition I occurrences occur frequently or regularly, they must be considered from the point of view of affecting the consequences of fault conditions (ANS Conditions II, III and IV). In this regard, analysis of each fault condition described is generally based on a conservative set of initial conditions corresponding to the most adverse set of conditions which can occur during ANS Condition I operation.

The list of steady state and shutdown conditions, permissible deviations, and operational transients is given in Chapter 15. Implicit in the definition of normal operation is proper and timely action by the reactor operator. That is, the operator follows recommended operating procedures for maintaining appropriate power distributions and takes any necessary remedial actions when alerted to do so by the plant instrumentation. Thus, as stated above, the worst or limiting power distribution which can occur during normal operation is to be considered as the starting point for analysis of ANS Conditions II, III, and IV events.

Improper procedural actions or errors by the operator are assumed in the design as occurrences of moderate frequency (ANS Condition II). Some of the consequences which might result are discussed in Chapter 15. Therefore, the limiting power shapes which result from such ANS Condition II events are those power shapes which deviate from the normal operating condition at the recommended axial offset band, e.g., due to lack of proper action by the operator during a xenon transient following a change in power level brought about by control rod motion. Power shapes which fall in this category are used for determination of the reactor protection system setpoints so as to maintain margin to overpower or DNB limits.

The means for maintaining power distributions within the required hot channel factor limits are described in the Technical Specifications. A complete discussion of power distribution control in Westinghouse pressurized water reactors used by AREVA is included in Reference 4.3.2-5. Detailed background information on the following design constraints on local power density in a Westinghouse pressurized water reactor, and the measures taken to preclude exceeding design limits is presented in the AREVA topical report "Power Distribution Control" in Westinghouse Reactors (Reference 4.3.2-5). The following paragraphs summarize these reports and describe the calculations used to establish the upper bound on peaking factors.

The calculations used to establish the upper bound on peaking factors, F_Q and $F\Delta H$, include all of the nuclear effects which influence the radial and/or axial power distributions throughout core life for various modes of operation, including load follow, reduced power operation, and axial xenon transients.

Radial power distributions are calculated for the full power condition and fuel and moderator temperature feedback effects are included for the average enthalpy plane of the reactor. The steady state nuclear design calculations are done for normal flow with the same mass flow in each channel and flow redistribution explicitly where it is important in the DNB analysis of accidents. The effect of xenon on radial power distribution is small (compare Figures 4.3.2-6 and 4.3.2-7) but is included as part of the normal design process. Radial power distributions are relatively fixed and easily bounded with upper limits.

The core average axial profile, however, can experience significant change which can occur rapidly as a result of rod motion and load changes and more slowly due to xenon distribution

and core burnup. For the study of points of closest approach to axial power distribution limits, several thousand cases are examined. Since the properties of the nuclear design dictate what axial shapes can occur, boundaries on the limits of interest can be set in terms of the parameters which are readily observed on the plant. Specifically, the nuclear design parameters which are significant to the axial power distribution analysis are:

1. Core power level
2. Core height
3. Reactor coolant temperature and flow
4. Reactor coolant temperature program as a function of reactor power
5. Fuel cycle lifetimes
6. Rod bank worths
7. Rod bank overlaps
8. Size and number of axial blankets

Normal operation of the plant assumes compliance with the following conditions:

1. Control rods in a single bank move together with no individual rod insertion differing by more than 12 steps (indicated) from the bank demand position.
2. Control banks are sequenced with overlapping banks.
3. The control full length bank insertion limits are not violated.
4. Axial power distribution procedures, which are given in terms of flux difference control and control bank position, are observed.

The axial power distribution procedures referred to above are part of the required operating procedures which are followed in normal operation. Limits placed on the axial flux difference are designed to assure that the total peaking factor F_Q^T is maintained within acceptable limits which satisfy LOCA and local power requirements. The Power Distribution Control (PDC) methodology described in Reference 4.3.2-5, requires control of the axial flux difference (AFD) between 50% and 100% full power within a permissible operating band about a target value corresponding to the full power value assuming equilibrium xenon and all rods out or the controlling bank inserted to a bite position.

Maximum operating flexibility is achieved by allowing for a 1% reduction in the AFD band widths about the target for each 1% the FQ might exceed the Technical Specification limit.

Calculations are performed for normal operation of the reactor including load following maneuvers. Beginning, middle, and end of cycle conditions are included in the calculations. Different histories of operation are assumed prior to calculating the effect of load follow transients on the axial power distribution. These different histories assume operation is

maintained within the specified PDC AFD band. For a characteristic fuel cycle six load follow maneuvers are studied to determine the general behavior of the local power density as a function of core elevation.

For the widest possible delta flux operating space to be defined, the power shapes over a wide range of delta flux values accounting for the RIL are analyzed. The widest delta operating space is the one in which the measured $F_Q(z)$ with the associated PDC V(z) applied does not violate the Technical Specification limits on F_Q.

The PDC power shapes generated are evaluated to determine if LOCA constraints are met or exceeded. The total peaking factor, F_Q^T is explicitly calculated using three-dimensional core calculations.

Finally, as previously discussed, the PDC AFD bands are based on methods which allow for operation within an allowed deviation from a target equilibrium value. The methods are detailed in the Technical Specifications and are followed by relying on the excore surveillance supplemented by the normal monthly full core map requirement and by computer-based alarms on deviation. The following numerical example shows how this surveillance ensures that Technical Specifications are met. Cycle specific Technical Specifications and Core Operating Limits Report (COLR) values may vary from this typical example.

Allowing for fuel densification effects the average linear power at 2948 Mwt is 5.77 kW/ft. From Figure 4.3.2-21, a typical conservative upper bound value of normalized local power density is 2.41 corresponding to a peak linear power of 14.0 kW/ft. at 100.34 percent power.

Accident analyses for SHNPP are presented in Chapter 15 of the FSAR. The results of these analyses will determine a limiting value of total peaking factor, F_Q, typically a value like 2.41 under normal operation, including load following maneuvers. This typical value would be derived from the conditions necessary to satisfy the limiting conditions specified in the LOCA analyses of FSAR Section 15.6.5. As noted above, this typical upper bound envelope of F_Q x Power equal to 2.41 x K(Z), as shown in FSAR Figure 4.3.2-21, results from operation in accordance with PDC-3 procedures.

Reactor protection system setpoints are determined assuming the core is operating within the four constraints described above.

To assure that the limiting operating conditions have been covered, axial power shapes are generated at a series of different power levels and rod configurations combined with unrealistically severe axial xenon shapes. These adverse xenon shapes are then applied to rodded and unrodded core configurations at different power levels. This produces axial power shapes which are more limiting than those which are reasonably achievable.

Analyses of possible operating power shapes show that the appropriate hot channel factors F_Q and $F\Delta H$ for peak local power density and for DNB analysis at full power are the values given in Table 4.3.2-2 and addressed in the Technical Specifications.

F_Q can be increased with decreasing power as shown in the Technical Specifications. Increasing $F\Delta H$ with decreasing power is permitted by the DNB protection setpoints and allows radial power shape changes with rod insertion to the insertion limits as described in Section 4.4.4.3. The allowance for increased $F\Delta H$ is located in the Technical Specifications. This

becomes a design basis criterion which is used for establishing acceptable control rod patterns and control bank sequencing. Likewise fuel loading patterns for each cycle are selected with consideration of this design criterion. The worst values of FΔH for possible rod configurations occurring in normal operation are used in verifying that this criterion is met. Typical radial factors and radial power distributions are shown in Figures 4.3.2-6 through 4.3.2-11. The worst values generally occur when the rods are assumed to be at their insertion limits. Maintenance of PDC-3 axial offset control bands allowing rod motion to the insertion limits provides margin to the FΔH criterion. These limits are taken as input to the thermal-hydraulic design basis as described in Section 4.4.4.3.1.

When a situation is possible in normal operation which could result in local power densities in excess of those assumed as the pre-condition for a subsequent hypothetical accident, but which would not itself cause fuel failure, administrative controls and alarms are provided for returning the core to a safe condition. These alarms are described in detail in Chapters 7 and 16.

The independence of the various individual uncertainties constituting the uncertainty factor on F_Q enables the uncertainty (F^U_Q) to be calculated by statistically combining the individual uncertainties on the limiting rod. The standard deviation of the resultant distribution of F^U_Q is determined by taking the square root of the sum of the variances of each of the contributing distributions. The values for F^E_Q and F^N_U are 1.03 and 1.05, respectively.

4.3.2.2.7 Experimental verification of power distribution analysis

This subject is discussed in depth in Reference 4.3.2-1. A summary of this report is given below. It should be noted that power distribution related measurements are incorporated into the evaluation of calculated power distribution information using an incore instrumentation processing code described in Reference 4.3.2 8. The measured versus calculational comparison is normally performed periodically throughout the cycle lifetime of the reactor as required by Technical Specifications.

In a measurement of the heat flux hot channel factor, F_Q, with the movable detector system described in Sections 7.7.1 and 4.4.6, the following uncertainties have to be considered:

1. Reproducibility of the measured signal.

2. Errors in the calculated relationship between detector current and local flux.

3. Errors in the calculated relationship between detector flux and peak rod power some distance from the measurement thimble.

The appropriate allowance for Category 1. above has been quantified by repetitive measurements made with several intercalibrated detectors by using the common thimble features of the incore detector system. This system allows more than one detector to access any thimble. Errors in Category 2. above are quantified to the extent possible, by using the fluxes measured at one thimble location to predict fluxes at another location which is also measured. Local power distribution predictions are verified in critical experiments on arrays of rods with simulated guide thimbles, control rods, burnable poisons. These critical experiments provide quantification of errors of Categories 1 and 3 above.

Reference 4.3.2-1 describes critical experiments used that were performed by Babcock & Wilcox and Battelle Pacific Northwest Laboratories and measurements taken on three Westinghouse plants with incore systems of the same type as used in the SHNPP. Reference 4.3.2-2 concludes that the uncertainty associated with F_Q (heat flux) and FΔH is 5% and 4% respectively.

The accumulated data on power distributions in actual operation is basically of three types:

1. Much of the data is obtained in steady state operation at constant power in the normal operating configuration.

2. Deleted by Amendment No. 49.

3. Data collected during power maneuvers and other transient xenon conditions yields useful information on power distributions.

   These data are presented in detail in References 4.3.2-8 and 4.3.2-9.

4.3.2.2.8 Testing

An extensive series of physics tests are performed during the initial plant startup prior to power ascension. The tests and the criteria for satisfactory results are described in Chapter 14. Low power physics testing during subsequent plant cycle initial startups and power ascensions will be guided by the following documents:

ANSI/ANS - 19.6.1, Reload Startup Physics Tests for Pressurized Water Reactors

Applicable fuel vendor approved documents with licensee concurrence.

Since not all limiting situations can be created at BOL, the main purpose of both test programs (initial and restart) is to provide a check on the calculational methods used in the predictions for the conditions of the test and to verify Technical Specifications limits for MTC.

4.3.2.2.9 Monitoring instrumentation

The adequacy of instrument numbers, spatial deployment, required correlations between readings and peaking factors, calibration and errors are described in References 4.3.2-1, 4.3.2-5, and 4.3.2-7. The relevant conclusions are summarized in Sections 4.3.2.2.7 and 4.4.6.

Provided the limitations given in Section 4.3.2.2.6 on rod insertion and flux difference are observed, the excore detector system provides adequate on-line monitoring of power distributions. Further details of specific limits on the observed rod positions and flux differences are given in the Technical Specifications together with a discussion of their bases.

Limits for reactor trip are given in the Technical Specifications. Descriptions of the systems provided are given in Section 7.7.

4.3.2.3 Reactivity Coefficients

The kinetic characteristics of the reactor core determine the response of the core to changing plant conditions or to operator adjustments made during normal operation, as well as the core response during abnormal or accidental transients. These kinetic characteristics are quantified in reactivity coefficients. The reactivity coefficients reflect the changes in the neutron multiplication due to varying plant condition such as power, moderator or fuel temperatures, or less significantly due to a change in pressure or void conditions. Since reactivity coefficients change during the life of the core, ranges of coefficients are employed in transient analysis to determine the response of the plant throughout life. The results of such simulations and the reactivity coefficients used are presented in Chapter 15. The reactivity coefficients are calculated on a corewise basis by radial and axial diffusion theory methods and with nodal analysis methods. The effect of radial and axial power distribution on core average reactivity coefficients is implicit in those calculations and is not significant under normal operating conditions. For example, a skewed axial xenon distribution which results in changing axial offset by 5 percent changes the moderator and Doppler temperature coefficients by less than 0.01 pcm/F and 0.03 pcm/F respectively.

An artificially skewed radial xenon distribution which results in changing the radial $F^N_{\Delta H}$ by 3 percent changes the moderator and Doppler temperature coefficients by less than 0.03 pcm/F and 0.001 pcm/F respectively. The spatial effects are accentuated in some transient conditions; for example, in postulated rupture of the main steam line break and rupture of a rod cluster control assembly mechanism housing described in Sections 15.1.5 and 15.4.8, and are included in these analyses.

The analytical methods and calculational models used in calculating the reactivity coefficients are given in Section 4.3.3.

Quantitative information for calculated reactivity coefficients, including fuel Doppler coefficient, moderator coefficients (density, temperature, pressure, void), and power coefficient is given in the following sections.

4.3.2.3.1 Fuel temperature (Doppler) coefficient

The fuel temperature (Doppler) coefficient is defined as the change in reactivity per degree change in effective fuel temperature and is primarily a measure of the Doppler broadening of U-238 and Pu-240 resonance absorption peaks. Doppler broadening of other isotopes such as U-236 and Np-237 is also considered but their contributions to the Doppler Effect is small. An increase in fuel temperature increases the effective resonance absorption cross section of the fuel and produces a corresponding reduction in reactivity.

The fuel temperature coefficient is calculated using CASMO-2E and XTGPWR (References 4.3.3-12 & 13) or CASMO-3G and PRISM (Reference 4.3.3-15). Moderator temperature is held constant and the power level is varied. Spatial variation of fuel temperature is taken into account by calculating the effective fuel temperature as a function of power density.

A typical Doppler-only contribution to the power coefficient, defined later, is shown in Figure 4.3.2 28 as a function of relative core power. The integral of the differential curve on Figure 4.3.2-28 is the Doppler contribution to the power defect and is shown in Figures 4.3.2-29 as a function of relative power. The Doppler coefficient becomes more negative as a function of life

as the Pu-240 content increases, thus increasing the Pu-240 resonance absorption. The upper and lower limits of the Doppler coefficient used in accident analyses are given in Chapter 15.

4.3.2.3.2 Moderator Coefficient

The moderator coefficient is a measure of the change in reactivity due to a change in the specific reactor coolant parameters, such as density, or temperature. The moderator temperature (density) coefficient is defined as the change in reactivity per degree change in the moderator temperature. Generally, the effects of the changes in moderator density, as well as the temperature are considered together. A decrease in moderator density means less moderation which results in a negative moderator coefficient. An increase in reactor coolant temperature, keeping the density constant, leads to a hardened neutron spectrum and results in an increase in resonance absorption in U-238, Pu-240 and other isotopes. The hardened spectrum also causes a decrease in the fission to capture ratio in U-235 and Pu-239. Both of these effects make the moderator coefficient more negative. Since water density changes more rapidly with temperature as temperature increases, the moderator temperature (density) coefficient becomes more negative with increasing temperature.

The soluble boron used in the reactor as a means of reactivity control also has an effect on moderator density coefficient since the soluble boron poison density as well as the water density is decreased when the reactor coolant temperature rises. An increase in the soluble poison concentration introduces a positive component in the moderator coefficient.

Thus, if the concentration of soluble poison is large enough, the net value of the coefficient may be positive. With the gadolinia bearing fuel pins present, however, the initial hot boron concentration is sufficiently low that the moderator temperature coefficient is negative at full-power operating temperatures, and within safety limits at part power operating temperatures. The effects of control rods are to make the moderator coefficient more negative by reducing the required soluble boron concentration and by increasing the "leakage" of the core.

With burnup, the moderator coefficient becomes more negative, primarily as a result of boric acid dilution, but also to a significant extent from the effects of the buildup of plutonium and fission products.

The moderator coefficient is calculated for the various plant conditions discussed above by performing two-group X-Y-Z calculations, varying the moderator temperature (and density) by about -10F about each of the mean temperatures. The moderator coefficient is shown as a function of core temperature and boron concentration for a typical unrodded and rodded core in Figures 4.3.2-30 through 4.3.2-32. The temperature range covered is from cold (68°F) to about 600°F. Figure 4.3.2-33 shows the hot, full power moderator temperature coefficient for a typical core plotted as a function of cycle exposure for the ARO critical boron concentration condition based on the design boron letdown condition.

The moderator coefficients presented here are calculated on a corewide basis, since they are used to describe the core behavior in normal and accident situations when the moderator temperature changes can be considered to affect the entire core.

4.3.2.3.3 Power coefficient

The combined effect of moderator temperature and fuel temperature change as the core power level changes is called the total power coefficient and is expressed in terms of reactivity change per percent power change. A typical power coefficient at BOL and EOL conditions is given in Figure 4.3.2-34.

It becomes more negative with burnup reflecting the combined effect of moderator and fuel temperature coefficients with burnup. The power defect (integral reactivity effect) at BOL and EOL is given in Figure 4.3.2-35.

4.3.2.3.4 Comparison of calculated and experimental reactivity coefficients

Experimental evaluation of the calculated coefficients will be done during the physics startup tests described in Chapter 14.

4.3.2.3.5 Reactivity coefficients used in transient analysis

Table 4.3.2-2 gives the best estimate values for the reactivity coefficients. The exact values of the coefficient used in the analysis depend on whether the transient of interest is examined at the BOL or EOL, whether the most negative or the most positive (least negative) coefficients are appropriate, and whether spatial nonuniformity must be considered in the analysis, are used in the transient analysis. This is described in Chapter 15.

4.3.2.4 Control Requirements

To ensure the shutdown margin stated in the Technical Specifications under conditions where a cooldown to ambient temperature is reached, concentrated soluble boron is added to the reactor coolant. Boron concentrations for several core conditions are listed in Table 4.3.2-2. For all core conditions including refueling, the boron concentration is well below the solubility limit. The rod cluster control assemblies are employed to bring the reactor to the hot standby condition. The minimum required shutdown margin is given in the Technical Specifications.

The ability to accomplish the shutdown for hot conditions is demonstrated in Table 4.3.2-3 by comparing the difference between the rod cluster control assembly reactivity available with an allowance for the worst stuck rod with that required for control and protection purposes. The shutdown margin includes an allowance of 10 percent for analytical uncertainties. The largest reactivity control requirement appears at the EOL when the moderator temperature coefficient reaches its peak negative value as reflected in the larger power defect.

The steps necessary to assure satisfactory control of plant reactivity include:

1. Insertion of control rods by reactor trip or by manual insertion with control rod switch.

2. Injection of boric acid into RCS with borated water supplied from boric acid tank or RWST.

3. Monitoring of control rod positions and volume of boric acid injected using appropriate indicators and charts.

4. Monitoring of reactor power level using power range, intermediate range, and source range flux monitors.

The above steps are normally completed at the Main Control Board. However, they can be completed outside of the Control Room if necessary, at local control stations and auxiliary equipment panels.

The control rods are required to provide sufficient reactivity to account for the power defect from full power to zero power and to provide the required shutdown margin. The reactivity addition resulting from power reduction consists of contributions from Doppler, variable average moderator temperature, flux redistribution, and reduction in void content, as discussed below.

4.3.2.4.1 Doppler

The Doppler Effect arises from the broadening of U 238 and Pu-240 resonance peaks with an increase in effective pellet temperature. This effect is most noticeable over the range of zero power to full power due to the large pellet temperature increase with power generation.

4.3.2.4.2 Variable average moderator temperature

When the core is shutdown to the hot, zero power condition, the average moderator temperature changes from the equilibrium full load value determined by the steam generator and turbine characteristics (steam pressure, heat transfer, tube fouling) to the equilibrium no-load value, which is based on the steam generator shell side design pressure.

The moderator coefficient becomes more negative as the fuel depletes because the boron concentration is reduced. This effect is the major contributor to the increased requirement at EOL.

4.3.2.4.3 Redistribution

During full power operation the reactor coolant density decreases with core height, and this, together with partial insertion of control rods, results in less fuel depletion near the top of the core. Under steady state conditions, the relative power distribution will be slightly asymmetric towards the bottom of the core. On the other hand, with a constant moderator temperature at equilibrium no load value, the reactor coolant density is uniform up the core and there is no flattening due to Doppler. The result will be a flux distribution which at zero power can be skewed toward the top of the core. The reactivity insertion due to the skewed distribution is calculated with an allowance for effects of xenon distribution.

4.3.2.4.4 Void content

A small void content in the core is due to nucleate boiling at full power. The void collapse coincident with power reduction makes a small reactivity contribution.

4.3.2.4.5 (Removed by Amendment 58)

4.3.2.4.6 Burnup

Excess reactivity is installed at the beginning of each cycle to provide sufficient reactivity to compensate for fuel depletion and fission products throughout the cycle. This reactivity is controlled by the addition of soluble boron to the reactor coolant and by burnable poison. Typical values for the soluble boron concentration for several core configurations, the unit boron worth, and burnable poison worth are given in Tables 4.3.2-1 and 4.3.2-2. Since the excess reactivity for burnup is controlled soluble boron and/or burnable poison, it is not included in control rod requirements.

4.3.2.4.7 Xenon and samarium poisoning

Changes in xenon and samarium concentrations in the core occur at a sufficiently slow rate, even following rapid power level changes, that the resulting reactivity change is controlled by changing the soluble boron concentration.

4.3.2.4.8 pH effects

Changes in reactivity due to a change in coolant pH, if any, are sufficiently small in magnitude and occur slowly enough to be controlled by the boron system. Further details are provided in Reference 4.3.2-10.

4.3.2.4.9 Control

Core reactivity is controlled by means of a chemical poison dissolved in the reactor coolant, rod cluster control assemblies, and gadolinia bearing fuel pins, as described below.

4.3.2.4.10 Chemical poison

Boron in solution as boric acid is used to control relatively slow reactivity changes associated with:

1. The moderator temperature defect in going from cold shutdown at ambient temperature to a constant moderator temperature at equilibrium no load value.

2. The transient xenon and samarium poisoning, such as that following power changes or changes in rod cluster control position.

3. The excess reactivity required to compensate for the effects of fissile inventory depletion and buildup of long-life fission products.

4. The burnable poison depletion.

The boron concentrations for various core conditions are presented in Table 4.3.2-2.

4.3.2.4.11 Rod cluster control assemblies

Full length rod cluster control assemblies are exclusively employed. The number of full length assemblies is shown in Table 4.3.2-1. The full length rod cluster control assemblies are used for shutdown and control purposes to offset fast reactivity changes associated with:

1. The required shutdown margin in the hot zero power, stuck rods condition.

2. The reactivity compensation as a result of an increase in power above hot zero power (power defect including Doppler and moderator reactivity changes).

3. Unprogrammed fluctuations of boron concentration, reactor coolant temperature, or xenon concentration (with rods not exceeding the allowable rod insertion limits).

4. Reactivity ramp rates resulting from load changes.

The allowed full length control bank reactivity insertion is limited at full power to maintain shutdown capability. As the power level is reduced, control rod activity requirements are also reduced and more rod insertion is allowed. The control bank position is monitored and the operator is notified by an alarm if the limit is approached. The determination of the insertion limit uses conservative xenon distributions and axial power shapes. In addition, the rod cluster control assembly withdrawal pattern determined from these analyses is used in determining power distribution factors and in determining the maximum worth of an inserted rod cluster control assembly ejection accident. For further discussion, refer to the Technical Specifications on rod insertion limits.

Power distribution, rod ejection, and rod misalignment analyses are based on the arrangement of the shutdown and control groups of the rod cluster control assemblies shown in Figure 4.3.2-36. All shutdown rod cluster control assemblies are withdrawn before withdrawal of the control banks is initiated.

In going from zero to 100 percent power, control banks A, B, C, and D are withdrawn sequentially. The limits of rod positions and further discussion on the basis for rod insertion limits are provided in the Technical Specifications.

4.3.2.4.12 Reactor coolant temperature

Reactor coolant (or moderator) temperature control has added flexibility in reactivity control of the Westinghouse pressurized water reactor. This feature takes advantage of the negative moderator temperature coefficient inherent in a pressurized water reactor to:

1. Maximize return to power capabilities.

2. Provide +5 percent power load regulation capabilities without requiring control rod compensation.

3. Extend the time in cycle life to which daily load follow operations can be accomplished.

Reactor coolant temperature control supplements the dilution capability of the plant by lowering the reactor coolant temperature to supply positive reactivity through the negative moderator

coefficient of the reactor. After the transient is over, the system recovers the reactor coolant temperature to the programmed value.

Moderator temperature control of reactivity, like soluble boron control, has the advantage of not significantly affecting the core power distribution. However, unlike boron control, temperature control can be rapid enough to achieve reactor power change rates of 5 percent/minute.

4.3.2.4.1 Burnable absorbers

Gadolinia bearing fuel is used for the control of the excess reactivity available during the beginning of the fuel cycle. In doing so, the gadolinia bearing fuel prevents the moderator temperature coefficient from violating safety limits at normal operating conditions. The gadolinia bearing fuel performs this function by reducing the requirement for soluble poison in the moderator at the beginning of the fuel cycle as described previously. In addition to controlling excess reactivity, gadolinia bearing fuel is used to control power peaking.

4.3.2.4.14 Peak xenon startup

Compensation for the peak xenon buildup is accomplished by using the Chemical Shim Control System. Startup from the peak xenon condition is accomplished with a combination of rod motion and boron dilution. The boron dilution may be made at any time, including during the shutdown period, provided the shutdown margin is maintained.

4.3.2.4.15 Load follow control and xenon control

During load follow maneuvers, power changes are accomplished by using control rod motion and dilution or boration by the Chemical Shim Control System as required. Control rod motion is limited by the control rod insertion limits on full length rods, as provided in the Technical Specifications and discussed in Sections 4.3.2.4.11 and 4.3.2.4.12. The power distribution is maintained within acceptable limits through the location of the full length rod bank. Reactivity changes due to the changing xenon concentration can be controlled by rod motion and/or changes in the soluble boron concentration.

Late in cycle life, extended load follow capability is obtained by augmenting the limited boron dilution capability at low soluble boron concentration by temporary moderator temperature reductions.

Rapid power increases (5 percent/min.) from part power during load follow operation are accomplished with a combination of rod motion, moderator temperature reduction, and boron dilution. Compensation for the rapid power increase is accomplished initially by a combination of rod withdrawal and moderator temperature reduction. As the slower boron dilution takes affect after the initial rapid power increase, the moderator temperature returns to the programmed value.

4.3.2.4.16 Burnup

Control of the excess reactivity for burnup is accomplished by using soluble boron and/or burnable poison. The boron concentration must be limited during operating conditions to ensure the moderator temperature coefficient is within safety limits. Sufficient burnable poison is

installed at the beginning of a cycle to give the desired cycle lifetime without exceeding the boron concentration limit. The practical minimum boron concentration is 10 ppm.

4.3.2.5 Control Rod Patterns and Reactivity Worth

The full length rod cluster control assemblies are designated by a function as the control groups and the shutdown groups. The terms "group" and "bank" are used synonymously throughout this report to describe a particular grouping of control assemblies.

The control banks are labeled A, B, C, and D and the shutdown banks are labeled SA, SB, and SC. Each bank, although operated and controlled as a unit, is comprised of two subgroups. The axial position of the full length rod cluster control assemblies may be controlled manually or automatically. The rod cluster control assemblies are all dropped into the core following actuation of reactor trip signals.

Two criteria have been employed for selection of the control groups. First, the total reactivity worth must be adequate to meet the requirements specified in Table 4.3.2-3. Second, in view of the fact that these rods may be partially inserted at power operation, the total power peaking factor should be low enough to ensure that the power capability requirements are met. Analyses indicate that the first requirement can be met either by a single group or by two or more banks whose total worth equals at least the required amount. The axial power shape would be more peaked following movement of a single group of rods worth 3 to 4 percent $\Delta\rho$; therefore, four banks (described as A, B, C, and D) each worth approximately 0.3 to 1.0 percent $\Delta\rho$ have been selected.

The position of control banks for criticality under any reactor condition is determined by the concentration of boron in the reactor coolant. On an approach to criticality, boron is adjusted to ensure that criticality will be achieved with control rods above the insertion limit set by shutdown and other considerations (see the Technical Specifications). Early in the cycle there may also be a withdrawal limit at low power to maintain the moderator temperature coefficient within safety limits. For the reference first core described in this section, however, no such withdrawal limit is required.

Ejected rod worths are given in Section 15.4.8 for several different conditions.

Allowable deviations due to misaligned control rods are discussed in the Technical Specifications.

A representative calculation for two banks of control rods withdrawn simultaneously (rod withdrawal accident) is given in Figure 4.3.2-37.

Calculation of control rod reactivity worth versus time following reactor trip involves both control rod velocity and differential reactivity worth. The rod position versus time of travel after rod release normalized to "Distance to Top of Dashpot" and "Drop Time to Top of Dashpot" is given in Figure 4.3.2-38. For nuclear design purposes, the reactivity worth versus rod position is calculated by a series of steady state calculations at various control rod positions assuming all rods out of the core as the initial position in order to minimize the initial reactivity insertion rate. Also to be conservative, the rod of highest worth is assumed stuck out of the core and the flux distribution (and thus reactivity importance) is assumed to be skewed to the bottom of the core. The result of these calculations is shown on Figure 4.3.2-39.

The shutdown groups provide additional negative reactivity to assure an adequate shutdown margin. Shutdown margin is defined as the amount by which the core would be subcritical at hot shutdown if all rod cluster control assemblies are tripped, but assuming that the highest worth assembly remains fully withdrawn and no changes in xenon or boron take place. The loss of control rod worth due to the material irradiation is negligible since only bank D may be in the core under normal operating conditions (near full power). The values given in Table 4.3.2-3 show that the available reactivity in withdrawn rod cluster control assemblies provides the design bases minimum shutdown margin allowing for the highest worth cluster to be at its fully withdrawn position. An allowance for the uncertainty in the calculated worth of N-1 rods is made before determination of the shutdown margin.

4.3.2.6 Criticality of Fuel Assemblies Outside of the Reactor

Criticality of fuel assemblies outside the reactor is precluded by adequate design of fuel transfer, shipping and storage facilities and by administrative control procedures. The two principal methods of preventing criticality are limiting the fuel assembly array size and limiting assembly interaction.

As described in FSAR Section 9.1.1 and 9.1.2 storage of fuel occurs in both pools and dry (new fuel) storage. Several rack designs are used and each has its own specific analytical method and storage restrictions. A brief summary of the rack types follows with reference to the subsection that contains the description of the criticality analysis. The rack design details are presented in FSAR Table 9.1.2-2.

Refer to Subsection 4.3.2.6.1 for BWR racks in Pools A and B. Fuel restrictions are based on limiting fuel design (GE 8x8R) and enrichment (3.2 w/o U235). The racks contain either a Boraflex or Boral as a neutron absorber.

Refer to Subsection 4.3.2.6.2 for BWR and PWR racks used in Pools C and D. These racks contain Boral/Metamic as a neutron absorber. The PWR racks use a burnup credit requirement for storage. The BWR racks use a criterion based on Standard Cold Core Geometry.

Refer to Subsection 4.3.2.6.3 for HNP new fuel stored in Pools A or B. These racks are "flux trap" style racks that were fabricated with Boraflex as a neutron absorber. Due to degradation by the high gamma flux from recently discharged fuel, the Boraflex is degrading and is no longer credited. New fuel must be stored in a 2-of-4 geometry. As described in Section 4.3.2.6.4 credit for soluble boron is required for normal storage.

Refer to Subsection 4.3.2.6.4 for PWR racks used in Pools A and B. The racks are "flux trap" style racks that were fabricated with Boraflex as a neutron absorber. Due to degradation by high gamma flux from recently discharged fuel, the Boraflex is degrading and no longer credited. A burnup enrichment restriction applies.

Refer to Subsection 4.3.2.6.5 for PWR racks used in the dry, new fuel storage area. These racks are "flux trap" style racks that were fabricated with Boraflex as a neutron absorber. For conservatism, no credit is taken for the Boraflex in the criticality analyses in dry storage.

The design basis for preventing criticality outside the reactor is that, considering possible variations, there is a 95 percent probability at a 95 percent confidence level that the effective multiplication factor (K_{eff}) of the fuel assembly array will be less than or equal to 0.95 as recommended in ANSI 57.2-1983. In the case of pools C and D, a more conservative factor K-infinity (K_{inf}) was calculated.

4.3.2.6.1 Criticality Evaluation Results for BWR Fuel Storage in Pools A and B

The following are the conditions that are assumed in meeting the design basis:

1. BWR fuel: The fuel assembly contains the highest enrichment authorized at its most reactive point in core life. No credit is taken for control rods or burnable poison. Refer to Section 9.1.2 for fuel storage rack parameters used in criticality calculations. Fuel parameters used in the criticality analysis are for General Electric (GE) 8 x 8R fuel design at 3.2 w/o U235. A study has been performed to confirm that other GE bundle designs currently stored at Brunswick (BSEP) are bounded by the analyzed 8 x 8R assembly at 3.2 w/o (Reference 4.3.2 28). From a reactivity standpoint, as measured by K-infinity, the existing criticality analysis conservatively bounds all fuel assemblies loaded in BSEP Unit 1 through reload 5 and all fuel assemblies loaded in BSEP Unit 2 through reload 6.

2. For flooded conditions, the moderator is pure water at the temperature within the design limits which yields the largest reactivity.

3. The array is infinite in lateral and axial extent and precludes any neutron leakage from the array.

4. Mechanical uncertainties are treated by either using "worst case" conditions or by performing sensitivity studies and obtaining appropriate uncertainties.

5. Credit is taken for the neutron absorption in structural materials and in solid materials added specifically for neutron absorption.

6. Credit for the dissolved boron is not taken except under postulated accident conditions where the double contingency principle of ANSI N16.1-1975 is applied. This principle states that it shall require at least two unlikely, independent, and concurrent events to produce a criticality accident.

The design method for the Westinghouse criticality analysis which insures the criticality safety of fuel assemblies outside the reactor uses the AMPX system of codes (Reference 4.3.2-12) for cross-section generation and KENO IV (Reference 4.3.2-13) for reactivity determination.

The cross-section library (Reference 4.3.2-11) that is the common starting point for all cross-sections has been generated from ENDF/B V data. The NITAWL program (Reference 4.3.2-12) includes in this library the self-shielded resonance cross-sections that are appropriate for a particular geometry. The Nordheim Integral Treatment is used.

Energy and spatial weighting of cross-sections is performed by the XSDRNPM program (Reference 4.3.2-12) which is a one-dimensional SN transport theory code. These multi-group

cross-section sets are then used as input to KENO IV (Reference 4.3.2-13) which is a three-dimensional Monte Carlo theory program designed for reactivity calculations.

A set of critical experiments has been analyzed using the above method to demonstrate its applicability to criticality analysis and to establish the method bias and variability. This benchmarking demonstrates that the calculational method is capable of determining the multiplication factor with an uncertainty less than 0.5 percent at a 95/95 percent probability/confidence level.

For the BWR analysis, the criticality design criteria are met when the calculated effective multiplication factor (K_{eff}) described is less than or equal to 0.95:

$$K_{eff} = K_{nominal} + B_{method} + B_{part} + [(ks_{nominal})^2 + (ks_{mech})^2 +$$

$$(ks_{method})^2 + (ks_{mat})^2]^{1/2}$$

where:

$K_{nominal}$ = nominal case KENO K_{eff}

B_{method} = method bias determined from benchmark critical comparisons

B_{part} = bias to account for poison particle self-shielding

$ks_{nominal}$ = 95/95 uncertainty in the nominal KENO K_{eff}

ks_{mech} = 95/95 uncertainty in the calculation of the bias due to construction tolerances

ks_{method} = 95/95 uncertainty in the method bias

ks_{mat} = 95/95 uncertainty associated with material thickness tolerances

It has been determined in Reference 4.3.2-27 that K_{eff} will remain less than or equal to 0.95 for BWR 8 x 8R fuel with a maximum lattice average enrichment of 3.2 w/o U235.

These methods conform with ANSI N18.2-1973, "Nuclear Safety Criteria for the Design of Stationary Pressurized Water Reactor Plants," Section 5.7, Fuel Handling System; ANSI 57.2-1983, "Design Objectives for LWR Fuel Storage Facilities at Nuclear Power Stations," Section 6.4.2; ANSI N16.9-1975, "Validation of Calculational Methods for Nuclear Criticality Safety;" NRC Standard Review Plan, Section 9.1.2, "Fuel Storage;" and the NRC guidance, "NRC Position for Review and Acceptance of Spent Fuel Storage and Handling Applications."

4.3.2.6.2 Criticality Evaluation Results for Fuel Storage in Pools C and D

The primary criticality analyses of the high-density spent fuel storage racks (Reference 4.3.2-39) were performed with a two-dimensional multigroup transport theory technique, using the CASMO-3 computer code (Reference 4.3.2-35). Since CASMO-3 cannot be directly compared to critical experiments, a calculational bias is not available for CASMO-3. Therefore, independent verification calculations were made with a three-dimensional Monte Carlo technique utilizing the MCNP-4A computer code (Reference 4.3.2-36).

CASMO-3 was also used for burnup calculations and for evaluation small reactivity increments associated with manufacturing tolerances. In the geometric model used in the calculations, each fuel rod and its cladding were described explicitly and reflecting boundary conditions (zero neutron current) were used in the axial direction and at the neutron absorber and steel plates between storage cells. These boundary conditions have the effect of creating an infinite array of storage cells in all directions.

MCNP-4A was used to determine reactivity effects, to calculate the reactivity for fuel misloading outside the racks and to determine the effect of having PWR and BWR racks adjacent to each other.

The following are the conditions that are assumed in meeting the design basis discussed above in Section 4.3.2.6:

1. PWR Fuel: The high-density racks designed for Pools C and D were evaluated for all of the PWR fuel assemblies listed in Table 4.3.2-7. The 15 x 15 Westinghouse fuel assembly, containing UO_2 at a maximum initial enrichment of 5.0 wt% ^{235}U, was shown to exhibit the highest reactivity at zero burnup and as a function of burnup. The design considers an infinite multiplication factor, k_{inf}, which is calculated for an infinite array, neglecting neutron losses due to leakage from the actual storage rack. This analytical technique produces a higher neutron multiplication factor, thus, producing a more conservative value than the effective multiplication factor k_{eff}. Therefore, the design basis criterion is a k_{inf} of less than 0.95, including statistically combined margins of uncertainty corresponding to mechanical tolerances. The calculated maximum reactivity includes burnup-dependent allowances for uncertainty in depletion calculations and for the axial distribution in burnup.

   To ensure that the true reactivity will always be less than the calculated reactivity, the following conservative assumptions were made:

   - Moderator is un-borated water at a temperature (4°C) that results in the highest reactivity.

   - In all cases (except for the assessment of peripheral effects and certain abnormal/accident conditions where neutron leakage is inherent), the infinite multiplication factor, k_{inf}, was used rather than the effective multiplication factor, k_{eff} (i.e., neutron loss from radial and axial leakage neglected).

   - Neutron absorption in minor structural members is neglected, i.e., spacer grids are analytically replaced by water.

   - The racks were assumed to be fully loaded with the most reactive fuel authorized to be stored in the facility. In the analysis performed for normal storage conditions, no credit was taken for any control rods or burnable poison (IFBA rods for the PWR fuel), or soluble boron in the pool water which may be present.

Consequences of abnormal and accident conditions have also been evaluated, where "abnormal" refers to conditions (such as higher water temperatures) which may reasonably be expected to occur during the lifetime of the plant and "accident" refers to conditions which are not expected to occur but nevertheless must be protected against.

The principal method of analysis for the racks was the CASMO-3 code, using the restart option in CASMO-3 to analytically transfer fuel of a specified burnup into the storage rack configuration at a reference temperature of 4°C (39°F). Calculations were made for fuel of several different initial enrichments and, at each enrichment, a limiting k_{inf} value was established which includes reactivity allowances for manufacturing tolerances, the uncertainty in the burnup analyses and for the effect of the axial burnup distribution on reactivity. The restart CASMO-3 calculations (cold, no-Xenon, rack geometry) were then interpolated to define the burnup value yielding the limiting k_{inf} value for each enrichment. A line was fitted to these converged burnup values and this line defines the boundary of the acceptable domain, as discussed below.

An independent MCNP-4A calculation was performed to verify the acceptability of the reference criticality analyses. Fuel of 5.0 wt% initial enrichment was analyzed by MCNP-4A and by CASMO-3. The results of this comparison are presented in Table 4.3.2-8. In comparing the MCNP values to the CASMO-3 values, the MCNP-4A calculational bias and calculational statistics were included. In addition the MCNP-4A model correctly included the effect of axial neutron leakage, which the CASMO-3 calculations conservatively neglect. Since the MCNP-4A model is at 20°C and the CASMO-3 model is at 4°C, a temperature correction had to be applied to the MCNP-4A result. The MCNP-4A result confirms that the reference CASMO-3 calculations are conservative.

The results of the criticality analyses for spent fuel storage in Pools C and D are summarized in Table 4.3.2-9 for the design basis storage conditions. The analyses are based on a reference PWR fuel assembly and storage cell. The reference storage cell includes the nominal dimensions provided in Table 9.1.2-2. The reference fuel is a 15 x 15 array of fuel rods with 21 rods replaced by 21 control rod guide tubes. The fuel has 5.0 wt.% ^{235}U maximum initial enrichment burned to 41,352 MWD/MTU. To provide additional margin against the acceptance criteria, the maximum k_{inf} is selected to be 0.9450 (95% probability at the 95% confidence level).

In order to meet this requirement, fuel with initial enrichments below 5.0 wt.% ^{235}U must have sufficient burnup to obtain the same effective reactivity as the design basis fuel and storage cell. For convenience, the minimum (limiting) burnup data for unrestricted storage can be described as a linear function of the initial enrichment (E, in weight percent ^{235}U) which conservatively encompasses the limiting burnup data. The equation for acceptable burnup-enrichment combinations is:

Minimum Burnup in MWD/MTU = 12114*E-19123

The burnup criteria is implemented by appropriate administrative procedures to ensure verified burnup as specified, prior to fuel transfer into Spent Fuel Pools C or D. The racks can safely accommodate fuel of various initial enrichments and discharge fuel burnups, provided the combination falls within the acceptable domain.

2. BWR Fuel: The high-density BWR racks designed for Pool C were evaluated for all of the BWR fuel assemblies listed in Table 4.3.2-10. The design basis BWR fuel assembly, used for uncertainty calculations, is a standard 8 x 8 array of BWR fuel rods containing UO_2 clad in Zircaloy (60 fuel rods with 4 water rods). A maximum planar average enrichment of 4.6 wt.% ^{235}U was assumed for all rods in the assembly and no credit was taken for gadolinia, which might be present. The design considers an infinite multiplication factor, kinf, which is calculated for an infinite array, neglecting neutron losses due to leakage from the actual storage rack. This analytical technique produces a higher neutron multiplication factor, thus,

producing a more conservative value than the effective multiplication factor k_{eff}. Therefore, the design basis criterion is a k_{inf} of less than 0.95, including statistically combined margins for uncertainty corresponding to mechanical tolerances.

The criticality safety was evaluated at the burnup corresponding to a k_{inf} of 1.32 in the Standard Cold Core Geometry (SCCG). SCCG is defined as an infinite array of fuel assemblies on a 6-inch lattice spacing at 20°C, without any control absorber or voids.

The two-dimensional CASMO-3 code was used as the principal method of analysis for the Harris spent fuel pool BWR racks. CASMO-3 was used to perform depletion calculations on the fuel assembly and using the restart option in CASMO-3 the fuel of a specified burnup was analytically transferred into the storage rack at a reference temperature of 4°C (39°F). The same fuel of a specified burnup was also analytically transferred into the standard cold core geometry (SCCG) configuration which is an infinite lattice with 6 inch spacing at a temperature of 20°C without any burnable absorber or control blades and no voids. All Xenon, which was present during the depletion calculations, was removed during the restarts in the rack and SCCG.

An independent MCNP-4A calculation was used to verify the acceptability of the reference criticality analyses. Fuel of 4.6 wt.% initial enrichment was analyzed by MCNP-4A and by CASMO-3. The results of this comparison are presented in Table 4.3.2-8. In comparing the MCNP values to the CASMO values, the MCNP-4A calculational bias and calculational statistics were included. In addition, the MCNP-4A model correctly included the effect of axial neutron leakage which the CASMO-3 calculations conservatively neglect. Since the MCNP-4A model is at 20°C and the CASMO-3 model is at 4°C, a temperature correction had to be applied to the MCNP-4A result. The MCNP-4A result confirms that the reference CASMO-3 calculations are conservative.

The maximum k_{inf} in the BWR storage rack was determined to be 0.9443 (95% probability at the 95% confidence level) including all known calculational and manufacturing uncertainties. In addition, a conservative allowance of 0.01 Δk for possible difference between fuel vendor calculations and those reported here was included. This allowance also encompasses any uncertainty in the burnup calculations.

The basis calculations supporting the criticality safety of the Pool C and D racks for the design basis fuel are summarized in Table 4.3.2-11. For the design bases fuel, the fuel storage rack satisfies the USNRC criterion of the maximum k_{eff} less than or equal to 0.95. For Unrestricted Storage of BWR fuel assemblies, the maximum planar average enrichment must be less than or equal to 4.6 wt.% 235U and the k_{inf} in standard cold core geometry must be less than or equal to 1.32.

4.3.2.6.3 Criticality Results for New PWR Fuel Storage in Pools A and B

The following are conditions that are assumed in meeting design basis.

1. HNP new fuel contains the highest enrichment authorized (4.95 w/o +0.05 w/o uncertainty). Refer to Section 9.1.2 for fuel storage rack parameters used in criticality calculations.

2. The new fuel for SHNPP is manufactured by AREVA and is of the HTP design with parameters identified in 4.3.2-38. The rack criticality was based on an Advanced HTP-17

assembly that is demonstrated to be conservative relative to the current fuel used at SHNPP. The fuel was analyzed without credit for gadolinia rods and without axial blankets or "cut back" zones in the pellet enrichment. Evaluation of new fuel with removable neutron absorbers such at Wet Annular Boron Absorber Assemblies (WABAs) or Burnable Poison Rods (BPRAs) was not included for current or future fuel designs. The Advanced HTP-17 details were as of August 2005. Any change in fuel from the current design requires comparison with the analyzed assembly to confirm that a new fuel reactivity (both initial and at calculated burnup points) is conservative relative to the analyses in Ref 4.2.3-38.

3. The criticality analyses ignored minor structural features of the rack design (e.g. the structural members that connect the individual cells); grid straps and flow mixing devices within the fuel assembly; and the presence of control rods or other absorbing components that may be inserted into an assembly. The PWR storage rack volumes occupied by the Boraflex are assumed to be moderator. Mechanical uncertainties are treated by either using "worst case" conditions or by performing sensitivity studies and obtaining appropriate uncertainties. A maximum normal pool temperature of 150°F was used.

4. The criticality analyses were performed using the SCALE 4.4 (Reference 4.3.2.-32). SCALE system was developed for use by the USNRC and its licensees. Methodology validation was by modeling critical experiments. The method has been benchmarked against critical experiments to demonstrate its applicability to criticality analyses and to establish the method bias and variability.

5. The tolerance evaluation uses the CASMO3 deterministic program to assess relative reactivity effects due to manufacturing tolerances.

6. The maximum k, $k_{95/95}$ used to compare with the criticality safety criterion consists of the summation of the absolute k, the bias, and a statistical combination of uncertainties. The benchmark determined the calculation method bias and bias uncertainty.

7. The criticality design criteria are met when the calculative effective multiplication factor (k_{eff}) described below is less than or equal to 0.95 for the new fuel as follows:

$$K_{95/95} = k_{keno} + k_{bias} + \Delta k_{sys} + [C^2(\sigma_k^2 + \sigma_{bias}^2 + \sigma_{sys}^2) + \Delta k_{tolerances}^2]^{1/2},$$

Where,

k_{keno} = the KENO V.a calculated k_{eff} result,

bias = the method uncertainty

C = confidence multiplier based upon the number of benchmark cases

σ_k, σ_{bias}, σ_{sys} = standard deviation of the KENO V.a, bias values, and normal system conditions

Δk_{sys} = reactivity penalties associated with normal system conditions such as moderator temperature, etc.

$\Delta k_{tolerances}$ = statistical combination of uncertainties due to manufacturing tolerances from CASMO tolerance calculations

The analyses concluded that a 2-of-4 checkerboard of new fuel within and between racks in the pool was necessary to maintain $k_{eff} \leq 0.95$. Interaction with adjacent PWR racks with a 4-of-4 storage, adjacent BWR racks and Non-fuel Bearing Container (NFBC, e.g. trash baskets containing irradiated core components) was considered. Credit for soluble boron is required to account for these interactions. The specific interaction requirements are described in FSAR Section 9.1.2.1. Minimum boron concentration of soluble boron is required to maintain $k_{eff} \leq 0.95$. Accident conditions analyzed are described in FSAR Section 9.1.2.2 along with the required soluble boron requirements.

4.3.2.6.4 Criticality Evaluation results for irradiated PWR fuel in Pools A and B

1. The criticality evaluation generally follows the methods and inputs described in Section 4.3.2.6.3 with several exceptions. The PWR fuel considered in the analyses is described in FSAR Table 4.3.2-7. In addition, the Advanced 17 x 17 HTP design was also considered. A limiting fuel design was identified and the reactivity of the fuel was evaluated at selected burnups as a function of initial enrichment, the specifics of this process are described in further detail below.

2. A target design criterion is applied to the burnup credit (BUC) analysis with the following equation:

   $K_{Design} = k_{KENO} + bias + [C^2(\sigma_k^2 + \sigma_{bias}^2) + \Delta k_{tolerances}^2]^{1/2}$,

   The BUC K_{Design} equation is the $K_{95/95}$ equation without the Δk_{sys} and σ_{sys} terms. The Δk_{sys} and σsys terms will represent those parameters and conditions which will require soluble boron PPM credit and will be handled separately after the BUC loading curve and requirements are determined. In most cases the parameters and conditions represented by Δksys is represented as a delta reactivity relative to the BUC design basis configuration conditions. The following approximate relationship is used:

   $K_{95/95}$ = K_{Design} (BUC Credit) + $\Sigma\Delta k_{sys}$ (Soluble Boron PPM Credit)

   A reasonable combination of BUC and PPM credit is used to demonstrate that $K_{95/95} \leq 0.95$ to meet the regulatory requirements.

   The BUC loading curve formulation is based upon a target K_{Design} that accounts for methods bias and normal tolerances / uncertainties. These values are determined in order to develop a simple relationship for BUC analysis:

   $K_{Design} = k_{KENO} + bias + [C^2(\sigma_k^2 + \sigma_{bias}^2) + \Delta k_{tolerances}^2]^{1/2} = k_{KENO} + N$

   Where $N = bias + [C^2(\sigma_k^2 + \sigma_{bias}^2) + \Delta k_{tolerances}^2]^{1/2}$ is a known, calculated value. The equation is used for selected initial enrichment values. Assembly average burnup is iterated until the resulting k_{eff} is just less than 1.0. The loci of these points for the BUC curve is presented in Technical Specification Figure 5.6-2.

3. Soluble boron is required for fuel storage at normal conditions without fuel handling activity as described in FSAR Section 9.1.2.2 to maintain $K_{95/95} < 0.95$. In the unlikely event that the pools are flooded with unborated water, the condition $K_{95/95} < 1.0$ is maintained.

4. Limiting fuel handling accidents are analyzed. The required limiting boron concentration is presented in FSAR Section 9.1.2.2.

4.3.2.6.5 Criticality Evaluation Results for New Fuel Storage in the New Fuel Inspection Pit

The following are the conditions that are assumed in meeting the design basis:

1. The analytical method used to calculate k_{eff} is the same as that described in Section 4.3.2.6.3 except where superseded by the items listed in this subsection.

2. PWR fuel: The fuel assembly contains the highest enrichment authorized (5 wt % U235).

3. The criticality analyses (Reference 4.3.2-38) models the new fuel storage racks in the Configuration shown in FSAR Figure 1.2.2-55. Each 6 x 10 module has alternating rows and columns locked out. Figure 2.3.3-1 of Reference 4.3.2-38 displays the arrangement analyzed. The arrangement results in use of 1-of-4 of the rack cells. The design physically prevents loading a fuel assembly in an incorrect location.

4. The k-effective of the fresh fuel in the fresh fuel storage racks is calculated assuming the racks are loaded with fuel of the maximum fuel assembly enrichment and flooded with pure (unborated) water at the temperature within the design limits which yields the largest reactivity. The k-effective resulting from these conditions is less than 0.95, at a 95 percent probability, 95 per cent confidence level.

5. Under optimum moderation conditions (low-density or heterogeneously distributed water), the resulting k-effective is less than 0.98, at a 95 percent probability, 95 percent confidence level.

4.3.2.7 Stability

4.3.2.7.1 Introduction

The stability of the pressurized water reactor cores against xenon-induced spatial oscillations and the control of such transients are discussed extensively in References 4.3.2-17, 4.3.2-18 and 4.3.2-19. A summary of these reports is given in the following discussion and the design bases are given in Section 4.3.1.6.

In a large reactor core, xenon-induced oscillations can take place with no corresponding change in the total power of the core. The oscillation may be caused by a power shift in the core which occurs rapidly by comparison with the xenon-iodine time constants. Such a power shift occurs in the axial direction when a plant load change is made by control rod motion and results in a change in the moderator density and fuel temperature distributions. Such a power shift could occur in the diametral plane of the core as a result of abnormal control action.

Due to the negative power coefficient of reactivity, pressurized water reactor cores are inherently stable to oscillations in total power. Protection against total power instabilities is

provided by the control and protection system as described in Section 7.7. Hence, the discussion on the core stability will be limited here to xenon induced spatial oscillations.

4.3.2.7.2 Stability index

Power distributions, either in the axial direction or in the X-Y plane, can undergo oscillations due to perturbations introduced in the equilibrium distributions without changing the total core power. The overtones in the current pressurized water reactors, and the stability of the core against xenon induced oscillations can be determined in terms of the eigenvalues of the first flux overtones. Writing, either in the axial direction or in the X-Y plane, the eigenvalue ξ of the first flux harmonic as:

$$\xi = b + ic \quad (1)$$

then b is defined as the stability index and T = 2π/c as the oscillation period of the first harmonic. The time-dependence of the first harmonic δφ in the power distribution can now be represented as:

$$\delta\varphi(t) = Ae^{\xi t} = ae^{bt} \cos ct \quad (2)$$

where A and a are constants. The stability index can also be obtained approximately by:

$$b = \frac{1}{T} \ln \frac{A_n+1}{A_n} \quad (3)$$

where A_n, A_n+1 are the successive peak amplitudes of the oscillation and T is the time period between the successive peaks.

4.3.2.7.3 Prediction of the core stability

The stability of the core described herein (i.e., with 17 x 17 fuel assemblies) against xenon-induced spatial oscillations is expected to be equal to or better than that of earlier designs. The prediction is based on a comparison of the parameters which are significant in determining the stability of the core against the xenon-induced oscillations, namely: 1) the overall core size is unchanged and spatial power distributions will be similar, 2) the moderator temperature coefficient is expected to be slightly more negative, and 3) the Doppler coefficient of reactivity is expected to be equal to or slightly more negative at full power.

Analysis of both the axial and X-Y xenon transient tests, discussed in Section 4.3.2.7.5, shows that the calculational model is adequate for the prediction of core stability.

4.3.2.7.4 Stability measurements

1. Axial measurements - Two axial xenon transient tests conducted in a pressurized water reactor with a core height of 12 ft. and 121 fuel assemblies are reported in Reference 4.3.2-20, and will be briefly discussed here. The tests were performed at approximately 10 percent and 50 percent of cycle life.

   Both a free-running oscillation test and a controlled test were performed during the first test. The second test at mid-cycle consisted of a free-running oscillation test only. In each of the free-running oscillation tests, a perturbation was introduced to the equilibrium power

distribution through an impulse motion of the control bank D and the subsequent oscillation was monitored to measure the stability index and the oscillation period. In the controlled test conducted early in the cycle, the part length rods were used to follow the oscillations to maintain an axial offset within the prescribed limits. The axial offset of power was obtained from the excore ion chamber readings (which had been calibrated against the incore flux maps) as a function of time for both free-running tests as shown in Figure 4.3.2-40.

The total core power was maintained constant during these spatial xenon tests, and the stability index and the oscillation period were obtained from a least square fit of the axial offset data in the form of Equation (2). The axial offset of power is the quantity that properly represents the axial stability in the sense that it essentially eliminates any contribution from even order harmonics including the fundamental mode. The conclusions of the tests are:

a. The core was stable against induced axial xenon transients both at the core average burnups of 1550 MWD/MTU and 7700 MWD/MTU. The measured stability indices were -0.041 $hr.^{-1}$ for the first test (Curve 1 of Figure 4.3.2-40) and -0.014 $hr.^{-1}$ for the second test (Curve 2 of Figure 4.3.2-40). The corresponding oscillation periods were 32.4 and 27.2 hours, respectively.

b. The reactor core becomes less stable as fuel burnup progresses and the axial stability index was essentially zero at 12,000 MWD/MTU.

2. Measurements in the X-Y plane - Two X-Y xenon oscillation tests were performed at a pressurized water reactor plant with a core height of 12 ft. and 157 fuel assemblies. The first test was conducted at a core average burnup of 1540 MWD/MTU and the second at a core average burnup of 12,900 MWD/MTU. The X-Y xenon tests show that the core was stable in the X-Y plane at both burnups. The second test shows that the core became more stable as the fuel burnup increased and all Westinghouse pressurized water reactors are expected to be stable throughout their burnup cycles.

   In each of the two X-Y tests, a perturbation was introduced to the equilibrium power distribution through an impulse motion of one rod cluster control unit located along the diagonal axis. Following the perturbation, the uncontrolled oscillation was monitored using the moveable detector and thermocouple system and the excore power range detectors. The quadrant tilt difference (QTD) is the quantity that properly represents the diametral oscillation in the X-Y plane of the reactor core in that the differences of the quadrant average powers over two symmetrically opposite quadrants essentially eliminates the contribution to the oscillation from the azimuthal mode. The QTD data were fitted in the form of Equation (2) through a least-square method. A stability index of -0.076 $hr.^{-1}$ with a period of 29.6 hours was obtained from the thermocouple data shown in Figure 4.3.2-41.

   It was observed in the second X-Y xenon test that the pressurized water reactor core with 157 fuel assemblies had become more stable due to an increased fuel depletion and the stability index was not determined.

4.3.2.7.5 Comparison of calculations with measurements

The analysis of the axial xenon transient tests was performed in an axial slab geometry by using a flux synthesis technique. The direct simulation of the axial offset data was carried out using the PANDA Code (Reference 4.3.2-21). The analysis of the X-Y xenon transient tests was

performed in an X-Y geometry using a modified TURTLE Code (Reference 4.3.1-2). Both the PANDA and TURTLE code solve the two-group time-dependent neutron diffusion equation with a time-dependent xenon and iodine concentrations. The fuel temperature and moderator density feedback is limited to a steady state model. All the X-Y calculations were performed in an average enthalpy plane.

The basic nuclear cross sections used in this study were generated from a unit cell depletion program which has evolved from the codes LEOPARD (Reference 4.3.1-1) and CINDER (Reference 4.3.2-22). The detailed experimental data during the tests, including the reactor power level, enthalpy rise, and the impulse motion of the control rod assembly, as well as the plant follow burnup data, were closely simulated in the study.

The results of the stability calculation for the axial tests are compared with the experimental data in Table 4.3.2-5. The calculations show conservative results for both axial tests with a margin of approximately -0.01 hr.-1 in the stability index.

An analytical simulation of the first X-Y xenon oscillation test shows a calculated stability index of -0.081 $hr.^{-1}$, which is in good agreement with the measured value of -0.076 $hr.^{-1}$ As indicated earlier, the second X-Y xenon test showed that the core had become more stable compared to the first test; therefore, no evaluation of the stability index was attempted. This increase in the core stability in the X-Y plane due to increased fuel burnup is due mainly to the increased magnitude of the negative moderator temperature coefficient.

Previous studies of the physics of xenon oscillations, including three-dimensional analysis, are reported in a series of topical reports, References 4.3.2-17, 4.3.2-18, and 4.3.2-19. A more detailed description of the experimental results and analysis of the axial and X-Y xenon transient tests is presented in Reference 4.3.2-20 and Section 1 of Reference 4.3.2-23.

4.3.2.7.6 Stability control and protection

The excore detector system is utilized to provide indications of xenon induced spatial oscillations. The readings from the excore detectors are available to the operator and also form part of the protection system.

1. Axial power distribution - For maintenance of proper axial power distributions, the operator is instructed to maintain an axial offset within a prescribed operating band, based on the excore detector readings. Should the axial offset be permitted to move far enough outside this band, the protection limit will be reached and the power will be automatically reduced.

   Twelve foot pressurized water reactor cores become less stable to axial xenon oscillations as fuel burnup progresses. However, free xenon oscillations are not allowed to occur except for special tests. The full length control rod banks are sufficient to dampen and control any axial xenon oscillations present. Should the axial offset be inadvertently permitted to move far enough outside the control band due to an axial xenon oscillation, or any other reason, the protection limit on axial offset will be reached and the power will be automatically reduced.

2. Radial power distribution - The core described herein is calculated to be stable against X-Y xenon induced oscillations at all times in life.

The X-Y stability of large pressurized water reactors has been further verified as part of the startup physics test program for pressurized water reactor cores with 193 fuel assemblies. The measured X-Y stability of the cores with 157 and 193 assemblies was in good agreement with the calculated stability as discussed in Sections 4.3.2.7.4 and 4.3.2.7.5. In the unlikely event that X-Y oscillations occur, backup actions are possible and would be implemented, if necessary, to increase the natural stability of the core. This is based on the fact that several actions could be taken to make the moderator temperature coefficient more negative, which would increase the stability of the core in the X-Y plane.

Provisions for protection against non-symmetric perturbations in the X Y power distribution that could result from equipment malfunctions are made in the protection system design. This includes control rod drop, rod misalignment and asymmetric loss of coolant flow.

A more detailed discussion of the power distribution control in pressurized water reactor cores is presented in Reference 4.3.2-5.

4.3.2.8 Vessel Irradiation

A brief review of the methods and analyses used in the determination of neutron and gamma ray flux attenuation between the core and the pressure vessel is given below. A more complete discussion on the pressure vessel irradiation and surveillance program is given in Section 5.3.

The materials that serve to attenuate neutrons originating in the core and gamma rays from both the core and structural components consist of the core baffle, core barrel, neutron pads, and associated water annuli, all of which are within the region between the core and the pressure vessel.

In general, few group neutron diffusion theory and nodal analysis codes are used to determine fission power density distributions within the active core and the accuracy of these analyses is verified by incore measurements on operating reactors. Region and rodwise power sharing information from the core calculations is then used as source information in two-dimensional S_n transport calculations which compute the flux distributions throughout the reactor.

The neutron flux distribution and spectrum in the various structural components varies significantly from the core to the pressure vessel. Representative values of the neutron flux distribution and spectrum are presented in Table 4.3.2-6. The values listed are based on time averaged equilibrium cycle reactor core parameters and power distributions and, thus, are suitable for long term nvt projections and for correlation with radiation damage estimates.

As discussed in Section 5.3.1, the irradiation surveillance program utilizes actual test samples to verify the accuracy of the calculated fluxes of the vessel.

4.3.3 ANALYTICAL METHODS

Calculations required in nuclear design consist of two distinct types, which are performed in sequence:

1. Generation of macroscopic few-group parameters.

2. Space-dependent, few-group diffusion calculations.

4.3.3.1 Macroscopic Group Constants

Macroscopic few-group constants and analogous microscopic cross sections are generated by MICBURN-2 and CASMO (References 4.3.3.14 & 4.3.3.12) or MICBURN-3 and CASMO-3G (Reference 4.3.3-15). MICBURN is a multigroup one-dimensional transmission probability code which calculates the microscopic burnup in an absorber rod containing initially homogeneously distributed gadolinia and generates effective cross-sections as a function of the gadolinia number density to be used in a CASMO assembly depletion. CASMO is a multi-group two-dimensional transmission probability code for burnup calculations on assemblies or pin cells. The nuclear cross-section library used by MICBURN and CASMO contains cross-section data based on a multi-energy-group structure derived from ENDF/B-IV files.

The first stage of the CASMO calculation, at each burnup step, consists of generating regional macroscopic cross sections from the nuclear data library and the current number densities. These cross-sections are then used in a micro group calculation to obtain detailed neutron energy spectra to be used for energy condensation to 7 groups and spatial homogenization for each pin type. This calculation is repeated for each pin type in an assembly.

A two-dimensional 7 energy group transport theory calculation is then made over the entire assembly with each pin cell being explicitly modeled. In the burnup calculation, the isotopic depletions are calculated separately in each fuel pin. The fluxes obtained from the transport theory calculation are used to condense cross sections to a two group structure to be used in XTGPWR (Reference 4.3.3-13) and PRISM (Reference 4.3.3-15). Group constants for control rods are calculated in a similar manner. CASMO, XTGPWR, and PRISM are capable of modeling all cell types necessary for PWR design applications. Validation of the cross section method is discussed in detail in Reference 4.3.3-10.

4.3.3.2 Spatial Few-Group Diffusion Calculations

Spatial few-group calculations consist primarily of two-group X-Y-Z calculations using XTGPWR (Reference 4.3.3-13) or PRISM (Reference 4.3.3-15). XTGPWR is a three-dimensional modified two group diffusion theory reactor simulator program which is designed to operate with large mesh sizes. XTGPWR uses diffusion theory to solve for the fast group flux in each node. The thermal flux is calculated from the fast flux assuming the only source of thermal neutrons is slowing from the fast group and no thermal leakage occurs within each node. After a specified number of iterations, the cross-sections are updated to reflect power dependence on xenon, Doppler broadening, thermal-hydraulic feedback, and iteration on critical boron concentration, power search, or control rod adjustment. XTGPWR and PRISM uses pin power data from CASMO to determine peak power information.

The usage of XTGPWR and PRISM is in safety analysis calculations in, X-Y-Z power and burnup distributions, critical boron concentrations, control bank worths, and reactivity coefficients and defects.

Axial calculations are used to determine differential control rod worth curves (reactivity versus rod insertion) and axial power shapes during steady state and transient xenon conditions.

4.3.4 REVISIONS

This section was deleted by Amendment No. 45.

REFERENCES: SECTION 4.3

4.3.1-1 Barry, R. F., "LEOPARD - A Spectrum Dependent Non-Spatial Depletion Code for the IBM-7094," WCAP-3269-26, September, 1963.

4.3.1-2 Barry, R. F. and Altomare, S., "The TURTLE 24.0 Diffusion Depletion Code," WCAP-7213-P-A (Proprietary) and WCAP-7758-A (Non-Proprietary) January, 1975.

4.3.1-3 Deleted by Amendment No.43.

4.3.1-4 "Westinghouse Anticipated Transients Without Reactor Trip Analysis," WCAP-8330, August, 1974.

4.3.1-5 "Generic Mechanical Licensing Report for Advanced 17 x 17 Fuel Design", EMF-93-074(P)(A) and Supplement 1, June, 1994.

4.3.1-6 "Extended Burnup Evaluation of Westinghouse Fuel", WCAP-10125-P-A, December 1985.

4.3.2-1 "EXXON Nuclear Analysis of Power Distribution Measurement Uncertainty for Westinghouse PWR's" XN-NF-79-6 (P) (A) Revision 1 and Amendment 1, October 1983.

4.3.2-2 "Power Distribution Measurement Uncertainty for INPAX-W In Westinghouse Plants" EMF-93-164(P) (A), February 1995.

4.3.2-3 Deleted by Amendment No. 45.

4.3.2-4 Deleted by Amendment No. 45.

4.3.2-5 "PDC-3: Advanced Nuclear Fuels Corporation Power Distribution Control for Pressurized Water Reactors and Application of PDC-3 to H.B. Robinson Unit 2" ANF-88-054(P)(A), October 1990.

4.3.2-6 Deleted by Amendment No. 45.

4.3.2-7 McFarlane, A. F., "Power Peaking Factors," WCAP-7912-P-A (Proprietary) and WCAP-7912-A (Non-Proprietary), January, 1975.

4.3.2-8 Meyer, C. E. and Stover, R. L., "Incore Power Distribution Determination in Westinghouse Pressurized Water Reactors," WCAP-8498, July, 1975.

4.3.2-9 "Augmented Startup and Cycle 1 Physics Program Supplement 1," WCAP-8575 Supplement 1, June 1976 (Westinghouse Proprietary) and WCAP-8576, June 1976 (Non-Proprietary).

4.3.2-10 Cermak, J. O., et.al., "Pressurized Water Reactor pH - Reactivity Effect Final Report," WCAP-3696-8 (EURAEC-2074), October, 1968.

4.3.2-11 Ford, W. E., III, et.al., "A 218-Group Neutron Cross-Section Library in the AMPX Master Interface Format for Criticality Safety Studies," ORNL/CSD/TM 4 (July, 1976).

4.3.2-12 Greene, N. M., et.al., "AMPX: A Modular Code System for Generating Coupled Multigroup Neutron-Gamma Libraries from ENDF/B," ORNL/TM 3706 (March 1976).

4.3.2-13 Petrie, L. M. and Cross, N. F., "KENO IV--An Improved Monte Carlo Criticality Program." ORNL 4398 (November, 1975).

4.3.2-14 Deleted by Amendment No. 40

4.3.2-15 Deleted by Amendment No. 40

4.3.2-16 Deleted by Amendment No. 40

4.3.2-17 Poncelet, C. G. and Christie, A. M., "Xenon-Induced Spatial Instabilities in Large PWRs," WCAP-3680 20 (EURAEC 1974), March, 1968.

4.3.2-18 Skogen, F. B. and McFarlane, A. F., "Control Procedures for Xenon-Induced X Y Instabilities in Large PWRs," WCAP-3680 21 (EURAEC 2111), February, 1969.

4.3.2-19 Skogen, F. B. and McFarlane, A. F., "Xenon Induced Spatial Instabilities in Three-Dimensions," WCAP-3680 22 (EURAEC 2116), September, 1969.

4.3.2-20 Lee, J. C., et.al., "Axial Xenon Transient Tests at the Rochester Gas and Electric Reactor," WCAP-7964, June, 1971.

4.3.2-21 Barry, R. F., et.al., "The PANDA Code," WCAP-7048 P A (Proprietary) and WCAP-7757 A (Non-Proprietary), January, 1975.

4.3.2-22 England, T. R., "CINDER - A One-Point Depletion and Fission Product Program," WAPD-TM-334, August, 1962.

4.3.2-23 Eggleston, F. T., "Safety Related Research and Development for Westinghouse Pressurized Water Reactors, Program Summaries Winter 1976", WCAP-8768, Revision 1, June, 1977.

4.3.2-24 Deleted by Amendment No. 42

4.3.2-25 Deleted by Amendment No. 45.

4.3.2-26 Deleted by Amendment No. 54

4.3.2-27 "Shearon Harris Unit 1 and Brunswick Units 1&2, Original Criticality Analysis Report," 89CP*-G-0005, NFS 404.0404.

4.3.2-28 "BWR 7 x 7, 8 x 8S, and 8 x 8 R K-Infinity Calculations," NFS 2489-0018, DeVoe, M. J., March 1989.

4.3.2-29 Deleted by Amendment 52

4.3.2-30 Deleted by Amendment No. 45.

4.3.2-31 Deleted by Amendment No. 54.

4.3.2-32 NUREG/CR-0200: "SCALE: A Modular Code System for Performing Standardized Computer Analyses for Licensing Evaluation."

4.3.2-33 NUREG/CR-0073: "Critical Separation Between Subcritical Clusters of 4.31 wt% Enriched UO_2 Rods in Water with Fixed Neutron Poison."

4.3.2-34 Deleted by Amendment No. 54.

4.3.2-35 M. Edenius and A. Ahlin, "CASMO-3: New Features, Benchmarking and Advanced Applications," Nuclear Science and Engineering, 100, 342-351, (1988).

4.3.2-36 J.F. Briesmeister, Editor, "MCNP - A General Mote Carlo N-Particle Transport Code, Version 4A," LA-12625, Los Alamos National Laboratory (1993).

4.3.2-37 Deleted by Amendment No. 54.

4.3.2-38 Shearon Harris Criticality Evaluation, Framatome ANP Report 77-5069740 (Proprietary)

4.3.2-39 HI-97,760, HOLTEC Report, "Licensing Report for Expanding Storage Capacity in Harris Pools C and D."

4.3.3-1 Deleted by Amendment No. 45.

4.3.3-2 Deleted by Amendment No. 45.

4.3.3-3 Deleted by Amendment No. 45.

4.3.3-4 Deleted by Amendment No. 45.

4.3.3-5 Deleted by Amendment No. 43.

4.3.3-6 Deleted by Amendment No. 43.

4.3.3-7 Deleted by Amendment No. 45.

4.3.3-8 Deleted by Amendment No. 45.

4.3.3-9 Deleted by Amendment No. 45.

4.3.3-10 "EXXON Nuclear Neutronics Design Methods For Pressurized Water Reactors" XN-75-27(P)(A), Supplement 4, December, 1986.

4.3.3-11 Deleted by Amendment No. 45.

4.3.3-12 CASMO-2E: "A Fuel Assembly Burnup Program", Studsvik/NR-81 (Restricted), Studsvik Energiteknik AB.

4.3.3-13 "XTG: A Two Group Three-Dimensional Reactor Simulator Utilizing Coarse Mesh Spacing", XN-CC-28(A) Revision 3, September, 1975.

4.3.3-14 MICBURN-2: "Microscopic Burnup in Burnable Absorber Rods", Studsvik/NR-82/153 (Restricted), Studsvik Energiteknik AB.

4.3.3-15 EMF-96-029(P)(A) Volumes 1 and 2, "Reactor Analysis System for PWRs Volume 1-Methodology Description, Volume 2 Benchmarking Results", Siemens Power Corporation,

4.4 THERMAL AND HYDRAULIC DESIGN

4.4.1 DESIGN BASIS

The overall objective of the thermal and hydraulic design of the reactor core is to provide adequate heat transfer which is compatible with the heat generation distribution in the core such that heat removal by the Reactor Coolant System (RCS) or the Emergency Core Cooling System (ECCS) (when applicable) assures that the following performances and safety criteria requirements are met;

1. Fuel damage (defined as penetration of the fission product barrier, i.e., the fuel rod clad) is not expected during normal operation and operational transients (ANS Condition I) or any transient conditions arising from faults of moderate frequency (ANS Condition II). It is not possible, however, to preclude a very small number of rod failures resulting in the release of fission products. The CVCS is designed to remove the fission products from the reactor coolant, keeping the reactor coolant activity within plant design bases limits.

2. The reactor can be brought to a safe state following a Condition III event with only a small fraction of the fuel rods damaged (see above definition) although sufficient fuel damage might occur to preclude resumption of operation without considerable outage time.

3. The reactor can be brought to a safe state and the core can be kept subcritical with acceptable heat transfer geometry following transients arising from Condition IV events.

4. In order to satisfy the above requirements, the following design bases have been established for the thermal and hydraulic design of the reactor core.

4.4.1.1 Departure from Nucleate Boiling Design Basis

1. Basis - There will be at least a 95 percent probability that departure from nucleate boiling (DNB) will not occur on the limiting fuel rods during normal operation, operational transients, or during transient conditions arising from faults of moderate frequency (ANS Condition I and II events), at a 95 percent confidence level. Historically this has been conservatively met by adhering to the following thermal design basis: there must be at least a 95 percent probability that the minimum departure from nucleate boiling ratio (DNBR) of the limiting power rod during ANS Condition I and II events is greater than or equal to the DNBR limit of the DNB correlation being used. The DNBR limit for the correlation is established based on

the variance of the correlation such that there is a 95 percent probability with 95 percent confidence that DNB will not occur when the calculated DNBR is at the DNBR limit.

The Shearon Harris reactor core is designed so that the minimum calculated DNB ratio during normal operation, including anticipated transients, is greater than or equal to the safety limit specified in Section 4.4.2.2.1.

2. Discussion - By preventing departure from nucleate boiling (DNB), adequate heat transfer is assured between the fuel clad and the reactor coolant, thereby preventing clad damage as a result of inadequate cooling.

   Maximum fuel rod surface temperature is not a design basis as it will be within a few degrees of the coolant temperature during operation in the nucleate boiling region. Limits provided by the Reactor Control System and the Reactor Protection System (RPS) are such that this design basis will be met for transients associated with ANS Condition II events, including overpower transients. There is an additional large DNBR margin at rated power operation and during normal operating transients.

4.4.1.2 Fuel Temperature Design Basis

1. Basis - During modes of operation associated with ANS Condition I and ANS Condition II events, fuel centerline melt will be precluded. By precluding fuel melting, the fuel geometry is preserved and possible adverse effects of molten fuel on the cladding are eliminated.

2. Discussion - Fuel rod thermal evaluations are performed at rated power, maximum overpower and during transients at various burnups. These analyses assure that this design basis as well as the fuel integrity design bases given in Section 4.2 are met. They also provide input for the evaluation of ANS Condition III and IV events given in Chapter 15.

4.4.1.3 DELETED

4.4.1.4 Hydrodynamic Stability Design Basis

1. Basis - Modes of operation associated with ANS Condition I and II events shall not lead to hydrodynamic instability.

4.4.1.5 Other Considerations

The above design bases together with the fuel clad and fuel assembly design bases given in Section 4.2.1 are sufficiently comprehensive that no additional limits are required.

Fuel rod diametral gap characteristics, moderator-coolant flow velocity and distribution, and moderator void are not inherently limiting. Each of these parameters is incorporated into the thermal and hydraulic models used to ensure that above mentioned design criteria are met. For instance, the fuel rod diametral gap characteristics change with time (see Section 4.2.3.3) and the fuel rod integrity is evaluated on that basis. The effect of the moderator flow velocity and distribution (see Section 4.4.2.2) are included in the core thermal evaluation and thus affect the design bases.

4.4.2 DESCRIPTION

4.4.2.1 Summary

The reactor is designed to a minimum DNBR limit as well as no fuel centerline melting during normal operation, operational transients and faults of moderate frequency.

All DNB analyses performed have considered the effects of transition cores.

4.4.2.2 Critical Heat Flux Ratio or Departure from Nucleate Boiling Ratio and Mixing Technology

DNBRs are calculated by using the correlation and definitions described in Sections 4.4.2.2.1 and 4.4.2.2.2. The XCOBRA IIIC computer code is used to determine the flow distribution in the core and the local conditions in the hot channel for use in the DNB correlation. The use of hot channel factors is discussed in Section 4.4.2.2.4.

4.4.2.2.1 Departure from nucleate boiling technology

The HTP DNB correlation (Reference 4.4.2-68) is used to evaluate critical heat flux in the AREVA fuel assemblies. The Biasi DNB correlation (Reference 4.4.2-69) is used in the evaluation of the Steamline Break cases because the hydraulic conditions are outside the range of the HTP correlation. A Mixed Core Penalty is imposed on the DNBR safety limit when the core is composed of hydraulically different fuel designs. Following SGR/PUR the entire core is comprised of 17 x 17 High Thermal Performance fuel assemblies with Intermediate Flow Mixers (HTP/IFM) supplied by AREVA thus no mixed core penalty is required.

4.4.2.2.2 Definition of departure from nucleate boiling ratio

The DNB ratio is defined as the ratio of the critical heat flux to the local heat flux at the same core location. A DNB ratio equal to the safety limit corresponds to a 95 percent probability at a 95 percent confidence level that DNB does not occur.

DNB is not an observable parameter during reactor operation. Therefore, the observable parameters, reactor power, reactor coolant temperature, flow rate, and pressure have been related to DNB through the DNB correlation. With the exception of steamline break, the coolant conditions commonly encountered during steady-state operation and Anticipated Operational Occurrences (AOO) in PWRs are within the range of the HTP correlation.

4.4.2.2.3 Mixing technology

The turbulent mixing parameter Bs/D, is defined with "B" as the ratio of the turbulent cross flow mass flux between adjacent subchannels to the average mass flux in the axial direction. The parameter "s" is the gap spacing and "D" is the hydraulic diameter. The turbulent mixing parameter is employed in XCOBRA-IIIC simulations of the fuel assembly to describe enthalpy transport between subchannels due to turbulent exchange and diversion crossflow. The turbulent mixing parameter for the HTP fuel is determined from hot mixing tests.

4.4.2.2.4 Hot channel factors

1. Hot channel factors for heat flux and enthalpy rise, F_q and FΔH -The total hot channel factors for heat flux and enthalpy rise are defined as the maximum-to-core average ratios of these quantities. The heat flux hot channel factor (F_q) considers the local maximum linear heat generation rate at a point (the hot spot), and the enthalpy rise hot channel factor (FΔH) involves the maximum integrated linear heat generation rate along a channel (the hot channel).

   Each of the total hot channel factors is composed of a nuclear hot channel factor describing the fission power distribution and an engineering hot channel factor, which allows for variations in flow conditions and fabrication tolerances. The engineering hot channel factors are made up of subfactors which account for manufacturing uncertainties in fuel pellet diameter, density, and enrichment as well as the effect of densification.

2. Engineering hot channel factor, F_E - The engineering hot channel factor is used to evaluate the maximum linear heat generation rate in the core. This subfactor is determined by statistically combining the fabrication uncertainties for fuel pellet diameter, density, and enrichment, as well as the effect of densification. A conservative value of 1.03 is used.

   The actual heat flux at each axial location in the assembly is calculated with the XCOBRA-IIIC code. That actual heat flux is then used in the calculation of MDNBR. To account for fuel manufacturing uncertainties and densification, the actual heat flux is increased by 3% in the MDNBR calculation. Application of this uncertainty factor in the MDNBR calculation does not affect the enthalpy rise in the subchannels.

3. Inlet flow maldistribution - A design basis of 5 percent reduction in reactor coolant flow to the hot assembly and the adjacent assemblies is used in the XCOBRA-IIIC analysis.

4. Flow redistribution - The flow redistribution accounts for the reduction in flow in the hot channel resulting from the high flow resistance in the channel due to the local or bulk boiling. The effect of the non-uniform power distribution is inherently considered in the XCOBRA-IIIC analysis for every operating condition which is evaluated.

5. Effects of rod bow on DNBR - The phenomenon of fuel rod bowing must be accounted for in the safety analysis of Condition I and Condition II events for each plant application. The impact of rod bowing on MDNBR and peak linear heat rate (LHR) is evaluated using the AREVA Rod Bowing Methodology (Reference 4.4.2-71).

4.4.2.2.5 DNB propagation

According to References 4.4.2-72 and 4.4.2 73, propagation of DNB failures is considered for PWRs when the following two conditions exist simultaneously:

1. When the DNB limiting rod of a bundle is calculated to have a MDNBR below the 95/95 limit value of the DNB correlation being used; and

2. When the internal pressure of the DNB limiting rod exceeds core pressure at the time of MDNBR.

Since internal rod pressures exceed core pressure only at high exposures where rod power levels are relatively low and DNB is not expected to occur, DNB propagation is not an issue for AREVA fuel.

4.4.2.3 Hydraulic Loads

The Fuel Assembly holddown springs are designed to keep the fuel assemblies in contact with the lower core plate under all ANS Condition I and II events with the exception of the pump overspeed transient associated with a loss of external load. The holddown springs are designed to tolerate the possibility of an over deflection associated with fuel assembly liftoff for this case and provide contact between the fuel assembly and the lower core plate following this transient. More adverse flow conditions occur during a loss-of-coolant accident. These conditions are presented in Section 15.6.5.

Hydraulic loads at normal operating conditions are calculated considering the mechanical design flow which is described in Section 5.1 and accounting for the minimum core bypass flow based on manufacturing tolerances. Core hydraulic loads at cold plant startup conditions are based on the cold mechanical design flow, but are adjusted to account for the coolant density difference. Conservative core hydraulic loads for a pump overspeed transient, which could possibly create flow rates 20 percent greater than the mechanical design flow, are evaluated to be almost 2 times the dry fuel assembly weight.

4.4.2.4 Thermal Effects of Operational Transients

DNB core safety limits are generated as a function of reactor coolant temperature, pressure, core power and axial power imbalance. Steady state operation within these safety limits insures that the minimum DNBR is not less than the safety analysis limit. This system provides adequate protection against anticipated operational transients that are slow with respect to fluid transients, e.g., uncontrolled rod bank withdrawal at power incident (see Section 15.4.2). Specific protection functions are provided as described in Section 7.2 and the use of these protection functions is described in Chapter 15.

4.4.2.5 Flux Tilt Considerations

Significant quadrant power tilts are not anticipated during normal operation since this phenomenon is caused by some asymmetric perturbation. A dropped or misaligned rod cluster control assembly could cause changes in hot channel factors; however, these events are analyzed separately in Chapter 15.

4.4.3 THERMAL HYDRAULIC COMPATIBILITY ANALYSIS

This section has been retained for historical purposes, even though the entire SGR/PUR core will be comprised of HTP/IFM fuel assemblies. None of the conclusions presented in this section are affected by the use of an all - HTP/IFM core.

The results of the thermal hydraulic compatibility analysis for SPC HTP/IFM fuel assemblies co-resident with Westinghouse LOPAR and VANTAGE 5 fuel assemblies in the Shearon Harris core are presented in this section.

As part of a general thermal hydraulic compatibility analysis, the HTP/IFM fuel has been evaluated relative to:

1. Core pressure drop
2. DNB performance
3. RCS loop Flow
4. Fuel centerline melt temperature
5. Guide tube and total core bypass flow
6. Control rod drop time
7. Mixed core liftoff effects

Key design parameters for the SPC and Westinghouse fuel assemblies are given in Table 4.4.3-1.

4.4.3.1 XCOBRA-IIIC Model

For the pressure drop, DNB performance, and RCS loop flow analyses, a core flow model is required to predict core pressure drop, core flow and enthalpy distributions, and rod surface heat fluxes. The XCOBRA-IIIC computer code (Reference 4.4.3-1) was used to calculate these parameters.

The XCOBRA-IIIC model represents a 1/8 symmetric segment of the core. Each fuel assembly in the 1/8 core model is treated as a hydraulic channel. Axial nodalization consists of 30 nodes in the fuel rod region, plus four additional nodes for the upper tie plate, the upper unheated region, the lower tie plate, and the inlet orifice region of each assembly. Within each hydraulic channel, the mass, axial momentum, and energy equations are solved to determine the local axial pressure gradient, axial flow, and enthalpy. Mass, axial momentum and energy contributions due to lateral crossflow between adjacent hydraulic channels are included in the calculations. The lateral crossflow between assemblies (channels) at each axial elevation is determined from the transverse momentum equation that is applied to each assembly-to-assembly interface.

XCOBRA-IIIC models the assembly inlet, outlet, and spacer loss coefficients, friction factors, flow areas, and power levels of the different fuel types in the core. Axial and lateral crossflows for any one fuel type are influenced by the loading pattern and the relative number of the various fuel type(s) present in the core. Hydraulic differences in upper and lower tie plate designs generally have only minor, if any, impact on DNB performance. This is because the axial extent of crossflows caused by these components is not large enough to impact hydraulic conditions at elevations where DNB occurs in a fuel assembly.

The loss coefficients for the SPC HTP/IFM fuel and for the Westinghouse VANTAGE 5 fuel are derived from pressure drop tests performed in SPC's Portable Hydraulic Test Facility (PHTF). The pressure drop testing characterized the component loss/flow coefficients of the lower tie

plate (including the adjacent spacer and the inlet hardware), bare rod friction, spacers, and the upper tie plate (including the adjacent spacer and the exit hardware).

Other inputs for the core flow model include the axial and radial power distributions, and plant operating conditions. A chopped cosine axial profile with a 1.55 peak-to-average ratio was assumed for the thermal hydraulic compatibility analysis. The axial profile distribution used in this analysis is presented in Figure 4.4.3-1. The Cycle 6 core loading pattern for 1/8 of a core is shown in Figure 4.4.3-2. Figure 4.4.3-3 shows the radial power distribution used in this analysis. This distribution is representative of the Cycle 6 transition core for EOC conditions. The plant operating conditions used in the thermal hydraulic compatibility analysis are presented in Table 4.4.3-2.

4.4.3.2 Core Pressure Drop

The purpose of this analysis is to define the change in core pressure drop for the transition from an all Westinghouse VANTAGE 5 core to the Cycle 6 mixed core and finally to an all SPC HTP/IFM core. The pressure drop is seen to decrease very slightly for the Cycle 6 mixed core as compared to an all Westinghouse VANTAGE 5 core. The decrease in core pressure drop is primarily due to a lower loss coefficient at the core inlet for the SPC assemblies. The pressure drop for an all SPC HTP/IFM core increases by a small amount over that of the Cycle 6 mixed core. This is primarily due to the decreased flow area in the SPC fuel assemblies relative to the VANTAGE 5 fuel assemblies.

4.4.3.3 RCS Loop Flow

The introduction of SPC HTP/IFM fuel changes the core pressure drop by a small amount and this will affect the actual RCS loop flow. The results of the RCS loop flow analysis show that the Cycle 6 core will experience a negligible increase in loop flow. A core fully loaded with SPC HTP/IFM fuel will experience a 0.3% decrease in loop flow. A decrease in actual loop flow rate will not reduce predicted DNB margins because the minimum technical specification flow rate is used in the Chapter 15 DNB event analyses.

4.4.3.4 DNB Performance

The objective of this analysis is to demonstrate that the DNB performance for Westinghouse fuel will not be degraded in Cycle 6 relative to an all VANTAGE 5 core. The DNB correlation for the VANTAGE 5 fuel is proprietary; therefore, XCOBRA-IIIC was not used to predict DNB for the VANTAGE 5 fuel. The DNB performance for VANTAGE 5 fuel was evaluated based on flow and enthalpy distributions from the XCOBRA-IIIC calculations. Since the DNB performance is strongly related to flow and enthalpy distributions, inferences can be made regarding the performance of the VANTAGE 5 fuel in the presence of the SPC HTP/IFM fuel. Enthalpy rise is primarily affected by the power to flow ratio. DNB performance of the VANTAGE 5 fuel will not be degraded if flow and enthalpy in the VANTAGE 5 fuel are not degraded by the introduction of SPC HTP/IFM fuel. DNB performance of LOPAR fuel is not of concern due to the low power level of LOPAR fuel relative to fresh SPC fuel.

The presence of LOPAR fuel will also influence the flow and enthalpy distributions in the VANTAGE 5 fuel. The Westinghouse LOPAR fuel has a lower spacer loss coefficient than either the Westinghouse VANTAGE 5 or the SPC HTP/IFM fuel and it also does not have IFM grids. However, the assembly flow area for LOPAR fuel is less than for VANTAGE 5 fuel and

similar to SPC fuel. There is a net flow diversion to LOPAR fuel from both VANTAGE 5 and SPC fuel.

Power differences between SPC and VANTAGE 5 and LOPAR fuel assemblies will also influence the flow and enthalpy distributions in the VANTAGE 5 assemblies. The SPC HTP/IFM fuel assemblies will operate at power levels greater than the VANTAGE 5 fuel assemblies during Cycle 6. This will result in flow diversion from SPC assemblies to VANTAGE 5 and LOPAR assemblies.

XCOBRA-IIIC calculations indicate that the net effect of differences in hydraulic resistances, flow area, and power distributions will be increased flow and decreased enthalpy in the VANTAGE 5 assemblies. Thus, DNB ratios in VANTAGE 5 fuel (Reference 4.4.3-5) will not be degraded in relation to an all VANTAGE 5 core and relative to Cycle 5.

4.4.3.5 Fuel Centerline Melt Temperature

The statistical setpoint analysis determined the LHR limit to preclude centerline melt for both UO_2 and gadolinia rods. The gadolinia rods result in a more limiting LHR than UO_2 rods for Cycle 6. The centerline melt limit represents the maximum allowable LHR on a UO_2 rod to preclude centerline melt on a gadolinia rod, and therefore, also precludes centerline melt on UO2 rods. Chapter 15 analyses for Condition II events assure that the centerline melt criteria is met.

4.4.3.6 Guide Tube and Total Core Bypass Flow

The objective of this evaluation was to determine the change in guide tube and total core bypass flow from Cycle 5 to the Cycle 6 transition core and to an all SPC HTP/IFM core. The evaluation considered:

1. Guide tube design effects,

2. Core pressure drop effect, and

3. Effects of changes in the relative distribution of guide tube inserts (rodlets).

The results from this analysis are presented in Table 4.4.3-3. The total core bypass flow fraction increases from 6.6% in Cycle 5 to 6.8% for the Cycle 6 transition core. For a core fully loaded with SPC fuel, the total core bypass flow fraction increases to 7.1%. The bypass flow increase is primarily due to guide tube design changes and the relative distribution of the different type of fuel inserts. The slightly increased pressure drop for the SPC core will cause a negligible increase in the core remainder, the vessel to upper head, and the inlet to exit nozzle bypass fractions.

The weep holes are larger in the SPC design than in the Westinghouse LOPAR and VANTAGE 5 designs. The upper guide tube diameter is also larger leading to increased diametral clearances in the annulus around partially inserted control rods and the thimble plugs. Both of these differences will lead to reduced flow resistance and greater guide tube bypass flow in the SPC design. The guide tube fluid exit temperature will be lower in the SPC design and the margin to boiling in the guide tube will be greater given the same heat generation in the absorbers.

4.4.3.7 Rod Drop Time

The objective of this evaluation was to verify that the control rod drop times for the Cycle 6 transition core are less than the Technical Specification allowed rod drop time of 2.7 seconds. The analysis also verified that the control rod drop times for an all SPC HTP/IFM core will meet the Technical Specification limits for rod drop time. The evaluation considered:

1. Guide tube design changes, and

2. Raising the starting position of the control rods from 228 steps to 231 steps.

The results of the evaluation verify that the SPC HTP/IFM fuel for Cycle 6 and for an all SPC core will meet the Technical Specification limits for rod drop time. The following provides a summary of the evaluation results:

1. The fall of the control rod is controlled by the fluid egress from the guide tube via the weep holes and the annular space between the guide tube and the control rod. Since the diameter of the weep holes and the upper guide tube inside diameter are larger for the SPC fuel design, it has less fluid resistance than the VANTAGE 5 design. The control rods will fall faster for the SPC HTP/IFM design as compared to the VANTAGE 5 design. The LOPAR design is very similar to the SPC HTP/IFM design.

2. The control rods for the SPC HTP/IFM and the Westinghouse LOPAR designs will arrive at the dashpot region sooner and with higher velocity than for the Westinghouse VANTAGE 5 design. Since the elevation of the dashpots are equivalent, the significant portion of the drop time is less for the SPC HTP/IFM and Westinghouse LOPAR designs than for the VANTAGE 5 design.

3. The dashpot inner diameter and the drain hole diameter at the bottom of the guide tube are identical for all designs. Since the velocity is higher at entry for the SPC HTP/IFM and the Westinghouse LOPAR designs, the drop time in this region will also be shorter.

4. The higher starting position is estimated to increase the drop time by 0.03 seconds. Based on Cycle 4 (Reference 4.4.3-2) and Cycle 5 (Reference 4.4.3-3) startup test date, the maximum drop time for the VANTAGE 5 design is 2.18 seconds. The added time provides a total drop time of 2.21 seconds for the VANTAGE 5 design. This is well within the 2.7 seconds required by the Technical Specifications.

5. The drop time for the SPC HTP/IFM and the Westinghouse LOPAR designs will be shorter than the Westinghouse VANTAGE 5 fuel assemblies for all phases of the drop. Since the Westinghouse VANTAGE 5 fuel assemblies satisfy the Technical specification for drop time, the SPC HTP/IFM fuel for Cycle 6 and an all SPC core will meet the Technical Specification limits for rod drop time.

4.4.3.8 Mixed Core Liftoff Effects

Because flow is diverted to the Westinghouse assemblies, there is a slight increase in hydraulic force on those assemblies. The objective of this evaluation was to determine whether this effect would negate the holddown margins of the co-resident fuel designs. Using results of XCOBRA-IIIC cases, comparisons were made of the pressure drop changes for the co-resident fuel

designs. The slight increases were then compared to the liftoff design margins for these assemblies. The comparison showed that sufficient holddown margin will be maintained in the mixed core condition (Reference 4.4.3-4).

The effect of momentary liftoff of the SPC assemblies on the holddown springs has been evaluated. After momentary liftoff due to pump overspeed, the holddown springs will properly seat the assemblies, and liftoff in normal operation is prevented (i.e., the function of the holddown springs is maintained).

No adverse effects are expected for either a lifted assembly or an adjacent seated assembly for the following reasons. Because of the interface between the core plate interface pins and the tie plates, no mechanical interaction between ends of the assemblies can occur. At the mid region of the core, contact between assemblies is possible because of assembly bow and cage flexibility. However, damage is precluded because the spacer grids are designed to align with the co-resident fuel (i.e., adjacent spacer side plates still overlap in this condition), and act as barriers between the two assemblies during this momentary liftoff. Finally, because the condition is momentary, no adverse effects from unusual cross flows are expected.

4.4.4 INSTRUMENTATION REQUIREMENTS

4.4.4.1 Incore Instrumentation

Instrumentation is located in the core so that movable neutron detectors provide radial, axial, and azimuthal core characteristics for all core quadrants and fixed thermocouples provide radial characteristics for all core quadrants.

The Incore Instrumentation System is comprised of thermocouples, positioned to measure fuel assembly coolant outlet temperatures at preselected positions, and fission chamber detectors that can be positioned in guide thimbles which run the length of selected fuel assemblies to measure the neutron flux distribution. Figure 4.4.4-1 shows the number and location of instrumented assemblies in the core.

The incore instrumentation is provided to obtain data from which fission power density distribution in the core, reactor coolant enthalpy distribution in the core, and fuel burnup distribution may be determined.

4.4.4.2 Overtemperature and Overpower ΔT Instrumentation

The overtemperature ΔT trip protects the core against low DNBR. The overpower ΔT trip protects against excessive power (fuel cladding protection).

As discussed in Section 7.2.1.1.2, factors included in establishing the overtemperature ΔT and overpower ΔT trip setpoints includes the reactor coolant temperature in each reactor coolant loop and the axial distribution of core power through the use of the two section excore neutron detectors.

4.4.4.3 Instrumentation to Limit Maximum Power Output

The output of the three ranges (source, intermediate, and power) of detectors, with the electronics of the nuclear instruments, are used to limit the maximum power output of the reactor within their respective ranges.

There are 7 radial locations containing a total of 11 neutron flux detectors installed around the reactor in the primary shield. There is one power range detector that is used for startup testing that is located on the 90 degree "flat" portion of the core. There are two proportional counters for the source range installed at opposite (0 degree and 180 degree) "flat" portions of the core at an elevation approximately one quarter of the core height. Two compensated ionization chambers for the intermediate range, located in the same instrument wells and detector assemblies as the source range detectors, are positioned at an elevation corresponding to 1/2 the core height. There are also two NFMS fission chamber detectors located in the same instrument wells and below the assemblies which house the source and intermediate range detectors. Four dual section uncompensated ionization chamber assemblies for the power range are installed vertically on the minor axis of the core (45 degree, 135 degree, 225 degree, and 315 degree) and are verified equidistant from the reactor vessel at the top and bottom of the detector and, to minimize neutron flux pattern distortions, as close as practical to the vessel. Each power range detector provides two signals corresponding to the neutron flux in the upper and in the lower sections of a core quadrant. The three ranges of detectors are used as inputs to monitor neutron flux from a completely shutdown condition to 120 percent of full power with the capability of recording (via ERFIS) overpower excursions up to 200 percent of full power.

The output of the power range channels is used for:

1. The rod speed control function,

2. Alerting the operator to an excessive power unbalance between the quadrants,

3. Protecting the core against the consequences of rod ejection accidents and

4. Protecting the core against the consequences of adverse power distributions resulting from dropped rods.

Details of the neutron detectors, nuclear instrumentation design, and the control and trip logic are given in Chapter 7. The limits on neutron flux operation and trip setpoints are given in the Technical Specifications.

4.4.4.4 Loose Parts Monitoring System (Metal Impact Monitoring System)

The SHNPP Metal Impact Monitoring System is designed to enable early detection of debris which may collect in the steam generators or the reactor vessel. The loose parts monitoring system used at SHNPP is the Westinghouse Digital Metal Impact Monitoring System (MIMS). The system consists of detectors, preamplifiers, signal processors, and display.

The detectors are high temperature accelerometers mounted on the lower head of each steam generator, on the reactor vessel head flange, and on incore instrument conduit near the bottom of the reactor vessel. The system accelerometer sensitivity is 25 pico coulombs/g $\pm$ 10 percent.

4.4.4.4.1 System description

There are ten (10) loose parts monitoring sensors (accelerometers) located in pairs to provide for sensor redundancy. Each of the five (5) pairs of sensors are located on equipment (reactor vessel, steam generators) to monitor natural collection regions of the primary system where loose parts are likely to be found.

The sensor provides an output of 25 pico coulombs/g to the charge preamplifier which converts this into a voltage of 25 millivolts/g. The sensor and charge preamplifier are designed to operate in normal containment environment.

A block diagram of the MIMS is shown in Figure 4.4.4-2.

The vendor supplies (as an option) operator training in the operation, trouble shooting, and calibration of the system.

4.4.4.4.2 Normal operation

Activities anticipated during normal operation include diagnostic tests of the MIMS, channel checks of the sensor channels, response to events identified by the MIMS as impacts, and reinitialization of the MIMS should power be interrupted for a prolonged period of time. The other activities which may be performed during normal operation include modification of the alert setpoint of each of the sensor channels, read out of data on impact events identified by the MIMS, and aural monitoring and recording of each of the sensor channels. The diagnostic tests include internal checks of the circuit logic used to analyze sensor signals, checks of channel integrity and internal CPU power supply, and checks of the keyboard and displays.

Additional activities which will be performed are a weekly aural monitoring of the operable channels and a quarterly measurement of the background noise level on each channel.

Appropriate procedure or qualified personnel using technical information provided by the manufacturer will be used to perform manual activities.

4.4.4.4.3 Response to alarms

As discussed in Section 4.4.4.4.1 upon detection of noise which matches the signature programmed into the MIMS for a loose part, the MIMS will automatically record the channel number, date, time, and maximum amplitude for the event. Data on events exceeding the alarm point are retained for up to 48 hours and the data can be obtained from the MIMS by a display, tape recorder, or a printer. An indication above the alarm setpoint will actuate an alarm on the main control board.

The MIMS is designed to preclude alarms during operation of the control rod drive system; however, the MIMS alarm is not inhibited on a Reactor Trip or other routine events or anticipated transients which may cause alarms. Operating Procedures will provide instruction for the response to an alarm. The procedures will direct the Operators to review other indications for integrity of the Reactor Coolant pressure boundary and the integrity of the fuel and note other events such as pump starts, reactor or turbine trip or other transients which were concurrent with the alarm.

The Operator will review alarms in an attempt to determine if they were caused by events other than a loose part. This review will be based upon previous experience with the MIMS system including the results of alarm evaluations previously performed by engineering personnel, and it will also include activities such as aural monitoring of current noise levels following the alarm. No further action is required if the alarm is determined to be the result of an event other than a loose part.

Otherwise, the Operators will record information on the status of the reactor control system, note any transients which were concurrent with the alarm, and provide this information in an alarm event report to engineering personnel by the beginning of the next working day.

The report will be evaluated to correlate diverse information from sources such as process instrumentation with the MIMS alarm and determine if a loose object exists. The diagnosis of an alarm event report may include review of any additional alarms, analysis of the background noise, comparison of the background noise with earlier measurements and review of the status of the reactor coolant system concurrent with the alarm.

Additional factors which may be used to confirm the existence or absence of a loose object are the geometry of the collection area being monitored, flow conditions in the collection areas, the impact acceleration and the location and number of channels which show concurrent events. Records of alarm report reviews will be maintained for future reference.

If the diagnosis concludes that a loose object is present, the significance of the object with respect to the integrity of the Reactor Coolant System and the fuel will be determined.

Reports of the determination that a loose object has been identified will be made to the NRC in accordance with the reporting requirements of the Technical Specifications for the SHNPP.

A Baseline Data Acquisition Study was performed on the Metal Impact Monitoring System to ensure compliance with the sensitivity requirements of Regulatory Guide 1.133, Revision 1. System alert (alarm) setpoint changes, incorporated as a result of this study, were reported to the NRC per Reference 4.4.4-3.

4.4.4.5 Reactor Coolant System Flow Rate Measurement

Total reactor flow (total flow through the vessel from all loops) is required to be above a minimum value as established by the Technical Specifications. In order to maintain this minimum flow rate a calorimetric flow measurement is performed at least once per 18 months.

Reactor coolant loop flow is determined from the steam generator thermal output, corrected for the loop's share of the net pump heat input, and the enthalpy rise (Δh) of the coolant. Total reactor flow is the sum of the individual loop flows. Table 4.4.4-1 lists the calorimetric equations and defines the terms.

To establish the overall flow measurement uncertainty, the accuracy and relationship to flow of each instrument used for the calorimetric measurements (see Table 4.4.4-2) has been determined. There are several components (transducer, converter, isolator, readout device, etc.) which contribute to the overall uncertainty of the measurement. Reference 4.4.4-1 provides a list of typical components involved in the calorimetric loop flow measurement, a corresponding conservative instrument error allowance and the effect of the instrument error

allowance on the calculated power or flow value. The overall loop flow measurement uncertainty is the statistical combination of the individual uncertainties as shown on Reference 4.4.4-1. Total reactor flow measurement uncertainty is the statistical combination of the individual loop flow uncertainties as shown on Reference 4.4.4-1.

Reference 4.4.4-2 has analyzed the HNP instrument configuration for its effect on calculation of RCS flow measurement when steam generator blowdown is secured. The total uncertainty of determining the RCS flow using the precision calorimetric calculation is 1.60%.

When blowdown is in service, the additional uncertainty contribution of the blowdown instrumentation is negligible per Reference 4.4.4-2. (Since blowdown is only approximately 1% of feed flow, the precision calorimetric calculation is relatively insensitive to blowdown uncertainties.) Per Reference 4.4.4-2, the small blowdown measurement uncertainties are not statistically significant as compared to the flow uncertainty calculated by Reference 4.4.4-1 and therefore do not contribute any additional uncertainty in normalization of the RCS elbow tap. This yields the same confidence in the RCS flow measurement as when blowdown is secured.

In summary, individual loop flow is determined by performance of a calorimetric flow measurement and these values summed to arrive at total reactor flow. The measurement uncertainty is determined by statistically combining individual component and loop uncertainties. A calorimetric flow measurement must be performed to take credit for this particular measurement uncertainty.

4.4.4.6 Reactor Vessel Level Indicating System (RVLIS)

Information utilized to give the operator an advance warning of the approach to ICC and to monitor the recovery from ICC, if it occurs, is obtained via a qualified instrumentation package. The information is obtained by the use of the Reactor Vessel Level Indicating System (RVLIS) and incore exit thermocouples.

4.4.4.6.1 System description

The Westinghouse RVLIS installed at SHNPP represents the most recent Westinghouse design. It is a fully qualified and redundant system for monitoring water inventory in the reactor vessel. Each of the two channels provide differential pressure cells and transmitters for narrow and wide range monitoring over the full length of the vessel, with the reactor coolant pumps off (natural circulation) and on, respectively. Additionally, narrow range monitoring is provided for each channel of the upper plenum during natural circulation. Each channel's microprocessor utilizes these D/P signals in conjunction with other inputs such as RCS pressure, RCS temperature, (loop RTDs or incore thermocouples), RVLIS reference leg temperature sensors, to compensate for density changes in the system reference legs so as to provide direct water level readings available for operator use.

Qualified incore thermocouples are utilized to determine core exit temperature. These 51 thermocouples (26 channel A, 25 channel B) are inputs to and processed by the RVLIS microprocessors. The minimum required number of thermocouples is two trains of two thermocouples per quadrant with the additional requirement that the two thermocouples per train are paired so that one is located near the center of the core and the other thermocouple is located near the core perimeter. This additional requirement ensures that a single failure will not disable the ability to determine the radial temperature gradient across any core quadrant.

Both RVLIS water level readings and incore exit thermocouple data are data-linked to the ERFIS computer for primary display on the SPDS display which is located on the MCB. The data link is supplied from an isolated non-Class 1E output from the qualified RVLIS microprocessors. Although ERFIS is non-Class 1E, it is powered from a high reliability power source and is located adjacent to the Main Control Room. The RVLIS Train A cabinet and associated isolation device is located on the 286 ft level of the RAB and the RVLIS Train B cabinet and associated isolation device is located on the 305 ft level of the RAB adjacent to the Main Control Room.

Additionally, qualified microprocessor outputs (RVLIS water level and thermocouple data) are transmitted to dedicated redundant backup displays. These backup displays are alpha-numeric and qualified (Class 1E), and are located in the control room. The primary and backup displays have a selective capability for providing RVLIS water level, thermocouple data, and temperature mapping functions.

The input to the ERFIS computer is also used to determine the margin of saturation which can be displayed on demand (at operator request) on the SPDS display. The plant computer (ERFIS) processes and calculates subcooling data using temperature and pressure signals from the reactor coolant system. Displayed information includes margin of subcooling data both graphically and in engineering units.

In accordance with the provisions of Regulatory Guide 1.97, Rev. 3, operator confirmation of subcooling data is provided through the use of qualified pressure and temperature signals and ASME steam tables.

Design analysis and an evaluation of instruments to monitor water level, and available test data to support the design described above may be found in NUREG CR 2628 regarding the Westinghouse RVLIS design and is available for the incore exit thermocouple instrumentation.

Although the system sensors and microprocessors are not directly testable at power for calibration, the calculated parameter of margin to saturation can be readily verified at power through use of the steam tables and observation of the independent indications of pressure and temperature. These observations should show higher margin to saturation since the system uses conservatively auctioneered values.

RVLIS meets the intent of Regulatory Guide 1.97.

Technical Specifications for the instrumentation specifically installed for the detection of inadequate core cooling will consider the recommendations of NRC's Standard Technical Specifications (STS) for Westinghouse PWRs (Rev. 4).

Thermocouples utilized for the core exit for each core quadrant (in conjunction with core inlet temperature data) are sufficient to provide indication of radial distribution of the coolant enthalpy (temperature) rise across representative regions of the core.

The primary display has the following capabilities:

1. A spatially oriented core map indicating the temperature or temperature difference across the core (at each thermocouple location) is displayed on the CRT.

2. A selective reading of core exit temperature, which is consistent with parameters pertinent to operator actions in connection with plant-specific inadequate core cooling procedures is continuous on demand.

3. Direct readout and hard copy capability is available for all thermocouple temperatures. The range meets the 200°F to 2300°F requirement of Regulatory Guide 1.97. Hard copy is provided by computer printout.

4. Trend capability showing the temperature-time history of representative core exit temperature values is available on demand.

5. Alarms are provided in the control room. These alarms will be set to be consistent with the decision points in the emergency operating procedures.

6. The operator display device (CRT) interface is located in accordance with human-factor design in order to provide rapid access to requested displays.

A backup display in the Control Room is provided with the capability for selective reading of each of the operable thermocouples. The range meets the 200°F to 2300°F requirement of Regulatory Guide 1.97.

The types and locations of displays and alarms will take into account the following:

1. The use of this information by an operator during both normal and abnormal plant conditions.

2. Integration into emergency procedures.

3. Integration into operator training.

4. Other alarms during an emergency and need for prioritization of alarms.

The instrumentation meets the requirements of Appendix B, "Design and Qualification Criteria for Accident Monitoring Instrumentation."

The primary and backup display channels are electrically independent, energized from independent station Class 1E power sources, and physically separated in accordance with Regulatory Guide 1.75 up to and including the isolation devices. The primary display and associated hardware beyond the isolation device are energized from a high reliability power source. The backup display, associated hardware, and power source is Class 1E.

Primary and backup display are located in the control room envelop. Backup display will be completely qualified in accordance with IEEE 323 (1974) and 344 (1975) as defined in WCAP-8587, "Methodology for Qualifying Westinghouse WRD Supplied Safety Related Electrical Equipment" and WCAP-8687, "Equipment Qualification Test Reports." The isolation device is located in an area which is accessible for maintenance following an accident.

The primary and backup display channels are designed to provide 99 percent availability for each channel with respect to functional capability to display a minimum of four thermocouples per core quadrant. This can be accomplished since each quadrant will contain a minimum of

two paired thermocouples for each of Train A and Train B. ICC systems will be addressed in the technical specifications.

Quality assurance meets the requirements of 10 CFR 50 as applicable. This is further addressed in Section 1.8 (Reg. Guide 1.97).

ICC instrumentation will be installed and preoperational tests will be completed before fuel load. Startup tests and calibrations which require the core to be in place will be completed prior to operation above 10 percent of full power.

SHNPP Emergency Operating Procedures (EOPs) and Functional Restoration Procedures (FRPs) incorporate the Westinghouse Owners' Group Emergency Response Guidelines and Functional Restoration Guidelines. These procedures employ inadequate core cooling (ICC) instrumentation (RVLIS, the core exit thermocouples, and the subcooling data) along with other post-accident monitoring capabilities (i.e., reactor coolant system pressure, reactor coolant pump status, and safety injection flow). Therefore, SHNPP instrumentation for monitoring ICC is used in accordance with the emergency response guidelines developed by the Westinghouse Owners' Group. The emergency response guidelines were accompanied by extensive analysis of the setpoints used in the critical safety function status tree and the functional restoration guidelines. These analyses are referenced in WOG Revision 1 (High Pressure Plant) Emergency Response Guidelines.

The SHNPP EOP for ICC will refer the operator to functional restoration procedures based on the readings on the ICC instrumentation. The SHNPP functional restoration procedures will incorporate the Westinghouse Owners' Group Functional Restoration Guidelines C.1, C.2, and C.3. The actions specified for the operator are fully addressed in WOG submittals.

REFERENCES: SECTION 4.4

4.4.1-1 Deleted by Amendment No. 45.

4.4.2-1 through 4.4.2-67 deleted by Amendment No. 45.

4.4.2-68 HTP: Departure from Nucleate Boiling Correlation for High Thermal Performance Fuel, EMF-92-153(P)(A) Revision 1, Siemens Power Corporation, Richland, WA 99352, January 2005.

4.4.2-69 L. Biasi et al, "Studies on Burnout, Part 3 - A New Correlation for Round Ducts and Uniform Heating and its Comparision with World Data", Energia Nucleare, Volume 14, Number 9, September 1967.

4.4.2-70 Application of Exxon Nuclear Company PWR Thermal Margin Methodology to Mixed Core Configurations, XN-NF-82-21(P)(A), Revision 1, Exxon Nuclear Company, Richland, WA 99352, September 1983.

4.4.2-71 Computational Procedure for Evaluating Fuel Rod Bowing, XN-75-32(P)(A), Supplements 1, 2, 3, and 4, Exxon Nuclear Company, Richland, WA 99352, October 1983.

4.4.2-72 Qualification of Exxon Nuclear Fuel for Extended Burnup, XN-NF-82-06(P)(A) Revision 1, and Supplements 2, 4, and 5, Exxon Nuclear Company, Richland, WA 99352, October 1986.

4.4.2-73 Qualification of Advanced Nuclear Fuels' PWR Design Methodology for Rod Burnups of 62 GWd/MTU, ANF-88-133(P)(A), and Supplement 1, Advanced Nuclear Fuels Corporation, Richland, WA 99352, December 1991.

4.4.2-74 Generic Mechanical Licensing Report for Advanced 17x17 Fuel Design, EMF-93-074(P)(A) and Supplement 1, Siemens Power Corporation, Richland, WA 99352, June 1994.

4.4.3-1 XCOBRA-IIIC: A Computer Code to Determine the Distribution of Coolant During Steady-State and Transient Core Operation, XN-NF-75-21(P)(A), Revision 2, Exxon Nuclear Company, Richland, WA 99352, January 1986.

4.4.3-2 Shearon Harris Cycle 4, Startup Up Test Report, File: NF-908.04, Serial: NF-91-297.

4.4.3-3 Shearon Harris Cycle 5, Startup Up Test Report, File: NF-908.04, Serial: NF-93-006.

4.4.3-4 Letter from D.D. Davis (CP&L) to L. Stephens (SPC), File: NF-404.0803, Serial: NF-93A-0756, dated November 12, 1993.

4.4.3-5 Westinghouse Cycle 5 Reload Transition Report Rev. 1 October, 1992.

4.4.4-1 Moomau, W.H., "Westinghouse Improved Thermal Design Procedure Instrument Uncertainty Methodology for Carolina Power and Light Harris Nuclear Plant (for Uprate to 2912.4 Mwt-NSSS Power and Replacement Steam Generators)," WCAP-12340 Rev. 1, January 2000.

4.4.4-2 Calculation HNP-I/INST-1011, "Harris (CQL) Calorimetric and Loop RCS Flow Uncertainty for Uprate to 2912.4 Mwt NSSS Power."

4.4.4-3 CP&L Letter to NRC, "Loose Parts Monitoring System - Alert Setpoint Revision," Serial: HNP-96-192, dated October 31, 1996.

4.5 REACTOR MATERIALS

4.5.1 CONTROL ROD DRIVE SYSTEM STRUCTURAL MATERIALS

4.5.1.1 Materials Specifications

All parts of the Control Rod Drive Mechanism (CRDM) that are exposed to reactor coolant are made of metals which resist the corrosive action of the water. Three types of metals are used exclusively: stainless steels, nickel chromium iron, and cobalt based alloys. In the case of stainless steels, only austenitic and martensitic stainless steels are used. The martensitic stainless steels are not used in the heat treated conditions which cause susceptibility to stress corrosion cracking or accelerated corrosion in the Westinghouse pressurized water reactor water chemistry. Precipitation hardening and martensitic stainless steels were not used as structural materials in control rod drive mechanism applications. Materials with yield strengths

greater than 90,000 psi are 410 SS, Haynes 25, and Inconel X-750. Their usage and properties are presented in the following paragraphs. No maximum yield strength has been specified for austenitic stainless steels used in fabricating the CRDM. Table 4.5.1-1 identifies the 400 series stainless steel items used in the fabrication of the CRDM.

a) Pressure vessel - All pressure containing materials of the CRDM comply with Section III of the ASME Boiler and Pressure Vessel Code, and are fabricated from austenitic (Type 304) stainless steel.

For those components of the CRDM outside the scope of the "code", Section 4.5.1 and those sections of Chapter 5 referenced in Section 4.5.1 discuss the acceptability of such components. In addition, Table 5.2.3-1 gives the material specifications for these components.

b) Coil stack assembly - The coil housings require a magnetic material. Ductile iron has been successfully tested and used for SHNPP. The finished housings are zinc flame sprayed to provide corrosion resistance.

Coils are wound on bobbins of molded Dow Corning 302 material, with double glass insulated copper wire. Coils are then vacuum impregnated with silicon varnish. A wrapping of mica sheet is secured to the coil outside diameter. The result is a well-insulated coil capable of sustained operation at 200 C.

c) Latch assembly - Magnetic pole pieces are fabricated from Type 410, ASTM-A-276, stainless steel. All non-magnetic parts, except pins and springs, are fabricated from Type 304 stainless steel. Haynes 25 is used to fabricate link pins. Haynes 25 is used in the solution treated and cold worked condition. Springs are made from nickel-chromium-iron alloy (Inconel-X). Latch arm tips are clad with Stellite-6 to provide improved wearability. Hard chrome plate and Stellite-6 are used selectively for bearing and wear surfaces.

d) Drive rod assembly - The drive rod assembly utilizes a Type 410 stainless steel drive rod. The coupling is machined from Type 403 stainless steel. Other parts are Type 304 stainless steel, with the exception of the springs which are nickel-chromium-iron alloy, and the locking button, which is Haynes 25.

4.5.1.2 Fabrication and Processing of Austenitic Stainless Steel Components

The discussions provided in Section 5.2.3 concerning the processes, inspections, and tests on austenitic stainless steel components to assure freedom from increased susceptibility to intergranular corrosion caused by sensitization, and the discussions provided in Section 5.2.3 on the control of welding of austenitic stainless steels, especially control of delta ferrite, are applicable to the austenitic stainless steel pressure housing components of the CRDM.

4.5.1.3 Contamination Protection and Cleaning of Austenitic Stainless Steel

The CRDMs are cleaned prior to delivery in accordance with the guidance of ANSI 45.2.1. Process specifications in packaging and shipment are discussed in Section 5.2.3. Westinghouse personnel conduct surveillance of these operations to assure that manufacturers and installers adhere to appropriate requirements, as discussed in Section 5.2.3.

4.5.2 REACTOR INTERNALS MATERIALS

4.5.2.1 Materials Specifications

All the major material for the reactor internals is Type 304 stainless steel. Parts not fabricated from Type 304 stainless steel include bolts and dowel pins, which are fabricated from Type 316 stainless steel, and radial support key bolts which are fabricated of InconelX-750. These materials are listed in Table 5.2.3 2. Strain hardened (cold worked) Type 316 stainless steel is used for threaded fasteners, fuel assembly guide pins ,and replacement guide tube support pins and nuts and these are the only applications of cold worked stainless steel. For SHNPP and strain hardened type 316, a maximum yield strength of 85 KSI (90 KSI for replacement guide tube support pins and nuts) was specified. There are no other materials used in the reactor internals or core support structures which are not included in the ASME Code, Section III, Appendix I with exception of ASTM A-511 material, which is an acceptable alternate replacement Thermal Sleeve material when lower section is removed to support head adapter nozzle inspections or Inside Diameter Temper Bead (IDTB) weld repairs. Precipitation hardening and martensitic stainless steels were not used in the construction of reactor internals for SHNPP.

4.5.2.2 Controls on Welding

The discussions provided in Section 5.2.3 are applicable to the welding of reactor internals and core support components. The core support component weld inspection requirements are in accordance with ASME Section III, NG-5000.

4.5.2.3 Nondestructive Examination of Wrought Seamless Tubular Products and Fittings

The nondestructive examination of wrought seamless tubular products and fittings is in accordance with Section III of the ASME Code.

4.5.2.4 Fabrication and Processing of Austenitic Stainless Steel Components

Conformance of reactor internals and core support structures with Regulatory Guide 1.44 is discussed in Section 5.2.3 and Section 1.8.

Conformance of reactor internals and core support structures with Regulatory Guide 1.31 is discussed in Section 5.2.3 and Section 1.8.

Conformance of reactor internals with Regulatory Guide 1.34 is discussed in Section 1.8.

Conformance of reactor internals and core support structures with Regulatory Guide 1.71 is discussed in Section 1.8.

4.5.2.5 Contamination Protection and Cleaning of Austenitic Stainless Steel

The discussions provided in Section 5.2.3 and Section 1.8 are applicable to the reactor internals and core support structures and verify conformance with ANSI 45 specifications and Regulatory Guide 1.37.

4.6 FUNCTIONAL DESIGN OF REACTIVITY CONTROL SYSTEMS

4.6.1 INFORMATION FOR CONTROL ROD DRIVE SYSTEM (CRDS)

The CRDS is described in Section 3.9.4.1. Figures 3.9.4-1 and 3.9.4-2 provide the details of the control rod drive mechanisms, and Figure 4.2.2-8 provides the layout of the CRDS. No hydraulic system is associated with its functioning. The instrumentation and controls for the Reactor Trip System are described in Section 7.2 and the Reactor Control System is described in Section 7.7.

4.6.2 EVALUATION OF THE CRDS

The CRDS has been analyzed in detail in a failure mode and effects analysis (Reference 4.6.2-1). This study, and the analyses presented in Chapter 15.0, demonstrates that the CRDS performs its intended safety function, a reactor trip, by putting the reactor in a subcritical condition when a safety system setting is approached, with any assumed credible failure of a single active component. The essential elements of the CRDS (those required to ensure reactor trip) are isolated from non-essential portions of the CRDS (the Rod Control System) as described in Section 7.2.

Despite the extremely low probability of a common mode failure impairing the ability of the Reactor Trip System to perform its safety function, analyses have been performed in accordance with the requirements of WASH-1270. These analyses documented in References 4.6.2-2 and 4.6.2-3 have demonstrated that acceptable safety criterion would not be exceeded even if the CRDS were rendered incapable of functioning during a reactor transient for which their function would normally be expected.

The design of the control rod drive mechanism is such that failure of the control rod drive mechanism cooling system will, in the worst case, result in an individual control rod trip or a full reactor trip. See Section 9.4 for a description of the Control Rod Drive Ventilation System.

4.6.3 TESTING AND VERIFICATION OF THE CRDS

The CRDS is extensively tested prior to its operation. These tests may be subdivided into five categories: 1) prototype tests of components, 2) prototype CRDS tests, 3) production tests of components following manufacture and prior to installation, 4) onsite preoperational and initial startup tests, and 5) periodic inservice tests. These tests which are described in Section 3.9.4.4, 4.2, 14.2, and 16.2 are conducted to verify the operability of the CRDS when called upon to function.

4.6.4 INFORMATION FOR COMBINED PERFORMANCE OF REACTIVITY SYSTEMS

As is indicated in Chapter 15.0, the only postulated events which assume credit for reactivity control systems other than a reactor trip to render the plant subcritical are the steam line break, feedwater line break, Anticipated Transient Without Scram (ATWS), and loss-of-coolant accident. The reactivity control systems which are available to mitigate these accidents are the Reactor Trip System and the Safety Injection System (SIS). The Reactor Trip System is not credited in the Large Break LOCA since the associated hydraulic forces due to the event may preclude rod insertion. Section 15.6.5 describes the single failures assumed in the Large Break LOCA event analyses and provides a summary of the analytical results relative to 50.46

acceptance criteria. Additional information on the CRDS is presented in Section 3.9.4 and on the SIS in Section 6.3. The Technical Specifications require that some combination of boron injection paths be available from the CVCS Boric Acid Tank and/or the Safety Injection Refueling Water Storage Tank to ensure that negative reactivity control is available in each mode of operation. Section 15.4.6 shows that for postulated dilution events, the operator has sufficient time to determine the cause of dilution, terminate the source of the dilution, and initiate reboration before shutdown margin is lost. Section 15.8 describes the use of boron injection to mitigate an ATWS event. Information on the capabilities of the CVCS is provided in Section 9.3.4. The adverse boron dilution possibilities due to the operation of the CVCS are investigated in Section 15.4.6. Prior proper operation of the CVCS has been presumed as an initial condition to evaluate transients and appropriate Technical Specifications have been prepared to ensure the correct operation or remedial action.

4.6.5 EVALUATION OF COMBINED PERFORMANCE

The evaluation of the steam line break, feedwater line break and the loss-of-coolant accident which presume the combined actuation of the Reactor Trip System to the CRDS and the SIS are presented in Sections 15.1.5, 15.2.8 and 15.6.5. Reactor trip signals and safety injection signals for these events are generated from functionally diverse sensors and actuate diverse means of reactivity control, i.e., control rod insertion and injection of soluble poison.

Non-diverse, but redundant types of equipment, are only utilized in the processing of the incoming sensor signals into appropriate logic which initiates the protective action. This equipment is described in detail in Section 7.2 and 7.3. In particular, note that protection from equipment failures is provided by redundant equipment and periodic testing. Effects of failures of this equipment have been extensively investigated as reported in Reference 4.6.5-1. This failure mode and effects analysis verifies that any single failure will not have a deleterious effect upon the Engineered Safety Features Actuation System. Adequacy of the Emergency Core Cooling System and SIS performance under faulted conditions is verified in Section 6.3.

REFERENCES: SECTION 4.6

4.6.2-1 Shopsky, W. E., "Failure Mode and Effects Analysis (FMEA) of the Solid State Full Length Rod Control System" WCAP-8976, August, 1977.

4.6.2-2 "Westinghouse Anticipated Transients Without Trip Analysis," WCAP-8330, August, 1974.

4.6.2-3 Gangloff, W. C. and Loftus, W. D., "An Evaluation of Solid State Logic Reactor Protection in Anticipated Transients," WCAP-7706 L (Proprietary) and WCAP-7706 (Non-Proprietary), July, 1971.

4.6.2-4 Eggleston, F.T., Rawlins, D. H. and Petrow, J.R., "Failure Mode and Effects Analysis (FMEA) of the Engineering Safeguard Features Actuation System" WCAP-8584 (Proprietary) and WCAP-8760 (Non Prietary), April, 1976.

TABLE 4.1.1-1 ORIGINAL CORE REACTOR DESIGN COMPARISON TABLE

	THERMAL AND HYDRAULIC DESIGN PARAMETERS	SHEARON HARRIS	VIRGIL C. SUMMER NUCLEAR STATION
1.	Reactor Core Heat Output, Mwt	2775	2775
2.	Reactor Core Heat Output, 10^6 Btu/hr.	9471	9471
3.	Heat Generated in Fuel, Percent	97.4	97.4
4.	System Pressure, Nominal, psia	2250	2250
5.	System Pressure, Minimum Steady-State, psia	2220	2220
6.	Minimum Departure from Nucleate Boiling Ratio for Design Transients	>1.30	>1.30
	COOLANT FLOW		
7.	Total Thermal Flow Rate, 10^6 lbm/hr.	108.9	109.6
8.	Effective Flow Rate for Heat Transfer, 10^6 lb./hr.	102.3	102.6
9.	Effective Flow Area for Heat Transfer, $ft.^2$	41.6	41.6
10.	Average Velocity Along Fuel Rods, ft/sec.	15.6	15.6
11.	Average Mass Flux, 10^6 lb_m/hr.-$ft.^2$	2.46	2.47
	COOLANT TEMPERATURE, F		
12.	Nominal Inlet	557.4	556.0
13.	Average Rise in Vessel	62.9	62.8
14.	Average Rise in Core	66.4	66.6
15.	Average in Core	592.6	591.2
16.	Average in Vessel	588.8	589.0
	HEAT TRANSFER		
17.	Active Heat Transfer, Surface Area, $ft.^2$	48,600	48,600
18.	Average Heat Flux, BTU/hr.-$ft.^2$	189,800	189,800
19.	Maximum Heat Flux for Normal Operation, BTU/hr.-$ft.^2$	440,400(1)	440,400
20.	Average Thermal Output, kW/ft.	5.44	5.44
21.	Maximum Thermal Output for Normal Operation, kW/ft.	12.6(1)	12.6
22.	Peak Linear Power Resulting From Overpower Transients, Operator Errors, Assuming a Maximum Overpower of 118 Percent, kW/ft.	18.0(2)	18.0
23.	Heat Flux Hot Channel Factor, F_Q	2.32(3)	2.32
24.	Peak Fuel Central Temperature at 100 Percent Power, F	3250	3250
25.	Peak Fuel Central Temperature at Maximum Thermal Output for Maximum Overpower Trip Point, F	<4700	<4700
	FUEL ASSEMBLIES		
26.	Design	RCC Canless	RCC Canless
27.	Number of Fuel Assemblies	157	157
28.	UO2 Rods per Assembly	264	264
29.	Rod Pitch, in.	0.496	0.496
30.	Overall Dimensions, in.	8.4 x 8.4	8.4 x 8.4
31.	Fuel Weight (as UO2), lb.	181,190	181,190
32.	Zircaloy Weight, lb.	41,415	41,415
33.	Number of Grids per Assembly	8 - Type R	8 - Type R
34.	Loading Technique	3 region nonuniform	3 region nonuniform
	FUEL RODS		
35.	Number	41,448	41,448
36.	Outside Diameter, in.	.374	0.374
37.	Diametral Gap, in.	.0065	0.0065

TABLE 4.1.1-1 ORIGINAL CORE REACTOR DESIGN COMPARISON TABLE

THERMAL AND HYDRAULIC DESIGN PARAMETERS	SHEARON HARRIS	VIRGIL C. SUMMER NUCLEAR STATION
38. Clad Thickness, in.	.0225	0.0225
39. Clad Material	Zircaloy-4	Zircaloy-4
FUEL PELLETS		
40. Material	UO_2 Sintered	UO_2 Sintered
41. Density (Percent of Theoretical)	95	95
42. Diameter, in.	0.3225	0.3225
43. Length, in.	0.530	0.530
ROD CLUSTER CONTROL ASSEMBLIES		
44. Neutron Absorber	Ag-In-Cd 80 Percent, 15 Percent, 5 Percent or Hafnium 100 Percent	Ag-In-Cd
45. Cladding Material	Type 304 SS-Cold Worked	Type 304 SS-Cold Worked
46. Clad Thickness, in.	0.0185	0.0185
47. Number of Clusters, Full/Part Length	52/0	48/0
48. Number of Absorber Rods per Cluster	24	24
CORE STRUCTURE		
49. Core Barrel, I.D./O.D., in.	133.85/137.875	133.85/137.875
50. Thermal Shield, I.D./O.D., in.	Neutron Pad design	Neutron Pad design
STRUCTURE CHARACTERISTICS		
51. Core Diameter, in. (Equivalent)	119.7	119.7
52. Core Height, in. (Active Fuel)	144	144
REFLECTOR THICKNESS AND COMPOSITION		
53. Top - Water plus Steel, in.	~10	~10
54. Bottom - Water plus Steel, in.	~10	~10
55. Side - Water plus Steel, in.	~15	~15
56. H_2O/U Molecular Ratio Core, Lattice (Cold)	2.42	2.42
FUEL ENRICHMENT, W/O		
57. Region 1	2.10	2.10
58. Region 2	2.60	2.60
59. Region 3	3.10	3.10

(1) This is the value associated with F_Q = 2.32.

(2) See Section 4.3.2.2.6.

(3) This is the value of F_Q used for Thermal Hydraulic Design. The plant operating F_Q limit is given the the Technical Specifications.

TABLE 4.1.1-2

ANALYTIC TECHNIQUES IN CORE DESIGN

Analysis	Technique	Computer Code	Section Referenced
Mechanical Design of Core Internals Loads, Deflections, and Stress Analysis	Static and dynamic modeling	Blowdown code, FORCE, finite element structural analysis code and others	3.7.2.1 3.9.1
Fuel Rod Design Fuel Performance Characteristics (temperature, internal pressure, clad stress, etc.)	Model of fuel rod including consideration of fuel density changes, heat transfer, fission gas release, etc.	Westinghouse or AREVA fuel rod design models	4.2.1.3.1 4.3.3.1 4.4.2.2
Nuclear Design			
1. Cross Sections and Group Constants	Microscopic data, Macroscopic constants for homogenized core regions	Modified ENDF/B-4 library CASMO-2E/CASMO-3G/MICBURN-2/MICBURN-3	4.3.3.14.3.3.1
2. X-Y Power Distribution, Fuel Depletion, Critical Boron Concentrations, X-Y Xenon Distributions, Reactivity Coefficients, Axial Power Distributions, Control Rod Worths, and Axial Xenon Distribution	Three Dimensional Modified 2-Group Diffusion Theory	XTGPWR/PRISM	4.3.3.2
Thermal-Hydraulic Design	Subchannel analysis of local fluid conditions in rod bundles, including inertial and crossflow resistance terms, solution progresses from core-wide to hot assembly to hot channel	XCOBRA-IIIC	4.4.3.1

TABLE 4.2.2-1 COMPARISON OF 17 X 17 LOPAR, 17 X 17 VANTAGE 5 AND 17 X 17 AREVA ASSEMBLY DESIGN PARAMETERS

PARAMETER	17 X 17 LOPAR DESIGN	17 X 17 VANTAGE 5 DESIGN	17 X 17 AREVA DESIGN	ADVANCED W17 HTP AREVA DESIGN	W17 GAIA DESIGN (AREVA)
Fuel Assy Length, in.	159.765[(1)], 159.915[(2)]	159.975	159.61	159.61	159.86
Fuel Rod Length, in.	151.56[(1)], 151.62[(2)]	152.285	151.50	151.5	151.89
Assembly Envelope, in.	8.426	8.426	8.426	8.426	8.426
Compatible with Core Internals	Yes	Yes	Yes	Yes	Yes
Fuel Rod Pitch, in.	0.496	0.496	0.496	0.496	0.496
Number of Fuel Rods/Assy.	264	264	264	264	264
Number/Guide Thimble Tubes/Assy.	24	24	24	24	24
Number/Instrumentation Tube/Assy.	1	1	1	1	1
Compatible with Movable Incore Detector System	Yes	Yes	Yes	Yes	Yes
Fuel Tube Material	Zircaloy 4	Zircaloy 4	Zircaloy 4 or M5	M5	M5®
Fuel Rod Clad OD., in.	0.374	0.360	0.376	0.376	0.374
Fuel Rod Clad Thickness, in.	0.0225	0.0225	0.024	0.024	0.0225
Fuel/Clad Gap, mil.	6.5	6.2	6.5	6.5	6.5
Fuel Pellet Diameter, in.	0.3225	0.3088	0.3215	0.3215	0.3225
Fuel Pellet Length					
Enriched Fuel, in.	0.530 [(1)] 0.387 [(2)]	0.370	0.402	0.402	0.402
Blanket Fuel, in.	0.545	0.500	0.500	0.500	0.500

TABLE 4.2.2-1 COMPARISON OF 17 X 17 LOPAR, 17 X 17 VANTAGE 5 AND 17 X 17 AREVA ASSEMBLY DESIGN PARAMETERS

PARAMETER	17 X 17 LOPAR DESIGN	17 X 17 VANTAGE 5 DESIGN	17 X 17 AREVA DESIGN	ADVANCED W17 HTP AREVA DESIGN	W17 GAIA DESIGN (AREVA)
Guide Thimble Material	Zircaloy 4	Zircaloy 4	Zircaloy 4	Zircaloy 4	Q12®
Guide Thimble OD (above dashpot), in.	0.484(1) 0.482(2)	0.474	0.480	0.482	0.496
Guide Thimble Wall Thickness., in	0.018(1) 0.016(2)	0.016	0.016	0.016 (above dashpot) 0.042 (in dashpot)	0.023 (above dashpot) 0.050 (in dashpot)
Structural Mat'l - Six Inner Grids	Inconel	Zircaloy 4	Zircaloy 4	Zircaloy 4	M5®
Structural Mat'l - Two End Grids	Inconel	Inconel	Zircaloy 4 + Alloy 718 Springs	Zircaloy 4 (Uppermost, HTP) Nickel Alloy 718 (Lowermost, HMP)	Nickel Alloy 718
Material – Intermediate Flow Mixer Grids	None	Zircaloy 4	Zircaloy 4	Zircaloy 4	M5®
Grid Inner Strip Thickness, mil.	10.5 (Inc.)	18 (Zirc.)	34 (HTP)	34 (HTP) 25 (HMP)	15 (V10) 25 (HMP)
Grid Outer Strip Thickness, mil.	17.0 (Inc.)	26 (Zirc.)	26 (HTP)	26 (HTP) 25 (HMP)	21 (V10) 25 (HMP)
Grid Support for Fuel Rods	6 points; 2 springs + 4 dimples	6 points; 2 springs + 4 dimples	End Grids: 5 points; 1 spring + 4 dimples. HTP Grids: 8 Line Contact. IFMs: 4 Line Contact	HMP Grid-8 Line Contact HTP Grid-8 Line Contact IFM-4 Line Contact	V10 Grid – 8 Line Contact HMP Grid – 8 Line Contact IGM – Non-Contacting
(1) Cycle 1/initial core fuel (2) Cycle 2/Region 4 fuel					

TABLE 4.3.2-1

REACTOR CORE DESCRIPTION
(Typical Cycle)

Average Core	
Equivalent Diameter (in.)	119.7
Core Average Active Fuel Height, First Core, in. (nominal)	144
Height-to-Diameter Ratio	1.20
Total Cross Section Area $ft.^2$	78.14
Reflector Thickness and Composition	
Top - Water plus Steel (in.)	~10
Bottom - Water plus Steel (in.)	~10
Side - Water plus Steel (in.)	~15
Fuel Pellets	
Material	UO_2 Sintered
Density (percent of Theoretical)	95-96
Maximum Fuel Enrichment	5.0
Average Blanket Enrichment	0.72 or 2.60
Rod Cluster Control Assemblies	
Neutron Absorber	Ag-In-Cd
Composition	80%-15%-5%
Diameter, in.	0.34
Density, $lbs/in.^3$	0.367
Cladding Material	Type 304, Cold Worked Stainless Steel (WESTINGHOUSE). Type 316L Low Contaminant Stainless Steel (AREVA).
Clad Thickness, in.	0.0185
Number of Clusters, Full Length	52
Number of Absorber Rods per Cluster	24
Full Length Assembly Weight (dry), lb.	149 (Ag-In-Cd)
Gadolinia Bearing Fuel Rods (Per Typical Reload)	
Number	1200 to 1600
Material	UO_2-Gd_2O_3
Clad Material	Zircaloy-4 or M5
Initial Reactivity Worth, pcm	5000 (approx.)
Excess Reactivity	
Maximum Fuel Assembly k_∞ (Cold, Clean Unborated Water)	1.470
Maximum Core Reactivity (Cold, Zero Power, Beginning of Cycle)	1.030

TABLE 4.3.2-2 NUCLEAR DESIGN PARAMETERS (TYPICAL CYCLE)

Core Average Linear Power, kW/ft;	5.77	
Total Heat Flux Hot Channel Factor, F_Q	2.52***	
Nuclear Enthalpy Rise Hot Channel Factor, $F_{\Delta H}$	AREVA: 1.73 [1 + 0.35(1-P)]***	
Reactivity Coefficients		Best Estimate
Doppler-only Power, Coefficients, pcm/% Power (upper limit)		-20.2 to -12.6
(See Figure 15.0.4-1), Lower Limit		-15.2 to -11.2
Doppler Temperature Coefficient, pcm/F		-1.9 to -1.2
Moderator Temperature Coefficient, pcm/F		-1.0 to -38.0
Boron Coefficient, pcm/ppm		-10 to -5
Delayed Neutron Fraction and Lifetime		
β_{eff} BOL, (EOL)	0.0061 (0.0054)	
ℓ, BOL, (EOL) μ sec.	17.4 (19.1)	
Control Rods		
Rod Requirements	See Table 4.3.2-3	
Maximum Rod Worth, pcm^{++}	<2000	
Maximum Ejected Rod Worth		
Boron Concentrations (PPM)		
Zero Power, k_{eff} = 1.00, Cold, Rod Cluster Control Assemblies Out, 100 ppm Uncertainty Included	1875	

Boron Concentrations (PPM) (Continued)

TABLE 4.3.2-2 NUCLEAR DESIGN PARAMETERS (TYPICAL CYCLE)

Zero Power, k_{eff} = 1.00, Hot, Rod Cluster Control Assemblies Out, 100 ppm Uncertainty Included	1950
Design Basis Refueling Boron Concentration	2000***
Zero Power, $k_{eff} \leq 0.95$, Cold, Rod Cluster Control Assemblies In, 100 ppm Uncertainty Included	1950
Zero Power, k_{eff} = 1.00, Hot, Rod Cluster Control Assemblies Out	1850
Full Power, No Xenon, keff = 1.00, Hot, Rod Cluster Control Assemblies Out	1600
Full Power, Equilibrium Xenon, keff = 1.00, Hot, Rod Cluster Control Assemblies Out	1249
Reduction with Fuel Burnup Reload Cycle, ppm/GWD/MTU	-100

*Gigawatt Day (GWD) = 1000 Megawatt Day (1000 MWD).

++Note: 1 pcm = 10^{-5} $\Delta\rho$ where $\Delta\rho$ is calculated from two statepoint values of k_{eff} by ln (k_2/K_1)

***Current limits are located in the Technical Specifications

TABLE 4.3.2-3

REACTIVITY REQUIREMENTS FOR ROD CLUSTER CONTROL ASSEMBLIES

Reactivity Effects (percent)	Beginning-of-Life (Typical Cycle)	End-of-Life (Typical Cycle)
1. Control Requirements		
Fuel Temperature, Doppler, pcm	1300	1600
Moderator Temperature(1), pcm	350	850
Redistribution, pcm	300	400
Rod Insertion Allowance, pcm	200	300
2. Total Content, pcm	2150	3150
3. Estimated Rod Cluster Control Assembly Worth (52 Rods)		
a. All but one (highest worth) assemblies inserted, pcm	7300	7500
4. Estimated Rod Cluster Control Assembly credit with 10 percent adjustment to accommodate uncertainties, (item 3b-10 percent), pcm	6570	6750
5. Shutdown margin available (item 4 - item 2) pcm	4420	3600
6. Required Shutdown Margin, pcm	1770	1770

(1) Includes void effects.

TABLE 4.3.2-5

AXIAL STABILITY INDEX PRESSURIZED WATER REACTOR CORE
WITH A 12 FOOT HEIGHT

Burnup (MWD/MTU)	F_Z	C_B (ppm)	Stability Index ($hr.^{-1}$) Exp	Calc
1550	1.34	1065	-0.041	-0.032
7700	1.27	700	-0.014	-0.006
	Difference:	+0.027	+0.026	

TABLE 4.3.2-6

TYPICAL NEUTRON FLUX LEVELS (n/cm^2-sec) AT FULL POWER

	E >1.0 Mev	5.53 Kev < E <1.0Mev	0.625 ev ≤ E E<5.53 Kev	0.625 ev <$(nv)_0$
Core Center	6.73×10^{13}	1.18×10^{14}	8.92×10^{13}	3.14×10^{13}
Core Outer Radius at Mid-height	3.39×10^{13}	6.03×10^{13}	4.85×10^{13}	9.03×10^{13}
Core Top, on Axis	1.60×10^{13}	2.54×10^{13}	2.20×10^{13}	1.71×10^{12}
Core Bottom, on Axis	2.48×10^{13}	4.13×10^{13}	3.67×10^{13}	1.53×10^{13}
Pressure Vessel Inner Wall,* Aximuthal Peak, Core Mid-height	2.90×10^{10}	6.03×10^{10}	6.32×10^{10}	8.78×10^{11}

*Values were estimated prior to plant operation. Refer to Reactor Vessel Irradiation Surveillance Program Results for actual values.

Table 4.3.2-7

PWR Fuel Characteristics

Fuel Assembly	Westinghouse 17X17 Std	Westinghouse 17X17 V5	Westinghouse 15x15	FANP 17x17	FANP 15x15	AREVA Adv. W17 HTP
NOTE: All Dimensions in inches						
Clad O.D.	0.374	0.360	0.422	0.376	0.424	0.376
Clad Material	Zr-4	Zr-4	Zr-4	Zr-4	Zr-4	M5
Maximum Enrichment	5.0	5.0	5.0	5.0	5.0	5.0
Active Fuel Length	144	144	144	144	144	144
Number Fuel Rods	264	264	204	264	204	264
Fuel Rod Pitch	0.496	0.496	.0563	0.496	0.563	0.496
Number of Thimbles	24/1	24/1	21	25	21	24/1
Thimble O.D.	0.482/0.484	0.474/0.476	0.546	0.480	0.544	0.482
Thimble I.D.	0.450/0.448	0.442/0.440	0.512	0.448	0.511	0.450

Table 4.3.2-8

Pool C and D Analysis
Comparison of MCNP-4A and CASMO-3 Calculations

	PWR Rack	BWR Rack
Fuel Assembly	W 15x15	GE 8
Enrichment	5.0	4.6
Temperature	4°C	4°C
MCNP-4A k_{eff}	1.2004	0.9993
Uncertainties		
Calculational Statistics 0.0020		
Bias Uncertainty 0.0011		
Total Uncertainty at 95%/95%	0.0023	0.0023
Termperature Correction from 20°C to 4°C	0.0020	0.0020
Bias	0.0009	0.0009
MCNP-4A Maximum k_{eff}	1.2056	1.0045
CASMO-3 k_{inf}	1.2076	1.0126

Notes:

1. The MCNP-4A calculation correctly includes the effect of axial neutron leakage.

Table 4.3.2-9

Pool C and D
Summary of Criticality Safety Calculations for the PWR Fuel Racks

Fuel Assembly		Westinghouse 15x15
Enrichment		5%
Temperature		4°C
Burnup from Calculation (MWD/MTU)		41,352
Burnup from Curve (MWD/MTU)		41,447
CASMO-3 k_{inf}		
Uncertainties		
UO_2 density	0.0014	
Inner Box dimension	0.0017	
Box wall thickness	0.0005	
Boral width	0.0009	
B-10 loading	0.0041	
Burnup	0.0160	
Total Uncertainty at 95%/95%		0.0167
Effect of Axial Burnup Distribution		0.0157
Maximum k_{inf}		0.9450
Regulatory Limit		0.9500

Notes:

1. Only the most reactive assembly is shown.
2. The total uncertainty is a statistical combination of the manufacturing uncertainties.

Table 4.3.2-10

BWR Fuel Characteristics

Fuel Assembly	GE 3	GE 4	GE 7	GE 8	GE 9	GE 10	GE 13
NOTE: All dimensions in inches							
Clad O.D.	0.563	0.493	0.483	0.483	0.483	0.483	0.440
Clad Material	Zr-2	Zr-2	Zr-2	Zr-2	Zr-2	Zr-2	Zr-2
Maximum Enrichment	4.6	4.6	4.6	4.6	4.6	4.6	4.6
SCCG k_{inf}	≤1.32	≤1.32	≤1.32	≤1.32	≤1.32	≤1.32	≤1.32
Fuel Rod Array	7x7	8x8	8x8	8x8	8x8	8x8	9x9
Number Fuel Rods	49	63	62	60	60	60	74
Fuel Rod Pitch	0.738	0.640	0.640	0.640	0.640	0.640	0.566
Number of Water Rods	0	1	2	4	1	1	2
Water Road O.D.		0.493	0.591	0.591/0.483	1.34	1.34	0.980
Channel I.D.	5.278	5.278	5.278	5.278	5.278	5.278	5.278
Channel Thickness	0.080	0.080	0.080	0.080	0.080	0.070	0.070

Notes:

1. The GE 13 assembly has 8 part length rods.
2. The GE 5 and GE 6 are identical to the GE 7 for the fuel parameters listed.
3. The enrichment is the maximum planar average enrichment.

Table 4.3.2-11

Summary of Criticality Safety Calculations for the Pool C BWR Fuel Racks

Temperature		4°C	4°C	4°C	4°C	4°C	4°C	4°C
SCCG k_{inf}		1.32	1.32	1.32	1.32	1.32	1.32	1.32
Enrichment		4.6	4.6	4.6	4.6	4.6	4.6	4.6
CASMO-3 k_{inf}		0.9163	0.9140	0.9192	0.9214	0.9207	0.9201	0.9227
Uncertainties								
UO_2 density	0.0023							
Inner box dimension	0.0037							
Box wall thickness	0.0005							
Boral width	0.0018							
B-10 loading	0.0053							
Total uncertainty at 95%/95%		0.0071	0.0071	0.0071	0.0071	0.0071	0.0071	0.0071
Channel bulging		0.0045	0.0045	0.0045	0.0045	0.0045	0.0045	0.0045
Uncertainty for burnup and vendor comparison		0.0100	0.0100	0.0100	0.0100	0.0100	0.0100	0.0100
Maximum k_{inf}		0.9379	0.9356	0.9408	0.9430	0.9423	0.9417	0.9443
Regulatory Limit		0.9500	0.9500	0.9500	0.9500	0.9500	0.9500	0.9500

Notes:

1) The total uncertainty is a statistical combination of the manufacturing uncertainties.

2) The GE 13 assembly has part length rods. Two CASMO-3 calculations were performed: one with all rods present and the other with only the full-length rods present. The most reactive configuration was the second and the k_{inf} from this configuration is presented.

3) The GE 5 and GE 6 are identical to the GE 7 for the fuel parameters analyzed and therefore the GE 5 and GE 6 have a maximum k_{inf} equivalent to the GE 7.

4) The enrichment is the planar average enrichment.

TABLE 4.4.3-1

CYCLE 6 FUEL DESIGN PARAMETERS

	Westinghouse LOPAR	Westinghouse VANTAGE 5	SPC HTP/IFM
Number of Assemblies	9	96	52
Assembly pitch (in)	8.466	8.466	8.466
Fuel rod OD (in)	0.374	0.360	0.376
Guide Tube OD (in)	0.484	0.474	0.480
Instrument Tube OD (in)	0.484	0.476	0.480
Assembly Flow area (in^2)	38.071	40.388	37.836
Assembly hydraulic diameter (in)	0.437	0.481	0.433

TABLE 4.4.3-2

OPERATING PARAMETERS FOR THERMAL HYDRAULIC COMPATIBILITY ANALYSIS

Operating Condition	Value
Rated Core Power	2775 MWt
Maximum Overpower	40%
Operating Pressure	2250 psia
Inlet Temperature	557.4°F
RCS Nominal Coolant Flow Rate	305478 gpm
Bypass Flow Fraction	6.6%

TABLE 4.4.3-3

COMPARISON OF GUIDE TUBE BYPASS FLOW FRACTIONS

Component	Cycle 5	Cycle 6	All SPC HTP/IFM
Guide Tube	2.0	2.2	2.5
Core Remainder	1.6	1.6	1.6
Vessel-to-Upper Head	2.0	2.0	2.0
Inlet-to-Exit Nozzle[a.]	1.0	1.0	1.0
Total Bypass Fraction	6.6	6.8	7.1

(a) 1.0% cold, 0.225% hot

TABLE 4.4.4-1

REACTOR COOLANT LOOP FLOW CALCULATION

$$W_l = \frac{\left[Q_{SG} - Q_P + \frac{(Q_L)}{N}\right] V_c \ 0.12471}{[h_H - h_c]}$$

where:

W_L		=	Loop flow (gpm)
Q_{SG}	=		Steam generator thermal output (Btu/hr.)
Q_L		=	Primary system net heat losses (Btu/hr.)
N		=	Number of loops
Q_P		=	Reactor coolant pump heat added (Btu/hr.)
h_H		=	Hot leg enthalpy (Btu/lb.)
h_c		=	Cold leg enthalpy (Btu/lb.)
V_c		=	Cold leg specific volume (cu. ft/lb.)

$$Q_{SG} = \left(h_s - h_f\right) W_f - \frac{(E_b)}{N}$$

where:

h_s	=	Steam enthalpy (Btu/lb.)
h_f	=	Feedwater enthalpy (Btu/lb.)
W_F	=	Feedwater flow (lb./hr.)
E_b	=	SG blowdown heat flux (Btu/hr.)
N	=	Number of loops

$$W_f = KF_a\sqrt{P_f \Delta P}$$

where:

K	=	Feedwater venturi flow coefficient
F_a	=	Feedwater venturi correction for thermal expansion
P_F	=	Feedwater density (lb./cu. ft.)
ΔP	=	Feedwater venturi pressure drop (inches H_2O)

$$E_b = W_b \left(\frac{h_{si}}{N} - hb\right)$$

where:

w_b	=	Total blowdown flow (lb./hr.)
h_{si}	=	Sum of steam generator steam enthalpy (Btu/lb.) (hs_{sg1} + hs_{sg2} +…+hs_{sgn})
h_b	=	Equivalent enthalpy for SG blowdown

TABLE 4.4.4-1 (Continued)

$$h_b = \frac{[(W_s * h_s + Wco * \Delta hco + W_d * h_d) - (W_c * h_c)]}{W_b}$$

where:

W_S= Flash tank steam flow (lb./hr.)
h_s= Flash tank steam flow enthalphy (Btu/lb.)
Wco= SGBD Regen Hx cooling flow (lb./hr.)
Δhco= Enthalpy rise of cooling flow through Regen. Heat Exchanger (Btu/lb.)
W_d= Flash tank drain flow (lb./hr.)
h_d= Enthalphy of flash tank drain flow (Btu/lb.)
W_c= Mixing tee flow (lb./hr.)
h_c= Enthalpy of mixing tee condensate cooling flow (Btu/lb.)

TABLE 4.4.4-2

MEASUREMENTS REQUIRED

Parameter	Instrument	Function
1. Feedwater venturi pressure differential	Differential pressure gauge	Feedwater flow
2. Feedwater temperature	RTD	Feedwater enthalpy and density
3. Steam pressure	Transducer	Steam enthalpy
4. Reactor coolant T_{hot}	Narrow range RTD	RCS hot leg enthalpy
5. Reactor coolant T_{cold}	Narrow range RTD	RCS cold leg enthalpy RCS specific volume
6. Reactor coolant pressure	Transducer	RCS enthalpy and specific volume

Other information required for the calculation is as follows:

7. Feedwater venturi coefficient from vendor calibration.
8. A. Steam generator blowdown secured during the measurement.
   B. If steam generator blowdown is in service, blowdown instrumentation is required:
      Flash tank steam flow
      Flash tank pressure
      Drain flow
      Drain temperature
      Drain pressure
      Condensate flow
      Condensate temperature
      Condensate pressure
9. Primary system heat losses and pump heat input obtained from calculations.

TABLE 4.5.1-1

CONTROL ROD DRIVE MECHANISM (CRDM)
400 SERIES STAINLESS STEEL ITEMS

ITEM	MATERIAL SPEC. NO.	GRADE, TYPE OR CLASS	MINIMUM UTS (ksi)	MINIMUM yp @ 0.2% (ksi)	MINIMUM ELONGATION (%)	HEAT TREATMENT	HEAT TREATMENT DETAILS
Latch Assy							a, b, c, e
Space-DimX Key Pole-Lift Pol-MG Plunger-MG Pole-SG Plunger Half Plunger-SG	AISI 410 ASTM A-240 ASTM A-276 ASTM A-479 ASTM A-276						
Drive Rod Assembly							a, b, c, e
Prot. Sleeve Disc Button Drive Rod Coupling Plunger-MG	ASTM A-479 ASTM A-276 ASTM A-268 AISI 403 (modified)						

FIGURE 4.2.2-1A

17 X 17 LOPAR FUEL ASSEMBLY CROSS SECTION

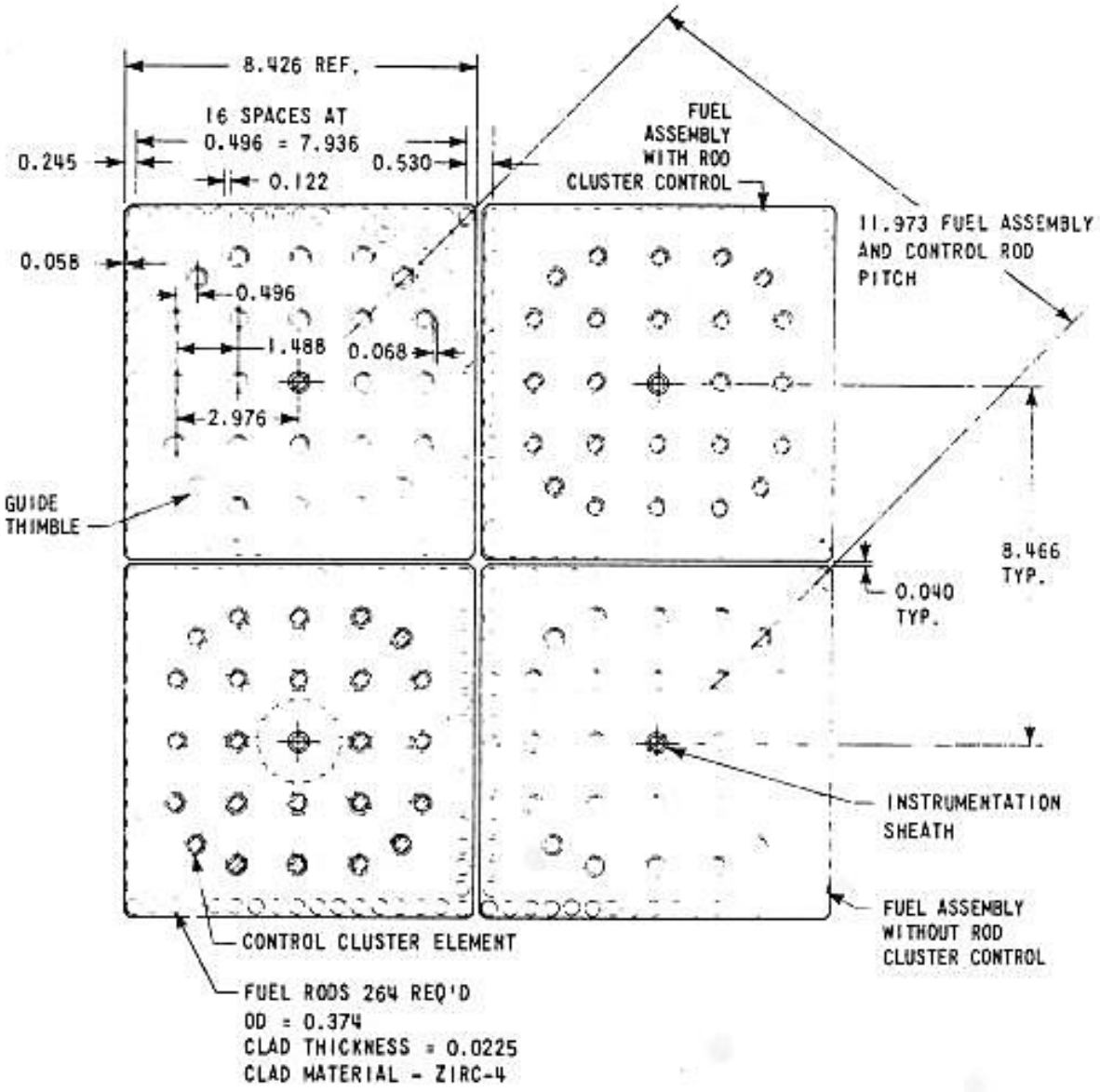

FIGURE 4.2.2-1B

17 X 17 VANTAGE 5 FUEL ASSEMBLY CROSS SECTION

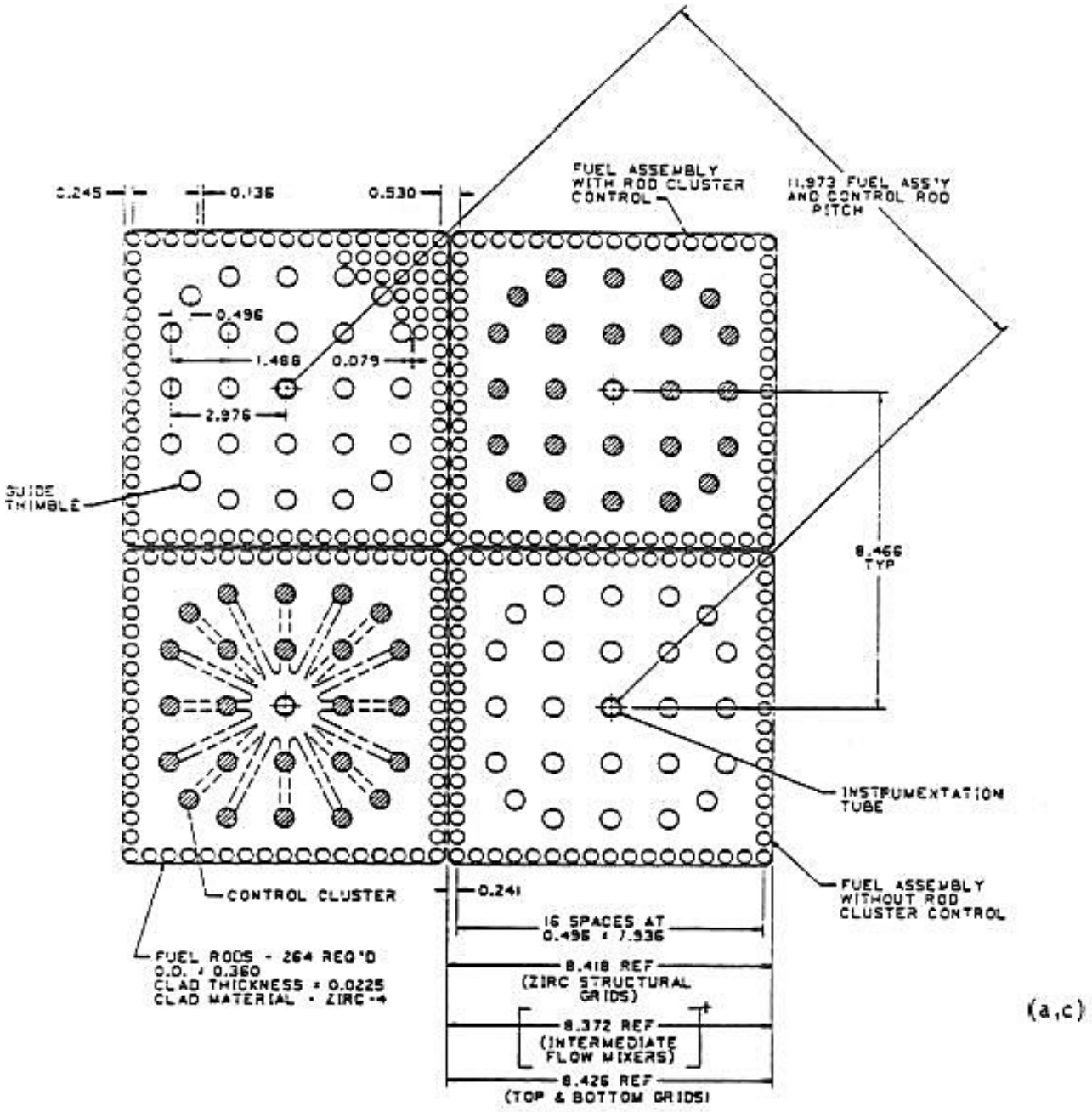

FIGURE 4.2.2-1C

17 X 17 AREVA FUEL ASSEMBLY CROSS SECTION ALL DIMENSIONS IN INCHES

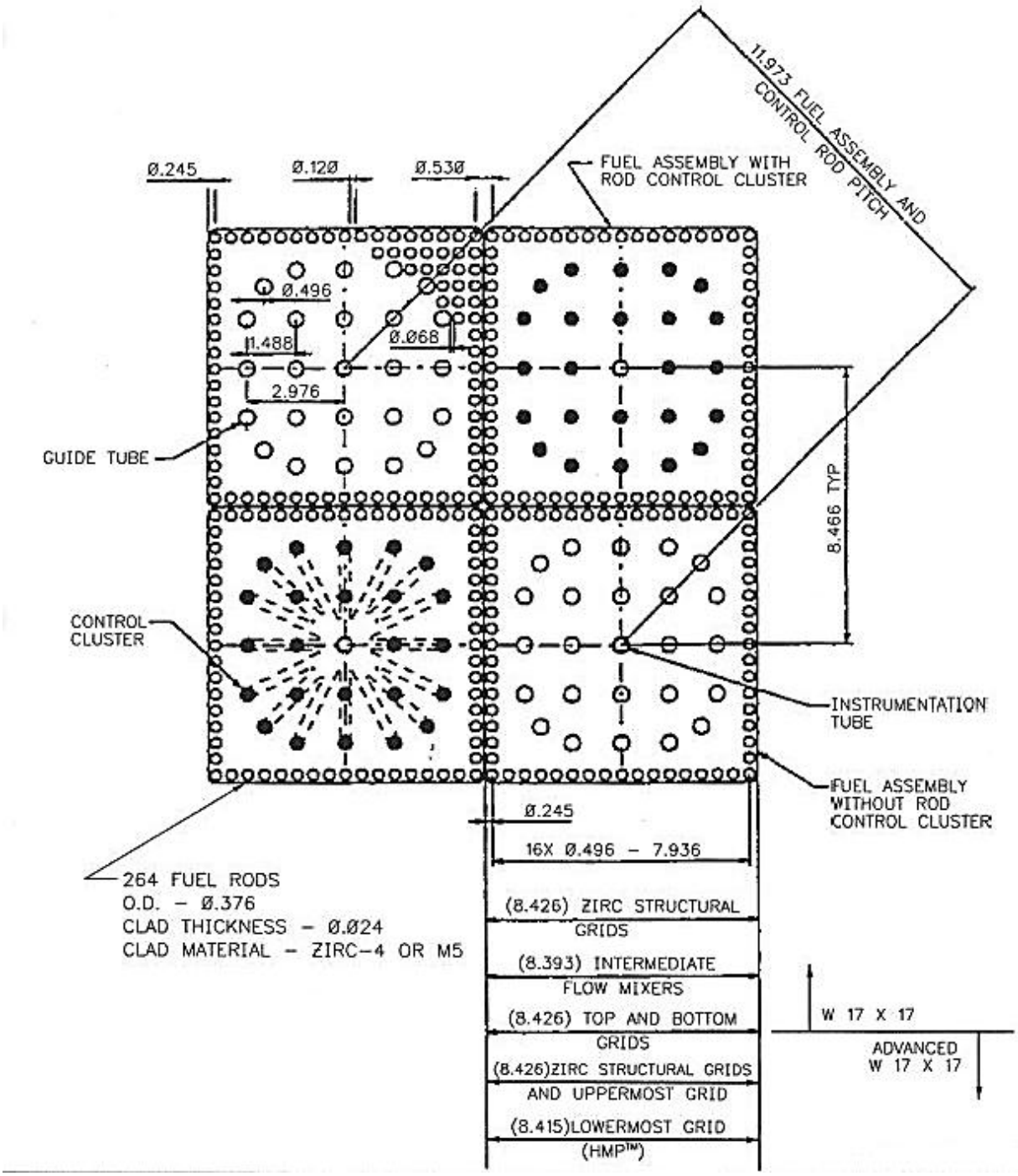

FIGURE 4.2.2-1D

17 x 17 AREVA GAIA FUEL ASSEMBLY
CROSS SECTION

ALL DIMENSIONS IN INCHES

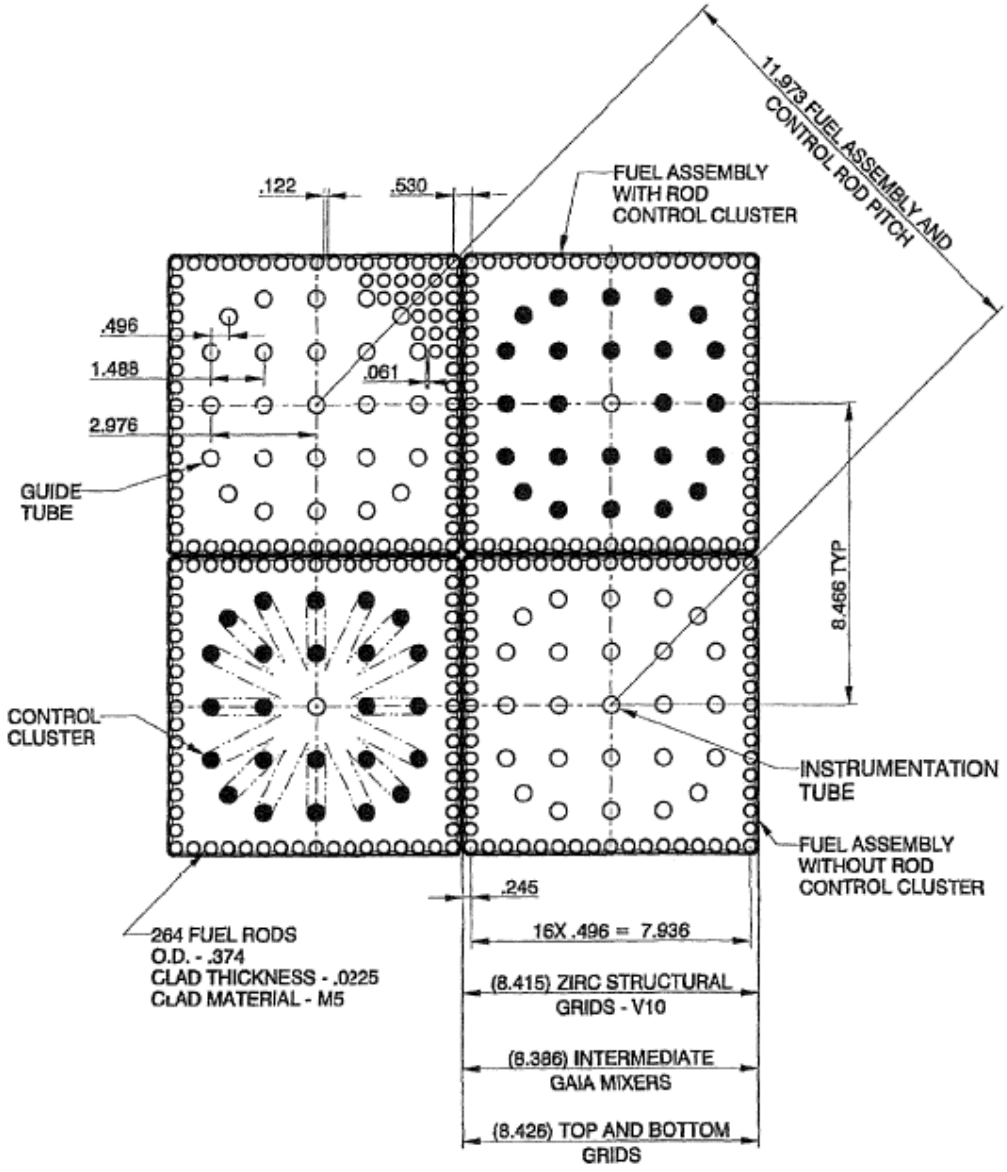

FIGURE 4.2.2-2A

17 X 17 VANTAGE 5/LOPAR FUEL ASSEMBLY OUTLINE

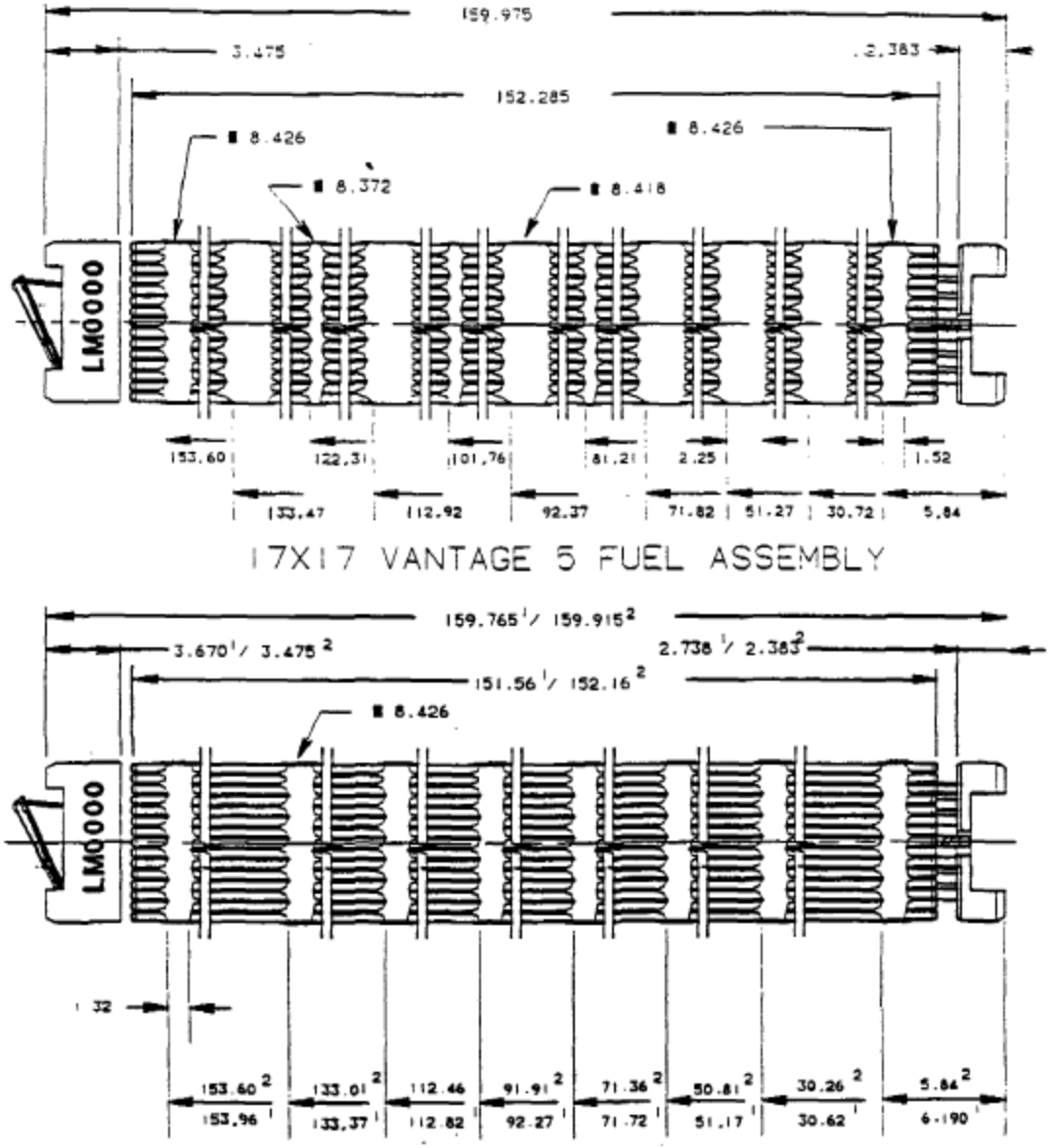

1-CYCLE 1
2-CYCLE 2

AMENDMENT NO. 48

FIGURE 4.2.2-2B

17 X 17 AREVA FUEL ASSEMBLY ALL DIMENSIONS IN INCHES

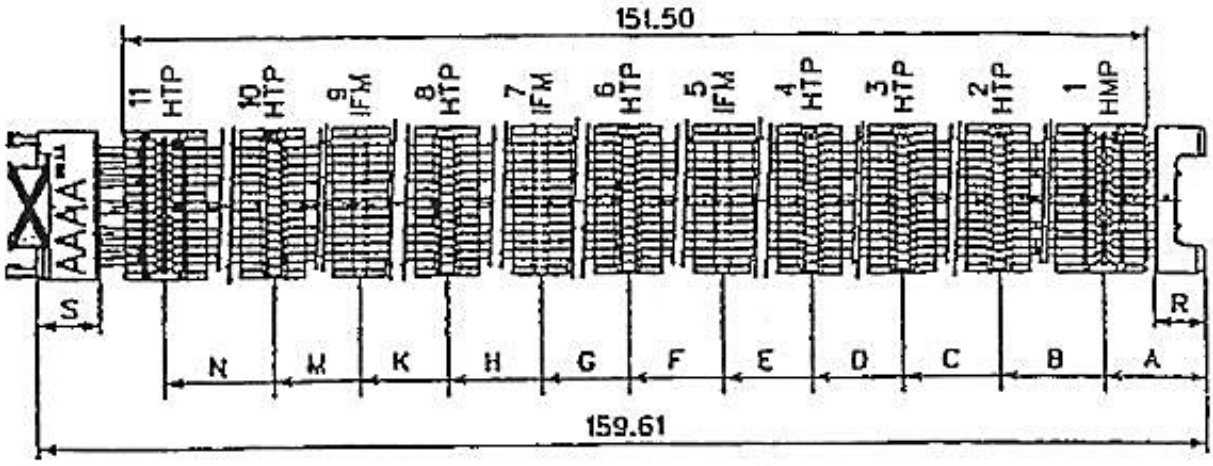

A	5.91
B	29.61
C	50.16
D	70.71
E	80.98
F	91.26
G	101.53
H	111.81
K	122.08
M	132.36
N	152.74
R	2.854
S	3.480

SPACER HEIGHTS

HTP = 1.75

IFM = 0.75

BASED ON INNER STRIP HEIGHT

HMP = 1.75

FIGURE 4.2.2-2C

17 X 17 AREVA GAIA FUEL ASSEMBLY

ALL DIMENSIONS IN INCHES

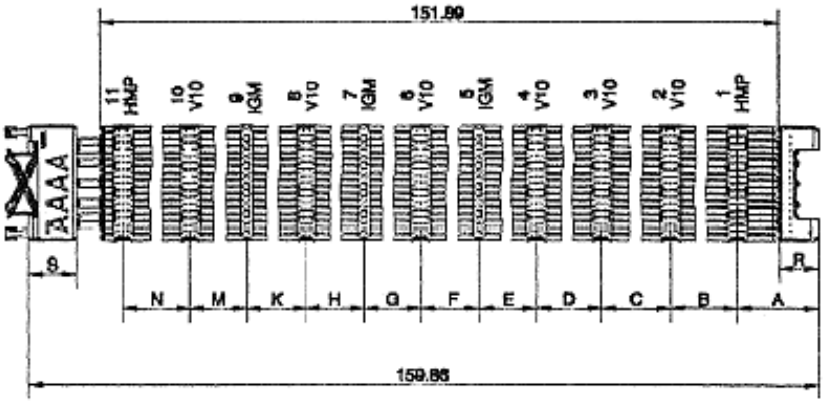

SPACER HEIGHTS

V10 = 1.77
IGM = 1.06
HMP = 1.75

A	5.53
B	29.97
C	50.52
D	71.07
E	81.39
F	91.62
G	101.94
H	112.17
K	122.49
M	132.72
N	152.68
R	2.736
S	3.551

FIGURE 4.2.2-3A

17 X 17 VANTAGE 5 / LOPAR FUEL ROD ASSEMBLY

BOTTOM END PLUG SHOWS INTERNAL GRIP TYPE FOR V-5 FUEL RODS.

NOT SHOWN IS THE EXTERNAL GRIP TYPE OF THE LOPAR FUEL ROD BOTTOM END PLUG.

1-CYCLE 1
2-CYCLE 2

DIM	17X17 V-5	17X17 LOPAR[1]	17X17 LOPAR[2]
A	152.285	151.56	152.16
B	7.525	6.90	7.32
C	144.00	144.00	144.00
DIA D	.315	.329	.329
DIA E	.360	.374	.374

DIMENSIONS ARE IN INCHES

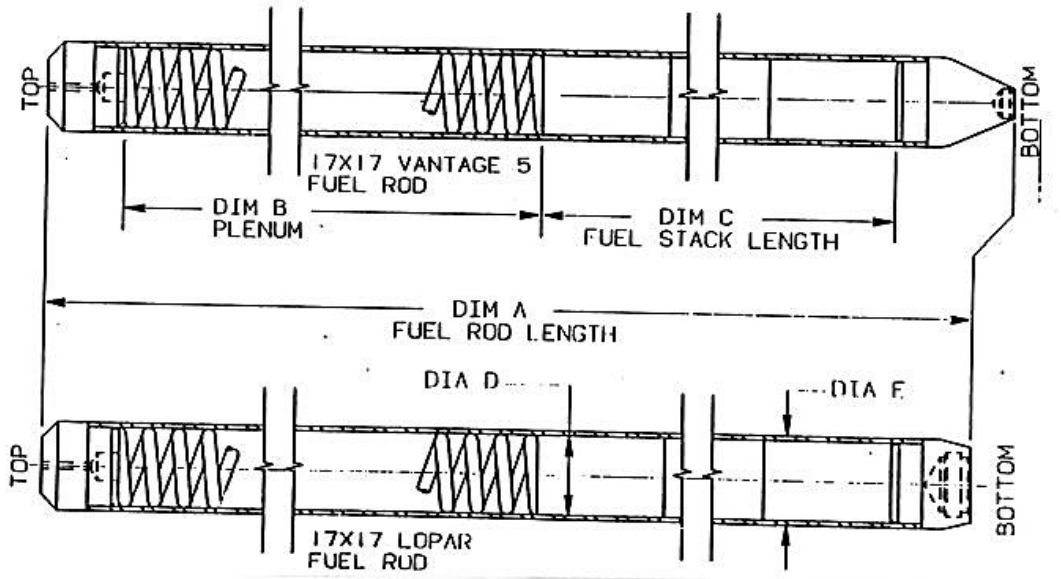

FIGURE 4.2.2-3B

17 X 17 AREVA FUEL ROD ALL DIMENSIONS IN INCHES

DIM	AREVA 17X17 FUEL ROD RELOADS SHA-1 TO SHA-7	AREVA 17X17 FUEL ROD RELOAD SHA-8 AND SHA1-14	AREVA 17 X 17 FUEL ROD RELOAD SHA1-15 AND BEYOND
A	151.50	151.50	151.5Ø
B	6.76	6.74	6.72
C	144.00	144.00	144.Ø
DIA D	0.328	0.328	Ø.328
DIA E	0.376	0.376	Ø.376

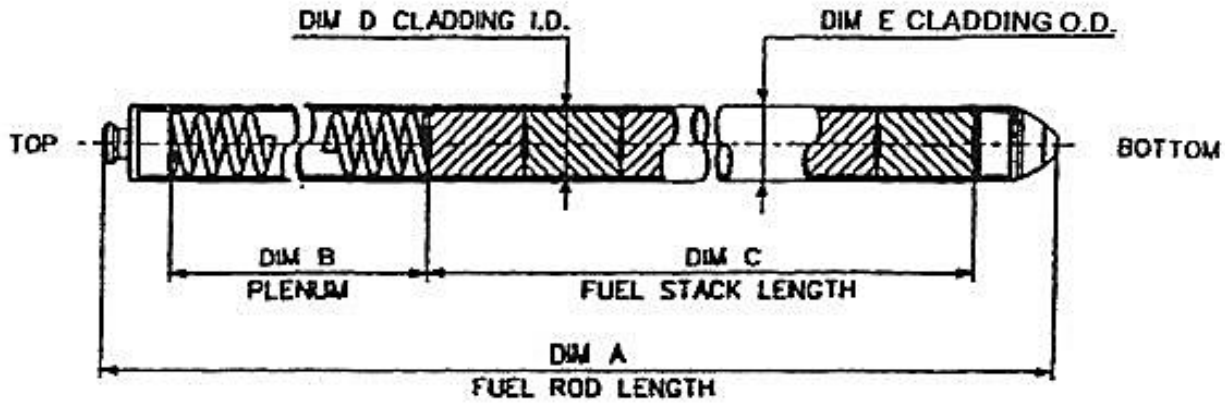

FIGURE 4.2.2-3C

17 X 17 AREVA GAIA FUEL ROD

ALL DIMENSIONS IN INCHES

DIM	AREVA 17X17 GAIA FUEL ROD SHA 1-20
A	161.89
B	6.90
C	144.00
DIA D	.329
DIA E	.374

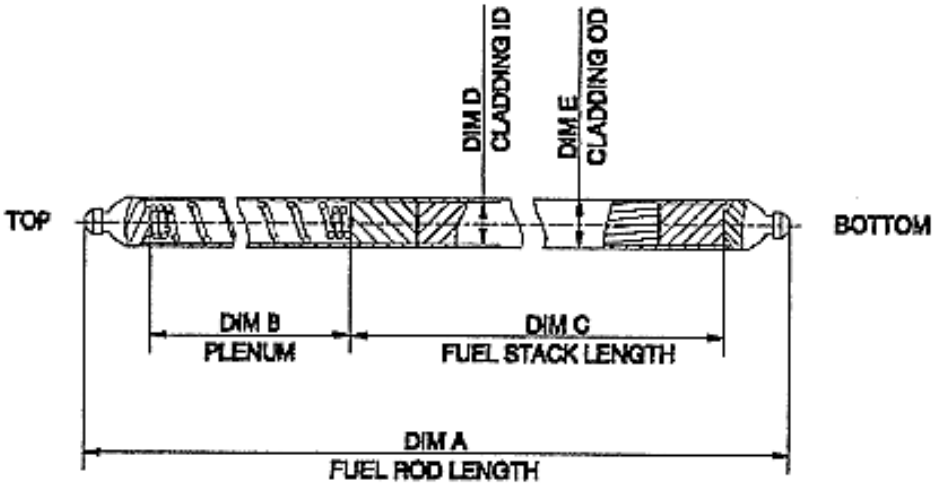

FIGURE 4.2.2-4

ZIRCALOY SPACER GRID ATTACHMENT

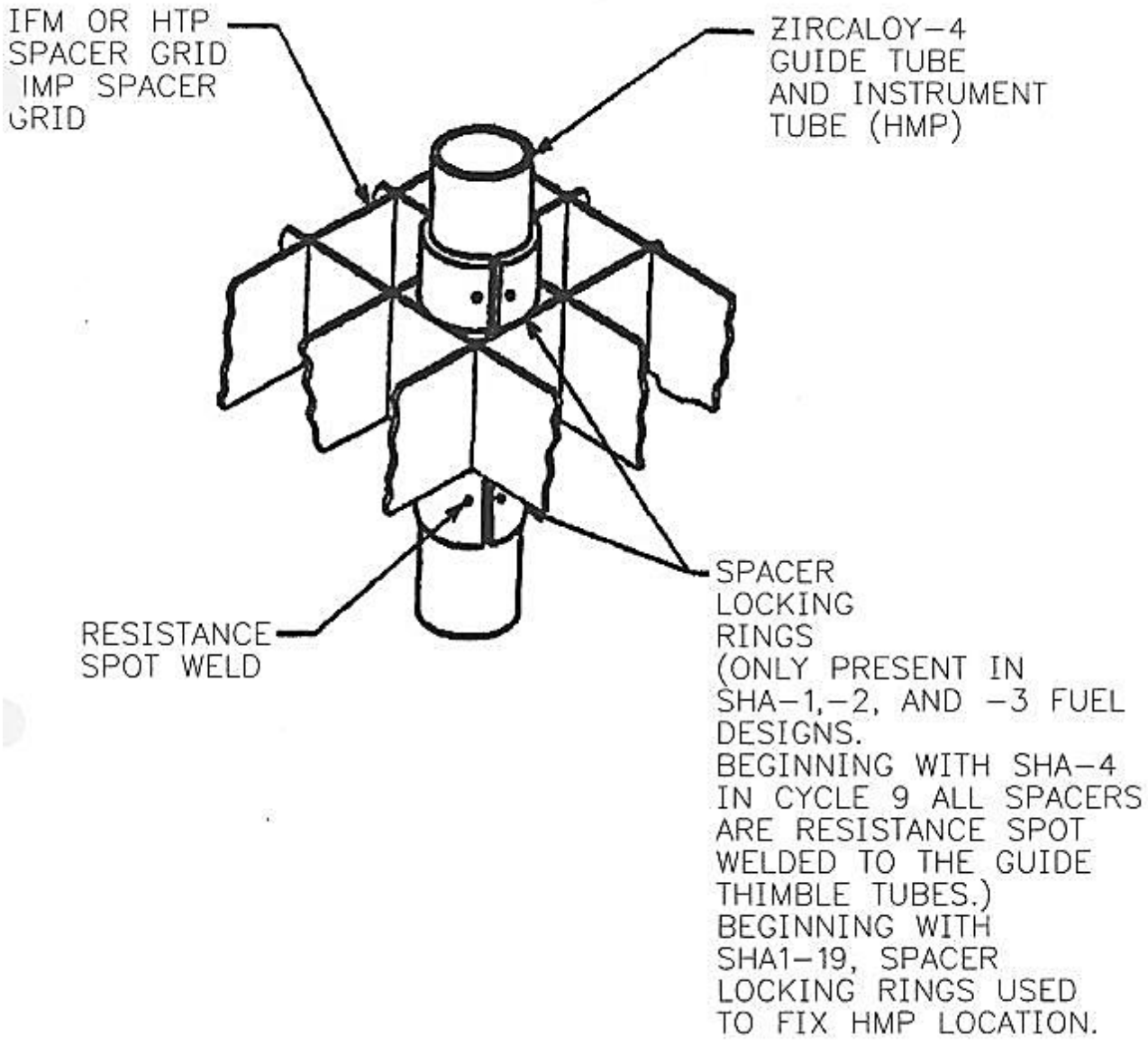

FIGURE 4.2.2-5A

PLAN VIEW MID GRID EXPANSION JOINT DESIGN

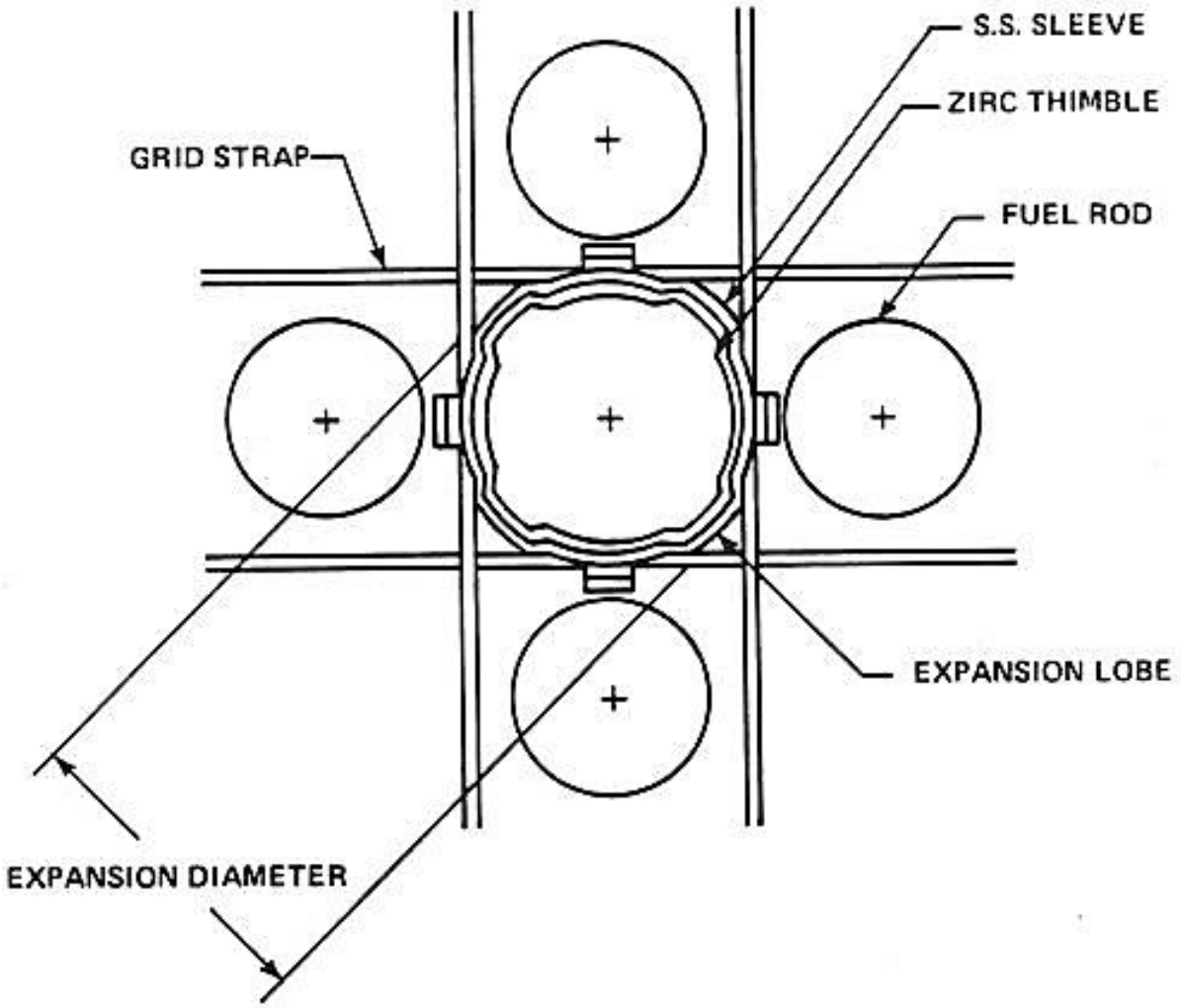

FIGURE 4.2.2-5B

ELEVATION VIEW GRID TO THIMBLE ATTACHMENT

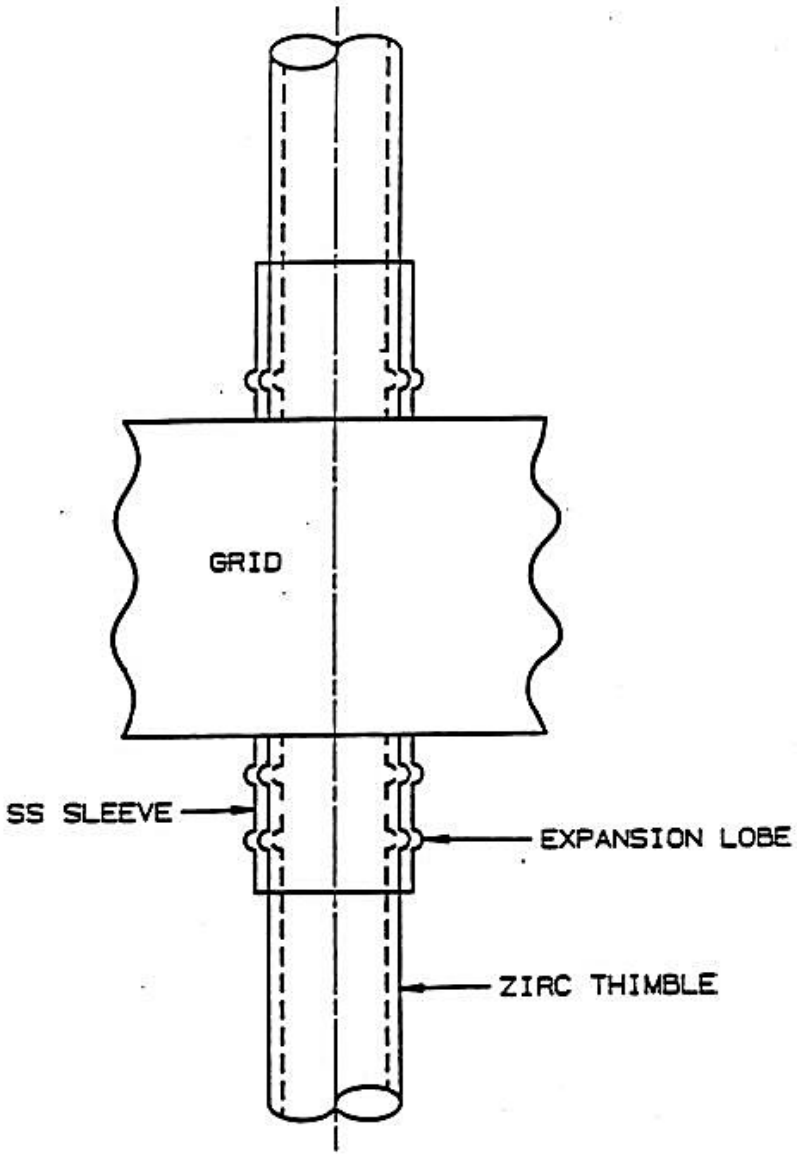

FIGURE 4.2.2-6

17 X 17 GUIDE THIMBLE TUBE COMPARISON

ALL DIMENSIONS IN INCHES

DIM	LOPAR CY1	LOPAR CY2	17X17 V5	17X17AREVA*	ADV. W17 HTP*	AREVA 17X17 GAIA
A	153.240	152.850	152.965	151.921	151.921	152.64
B	23.690	23.690	23.690	23.97	22.82	25.33
C	0.018	0.016	0.016	0.016	Ø.Ø16	Ø.Ø23
DIA D	0.448	0.450	0.442	0.448	Ø.45Ø	Ø.451
DIA E	0.484	0.482	0.474	0.480	Ø.482	Ø.496
DIA F	0.395	0.397	0.397	0.397	Ø.397	Ø.397
DIA G	0.431	0.430	0.430	0.430	Ø.482	Ø.496

* GUIDE TUBE END FITTING AND FLARED TUBE END ARE NOT INCLUDED IN LENGTH DIMENSIONS

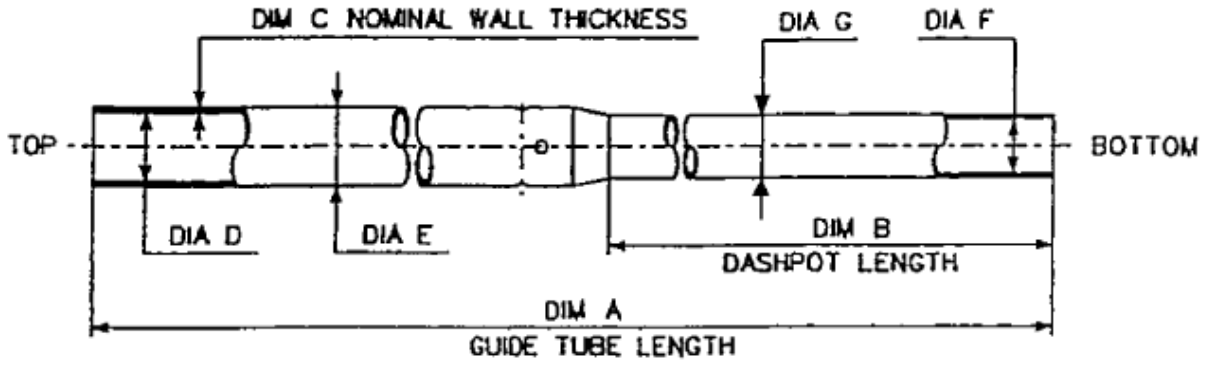

FIGURE 4.2.2-7

17 X 17 INSTRUMENTATION TUBE COMPARISON

ALL DIMENSIONS IN INCHES

DIM	LOPAR CY1	LOPAR CY2	17X17 V5	17X17AREVA	ADV. W17 HTP	AREVA 17X17 GAIA
DIA A	0.448	0.448	0.440	0.448	Ø.450	Ø.451
DIA B	0.484	0.484	0.476	0.480	Ø.482	Ø.496
C	154.23	154.23	154.23	154.00	154.00	154.21
D	0.018	0.018	0.018	0.016	Ø.016	Ø.023

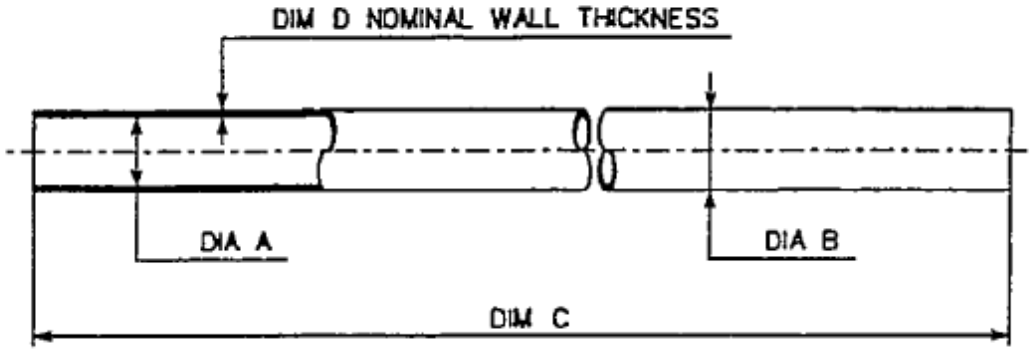

FIGURE 4.2.2-8

ROD CLUSTER CONTROL AND DRIVE ROD ASSEMBLY WITH INTERFACING COMPONENTS

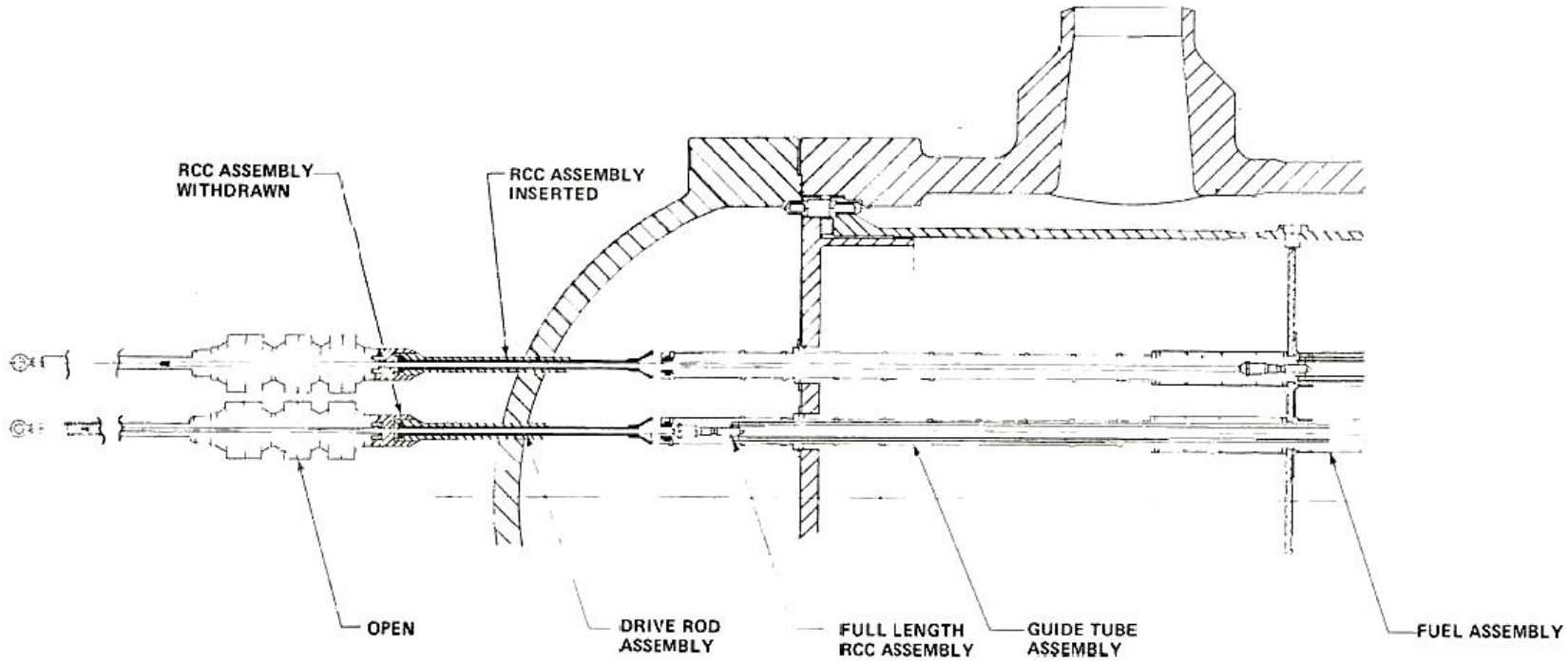

FIGURE 4.2.2-9

WESTINGHOUSE ROD CLUSTER CONTROL ASSEMBLY OUTLINE

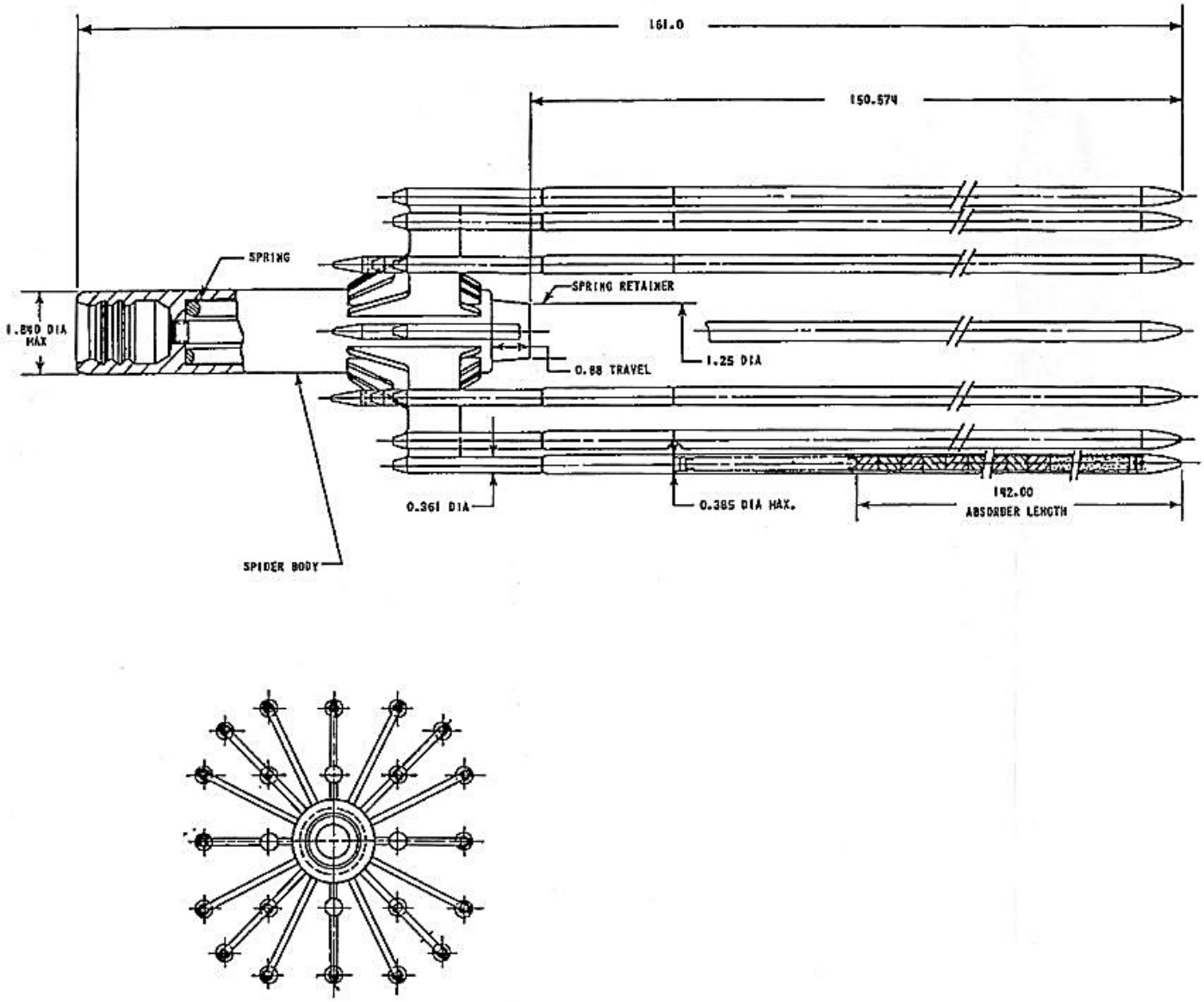

FIGURE 4.2.2-10

WESTINGHOUSE ABSORBER ROD

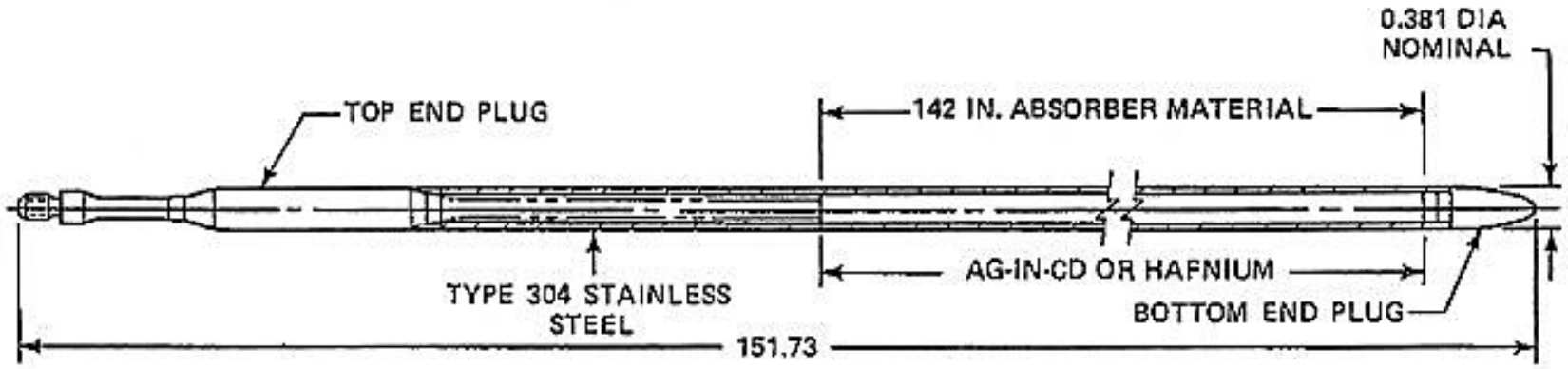

FIGURE 4.2.2-15

THIMBLE PLUG ASSEMBLY

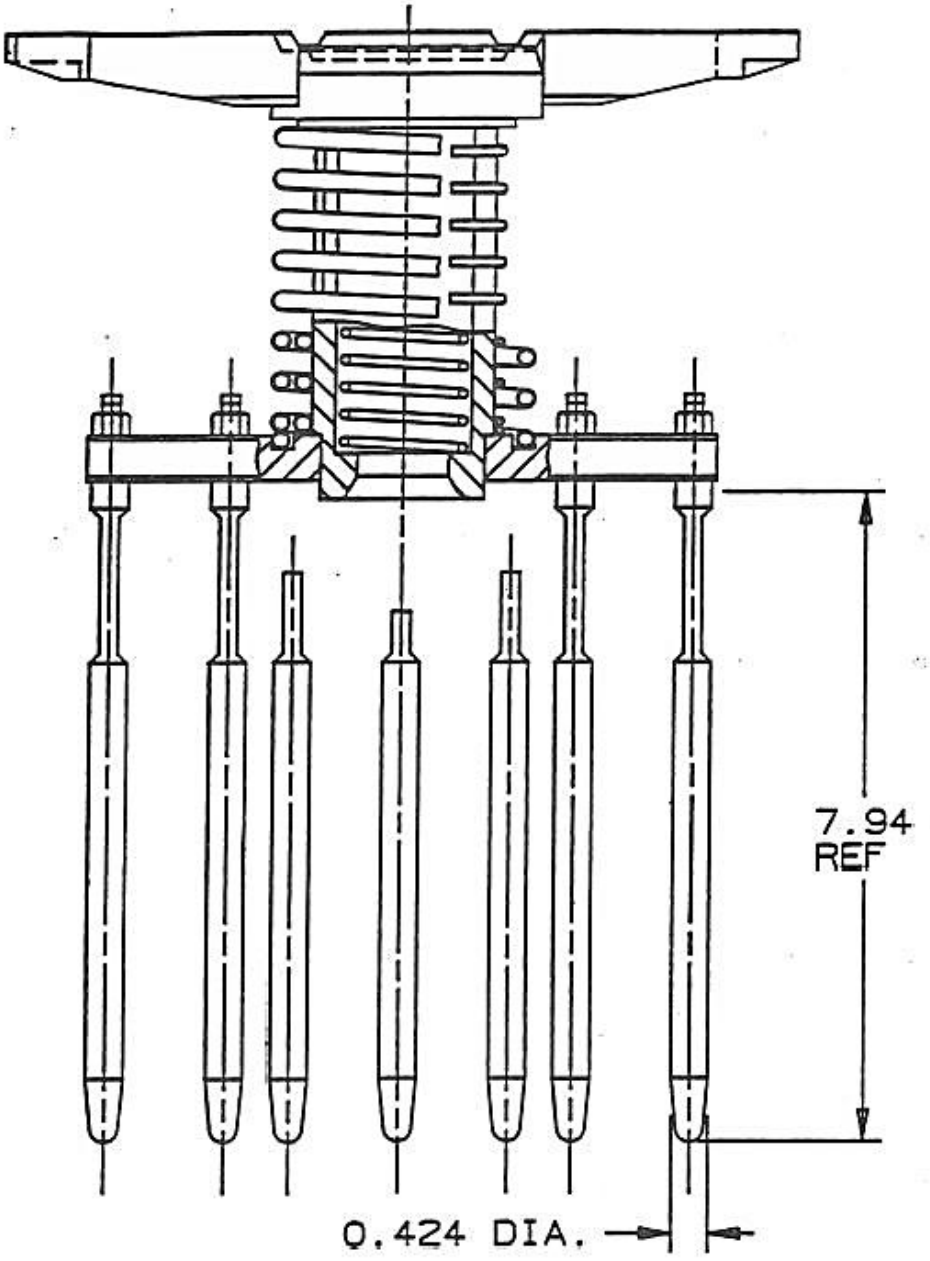

FIGURE 4.3.2-1A

AXIAL ZONING OF URANIUM ENRICHMENT AND GADOLINIA POISONING

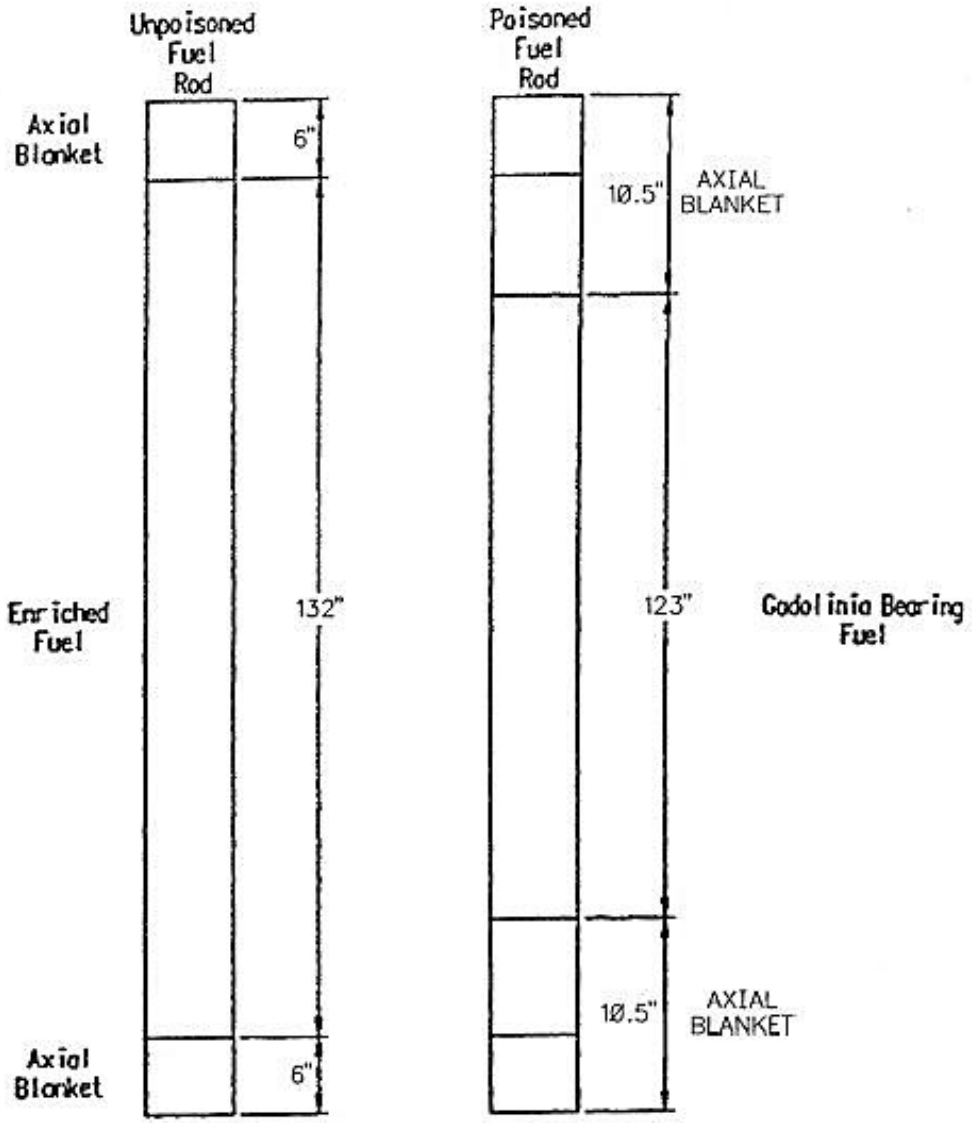

Note A:

Axial Zone dimensions are typical. Refer to Cycle Design reports for specific dimensions applicable to each reload. THE LISTED DIMENSIONS ARE APPLICABLE TO BATCH 21 (SHA1-19) AND ABOVE.

FIGURE 4.3.2-1B

TYPICAL LOW LEAKAGE FUEL LOADING ARRANGEMENT

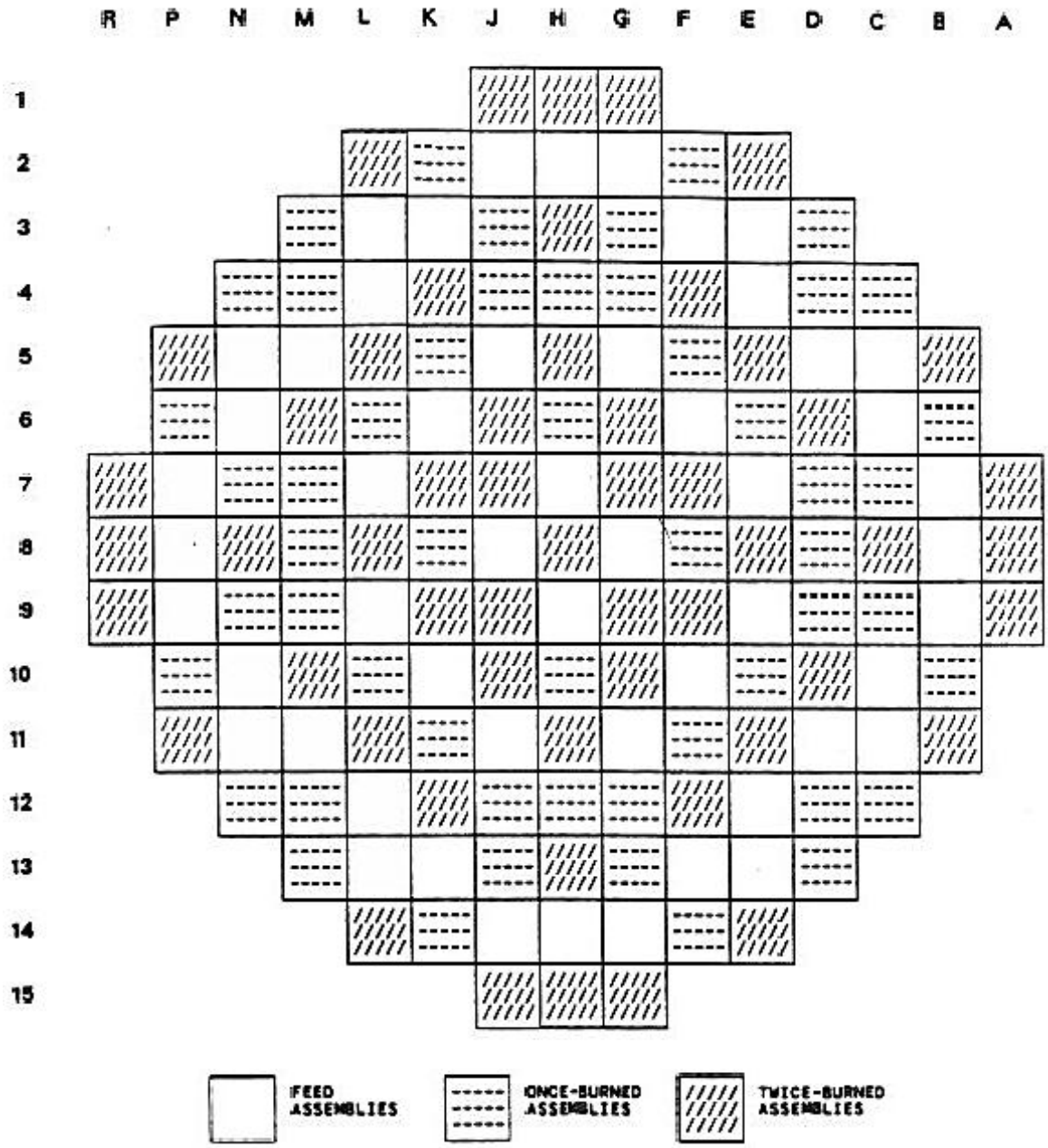

FIGURE 4.3.2-2

PRODUCTION AND CONSUMPTION OF HIGHER ISOTOPES

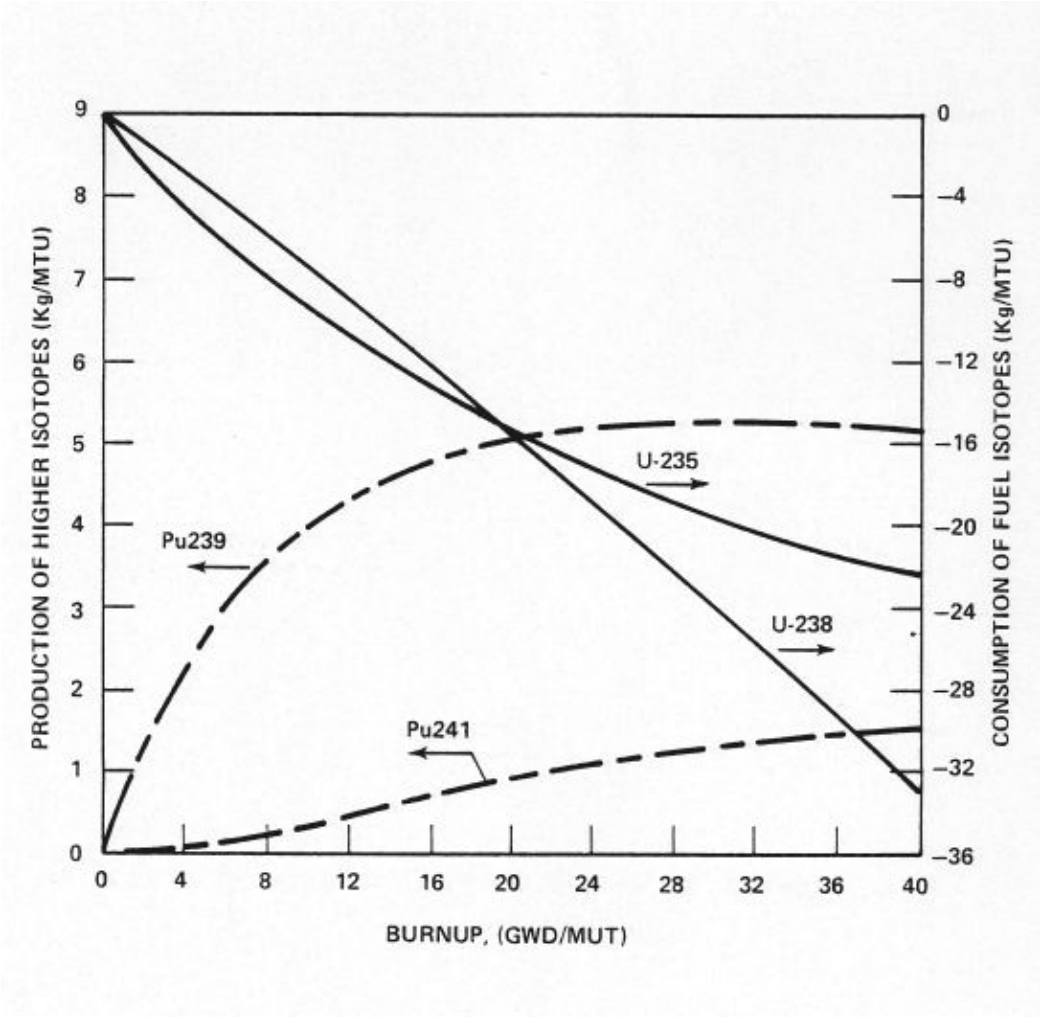

FIGURE 4.3.2-4A

TYPICAL GADOLINIA ARRANGEMENTS WITHIN AN ASSEMBLY

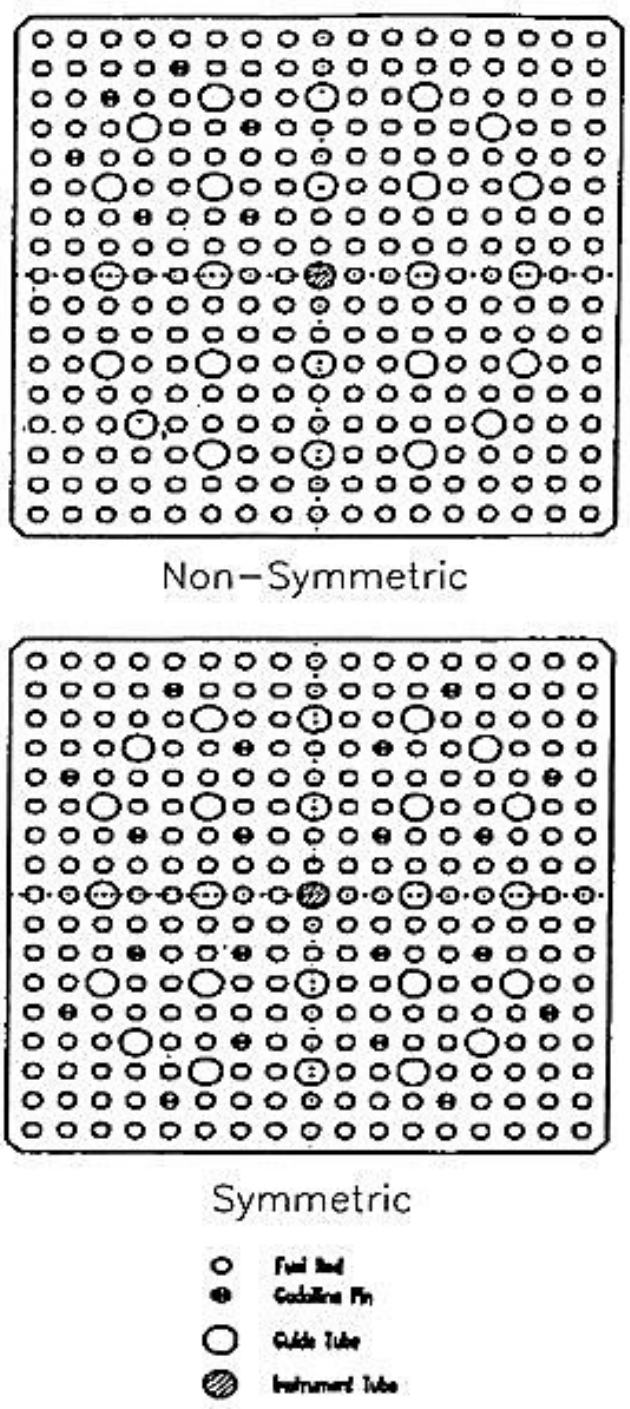

FIGURE 4.3.2-6

NORMALIZED POWER DENSITY DISTRIBUTION NEAR BEGINNING OF LIFE, UNRODDED CORE, HOT FULL POWER, NO XENON

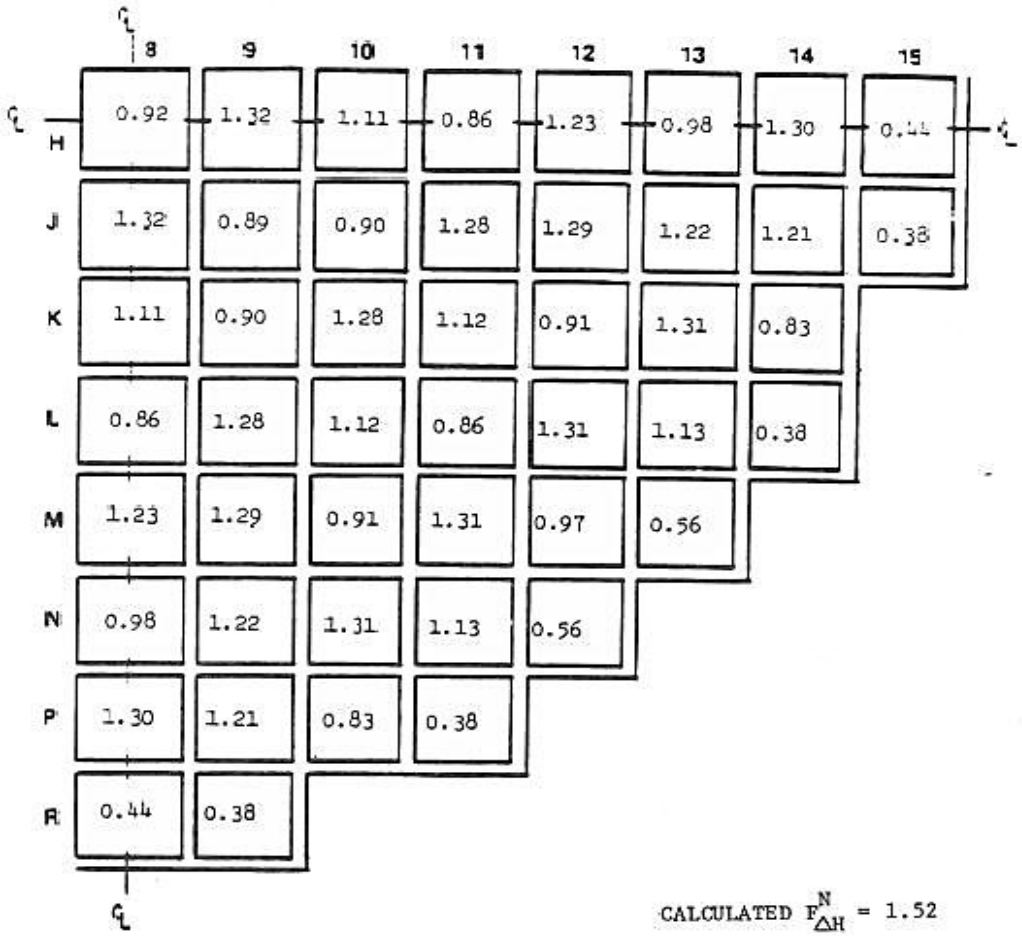

FIGURE 4.3.2-7

NORMALIZED POWER DENSITY DISTRIBUTION NEAR BEGINNING OF LIFE, UNRODDED CORE, HOT FULL POWER, EQUILIBRIUM XENON

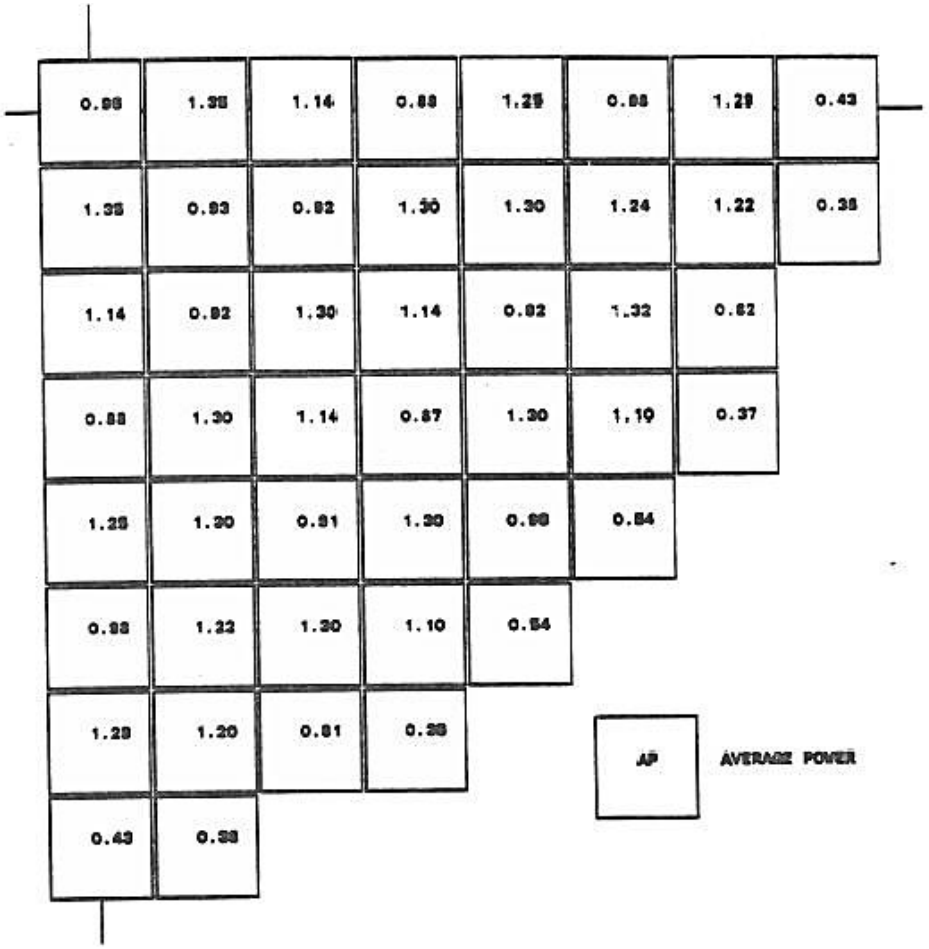

Calculated $F^{N}_{\Delta H} = 1.49$

FIGURE 4.3.2-8

NORMALIZED POWER DENSITY DISTRIBUTION NEAR BEGINNING OF LIFE, BANK D AT INSERTION LIMIT, HOT FULL POWER, EQUILIBRIUM XENON

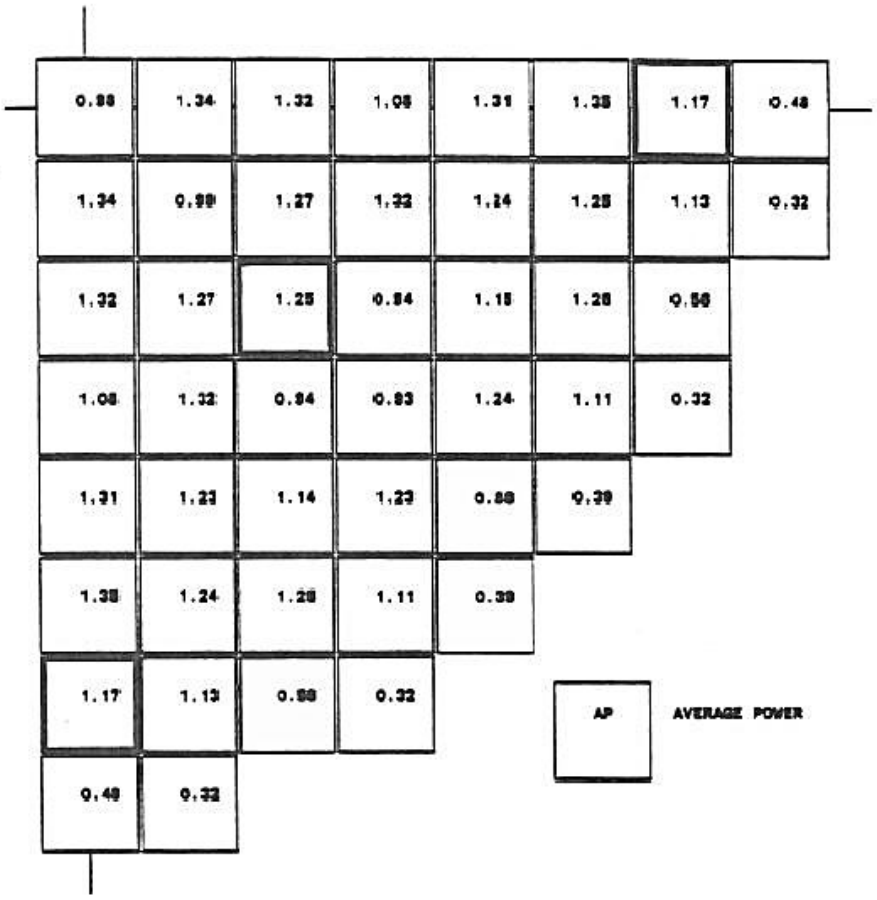

$F^{N}_{\Delta H} = 1.52$

FIGURE 4.3.2-9

NORMALIZED POWER DENSITY DISTRIBUTION NEAR MIDDLE OF LIFE, UNRODDED CORE, HOT FULL POWER, EQUILIBRIUM XENON

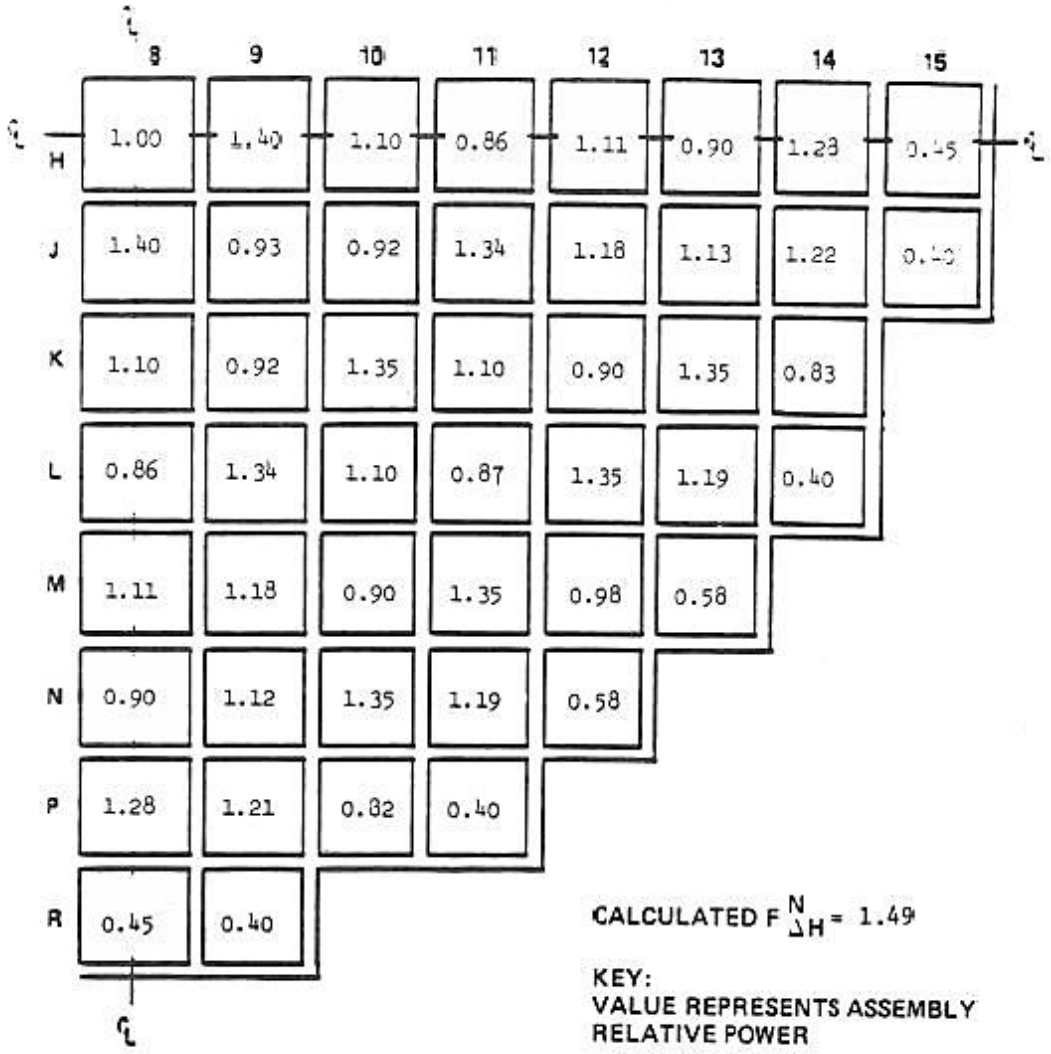

FIGURE 4.3.2-10

NORMALIZED POWER DENSITY DISTRIBUTION NEAR END OF LIFE, UNRODDED CORE, HOT FULL POWER, EQUILIBRIUM XENON

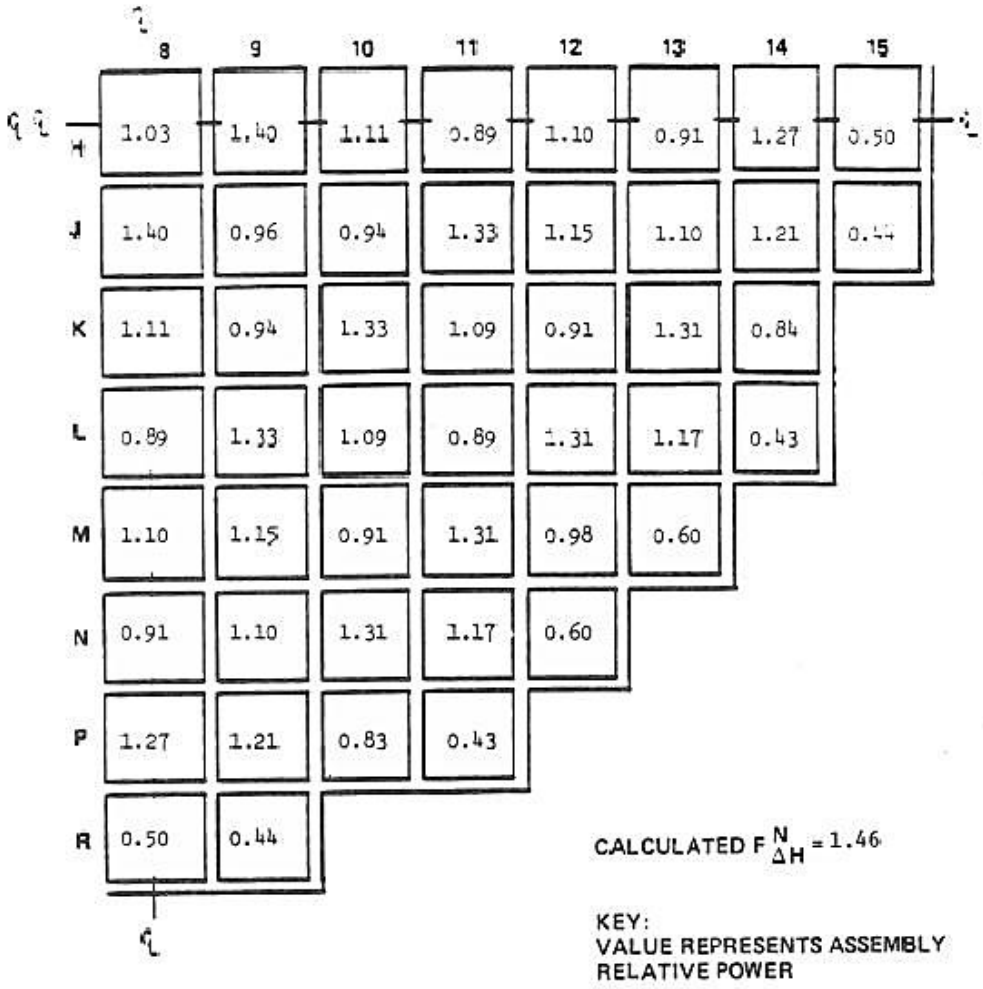

FIGURE 4.3.2-11

NORMALIZED POWER DENSITY DISTRIBUTION NEAR END OF LIFE, BANK D AT INSERTION LIMIT, HOT FULL POWER, EQUILIBRIUM XENON

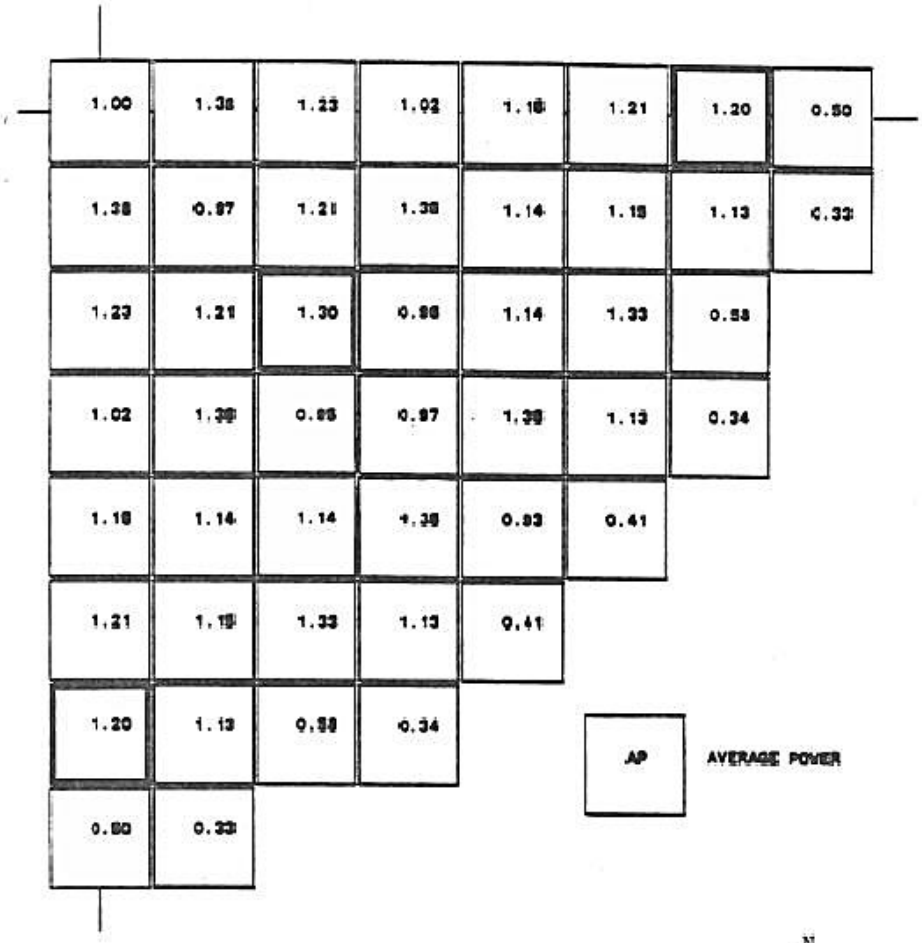

FIGURE 4.3.2-12

POWER DISTRIBUTION WITHIN A TYPICAL ASSEMBLY NEAR BOL, HFP, EQUILIBRIUM XENON, UNRODDED CORE

1.16

1.18 1.10

1.19 1.11 1.14

1.22 1.15 1.28 XX

1.24 1.18 1.31 1.34 1.25

1.27 1.29 XX 1.34 1.34 XX

1.27 1.20 1.32 1.22 1.23 1.34 1.24

1.27 1.21 1.33 1.22 1.23 1.35 1.24 1.25

1.29 1.30 XX 1.32 1.33 XX 1.34 1.34 XX

1.29 1.23 1.34 1.24 1.24 1.36 1.25 1.25 1.36 1.27

1.30 1.23 1.35 1.25 1.25 1.36 1.25 1.26 1.36 1.27 1.27

1.32 1.34 XX 1.38 1.38 XX 1.37 1.38 XX 1.39 1.39 XX

1.30 1.24 1.38 1.40 1.31 1.39 1.27 1.27 1.36 1.27 1.28 1.40 1.32

1.29 1.21 1.35 XX 1.41 1.41 1.28 1.27 1.37 1.27 1.28 1.41 1.42 XX

1.28 1.19 1.22 1.36 1.40 XX 1.39 1.39 XX 1.38 1.38 XX 1.39 1.36 1.22

1.28 1.19 1.20 1.23 1.27 1.38 1.28 1.28 1.36 1.27 1.27 1.37 1.26 1.22 1.19 1.19

1.26 1.28 1.29 1.31 1.33 1.36 1.35 1.35 1.35 1.33 1.33 1.34 1.32 1.29 1.28 1.27 1.24

XX = Guide Tube Locations

FIGURE 4.3.2-13

POWER DISTRIBUTION WITHIN A TYPICAL ASSEMBLY NEAR EOL, HFP, EQUILIBRIUM XENON, UNRODDED CORE

1.22

1.21 1.21

1.21 1.22 1.24

1.23 1.24 1.28 XX

1.25 1.27 1.31 1.33 1.34

1.27 1.29 XX 1.33 1.34 XX

1.27 1.29 1.32 1.32 1.33 1.35 1.35

1.27 1.30 1.33 1.32 1.34 1.36 1.36 1.36

1.28 1.30 XX 1.33 1.34 XX 1.35 1.36 XX

1.29 1.31 1.34 1.33 1.34 1.36 1.35 1.35 1.36 1.37

1.30 1.32 1.34 1.34 1.35 1.36 1.35 1.35 1.36 1.37 1.37

1.31 1.33 XX 1.36 1.37 XX 1.37 1.37 XX 1.38 1.38 XX

1.30 1.32 1.35 1.37 1.38 1.37 1.36 1.36 1.36 1.36 1.36 1.37 1.38

1.29 1.30 1.33 XX 1.38 1.38 1.36 1.36 1.35 1.35 1.35 1.37 1.37 XX

1.28 1.28 1.31 1.34 1.36 XX 1.36 1.37 XX 1.35 1.35 XX 1.35 1.32 1.29

1.28 1.28 1.28 1.31 1.33 1.35 1.35 1.35 1.33 1.33 1.32 1.32 1.31 1.28 1.26 1.25

1.29 1.28 1.28 1.29 1.31 1.32 1.32 1.32 1.31 1.29 1.29 1.30 1.28 1.26 1.25 1.24 1.2

XX = Guide Tube

FIGURE 4.3.2-14

TYPICAL AXIAL POWER SHAPES OCCURRING AT BEGINNING-OF-LIFE

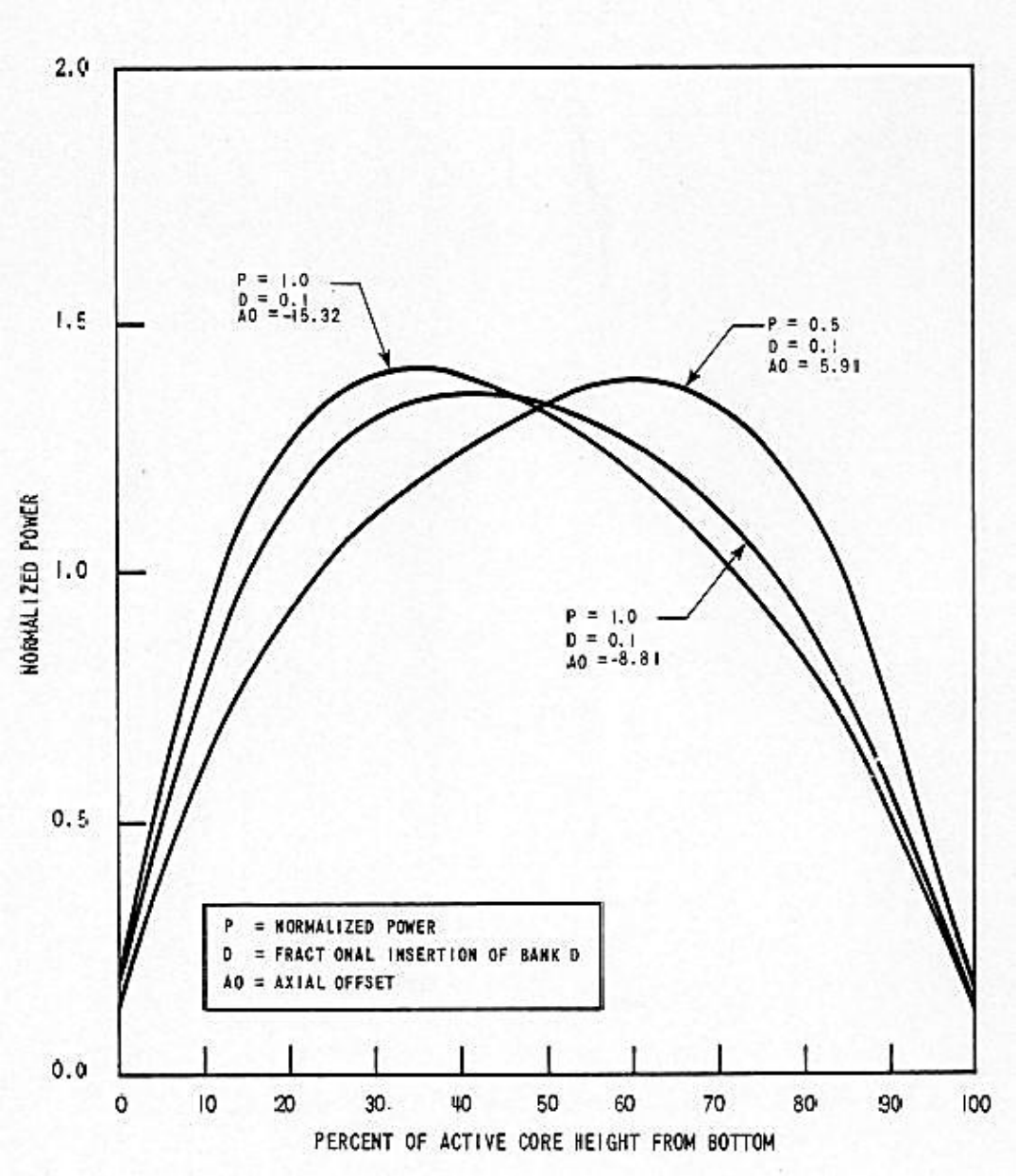

FIGURE 4.3.2-15

TYPICAL AXIAL POWER SHAPES OCCURRING AT MIDDLE-OF-LIFE

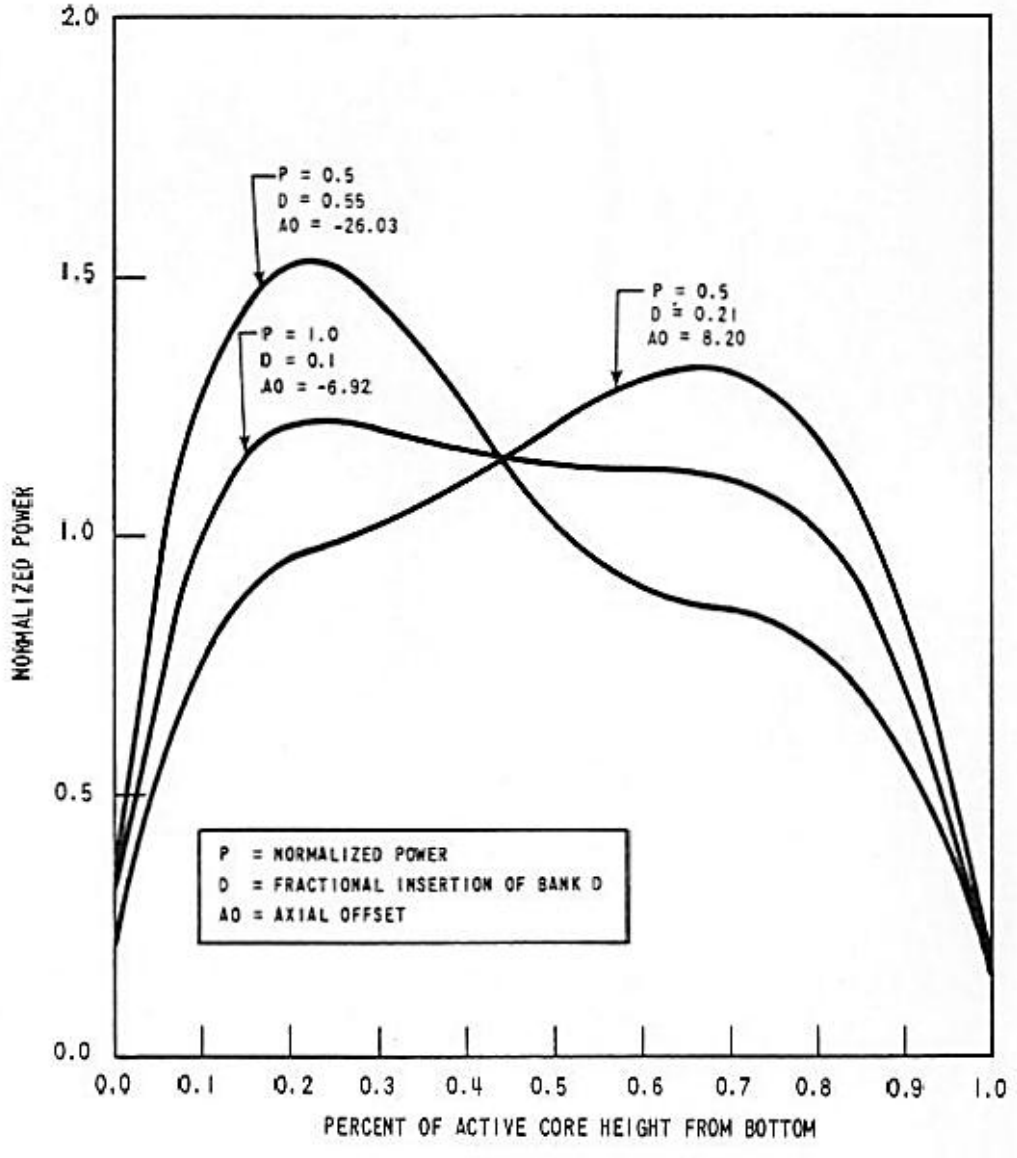

FIGURE 4.3.2-16

TYPICAL AXIAL POWER SHAPES OCCURRING AT END-OF-LIFE

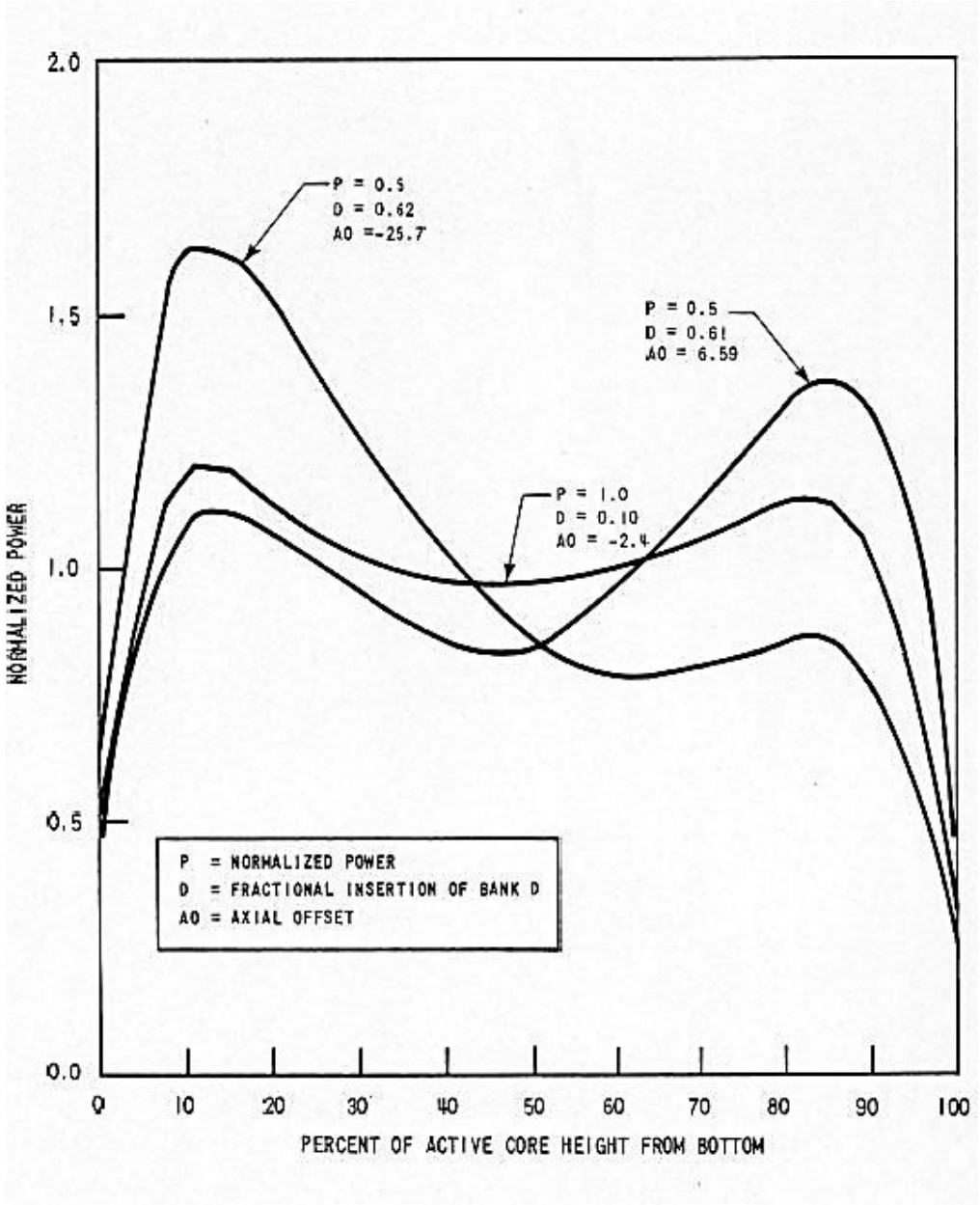

FIGURE 4.3.2-17

COMPARISON OF A TYPICAL ASSEMBLY AXIAL POWER DISTRIBUTION WITH CORE AVERAGE AXIAL DISTRIBUTION BANK SLIGHTLY INSERTED

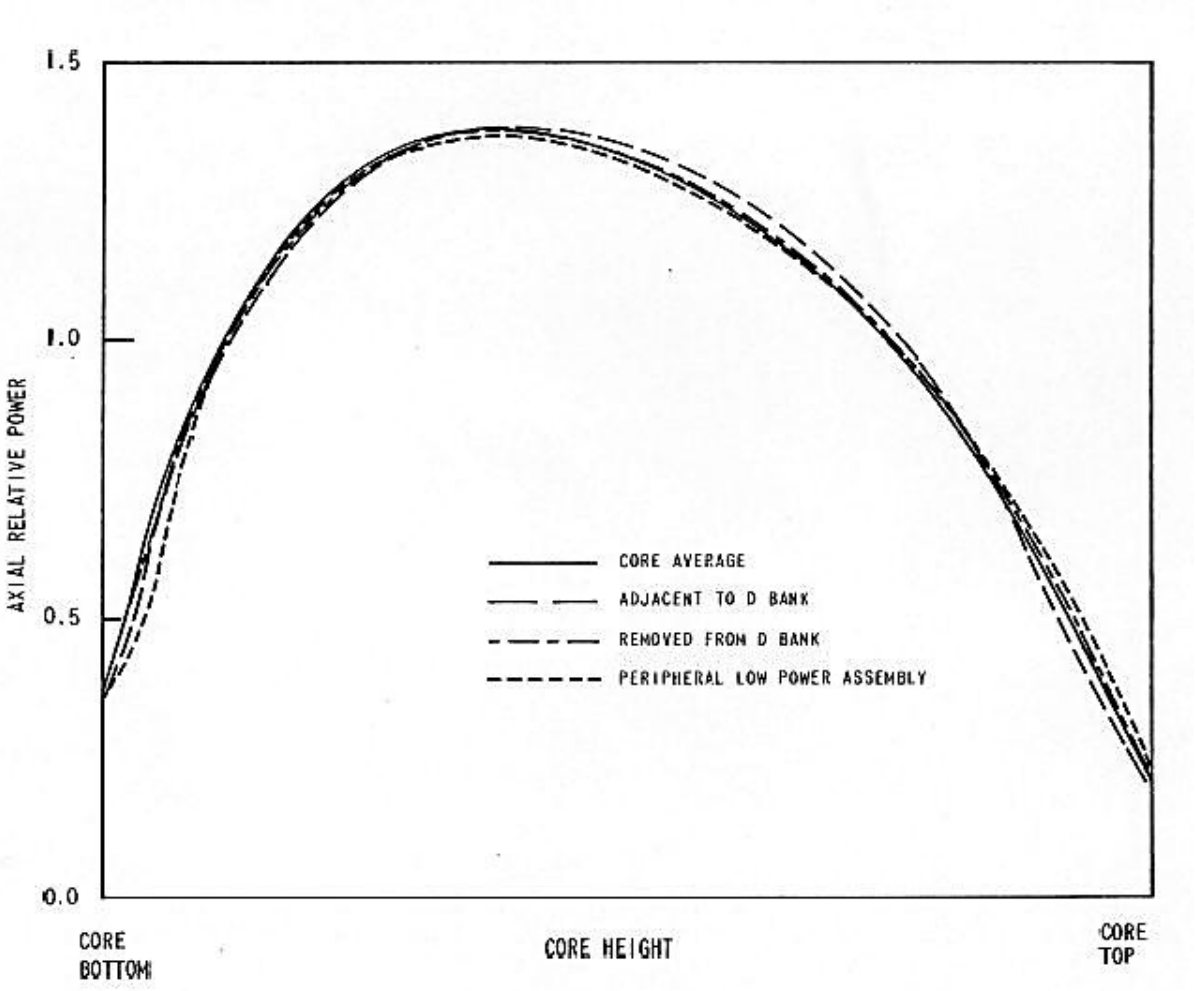

FIGURE 4.3.2-21

TYPICAL MAXIMUM FQ X K(Z) PEAKING FACTOR VERSUS CORE HEIGHT DURING NORMAL OPERATION

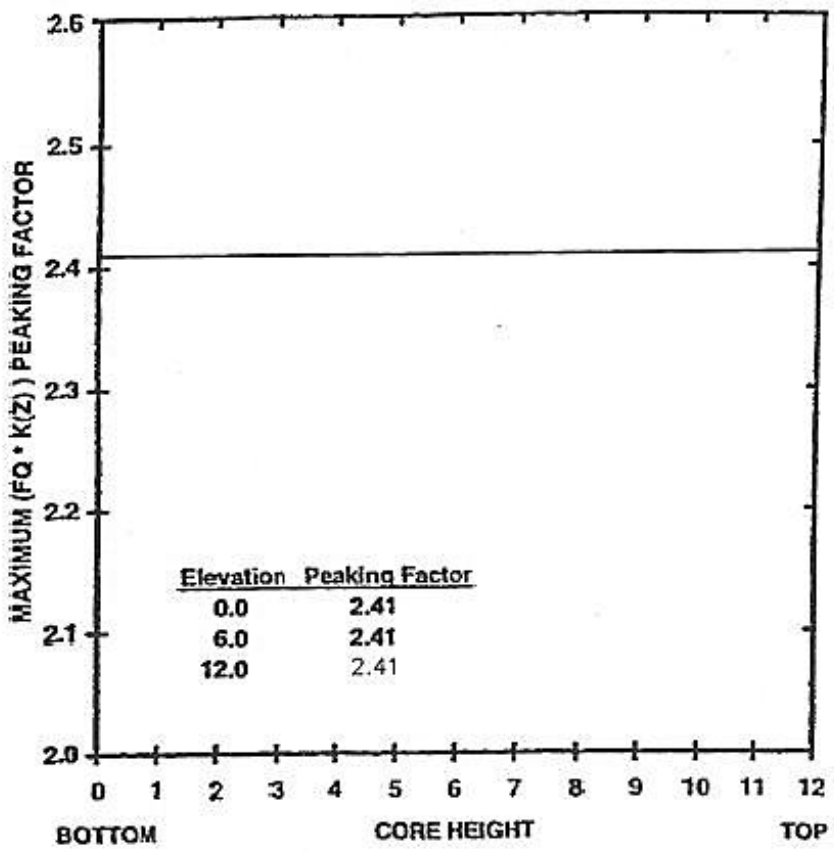

FIGURE 4.3.2-28

DOPPLER ONLY POWER COEFFICIENT VS POWER LEVEL
AT BOL AND EOL TYPICAL CYCLE

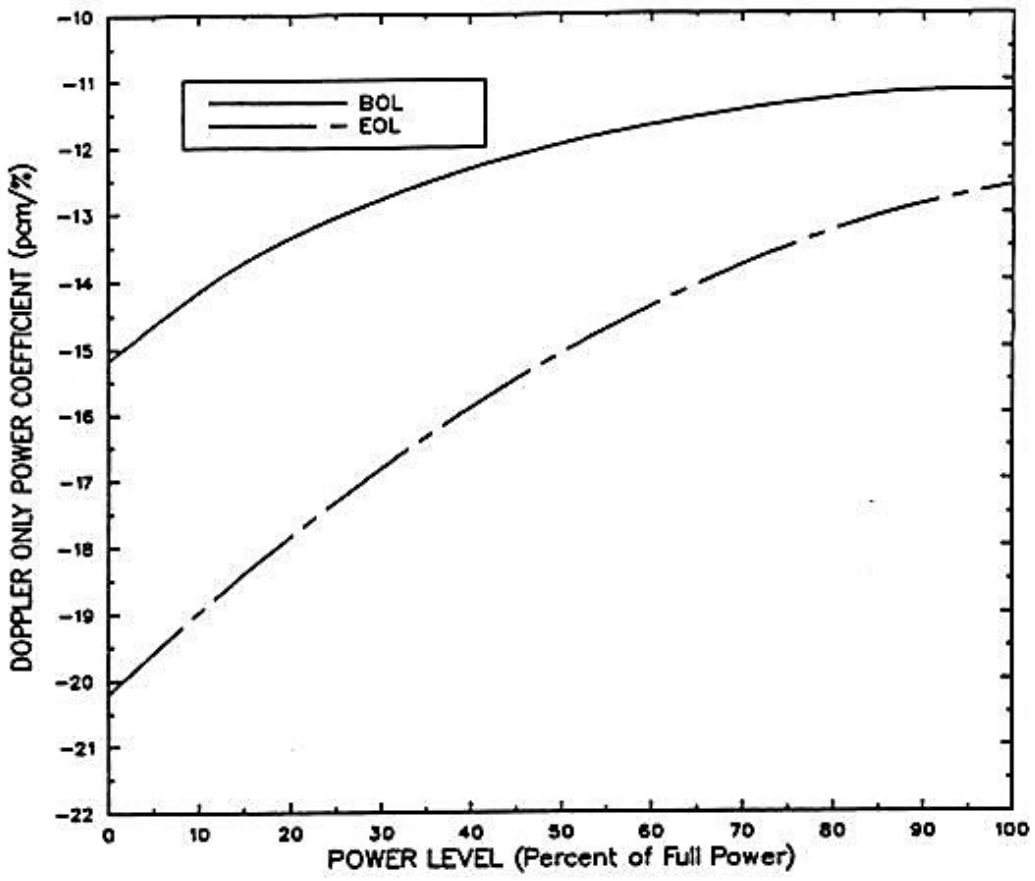

FIGURE 4.3.2-29

DOPPLER ONLY POWER DEFECT VS PERCENT POWER BOL AND EOL, TYPICAL CYCLE

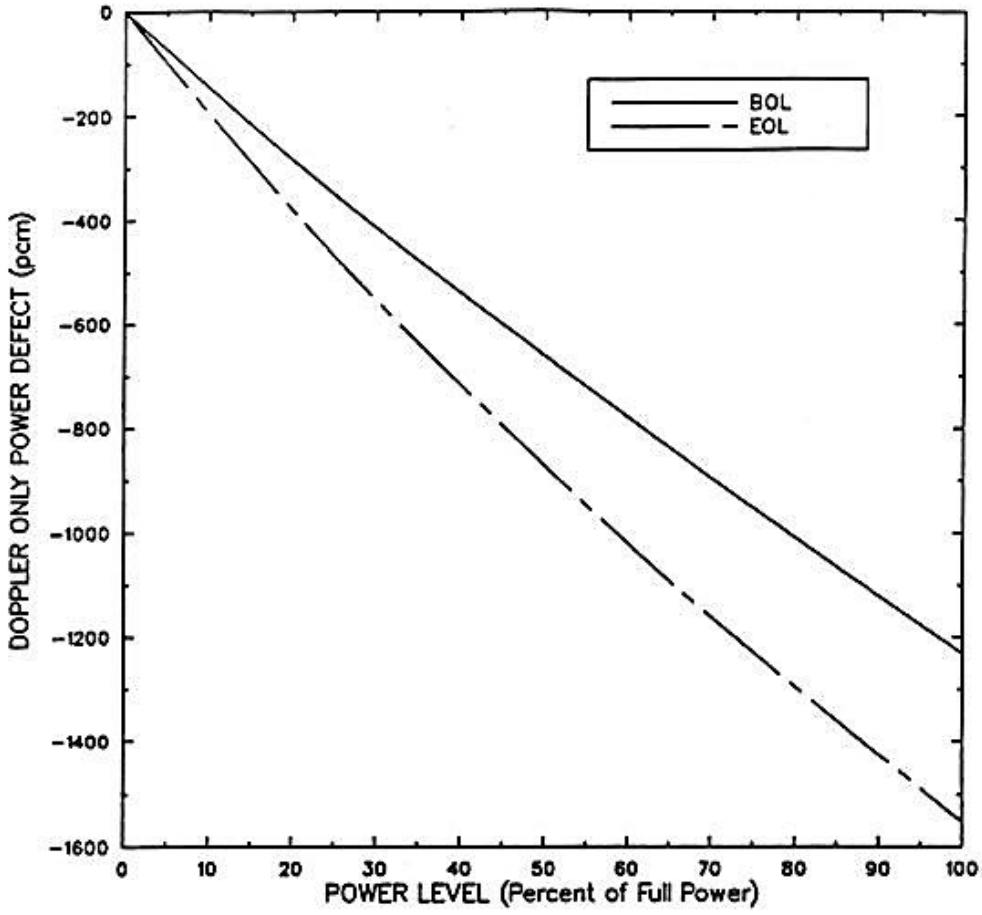

FIGURE 4.3.2-30

TYPICAL MODERATOR TEMPERATURE COEFFICIENT AT BOL, NO RODS

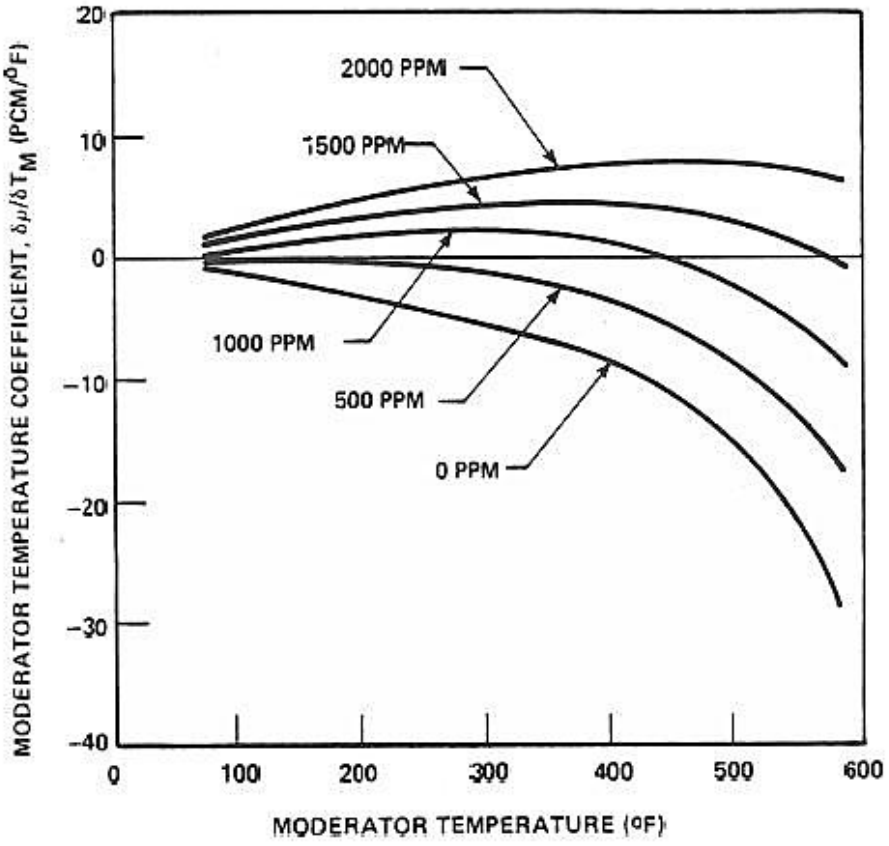

FIGURE 4.3.2-31

TYPICAL MODERATOR TEMPERATURE COEFFICIENT AT EOL

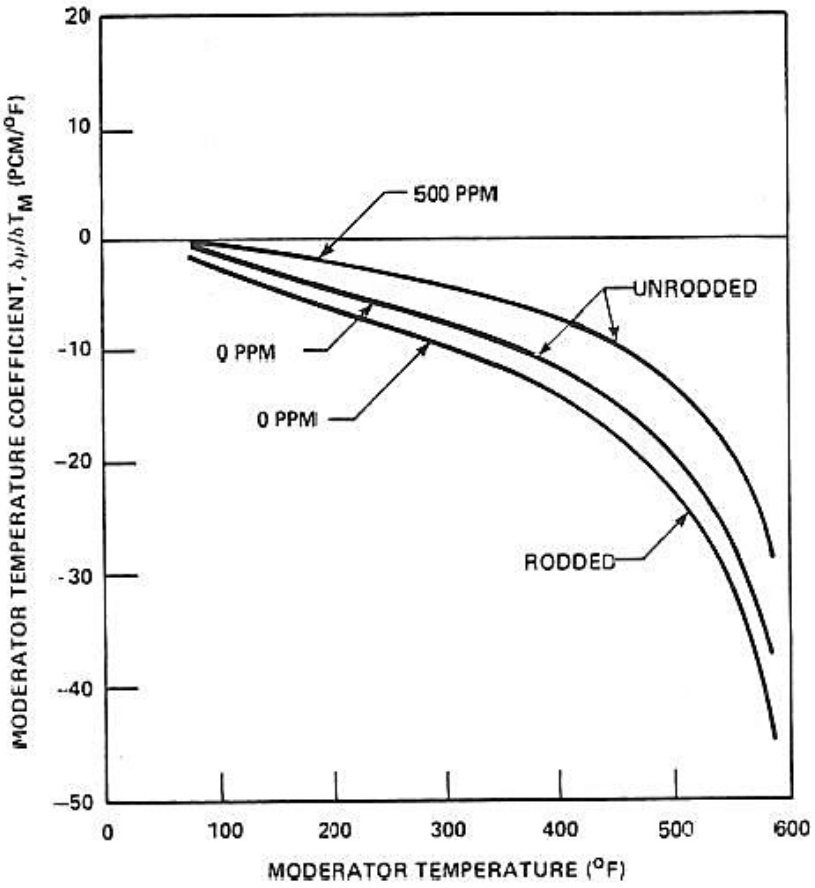

FIGURE 4.3.2-32

TYPICAL MODERATOR TEMPERATURE COEFFICIENT AS A FUNCTION OF BORON CONCENTRATION AT BOL, NO RODS

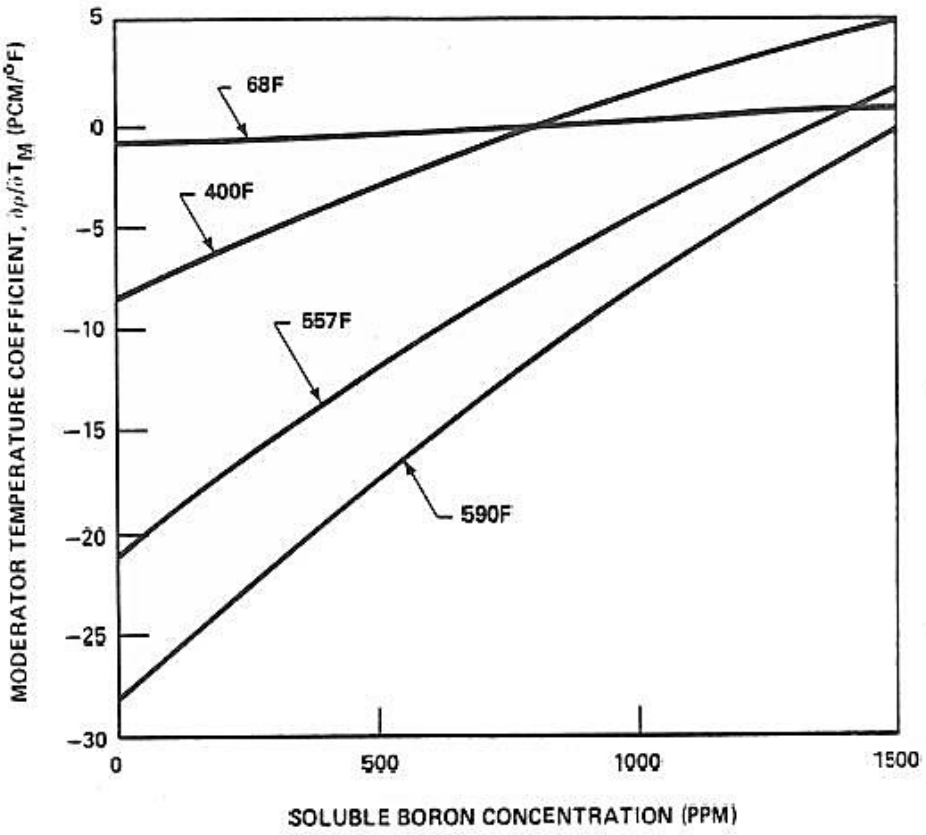

FIGURE 4.3.2-33

HOT FULL POWER TEMPERATURE COEFFICIENT DURING
TYPICAL CRITICAL BORON CONCENTRATION

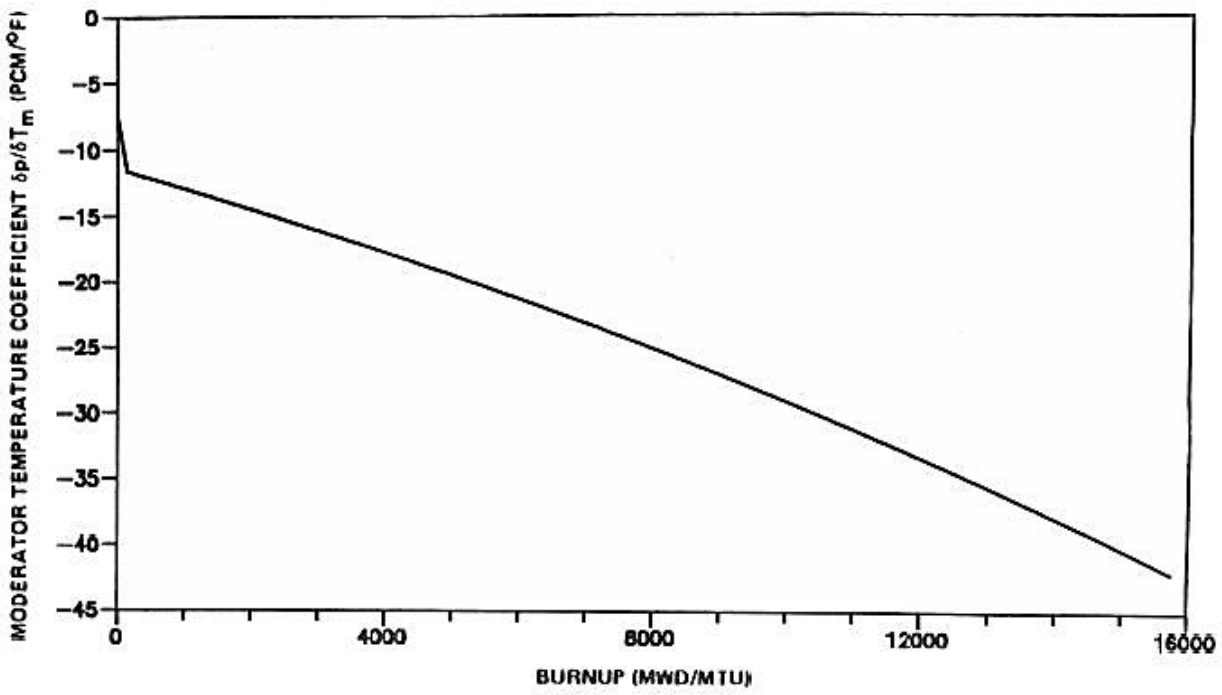

FIGURE 4.3.2-34

TOTAL POWER COEFFICIENT VS PERCENT POWER FOR BOL AND EOL

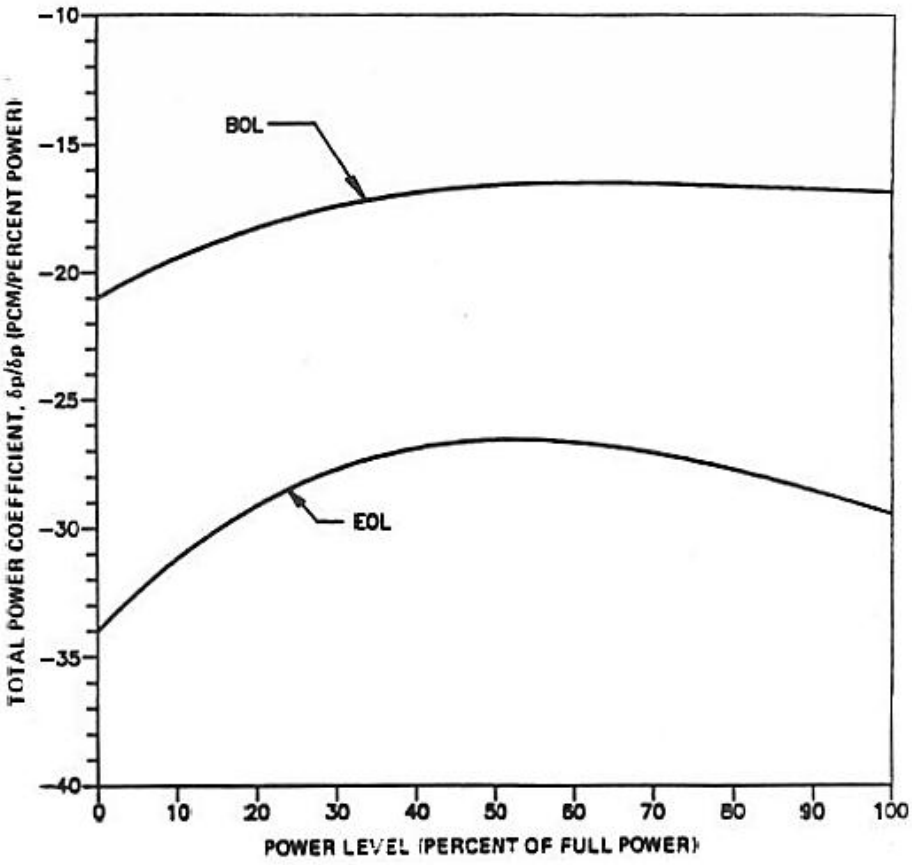

FIGURE 4.3.2-35

TOTAL POWER DEFECT BOL, EOL, TYPICAL

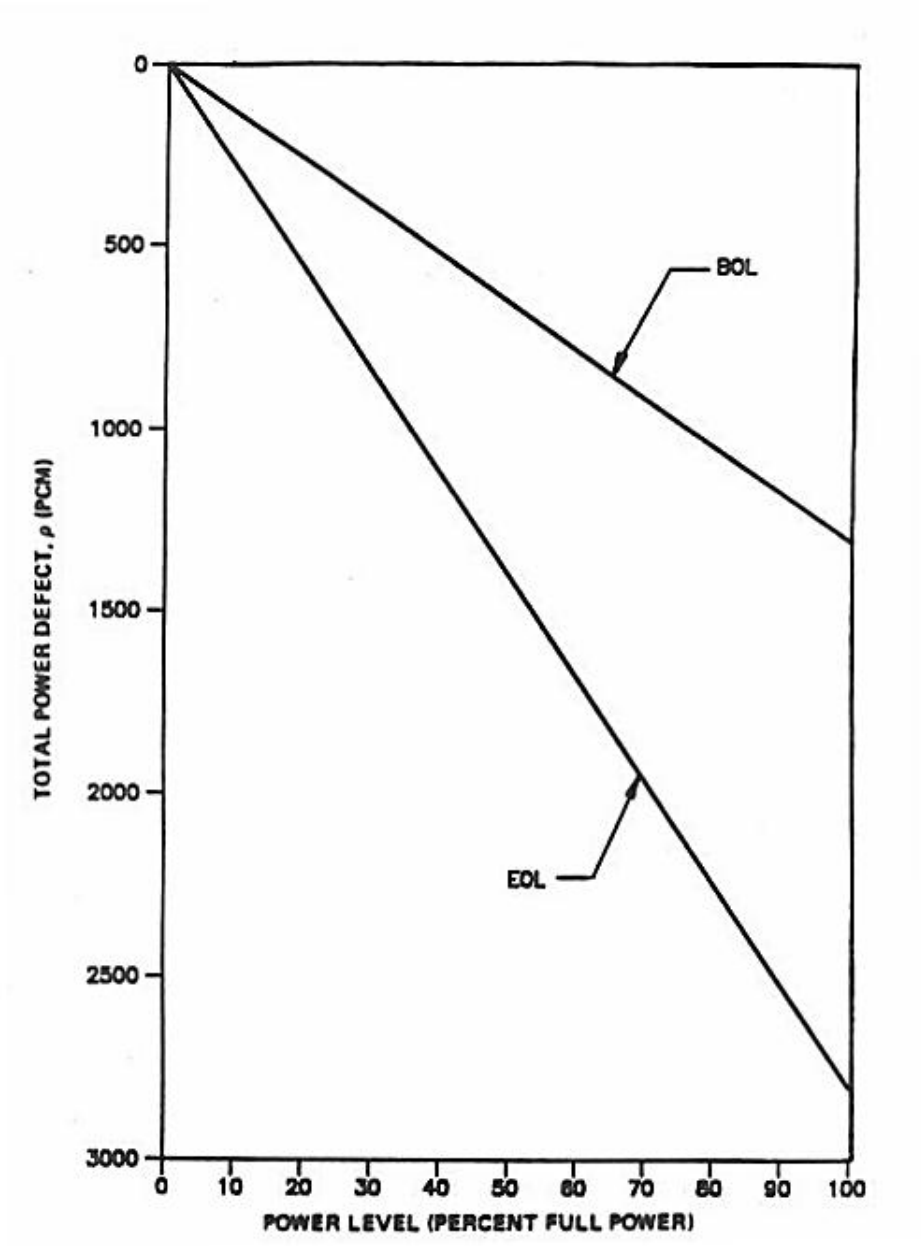

FIGURE 4.3.2-36

ROD CLUSTER CONTROL ASSEMBLY PATTERN

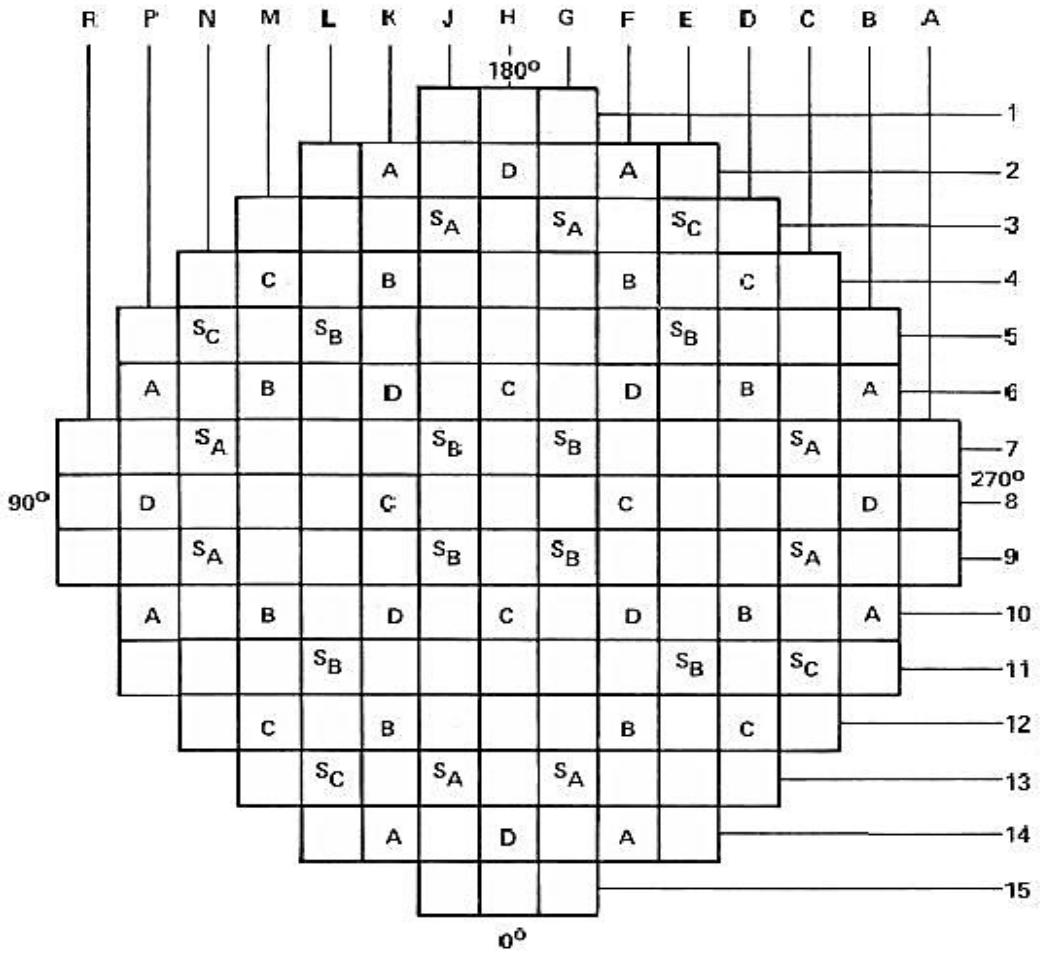

CONTROL BANK	NUMBER OF RODS
CONTROL D	8
CONTROL C	8
CONTROL B	8
CONTROL A	8
TOTAL	32

SHUTDOWN BANK	NUMBER OF RODS
SHUTDOWN B	8
SHUTDOWN A	8
SHUTDOWN C	4
TOTAL	20

FIGURE 4.3.2-37

TYPICAL ACCIDENTAL SIMULTANEOUS WITHDRAWAL OF TWO CONTROL BANKS AT EOL, HZP, BANKS “D” AND “B” MOVING INTO THE SAME PLACE

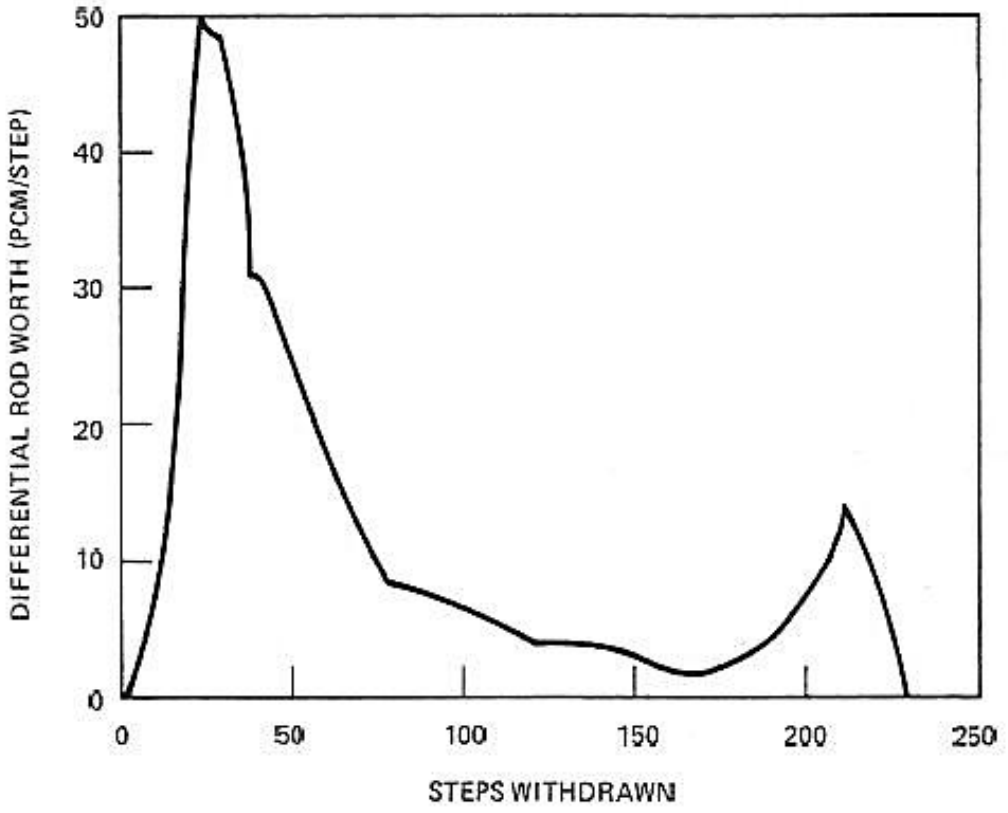

FIGURE 4.3.2-38

ROD POSITION VS TIME AFTER ROD DROP BEGINS

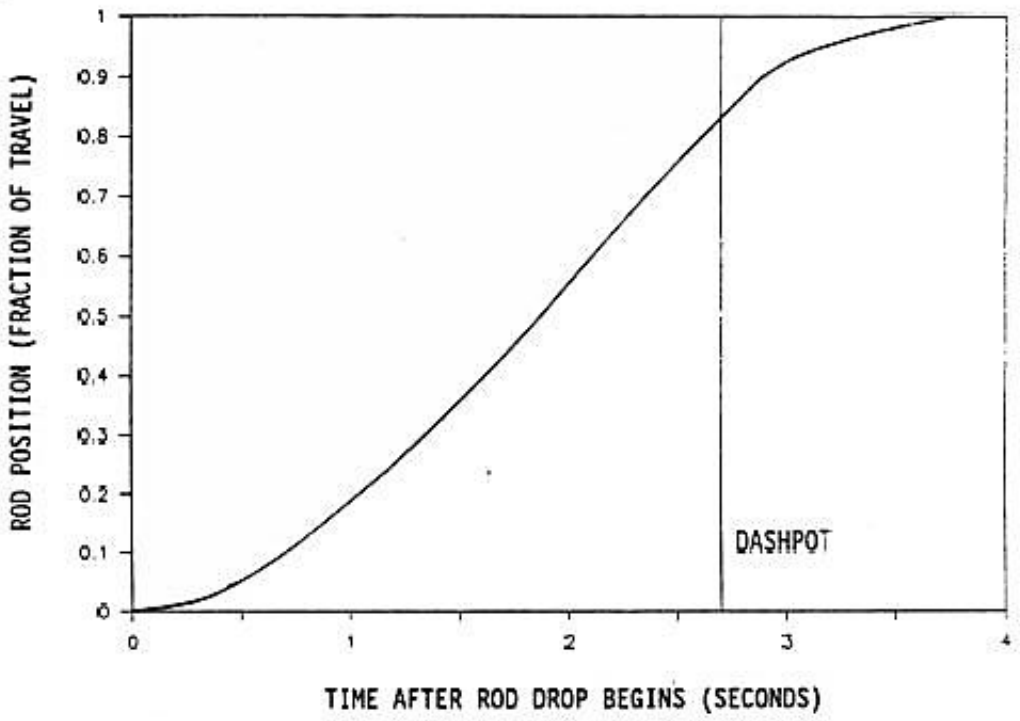

FIGURE 4.3.2-39

TYPICAL NORMALIZED ROD WORTH VS PERCENT INSERTION,
ALL RODS OUT BUT ONE

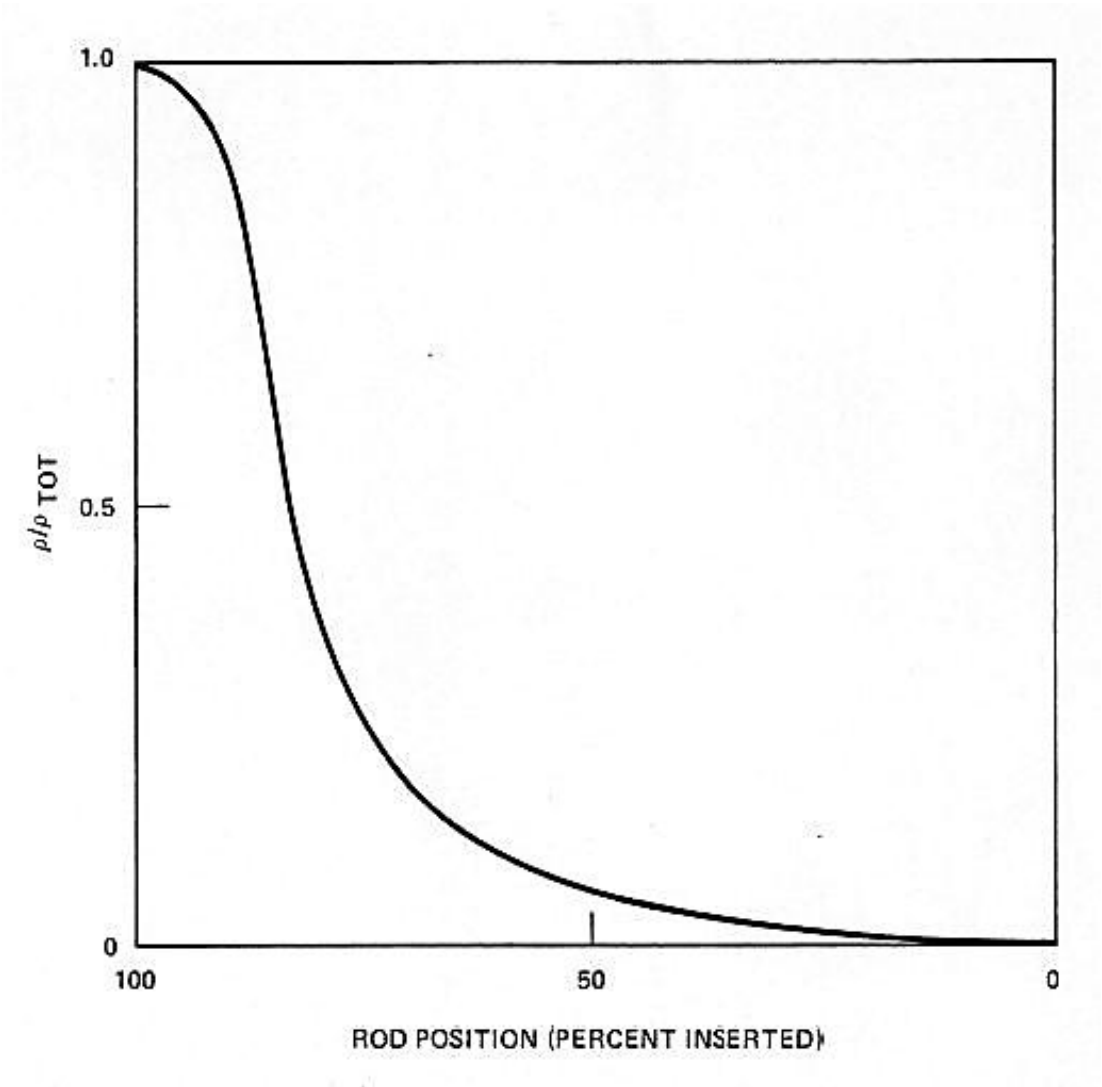

FIGURE 4.3.2-40

AXIAL OFFSET VS TIME, PWR CORE WITH A 12 FOOT HEIGHT AND 121 ASSEMBLIES

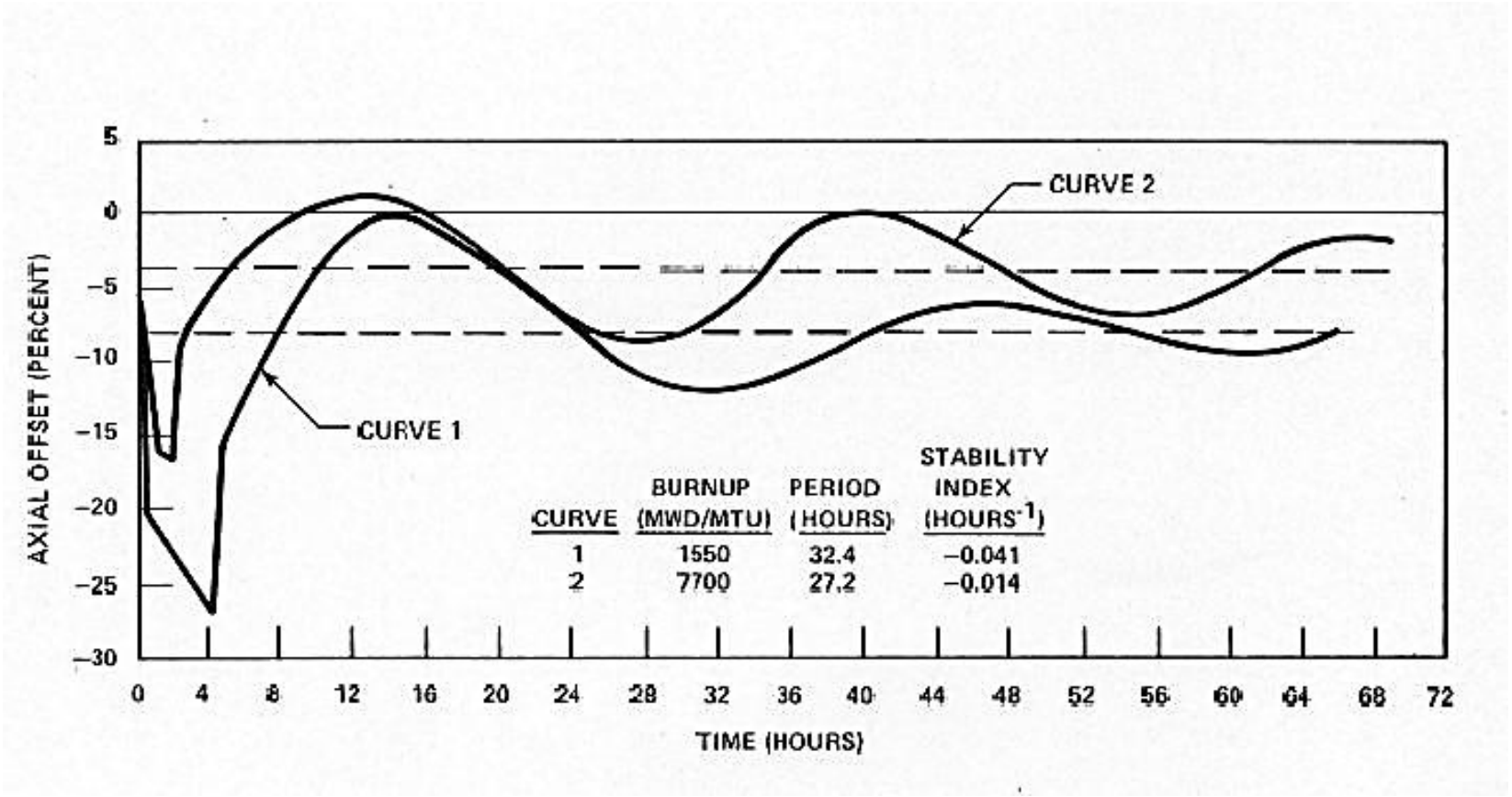

FIGURE 4.3.2-41

X-Y XENON TEST THERMOCOUPLE RESPONSE QUADRANT TILT DIFFERENCE VS TIME

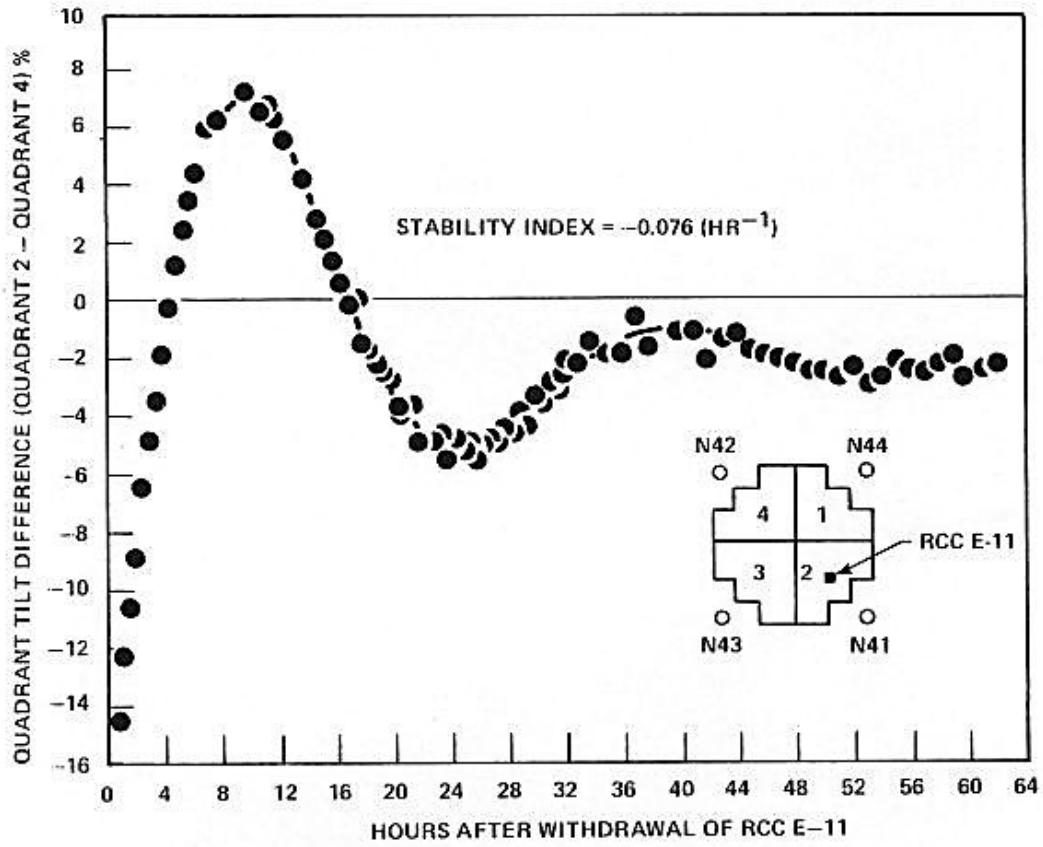

FIGURE 4.4.3-1

AXIAL POWER DISTRIBUTION FOR THERMAL HYDRAULIC COMPATIBILITY ANALYSIS

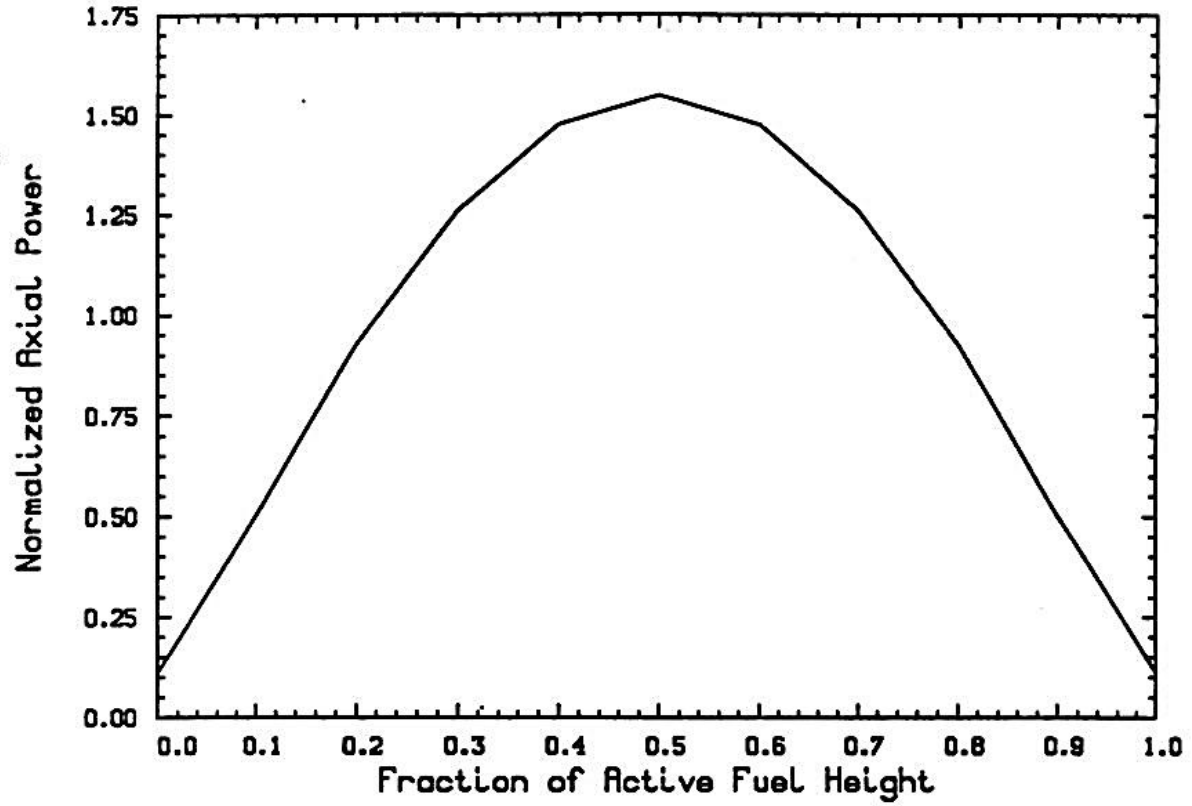

FIGURE 4.4.3-2

CYCLE 6 CORE LOAD PATTERN

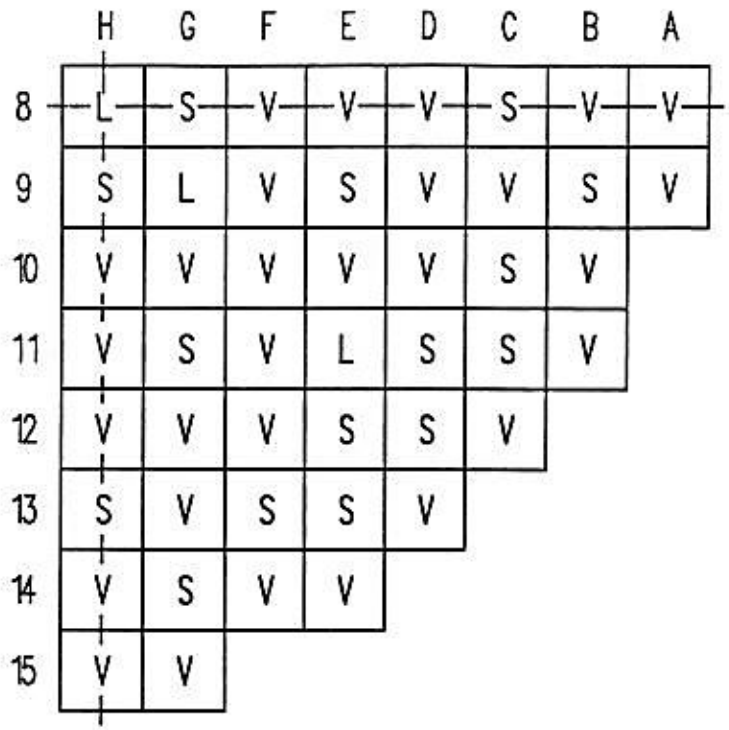

FIGURE 4.4.3-3

RADIAL POWER DISTRIBUTION FOR THERMAL HYDRAULIC COMPATIBILITY ANALYSIS

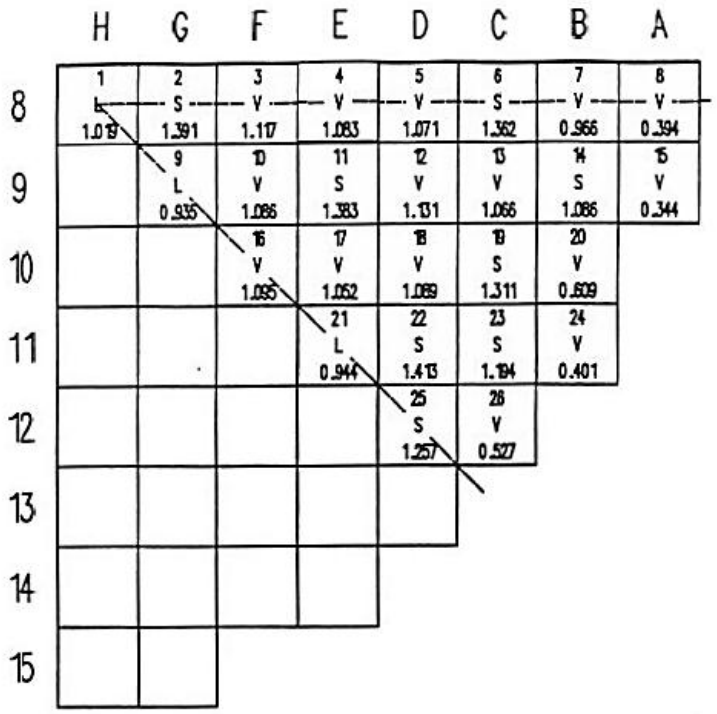

FIGURE 4.4.4-1

DISTRIBUTION OF INCORE INSTRUMENTATION

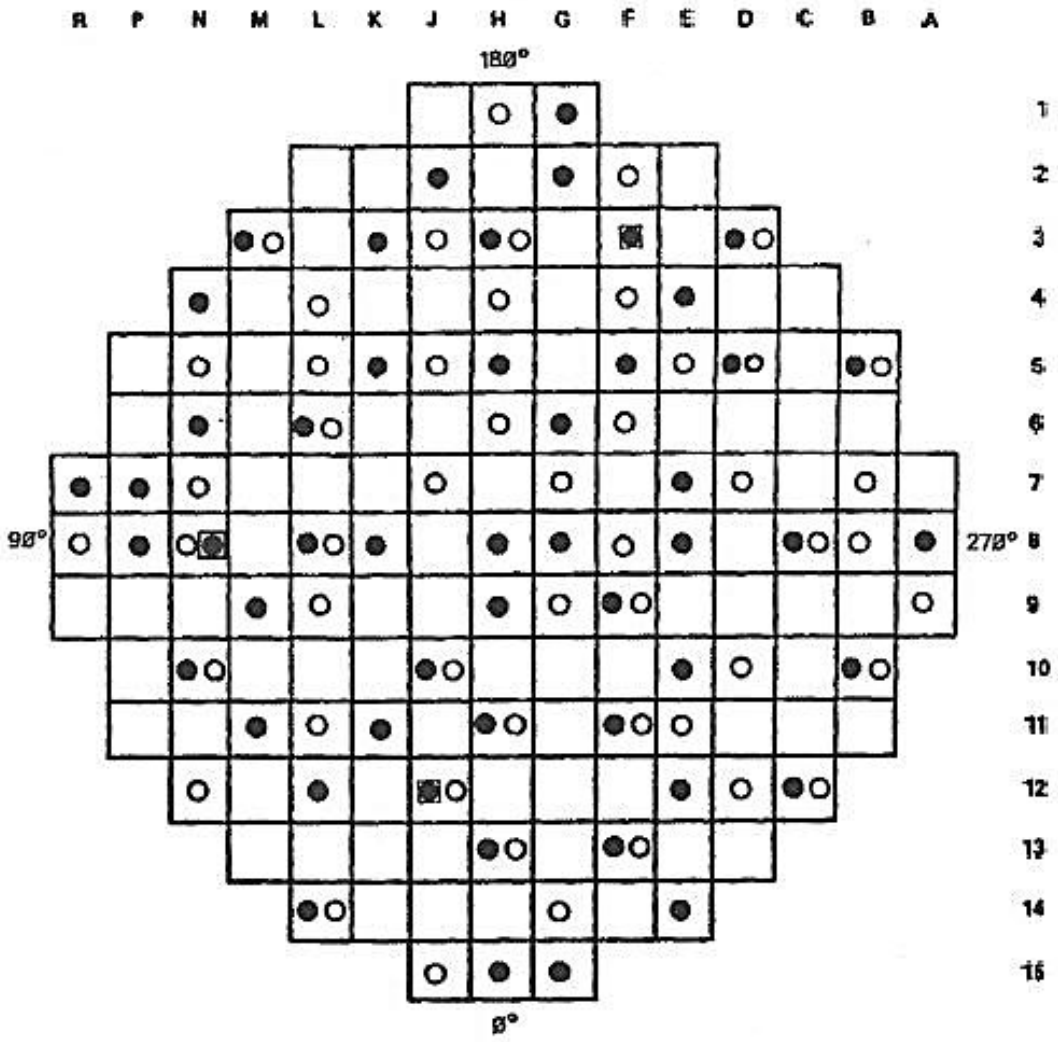

LEGEND

○ INCORE MOVABLE DETECTORS (58)

● THERMOCOUPLE LOCATIONS SHEARON HARRIS PLANT

▩ ABANDONED THERMOCOUPLE ASSEMBLIES

FIGURE 4.4.4-2

BLOCK DIAGRAM OF DMIMS